

Control of sediment diversion in run-of-river hydropower schemes

by

Morné Jandré van Heerden



A thesis submitted in partial fulfilment of the requirements for the degree
Master of Science in Hydraulic Engineering
at Stellenbosch University

Supervisor: Professor GR Basson

Department of Civil Engineering

December 2012

Copyright © 2012 University of Stellenbosch
All rights reserved.

Declaration

By submitting this thesis, I declare that this thesis and the entirety of the work contained therein is my own, that I am the authorship owner thereof (unless to the extent explicitly otherwise stated) and that I have not previously submitted it for any degree or examination in any other university.

Signature:

Date :

Synopsis

Sedimentation and the effects it has on turbine blades was the primary problem identified in run-of-river (RoR) hydropower schemes. Sedimentation in RoR hydropower schemes also increases trash rack blockage and reduces energy output in the long-term.

Damage occurs to all underwater parts that come into contact with sediment. The main concern is sediment passing through the hydropower intake and causing turbine damage. The reason for the abrasion and cavitation of turbine blades is increased sediment loads in river channels. This problem can be overcome in two ways. The first is the use of existing lakes or reservoir storage upstream as natural sand traps, and the second is by investigating the three features associated with river bend diversion, which are: the optimum diversion location in a river bend to minimise the abstraction of sediment, the optimum diversion structure angle to limit coarse sediment diversion, and the sediment load diverted through the intake.

The first objective of the research was investigated by construction of a physical model of a curved river channel to determine the location of the deepest scour forming on the outside of the bend. The second objective was to test the diversion orientation to maximize the local scour and thereby limiting sediment diversion at the intake. A third objective was to compare mathematical 2D model simulated scour results with the findings of the laboratory tests to evaluate the reliability of the numerical model predictions.

Finally different diverted discharge ratios were tested with different intake setups in the physical model, to evaluate the sediment load diverted. .

The first experiment in the curved laboratory channel was to predict where the deepest scour takes place without a diversion structure. This was then followed by placing a diversion structure at the maximum scour position, retrieved from experiment one, and by angling the structure with reference to the flow direction. The flow direction vector was placed as a tangent to the bend and orientated at angles of 0° , 30° , 45° and 60° into the bend direction.

The optimum diversion location was found to be positioned on the outside of the bend, approximately 60° into the channel bend. The final position of maximum scour in a 90° bend corresponds with the Sediment Committee and the Chinese Hydraulic Engineering Societies (1992) prediction of 60° into the bend. The optimal diversion had a 30° angle to the flow direction, as this presented the most efficient and effective scouring in front of the model intake.

Numerical simulations were performed with the CCHE 2D (hydrodynamics and sediment dynamics) modelling program. The numerical results were compared to the physical results to validate CCHE as a beneficial simulation tool. It was found that the numerical model predicted the scour depths at the

intakes tested with an accuracy of 43.8%, which is within the accuracy range of the sediment transport equation used by the numerical model.

The final experiment was the diversion of sediment with different intake level heights and discharges. It was evident from the results that low sediment diversion ratios were achieved with a diverted discharge ratio of 50% or less. The intake elevation highest above the channel bed diverted the least sediment. The interrelationship between Diverted Discharge Ratio (DDR), Diverted Froude number Ratio (DFrR) and Diverted Sediment load Ratio (SDR) was established in the study.

It is recommended that RoR schemes have sand traps downstream of the diversion structures and that turbines are coated with HVOF to overcome the power loss arising due to the excessive erosion of hydro turbines.

Samevatting

Sedimentasie en die invloed wat dit het op turbines was die primêre probleem geïdentifiseer in “run-of-river” (RoR) hidrokragskemas. Die sediment wat saam met die water uit ’n rivier uitgekeer word beskadig die inlaatrooster en verlaag kragopwekking in die langtermyn.

Skade word aangerig aan alle onderwatertoerusting en masjinerie wat aan sediment blootgestel word. Die grootste probleem tydens die uitkering van water is die growwe sediment wat daarmee deur die onttrekking inlaat gaan en turbineskade veroorsaak. Soos wat die sedimentlading in die rivier drasties toeneem, sal afslyting en kavitasie van turbinelemme meer gereeld voorkom. Dié probleem kan op twee maniere beperk word. Die een is die gebruik van bestaande opgaardamme stroomop, en die tweede is deur die ondersoek van drie kenmerke van rivierdraai en uitkeringstrukture, bv. die optimale uitskurings posisie in 'n rivierdraai (sonder 'n struktuur) om die diepste uitskuringposisie op die buitekant van die draai te bepaal, die optimale uitkeringsstruktuuriëntasie wat maksimum uitskuring verseker en die sediment uitkering beperk, en die lading van sedimentonttrekking deur die inlaat.

Die eerste doelwit van die navorsing is ondersoek deur 'n fisiese model te bou van 'n kronkelkanaal en te bepaal waar die diepste uitskring plaasvind op die buitekant van die draai. Die tweede doelwit van die studie was om die optimale uitkeringshoek te bepaal vir 'n uitkeringstruktuur sodat die uitskuring by the inlaat 'n maksimum is om die uitkering van sediment te beperk. 'n Derde doelwit was om die akkuraatheid van 'n wiskundige model se uitskuring voorspelling te toets teen die waargenome laboratorium resultate. Die finale doelwit was om vir verskillende inlaatontwerpe, rivier- en uitkeervloei die sedimentladings wat uitgekeer word te ondersoek. Die eerste eksperiment in die kronkelende kanaal was voorberei om die optimale uitskuring in die draai te bepaal. Dit is gevolg deur toetse met uitkeerstrukture by die maksimum uitskurings posisie te plaas en die hoek van die struktuur dan te verander met verwysing na die vloei rigting. Die vloei rigting vektor was as 'n raaklyn geplaas op die kanaal draai en georiënteer met hoeke: 0° , 30° , 45° en 60° , in die rigting van die draai.

Die optimale uitskurings posisie was aan die buiterand van die kanaal draai gevind, ongeveer 60° in die draai in. Die maksimum uitskuur posisie van 'n 90° kanaal draai stem ooreen met SC en CHES (1992) se resultaat van 60° in die draai in. Daar was ook genoegsame bewyse dat 'n optimale uitkeerwerke oriëntasie van 30° die doeltreffendste en effektiëste uitskuring sal gee.

Numeriese simulاسies is deur middel van 'n twee dimensionele wiskundige model CCHE 2D (hidro- en sedimentdinamika) uitgevoer. Die numeriese resultate was vergelyk met die laboratoriumresultate om die CCHE program te verifieer as 'n voordelige simulاسie program. Daar is gevind dat die wiskundige model die uitskuur dieptes by die inlate met 'n akkuraatheid van 43.8 % voorspel, wat

binne die akkuraatheid is van die sedimentvervoervergelyking wat deur die numeriese model gebruik word.

Die finale eksperiment was die uitkering van sediment met verskillende inlaathogtes en uitkerings sedimentladings. Uit die toetse was dit duidelik dat 'n lae sediment uitkeerverhouding behaal kan word met 'n uitkeerverhouding van 50% en minder. Verdere waarnemings het ook gewys dat die inlaathogte van die uitkeerstruktuur met die optimale resultate die hoogste bokant die rivierbedding was. Die verwantskap tussen die uitgekeerde deurstromingverhouding, die uitgekeerde Froude getal verhouding en die uitgekeerde sedimentlading is bepaal in die navorsing.

Dit word aanbeveel dat sandvangkanale stroomaf van uitkeerwerke geplaas word en dat turbines met HVOF as bedekkingsmateriaal beskerm word om kragverliese as gevolg van buitensporige erosie van die turbines te voorkom.

Acknowledgements

This document is dedicated to my parents, Nico and Corlette van Heerden, my brother, Stefan van Heerden, and Michelle Heyns for supporting and motivating me during the long hours and difficult times in my Master's studies.

To my parents, thank you for providing me with a fulfilling life full of fun and love. Thanks for all the sacrifices you had to make over my lifetime and for being such influential role models to pursue not only my Master's dreams, but my life dreams as well.

Professor G.R. Basson, thank you for your guidance and advice throughout my undergraduate and postgraduate studies. Thank you for the experience and knowledge that I can use throughout my life.

I would like to acknowledge the following people who enabled me to compile and successfully complete my studies for all their support:

- ESKOM, thank you for providing me with a bursary for the duration of my studies.
- Mr G.K.R. Robertson, for assistance with CCHE.
- Mr N. Combrinck, Mr A. Lindoor and Mr E. Wanza of the Hydraulic Laboratory of Stellenbosch University, for their support in building the physical model and always being available to lend a helping hand.
- Mr A.D.D. van den Heever, for helping in the river model as colleague.

Table of Contents

SYNOPSIS	IV
SAMEVATTING	VI
ACKNOWLEDGEMENTS.....	VIII
LIST OF FIGURES	VIII
LIST OF TABLES	XII
LIST OF SYMBOLS AND ABBREVIATIONS.....	XIII
CHAPTER 1.....	1-1
1.1 INTRODUCTION.....	1-1
1.2 PROBLEM STATEMENT AND OBJECTIVES.....	1-2
1.2.1 <i>Research question and hypothesis</i>	1-4
1.3 RESEARCH METHOD.....	1-5
1.4 METHODOLOGY	1-6
CHAPTER 2.....	2-1
2.1 LITERATURE STUDY	2-1
2.1.1 <i>Damage Analysis</i>	2-1
2.1.1.1 Sediment Deposition	2-1
2.1.1.2 Corrosion and Rusting.....	2-2
2.1.1.3 Hydro Erosion	2-3
2.1.2 <i>Sediment Characteristics</i>	2-6
2.1.2.1 Geological Studies.....	2-6
2.1.2.3 Sediment Movement.....	2-6
2.1.3 <i>Design of a RoR hydropower station to limit sediment diversion</i>	2-9
2.1.3.1 Open Channel River Mechanics	2-9
2.1.3.2 Site Configuration	2-17
2.1.3.3 Intake Structures.....	2-18
2.1.3.4 Trashrack	2-29
2.1.3.5 Vortices	2-35
2.1.3.6 Settlers and Sediment Trap design	2-38
2.1.3.7 Turbine Specifications and Parameters.....	2-43
CHAPTER 3.....	3-1
3.1 OBJECTIVES.....	3-1
3.2 PHYSICAL HYDRAULIC MODEL DESIGN	3-2
3.2.1. <i>Sediment Slide Angle</i>	3-7
3.3 LABORATORY TEST PROCEDURE.....	3-9
3.3.1 <i>Experiment 1: Maximum scour location without structure</i>	3-9
3.3.2 <i>Experiments 2 to 9: Angle of diversion structure</i>	3-10
3.3.3 <i>Experiment 10</i>	3-15
3.4 ANALYSIS AND RESULTS OF PHYSICAL EXPERIMENT.....	3-17
3.4.1 <i>Experiment 1 (without diversion structure, 20 l/s)</i>	3-18
3.4.2 <i>Experiment 2 (0° with flow, 17.5 l/s)</i>	3-22
3.4.3 <i>Experiment 3 (0° L-shape with flow, 14.5 l/s)</i>	3-23
3.4.4 <i>Experiment 4 (30° with flow, 18.8 l/s)</i>	3-24
3.4.5 <i>Experiment 5 (30° L-shape with flow, 17.8 l/s)</i>	3-26
3.4.6 <i>Experiment 6 (45° with flow, 17.2 l/s)</i>	3-27
3.4.7 <i>Experiment 7 (45° L-shape with flow, 15.5 l/s)</i>	3-28
3.4.8 <i>Experiment 8 (60° with flow, 18.4 l/s)</i>	3-29
3.4.9 <i>Experiment 9 (60° L-shape with flow, 15.5 l/s)</i>	3-31
3.4.10 <i>Experiment 10</i>	3-32

3.4.10.1 Experiment 10A (Sediment Load Test without Structure).....	3-33
3.4.10.2 Experiment 10B (Concentration Test with Greater Diversion Flows)	3-36
3.4.10.3 Experiment 10C (Concentration Test with Greater Flows)	3-39
3.4.10.4 Experiment 10D (Concentration Test, Change of Intake Level).....	3-43
3.5 SUMMARISED DISCUSSION OF RESULTS	3-48
3.5.1 <i>Sediment diversion</i>	3-48
CHAPTER 4.....	4-1
4.1 CCHE 2D.....	4-1
4.1.1 <i>Numerical Description of 2D Mesh Generator</i>	4-1
4.1.2 <i>Description of Hydrodynamics</i>	4-2
4.1.2.1 Flow Parameters for Diversion Model.....	4-2
4.1.3 <i>Sediment Transport Description</i>	4-2
4.1.3.1 Total Load	4-3
4.1.3.2 Initial Conditions.....	4-3
4.1.3.3 Empirical Formulas	4-3
4.1.3.4 Sediment Parameters for Diversion Model.....	4-4
4.2 OBJECTIVE	4-5
4.3 NUMERICAL MODEL CALIBRATION.....	4-5
4.4 NUMERICAL RESULTS	4-6
4.4.1 <i>Simulation Test 1 (Without Diversion Structure, $Q = 20$ l/s)</i>	4-9
4.4.2 <i>Simulation Test 2 (0° with flow, $Q = 17.5$ l/s)</i>	4-11
4.4.3 <i>Simulation Test 3 (0° L-shape with flow, $Q = 14.5$ l/s)</i>	4-13
4.4.4 <i>Simulation Test 4 (30° with flow, $Q = 18.8$ l/s)</i>	4-15
4.4.5. <i>Simulation Test 5 (30° L-shape with flow, $Q = 17.8$ l/s)</i>	4-17
4.4.6. <i>Simulation Test 6 (45° with flow, $Q = 17.2$ l/s)</i>	4-19
4.4.7. <i>Simulation Test 7 (45° L-shape with flow, $Q = 15.5$ l/s)</i>	4-21
4.4.8. <i>Simulation Test 8 (60° with flow, $Q = 18.4$ l/s)</i>	4-23
4.4.9. <i>Simulation Test 9 (60° L-shape with flow, $Q = 15.5$ l/s)</i>	4-25
4.4.10. <i>Simulation Test 10S 1 (30° 1 metre wide, $Q = 37.6$ l/s)</i>	4-27
4.4.11. <i>Simulation Test 10S 2 (60° 1 metre wide, $Q = 36.9$ l/s)</i>	4-28
4.5. SUMMARISED DISCUSSION OF RESULTS	4-30
CHAPTER 5.....	5-1
5.1 BACKGROUND	5-1
5.2 CASE STUDIES ON SCOPE OF WORK	5-1
5.3 SITE VISIT	5-2
5.4 HYDRAULICS OF THE PROPOSED ABSTRACTION WORKS SITE	5-4
CHAPTER 6.....	6-1
6. CONCLUSIONS AND RECOMMENDATIONS.....	6-1
Reference.....	R-1
Appendix A.....	A-a
Appendix B.....	B-a
Appendix C.....	C-a

List of Figures

Figure 1.1: Eroded runner and guide vanes (Olesen and Pradhan, 2010).....	1-5
Figure 1.2: Optimum sediment exclusion (OSE) research as a cyclic process (Bishwakama, 2007)..	1-6
Figure 1.3: Orientation of structure with reference to flow direction	1-7
Figure 2.1: Erosion on turbine blades (Central Board of Irrigation & Power and INCOLD, 2008)....	2-3
Figure 2.2: Cavitation mechanics of erosion	2-4
Figure 2.3: Ripple formation due to turbulence (Karimi and Schmid, 1992)	2-5
Figure 2.4: Damage of subsurface regions (Central Board of Irrigation & Power and INCOLD, 2008)	2-5
Figure 2.5: Modified Lui diagram (Rooseboom et al., 1983)	2-7
Figure 2.6: Settling velocity as a function of sediment size (Rooseboom et al., 1983)	2-8
Figure 2.7: Typical velocity distributions for open channel flow (Penche, 2004).....	2-9
Figure 2.8: Curvilinear flows in a channel bend (Bouvard, 1992) and (Thompson, 1876)	2-9
Figure 2.9: Secondary currents in river bends (Penche, 2004)	2-10
Figure 2.10: Flow behaviour in a channel bend (Henderson, 1967).....	2-10
Figure 2.11: Maximum scour in a river bend (Raudkivi, 1993)	2-12
Figure 2.12: Simulated scour and deposition (Brink et al., 2005)	2-13
Figure 2.13: Simulated helical flow intensity (Brink et al., 2005).....	2-13
Figure 2.14: Model experiment of diversion structures (Mosoyi, 1965)	2-14
Figure 2.15: High head scheme (Penche and De Minas, 1998).....	2-17
Figure 2.16: Short penstock for low heads (Penche and De Minas, 1998).....	2-18
Figure 2.17 : Side intake with cross weir (Avery, 1989)	2-20
Figure 2.18: Canal diversion works (Avery, 1989).....	2-21
Figure 2.19: Schematic view of a morning glory spillway (Penche, 2004).....	2-21
Figure 2.20: Vertical strata scheme (Penche and De Minas, 1998).....	2-22
Figure 2.21: Bottom intake across river (Penche, 2004).....	2-22
Figure 2.22: “Tyrolean” intake (Penche, 2004)	2-23
Figure 2.23 : Curved sluicing flumes (Tan, 1996).....	2-23
Figure 2.24: Pressy water intake (Bouvard, 1992) (Note: can also be designed as a frontal intake).	2-24
Figure 2.25: Bottom outlet scheme (Penche and De Minas, 1998)	2-24
Figure 2.26: Types of intakes (Raudkivi, 1993)	2-25
Figure 2.27: Intake raised above the river bottom (Penche and De Minas, 1998).....	2-26
Figure 2.28: Sediment trap (Penche and De Minas, 1998)	2-26
Figure 2.29: Layout of run-of-river power station scheme (Penche and De Minas, 1998).....	2-27
Figure 2.30: Oleo hydraulic cylinders (Penche and De Minas, 1998)	2-29
Figure 2.31: Prefabricated booms (Penche, 2004).....	2-30
Figure 2.32: Trash boom layout (Penche, 2004).....	2-30
Figure 2.33: French drop intake (Penche, 2004).....	2-32
Figure 2.34: Loss coefficient (Penche, 2004)	2-32
Figure 2.35: Formula for computing head losses (Penche, 2004).....	2-33
Figure 2.36: Trashrack design according to Ramos (2000)	2-34
Figure 2.37: Schemes of different types of vortices (Ramos, 2000).....	2-36
Figure 2.38: Minimum degree of submergence (Penche and De Minas, 1998).....	2-37
Figure 2.39: Different degrees of submergence (Penche, 2004).....	2-37
Figure 2.40: Different zones in a sedimentation basin (Ramos, 2000).....	2-38
Figure 2.41: Dufour sediment trap (Bouvard, 1992).....	2-39

Figure 2.42: Settler design (Bouvard, 1992).....	2-40
Figure 2.43: Diversion hopper design with jet pump.....	2-42
Figure 2.44: High-head turbines	2-44
Figure 3.1: Layout plan of diversion intake shape.....	3-1
Figure 3.2: Berg River with consecutive 90 ⁰ bends.....	3-2
Figure 3.3: Breede River with consecutive 90 ⁰ bends	3-3
Figure 3.4: Vaal River bends for RoR positioning	3-3
Figure 3.5: Sinusoidal test of 90 ⁰ bend.....	3-4
Figure 3.6: Layout plan of physical model to determine diversion position and angle	3-5
Figure 3.7: Test 1 for sediment slide angle.....	3-8
Figure 3.8: Test 2 for sediment slide angle.....	3-8
Figure 3.9: Cross section layout of physical model	3-9
Figure 3.10: Orientation of structure with reference to flow direction	3-10
Figure 3.11: Diversion angle with 0 ⁰ orientation to channel flow.....	3-12
Figure 3.12: Diversion angle with 30 ⁰ orientation to channel flow.....	3-12
Figure 3.13: Diversion angle with 45 ⁰ orientation to channel flow.....	3-13
Figure 3.14: Diversion angle with 60 ⁰ orientation to channel flow.....	3-13
Figure 3.15: 30 ⁰ diversion angle with L-shaped attachment.....	3-14
Figure 3.16: Origin of L-shaped structure	3-14
Figure 3.17: Model abstraction structure (scale 1:40)	3-15
Figure 3.18: V-notch weir at inlet of river and outlet of intake structure	3-16
Figure 3.19: Bed change result for physical experiment 1 (without diversion structure, Q = 20 l/s).....	3-18
Figure 3.20: Change in location of maximum diversion from low to high flow	3-19
Figure 3.21: Change in scour location due to different river flows (see Experiment 10A)	3-20
Figure 3.22: Location of optimum diversion in channel bend.....	3-21
Figure 3.23: Bed change result for physical experiment 2 (0 ⁰ with flow, Q = 17.5 l/s).....	3-22
Figure 3.24: Bed change result for physical experiment 3 (0 ⁰ L-shape structure, Q = 14.5 l/s).....	3-23
Figure 3.25: Bed change result for physical experiment 4 (30 ⁰ with flow, Q = 18.8 l/s).....	3-24
Figure 3.26: Bed change result for physical experiment 5 (30 ⁰ L-shape structure, Q = 17.8 l/s).....	3-26
Figure 3.27: Bed change result for physical experiment 6 (45 ⁰ with flow, Q = 17.2 l/s).....	3-27
Figure 3.28: Bed change result for physical experiment 7 (45 ⁰ L-shape structure, Q = 15.5 l/s).....	3-28
Figure 3.29: Bed change result for physical experiment 8 (60 ⁰ with flow, Q = 18.4 l/s).....	3-29
Figure 3.30: Bed change result for physical experiment 9 (60 ⁰ L-shape structure, Q = 15.5 l/s).....	3-31
Figure 3.31: Head details of experiment 10 series.....	3-32
Figure 3.32: Sediment loads (mg/s.m) at different river flows (m ³ /s) without a structure on the outside of the channel bend	3-35
Figure 3.33: Prevention slope of 1:5 in front of diversion intake	3-36
Figure 3.34: Diverted sediment concentration (g/l) at different DDRs through the intake (same Q _{Riv}).....	3-38
Figure 3.35: Diverted sediment concentration (g/l) at different intake levels (m) through the intake (same Q _{Riv})	3-39
Figure 3.36: Diverted sediment concentration (g/l) at different DDRs through the intake (Q _{Riv} varied)	3-42
Figure 3.37: Diverted sediment concentration (g/l) at different heads above intake (m) (Q _{Riv} varied).....	3-43
Figure 3.38: Diverted sediment concentration (g/l) at different DDRs through the intake (H3 increase)	3-45

Figure 3.39: Diverted sediment concentration (g/l) at different intake levels (m) through the intake (H3 increase).....	3-45
Figure 3.40: Graph of SDR versus DDR	3-49
Figure 3.41: Detail A of SDR versus DDR graph.....	3-52
Figure 3.42: Sediment diversion ratio vs. diverted Froude ratio with reference to the diverted discharge ratios	3-53
Figure 4.1: River mesh generated from numerical model.....	4-7
Figure 4.2: Bed change (m) result for numerical model test 1.....	4-9
Figure 4.3: Bed change (m) result for physical model test 1	4-9
Figure 4.4: Velocity magnitude (m/s) result for numerical model test 1	4-10
Figure 4.5: Bed change (m) result for numerical model test 2.....	4-11
Figure 4.6: Bed change (m) result for physical experiment 2.....	4-11
Figure 4.7: Velocity magnitude (m/s) result for numerical model test 2	4-12
Figure 4.8: Bed change (m) result for numerical model test 3.....	4-13
Figure 4.9: Bed change (m) result for physical result 3	4-13
Figure 4.10: Velocity magnitude (m/s) result for numerical model test 3	4-14
Figure 4.11: Bed change (m) result for numerical model test 4.....	4-15
Figure 4.12: Bed change (m) result for physical experiment 4.....	4-15
Figure 4.13: Velocity magnitude (m/s) result for numerical model test 4	4-16
Figure 4.14: Bed change (m) result for numerical model test 5.....	4-17
Figure 4.15: Bed change (m) result for physical experiment 5.....	4-17
Figure 4.16: Velocity magnitude (m/s) result for numerical model test 5	4-18
Figure 4.17: Bed change (m) result for numerical model test 6.....	4-19
Figure 4.18: Bed change (m) result for physical result 6.....	4-19
Figure 4.19: Velocity magnitude (m/s) result for numerical model test 6	4-20
Figure 4.20: Bed change (m) result for numerical model test 7.....	4-21
Figure 4.21: Bed change (m) result for physical experiment 7	4-21
Figure 4.22: Velocity magnitude (m/s) result for numerical model test 7	4-22
Figure 4.23: Bed change (m) result for numerical model test 8.....	4-23
Figure 4.24: Bed change (m) result for physical result 8.....	4-23
Figure 4.25: Velocity magnitude (m/s) result for numerical model test 8	4-24
Figure 4.26: Bed change (m) result for numerical model test 9.....	4-25
Figure 4.27: Bed change (m) result for physical result 9.....	4-25
Figure 4.28: Velocity magnitude (m/s) result for numerical model test 9	4-26
Figure 4.29: Bed change (m) result for numerical model test 10S 1	4-28
Figure 4.30: Velocity magnitude (m/s) result for numerical model test 10S1	4-28
Figure 4.31: Bed change (m) result for numerical model test 10S 2	4-29
Figure 4.32: Velocity magnitude (m/s) result for numerical model test 10S2	4-29
Figure 5.1: Satellite image of the Berg River near Voëlvlei Dam	5-2
Figure 5.2: 2D model bathymetry of Berg River abstraction works (elevation based on survey data as masl).....	5-2
Figure 5.3: Sediment sampling locations	5-3
Figure 5.4: Two-year flood water depth (m) with velocity vectors	5-5
Figure 5.5: Two-year flood velocity magnitude (m/s) with velocity vectors.....	5-6
Figure 5.6: Ten-year flood (water depth) with velocity vectors	5-6
Figure 5.7: Ten-year flood (velocity magnitude) with velocity vectors	5-7
Figure 5.8: Hundred-year flood (water depth) with velocity vectors.....	5-7

Figure 5.9: Hundred-year flood (velocity magnitude) with velocity vectors.....	5-8
Figure 5.10: Two-year flood (bed change)	5-9
Figure 5.11: Ten-year flood (bed change)	5-9
Figure 5.12: Hundred-year flood (bed change).....	5-10
Figure 5.13: Plan view of layout of proposed abstraction works.....	5-11
Figure 6.1: Mathematical model simulated bed change results for a 30 ⁰ diversion angle.....	6-2
Figure 6.2: Laboratory bed change results for a 30 ⁰ diversion angle	6-2
Figure 6.3: Sediment level of physical model before experiment run	6-3
Figure 6.4: Sediment bed level of physical model after experiment run	6-3
Figure 6.5: Sediment level of numerical model before simulation.....	6-3
Figure 6.6: Sediment level of numerical simulation after test run.....	6-3
Figure 6.7: SDR versus DDR for RoR hydropower generation.....	6-4
Figure 6.8: Sediment diversion ratio vs. diverted Froude ratio with reference to the diverted discharge ratios.....	6-1

List of Tables

Table 1.1: Definition of hydro power facility size (Atkins, 2003).....	1-3
Table 2.1: Sediment characteristics	2-2
Table 2.2: Relationship between central angle of a bend and optimal location of intake (SC and CHES, 1992).....	2-11
Table 2.3: Intake characteristics (Penche, 2004)	2-19
Table 2.4: Spacing between bars for different turbine types (Lencastre and Holmes, 1987)	2-34
Table 2.5: Strouhal number for different types of bars (Lencastre and Holmes, 1987).....	2-34
Table 2.6: Safety coefficient for Strouhal number (Lencastre and Holmes, 1987)	2-35
Table 2.7: Application range of standard turbines and their power output (Ramos, 2000)	2-44
Table 2.8: Low-head turbines	2-45
Table 3.1: Sediment movement in laboratory model	3-7
Table 3.2: Difference in terminology	3-11
Table 3.3: Weight adjustment	3-33
Table 3.4: Summary of results of physical experiments 1 to 9	3-46
Table 3.5: Summary of results of physical experiments 10 A to 10 D	3-47
Table 3.6: Sediment data for SDRs at specific DDRs	3-49
Table 4.1: CCHE 2D properties for all simulations.....	4-4
Table 4.2: Water level comparison at measuring points 1, 2 and 3	4-6
Table 4.3: Summary of numerical model setup	4-8
Table 4.4: Percentage error between the maximum scour depths (mm) of the numerical and physical tests (60° into the channel bend).....	4-30
Table 5.1: Site visit sample coordinates.....	5-3
Table 5.2: Summary of sediment grading results	5-4
Table 5.3: Flood peaks	5-5

List of Symbols and Abbreviations

(V:H)	(Vertical: Horizontal)
$^{\circ}\text{C}$	Degrees Celsius
A	Area (m^2)
b	Width between bars
B, w	Channel width
C_{Sediment}	Concentration of sediment diverted
$D F_r R$	Diverted Froude ratio
D	Normal depth (m)
d_{50}	Average particle diameter
DDR	Diverted discharge ratio (%)
E_b	Elasticity modulus (N/m^2)
F	Safety factor
f_b	Bars frequency
$F_{r \text{ Diverted}}$	Froude number through intake diversion
$F_{r \text{ River}}$	Froude number of river
Fr	Froude number
f_s	Swirl frequency
g	Gravity constant (m/s^2)
g/s	Grams per second
H	Water level above V-notch
H_2	Intake height
HVOF	High velocity oxygen fuelled
I_{max}	Nodes in x-direction (numerical model)
J_{max}	Nodes in y-direction (numerical model)
K	Kelvin
kg/s	kilograms/second
k_s	Surface roughness (m)
kW	Kilowatt
l/s	litres per second
L_b	Distance between bar supports (m)
L_B	Length of bend

L_D	Length of diversion structure
L_m	Model length
L_p	Prototype length
m	Metres
m/s	Metres per second
masl	Metres above sea level
mg	Milligrams
Ml/day	Megalitres per day
m_m	Mass (kg)
mm	Millimetres
MOL	Minimum operating level
MW	Megawatt
n	Manning n ($s/m^{0.333}$)
N	Rotational speed (revolutions per minute)
n_l, n_v, n_Q, n_t	Scale size
ϕ	Angle of inclination
P	Power output (kW)
Q	River flow/discharge
$Q_{Diverted}$	Diverted discharge (m^3/s)
Q_m	Model discharge
Q_p	Prototype discharge
Q_{River}	River discharge (m^3/s)
Q_s	Sediment load (grams/second)
Q_{sDiv}	Diverted sediment load (g/sm^2)
Q_{sRiver}	Incoming sediment load in river (g/sm^2)
R	Hydraulic radius (m)
r_c	Average radius of curvature
r_c/w	Radius of curvature to width ratio
Re	Reynolds number
ROR	Run-of-river
S	Slope of the river
SDR	Sediment diversion ratio
SPLASH	Spatial plans and local arrangement for small hydro
St	Strouhal number

t	Bar thickness
T	Time of run (seconds)
TDS	Total dissolved solids
T_m	Model time
T_p	Prototype time
V	Average velocity
V_{*C}	Shear velocity
V_m	Model velocity
V_o	Mean velocity (Q/A)
V_p	Prototype velocity
V_{ss}	Settling velocity
w/d	Width to depth ratio
y	Dry sediment mass
γ	Specific weight of water
γ_b	Specific weight (N/m ³)
ΔH	Change in water level
θ	V-notch angle (°)
$\mu S/m$	Micro Siemen per metre
ν	Kinematic viscosity (m ² /s)
ξ	Coefficient
ρ	Density (kg/m ³)

Chapter 1

1.1 Introduction

The way people interact with water and energy is changing. Electrical engineers working on energy projects and who are dependent on water are usually trained to understand this energy. The engineers who are trained in water do not necessarily understand this energy concept.

Combining electricity and water hydraulics will introduce a source of unlimited energy to the world. This source is not newly invented, and in fact has been around for centuries. This source is hydropower and dates back to the third century B.C.E. (Pruess, 2010). The Greeks introduced the mechanical water wheel to mechanise grain mills (Philo of Byzantium, n.d.). In the fourth century, the first water turbine was invented by Roman engineers. The world has changed, but the foundation of modern hydropower turbine genesis lies in *Architecture Hydraulique*, published in the 1770s by French engineer Bernard Forest de Belidor (De Belidor, 2010). The technology has not changed much since the Industrial Revolution, for example small hydro applications today use reactive turbines that are similar to those developed by Jan Andrej Segner in the 1750s (O'Connor and Roberson, 2004).

As time passed, hydroelectric power advanced, unlike the turbine. Thomas Edison invented the electromagnetic generator in 1879 (The Thomas Edison Papers, 2012) and, in 1882, HJ Rogers coupled Edison's generator with a water turbine and introduced the first hydroelectric plant on the Fox River in Appleton, Wisconsin (Library of Congress, n.d.). In 1936 the Hoover Dam was set into operation and became the largest hydropower plant in the world (Donegan et al., 2002). In later years, the Brazilian Itaipu Dam became the largest hydropower plant and, in 2008, the Chinese Three Gorges Dam surpassed it by producing 22 500 MW (Atkins, 2003). Hydropower has become prominent in certain countries, some of which receive 90% of their power from hydropower stations (Atkins, 2003). Globally, 20% of electricity comes from hydraulic sources and the world will continue to look at hydropower as a source of economical, efficient and sustainable electricity.

Hydropower has two major components that determine the efficiency and the output of the power station. The components entail different hydro schemes, with their individual components, and river hydraulics to ensure that clean water will be diverted to the maximum.

To understand the idea behind this study it will be necessary to discuss a few concepts. A full discussion of methods and devices for hydropower stations are provided in the literature review. The first concept to understand is the characteristics of an alluvial river.

Alluvial rivers change continuously in position and shape as a consequence of hydraulic forces acting on the river beds and banks. The changes occur slowly or rapidly, depending on the natural

environmental changes or changes caused by human activities (Simons and Senturk, 1992). Simons (1992) explained that when changes are made in a river channel they are made locally. These changes frequently cause upstream and downstream changes to the bathymetry of the river bed. To reduce these radical changes in alluvial river beds, small changes have to be made by man, which will provide the river with enough natural shape to keep its original flow pattern. Thus, the study at hand will observe changes in the sediment bed and the positioning of hydropower intake structures in rivers.

The other component is the different hydropower schemes that are presented for analysis. Ramos (2000) identified the following hydropower scheme types on the basis of their mode of discharge exploitation:

Run-of-river scheme – Power is generated without inflow regulation. This is a scheme applied commonly to mini- or micro-hydropower plants.

Daily regulation scheme – Power is generated according to the natural fluctuation of the daily demand, the water being stored in a regulating pond or small reservoir at off-peak times and being discharged at peak hours, resulting in an energy output bigger than what it would be without the capability of regulation.

Seasonal regulation scheme – This scheme is commonly applied in larger power plants, which need a reservoir to store water in the rainy season and discharge it in the dry season, enhancing a steady supply of energy all year (it is not a common scheme in small power plants).

Cascade scheme – The cascade scheme is a typical exploitation of the river in order to make the best use of river falls.

As part of this research study, run-of-river hydropower was selected as the hydro scheme and all the problem solving, results and methods used to overcome the sediment intake problems for this specific scheme are discussed in full detail.

1.2 Problem Statement and Objectives

Run-of-river (RoR) schemes present themselves as the new optimum and most environmentally friendly schemes. A large majority of small hydro plants are RoR schemes, meaning simply that the turbine generates power when the water is available and provided by the river. RoR schemes were chosen as the topic of research because the present level of knowledge and experience of RoR systems is not adequate for a thorough understanding of RoR power plants (Bishwakarma and Stole, 2008).

RoR hydropower schemes rely on the natural flow of rivers. When the river dries up and the flow falls below some predetermined amount, the generation ceases. This means, of course, that small

independent schemes may not always be able to supply energy, unless they are so sized and placed that there is always enough water. To ensure that water almost always flows through the scheme involves the placing of small, micro or pico hydro turbines in river bends without any damming of water. The definition of hydropower facility sizes are given in Table 1.1.

Table 1.1: Definition of hydro power facility size (Atkins, 2003)

Unit	Definition	Size (MW)
Small	Small hydro is a term used for the development of hydroelectric power for a small community or industrial plant.	10 MW-30 MW
Micro	Micro hydro is a term used for hydroelectric power distribution to isolated homes or small communities.	100 kW
Pico	Pico hydro is a term used for hydroelectric power generation in small, remote communities that require very small amounts of electricity.	< 5 kW

Brink et al. (2005) describe river bends as being ideal for diversion structures, and says that diversion structures should be placed on the outside of the bend to take advantage of the secondary spiral flow. Secondary spiral flow has a tendency to direct the heavy, sediment-laden bottom layers away from the diversion intake structure (scour) and to allow the top layers with lower sediment concentration to flow towards the intake of the diversion structure. Thus, the placing and orientation of the intake structure is very important.

RoR schemes are very versatile and can be placed in rivers in such a way as to produce sufficient electricity for a single house, a smallholding or a town. A RoR hydropower scheme can be very reliable and, if sufficient flow is available, it can generate continuous power for 365 days a year.

A problem identified in the river scheme is sedimentation and the effects it has on the turbine blades. This problem can be overcome in two ways. The first is by using any existing lakes or reservoir storage upstream, and the second is by investigating the three features associated with river bend diversions, i.e. the optimum diversion *location* to minimise the abstraction of sediment in a river channel, the optimum diversion *angle* to ensure scour upstream of the intake, and the diversion of minimum channel sediment through the intake.

When comparing RoR schemes in South Africa to international hydropower schemes it can be concluded that the international schemes have very high pressure heads, which cause a large amount of damage to the mechanical hardware if this sediment passes through the intake system and flows into the turbine.

According to the head, schemes can be classified into three categories:

- High head: 100 m and above
- Medium head: 30 to 100 m
- Low head: 2 to 30 m

The damage caused by high pressure is more severe than would be the case for South African lower pressure schemes. The reason for this damage is high concentrations of sediment-rich water, which leads to the following problem:

Sediment and coarse sediment are a serious problem in RoR hydropower stations. The erosion causes a loss of US\$ 120 to 150 million per year for these hydropower stations due to a drop in efficiency, forced outages, and repairs (Mann and Arya, 2001).

The literature clarified that turbines are very easily damaged if sediment-laden water is diverted through a diversion intake. Combining cost-effective principles and optimal design with effective efficiency through the diversion of low sediment-laden water would increase performance by maximising the benefits of hydropower operation. This would contribute to cost-effective construction and minimise the environmental impacts caused by newly constructed RoR hydropower plants.

For this reason it was very important to research the current thesis topic, as it would lead to the production of additional electricity where it was needed. The sooner these environmentally friendly RoR schemes can be implemented and used to their full extent, the sooner all people can benefit from them.

The aim of this research was to investigate possible methods to limit sediment diversion at RoR hydropower schemes. This investigation involved the placement first, of the diversion location in relation to curvilinear effects in the river, secondly, the orientation of the diversion structures and thirdly the intake design according to the intake elevation and the DDR.

Introducing this study, with all its results and recommendations, to power generation companies could result in the greater use of RoR systems after exploring all the possibilities of a RoR scheme.

1.2.1 Research question and hypothesis

The proposed research on run-of-river schemes can benefit Eskom and power supply companies in any countries experiencing continuous power shortages.

The following problem areas can be observed:

- The site selection determines the reliability of the power output and the site should therefore be properly studied.

- RoR hydropower relies on the flow of the river. If the water flow reduces, the power output of the hydro turbine placed in the stream will also generate less power. Thus, the availability of water at a specific location determines the flow of the rivers and establishes the power output, as stated above.
- The optimum placing of the hydro turbines is very specific and has to be studied for maximum power output.
- Notes should be taken of the sediment particles breaking the turbine blades and eroding the runners (see Figure 1.1).



Figure 1.1: Eroded runner and guide vanes (Olesen and Pradhan, 2010)

1.3 Research Method

The research method that was used was natural observation and quantitative research. The quantitative method comprised the design, selection and assembly of experimental equipment in the Stellenbosch University Hydraulics Laboratory. Empirical modelling was used for the theoretical calculations, and the scaled models for analysis. The effect of the sediment on specific designs was observed in detail.

The primary objectives of the thesis entailed a full literature study on diversion and sediment extraction methods, a physical model analysis of diversion orientation and sediment diversion capabilities, and the carrying out of a hydrodynamic mathematical model validation. Numerical simulations were done using CCHE 2D, a modelling program used to simulate real-time modelling situations, in order to compare with the results obtained from the laboratory experiments.

The research on optimum sediment exclusion in Run-of-River schemes is a cyclic approach, as shown in Figure 1.2, where the series of activities in the method of approach is specified.

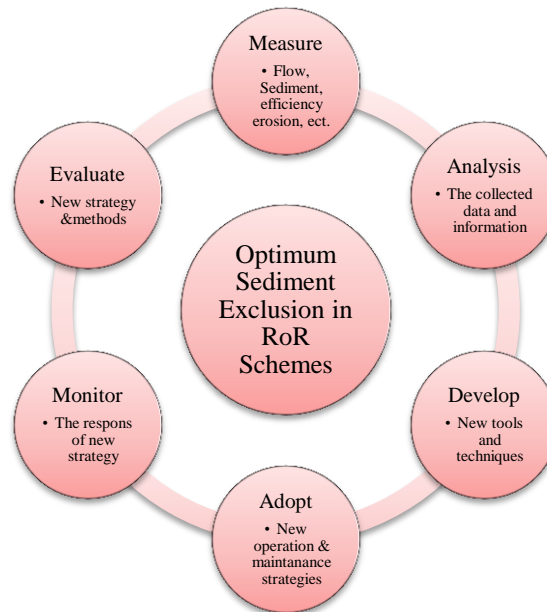


Figure 1.2: Optimum sediment exclusion (OSE) research as a cyclic process (Bishwakama, 2007)

A hydrodynamic mathematical model was used to simulate the sediment transport, sediment build-up and sediment scour effects on different tests. As the data is quantitative and only a simulation, the accuracy and reliability of the data processed is very dependent on the accuracy of the input data.

1.4 Methodology

The aim of the research was to enable power plant designers and operators to optimise power generation in respect of sediment and flow characteristics. The study of optimum sediment exclusion structures to divert sediment was to improve the performance of existing and upcoming RoR hydropower projects.

Following the literature review of this thesis on the hydraulics and sediment dynamics of river bends, laboratory experiments were carried out on a sinusoidal trapezoidal curved channel to determine the location and orientation of the optimum diversion. A radius-to-curvature width ratio was used for the curvature effect. The sediment used in the test procedure was crushed peach pips.

The first experiment in the curved channel was to predict where the optimum scour takes place without a diversion structure in place. This was then followed by placing a diversion structure at the maximum scour position, retrieved from experiment one, and angling the structure with reference to the flow direction. The flow direction vector was placed at a tangent to the bend (See Figure 1.3), and oriented with angles 0° , 30° , 45° and 60° , in the direction of the bend.

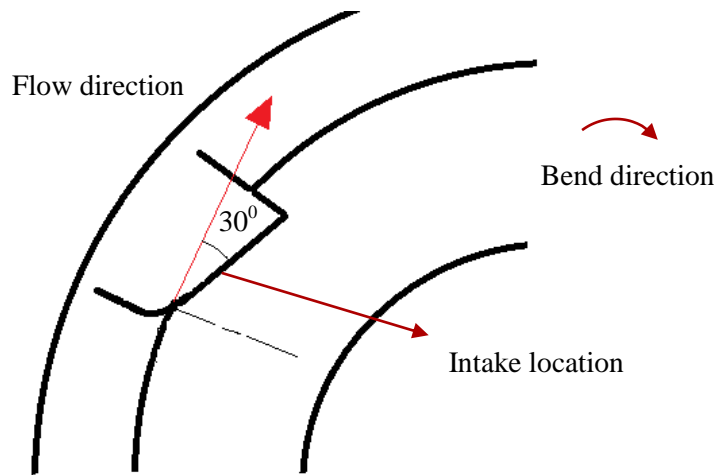


Figure 1.3: Orientation of structure with reference to flow direction

The angles of the structures used in the experiments are explained in Chapter 3. The optimum structure diversion angle relative to the volume of sediment diverted was tested. A total of 23 tests were carried out.

A two-dimensional hydrodynamic computational model was used (CCHE 2D), with a sediment module to simulate the sediment dynamics of the laboratory experiments. The calibration of the numerical model with the laboratory model will provide validation of the correctness of the numerical model results.

The physical models and numerical models were constructed to be analysed. These models were then used to determine the optimal design to reduce the sediment intake through the system. Sediment characteristics, damage that may occur and design layouts of the system were observed to establish possible future designs.

Chapter 2

2. Literature Review

2.1 Literature Study

Run-of-river (RoR) hydropower plants are found all over the world, and challenges occur as a result of the deposition of sediment in most sediment-laden rivers. Research on the design and operation of RoR hydropower plants and sedimentation is becoming more and more pertinent. Methods to monitor and divert the sedimentation in front of the turbine intake have been devised and studied and the outcomes have been recorded. This literature review will briefly discuss the methods and information available on RoR hydropower schemes.

An extensive literature study was carried out on curvilinear flow, scour depth relationships, bed configuration and hydropower design guidelines. Aspects discussed in the literature review are the following:

- Damage analysis of sediment deposition, corrosion and hydro-erosion,
- Sediment characteristics,
- Curvilinear and secondary current flow in meandering rivers,
- Intake structures and sediment control,
- Weirs, trashracks, vortices and sediment traps, and
- Turbine specifications.

2.1.1 Damage Analysis

2.1.1.1 Sediment Deposition

A study of sediment estimation for 30 hydropower reservoirs revealed that 30 to 40 per cent of river sediment is deposited in the reservoir. The remainder of sediment transported will either flow over the spillway or be diverted into the intake of the abstraction works. Over the life of the reservoir, a very high percentage of capacity is replaced with sediment, and thus it is a high priority to minimise the deposition (Central Board of Irrigation & Power and INCOLD, 2008).

This was the case at the Mbashe Dam in the Eastern Cape, where the capacity of the dam was reduced by 85 per cent and the sediment damaged the turbines in the RoR scheme (Murray and Watermeyer, 2011). It was established that the scouring sluices were buried under heavy sediment, which made them non-operational. As sediment deposition is a problem in 40 per cent of large reservoirs, it might be assumed that large reservoirs should be discarded. This is very problematic, as South Africa is a water-scarce country and reservoir water is the main source for drinking, agriculture and hydropower.

According to Kuun (2009), the reservoir solution for hydropower should not be discarded, but ought to be managed. Reservoir storage for hydropower and abstraction methods in rivers with low or no weir must be studied to ensure security of water and electricity.

South African rivers typically transport up to 80 percent of their sediment as wash load (silt and clay), bedload and suspended sediment load (sand and gravel). Sediment transport makes up about 20 percent of the total load in sand bedded alluvial rivers. The fine particles have a near uniform vertical and lateral distribution. Thus, diverting water can lead to sedimentation in the diversion structure which, in the case of high head systems, can be very harmful to turbines.

Normally, the median diameter of the particles (d_{50}) considered acceptable for small turbines is approximately 0.2 mm (Ramos, 2000). Raudkivi (1993) concluded that the particle sizes are dependent on the head of the system, where the head of the system determines the output of the system. According to Raudkivi (1993), a system head of 50 m should allow grain sizes of not more than 100 μm , and exclude clay particles for system heads of 200 m and greater. A grading of sediment size diameters are given in Table 2.1.

Table 2.1: Sediment characteristics

Sediment type	Grading size diameter (mm)
Clay	< 0.002 mm
Silt	0.002 mm - 0.05 mm
Sand	> 0.05 mm

Sediment deposition is a common occurrence in upstream channels, penstocks and chambers connecting the river intake with the turbines. The flushing and sediment control of chambers are challenging processes, but the use of sand traps can provide less daunting scenarios.

2.1.1.2 Corrosion and Rusting

The mechanical hardware that is submerged in water is continuously subjected to the salt contained in the water. South African rivers with total dissolved solids (TDS) that exceed the sediment load of 450 000 $\mu\text{S/m}$ (micro Siemen per metre) are in the Cape Provinces, KwaZulu-Natal and the Vaal River (Department of Environmental Affairs and Tourism, 1999). Naidu (1996) provided a cut-off sediment concentration of 200 mg/l that should preferably not to be exceeded. Turbine blades start corroding when components endure repetitive drying and wetting conditions (Central Board of Irrigation & Power and INCOLD, 2008).

2.1.1.3 Hydro Erosion

Damage occurs to all underwater components that come into contact with sediment. The initial stages of turbine erosion appear as erosion tails. Erosion tails take shape with the impact of the sediment particles on the “weak spots” of the surface. These erosions tails could initiate one of the following (Central Board of Irrigation & Power and INCOLD, 2008):

- i. Soft points in the metallographic structure of underwater parts due to faulty heat treatment.
- ii. Surface roughness.
- iii. Blow holes.
- iv. Points of high stress concentration in the underwater parts.

The concentration of sediment particles in the river determines whether the diversion of water has to be paused. If the concentration of the sediment in the river increases drastically, abrasion and cavitation of the turbine blades are greater. Constant exposure to cavitation and abrasion could result in holes in the turbine blade. Turbine blade erosion varies in appearance, from small patches to deep cavities and cracks. The damage can become so severe that the blade profiles are totally disfigured (Central Board of Irrigation & Power and INCOLD, 2008). Figure 2.1 provides images of turbine erosion. Once the damage starts, the turbulence in the assembly increases and the problem of erosion becomes compounded.

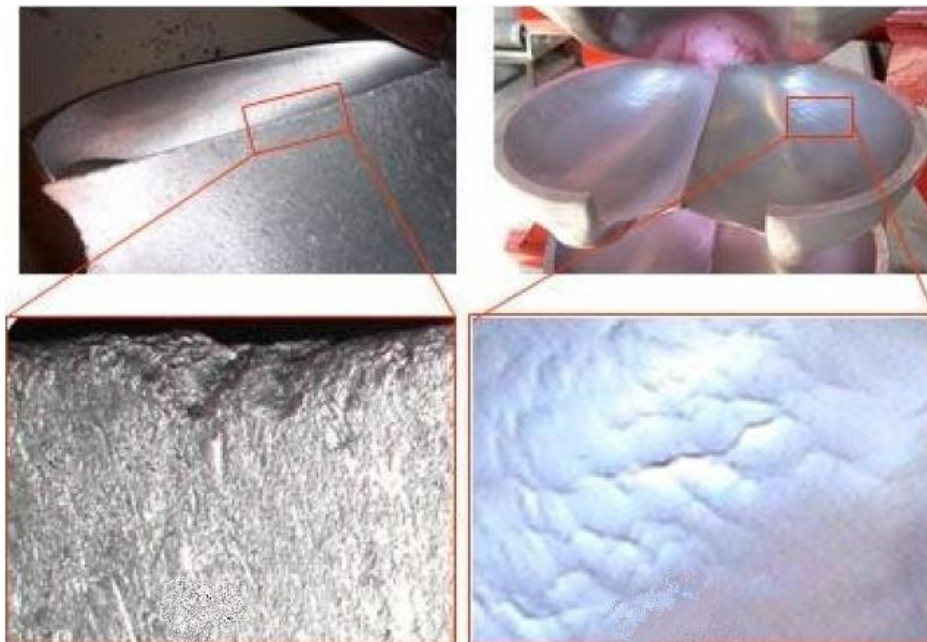


Figure 2.1: Erosion on turbine blades (Central Board of Irrigation & Power and INCOLD, 2008)

Due to the turbulent flow of water on the surface of underwater components, air bubbles are formed. These bubbles are transported on the surface of the underwater parts. A high pressure water stream causes the bursting of these air bubbles, which generates high-intensity shock waves (Central Board of Irrigation & Power and INCOLD, 2008). As these bubbles burst, the metal face of the turbine is damaged and ripples are formed on the blade surface. These ripples may also be caused by sediment impinging the turbine blade. In Figure 2.2, the process of erosion and cavitation caused by the turbulent bubbles is represented.

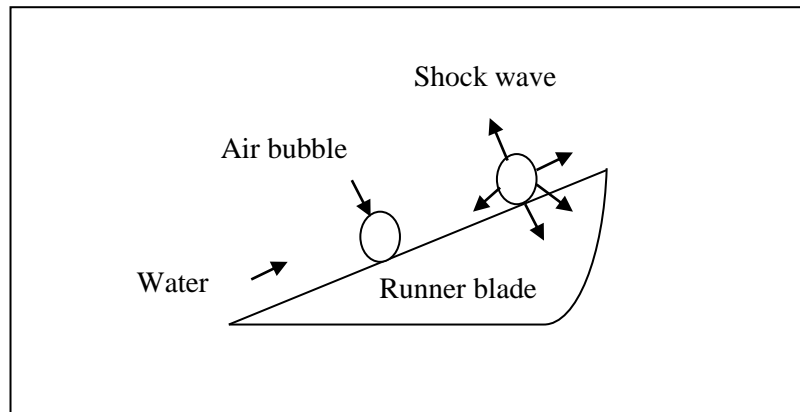


Figure 2.2: Cavitation mechanics of erosion

Sediment particles are transported by water jets through the RoR intake, which causes damage to the surface of the underwater components. Direct streams of water on the turbine causes rippled patterns. These rippled patterns can be reduced when small turbine blade angles are introduced. It was observed that ripples are a function of flow parameters and time of exposure. It was also established that ripple patterns are between 0.2 to 0.3 mm wide and 0.7 to 0.8 mm high, even if solid particles are not present in the flow. It was concluded that the reason could be cavitation, liquid jet impact or turbulent bursting (Karimi and Schmid, 1992).

The angles at which the sediment particles impinge on the target surface affect the erosion. For turbine blades with angles of 30° , erosion occurs through the formation of surface ploughs and lips. The impinging sediment particles and eddies provide tangential forces on the surface of the blades, causing abrasion in the direction of the particle flow. At 90° , plastic shear is very limited and the pure force of the particle on the face of the blade causes cavitation. It can be concluded that, at worst, pebble-sized holes will form in the turbine blade (Central Board of Irrigation & Power and INCOLD, 2008).

Based on experimental observation, Karimi and Schmid (1992) provided a descriptive model of the ripple formation that takes place on the face of a turbine blade. In the final stage (Figure 2.3 d), the flow was highly turbulent and deep ripples were formed.

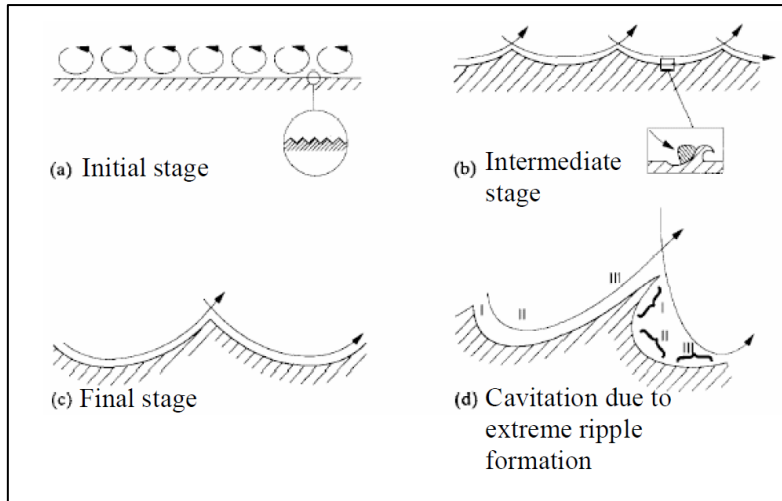


Figure 2.3: Ripple formation due to turbulence (Karimi and Schmid, 1992)

The Central Board of Irrigation & Power and INCOLD (2008) concluded that the high kinetic energy of impinging sediment particles has a tendency to penetrate into the body of the target material. This causes damage to the sub-surface regions and forms cavitation on the turbine blade. Figure 2.4 shows a schematic view of the damaged layers and the erosion caused by the sediment particles (Central Board of Irrigation & Power and INCOLD, 2008).

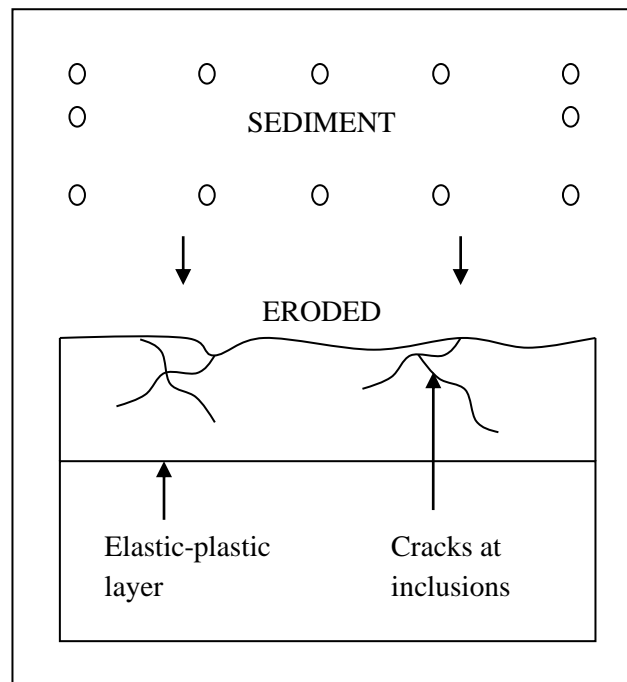


Figure 2.4: Damage of subsurface regions (Central Board of Irrigation & Power and INCOLD, 2008)

Plastic deformation and cavitation plays a decisive role in the failure of the component. It is thus important that the turbine blade should be made from a material possessing high strength.

2.1.2 Sediment Characteristics

2.1.2.1 Geological Studies

The most common problems that occur with RoR schemes in high mountainous areas are weathered surface zones. These surface zones are affected by different geomorphologic features, such as soil creep, solidification and rotational soil slides (Penche, 2004).

Sediment characteristics determine the sediment movement externally and internally in the RoR. RoR schemes are very dependent on orientation and location, which determine the sediment intake through the system. Geological testing can be done to determine the characteristics of the surroundings by using geomorphologic techniques. Penche (2004) defines the techniques in his book, *Guide on how to develop a small hydropower plant*. The techniques are as follows:

Photogeology: Photogrammetry - at scales from 1:10 000 to 1:5 000. This method allows the geologist to identify rock types, determine geological structures, and detect slope instability.

Laboratory analysis: Traditional laboratory tests such as soil grading and classification. The results should be included in the geomorphic map.

Geophysical studies: A geophysical investigation will contribute to better knowledge of the superficial formation thickness, the location of the landslide sections, the internal water circulation, and the volumetric importance of potentially unstable formations.

Structural geological analysis: The stability of the rock and seepage in the foundations of hydraulic structures are problems that can be solved by this method.

Direct investigations: This is when dams or weirs are placed on unconsolidated soil and require a drilling programme. Some of these recommended tests are:

- Permeability tests in boreholes, such as the Lugeon or low pressure test, to define the water circulation in the foundation.
- Laboratory tests to determine the compressive strength of the samples to define their characteristics.

2.1.2.3 Sediment Movement

Sediment movement and erosion in rivers have various relationships that define the critical condition. However, Rooseboom et al. (1983) recommended the use of stream power in alluvial rivers as an enhanced representation of the transportability of sedimentation.

According to Rooseboom et al. (1983), SANRAL's 5th Edition of the Drainage Manual describes the method to analyse sediment movement. The modified Lui diagram was the method used to express

the boundary between sediment movement and no sediment movement. The sediment movement can be explained in terms of the ‘shear Reynolds number’ against the ratio between shear velocity and settling velocity. The modified Lui diagram is given in Figure 2.5 below.

For turbulent flow, the ratio between shear velocity and settling velocity is constant (Equation 2-2), whereas for laminar flow the critical conditions between sediment movement and no sediment movement are given in Equation 2-3 below:

$$V_* = \sqrt{gDS} \quad \text{Equation 2-1}$$

$$\frac{V_{*c}}{V_{ss}} = 0.12 \quad \text{Turbulent flow} \quad \text{Equation 2-2}$$

$$\frac{V_{*c}}{V_{ss}} = \frac{0.16}{\frac{v_* d_{50}}{\nu}} \quad \text{Laminar flow} \quad \text{Equation 2-3}$$

where

V_{*c} = Critical shear velocity (m/s)

V_{ss} = Particle settling velocity (m/s)

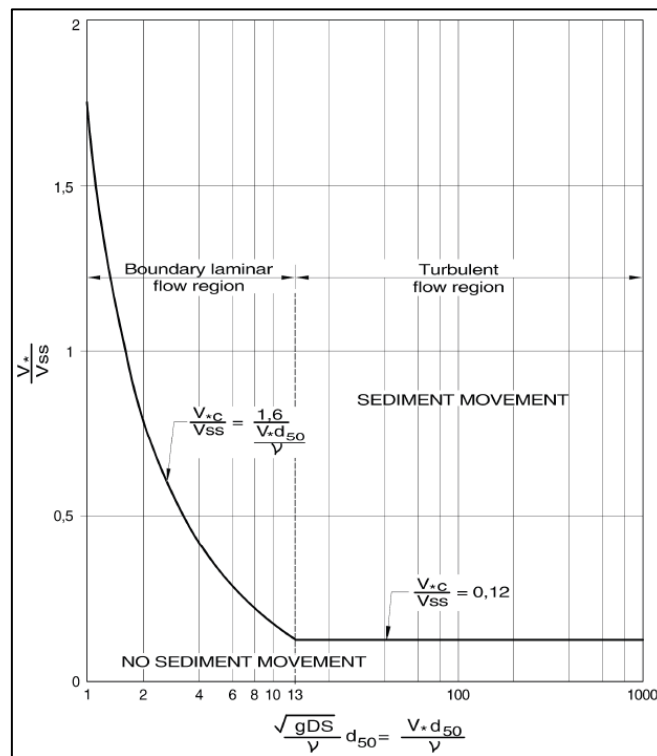


Figure 2.5: Modified Lui diagram (Rooseboom et al., 1983)

The relationship between settling velocity and particle diameter is given in Figure 2.6.

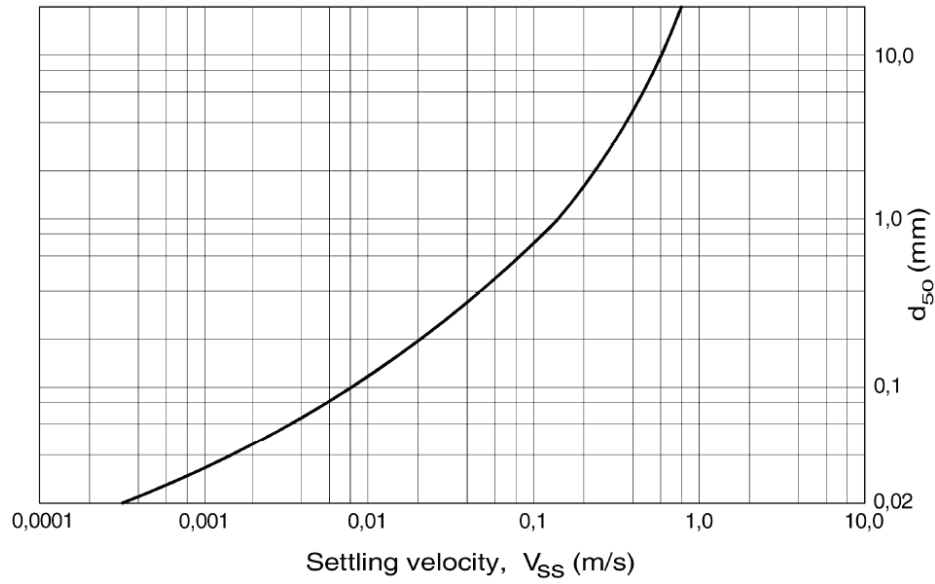


Figure 2.6: Settling velocity as a function of sediment size (Rooseboom et al., 1983)

Rooseboom et al.'s (1983) methods for determining sediment movement in alluvial rivers and sediment basins improve the knowledge of the procedures needed to exclude sediment.

2.1.3 Design of a RoR hydropower station to limit sediment diversion

2.1.3.1 Open Channel River Mechanics

Generally, an open channel has a free water surface that is subjected to atmospheric pressure. This is universally referred to as the zero pressure boundary layer and considered as constant along the full length of the channel (Penche, 2004).

All channels have a three-dimensional distribution of velocity. Penche (2004) researched this specific topic and simulated velocity profiles with two-dimensional hydrodynamic river flow depth averages. Figure 2.7 illustrates the velocity layers in channels of different profiles in a straight river flow (Penche, 2004).

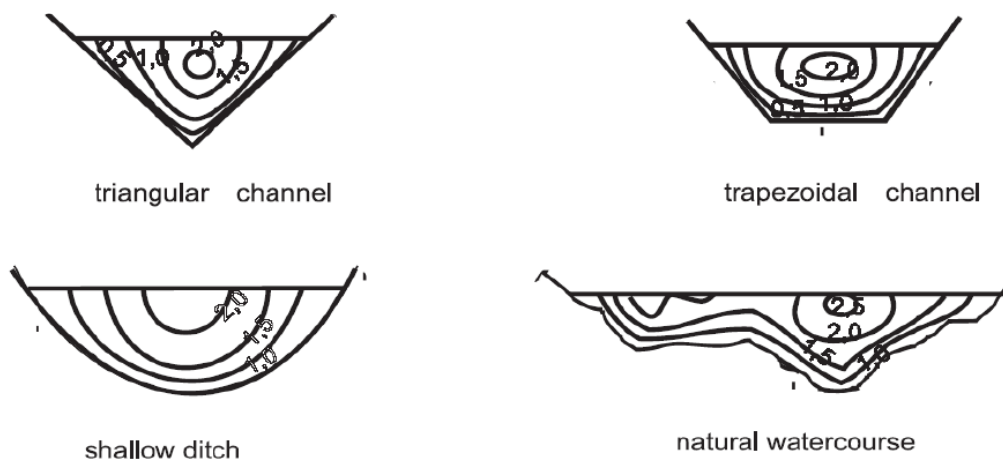


Figure 2.7: Typical velocity distributions for open channel flow (Penche, 2004)

When the velocity profile is known, Bouvard (1992) explains that a spiral motion with an anti-clockwise direction is created for a bend to the right. An illustration of the specific movement in the channel is given in Figure 2.8. The bedload deposition occurs mainly on the inside of the bend as the velocity reduces, thus the conclusion was that the diversion intake should be placed on the outside of the bend.

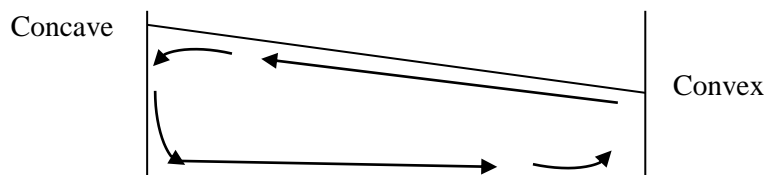


Figure 2.8: Curvilinear flows in a channel bend (Bouvard, 1992) and (Thompson, 1876)

The main purpose behind placing the diversion structure on the outside bend is to ensure that as little sediment as possible is abstracted from the main channel. This is achieved with the aid of the secondary flow that develops in bends and creates this spiral motion. The spiral motion moves the sediment-laden bottom flow towards the inside of the river bend, whereas the upper flow with less suspended sediment moves towards the outside of the bend. An illustration of river deposition in bends is provided in Figures 2.9 and 2.10.

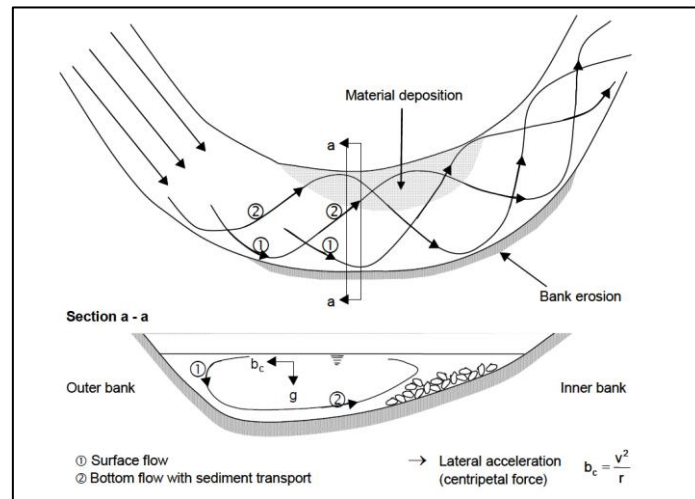


Figure 2.9: Secondary currents in river bends (Penche, 2004)

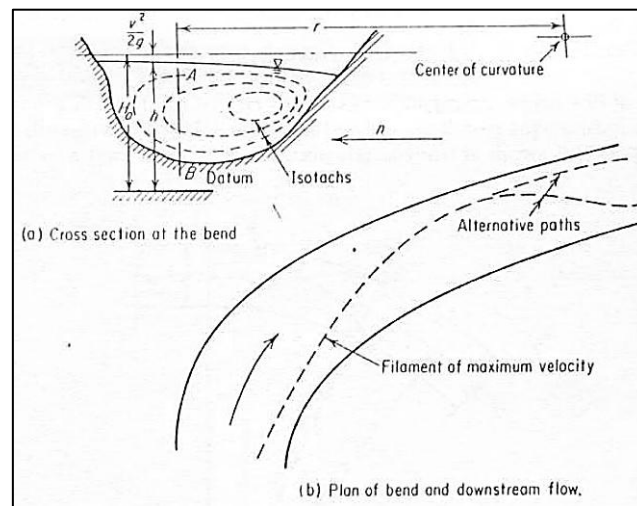


Figure 2.10: Flow behaviour in a channel bend (Henderson, 1967)

In all designs, the local geology of the proposed diversion structure is a very important parameter to take into account. Special attention should be given to the river topography with reference to curvilinear flow characteristics, as intake bypassing does occur (Basson, 2005).

River channels change locations and flow patterns according to the eroded topography. Thus the favourite locations to place intake structure for diversion are in stable bends, cliff faces and gorges (Raudkivi, 1993).

Brink et al. (2005) did a study on bend diversions to minimise sediment at an intake. According to Brink et al. (2005) the position of the maximum scour moves downstream as the bend angle increases.

Shen (1971) described the formation of bends as usually being part of a meander or deformed meander system. Bends are formed as a natural result of sinuous flow tendencies in channels. The tendency for bends to develop in alluvial channels that flatten over time was demonstrated by Lane (1955), cited in Shen (1971). The shape of the bend varies from symmetrical patterns to deformed bends, which are more frequently encountered in nature (Shen, 1971).

South African rivers tend to be symmetrically shaped rivers with sinusoidal factors of between 1.1 and 1.9. To ensure that the river fitted into the laboratory, a 90° bend with a sinuosity of 1.11 was designed. Tan (1996) recommended a length-to-radius ratio (L_{tot}/r_c) between 1.0 and 1.4. The intake of the power station should be placed on a stable reach, where the intake is just below the vertex of a concave bank (Tan, 1996). Literature on the position of the intake and maximum scour can be found in the following sources: Avery (1989), Basson (2005), Vanoni (1977), Yen and Lee (1995) and Raudkivi (1993). According to Brink et al. (2005) and Basson (2005), the relationship between the central angle of a bend and the optimal location is based on experimental data (SC and CHES, 1992), which is given in Table 2.2.

Experimentation with numerous empirical rules has taken place in the past to establish the best location for the intake structure. The results gave the best position as being on the outside of a bend in the river (Basson, 2005). The research provides results on the accuracy of the predicted scour position on a 90 degree bend, which was tested with a physical and numerical simulation.

Past experiments by the Sediment Committee (SC and CHES, 1992) established that the relationship between the central angle of a bend and the optimal location is as follows:

Table 2.2: Relationship between central angle of a bend and optimal location of intake (SC and CHES, 1992)

Central angle of bend (°)	< 45	60	90	120	150	180
Optimal location of intake (°)	0 (end)	45	60	80	95	110

The Basson (2005) guidelines for river abstraction state that, according to SC and CHES (1992), the optimal location of an intake can be provided by the following empirical equation:

$$L = \xi B \sqrt{\frac{4R_c}{B} + 1}$$

Equation 2-4

where L = distance
 $\xi = 0.8$ (coefficient)
 r_c = average radius of curvature
 B = river width

According to the method of Raudkivi (1993), the deepest scour hole would form twice the river width downstream from the upstream river intersection (see Figure 2.11). Brink et al. (2005) proved that the optimum diversion location was at a distance 8.8 times the width of the river. An experiment was done on two different canals and it was established that, in a 0.3 m curved canal, sediment-related tests corresponded with the Raudkivi (1993) method. The second canal was 0.6 m wide and provided results that did not conform to the Raudkivi (1993) method.

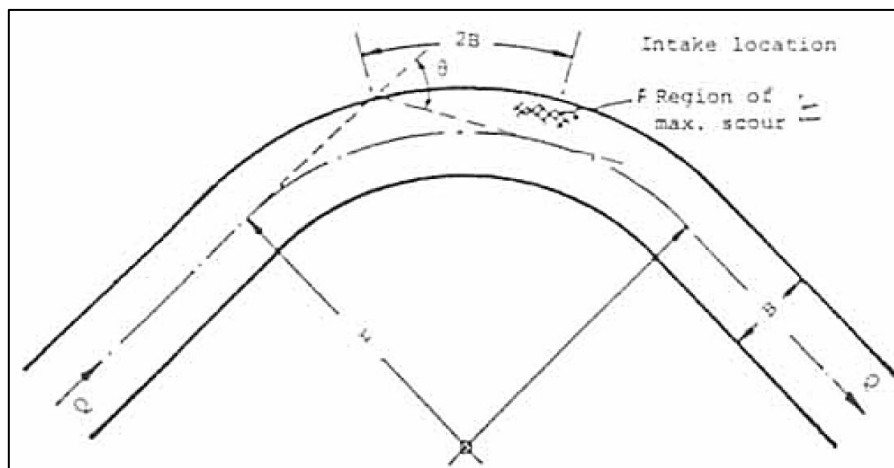


Figure 2.11: Maximum scour in a river bend (Raudkivi, 1993)

To establish if these experiments were trustworthy, another experiment was done in a 70 m wide river. This river was analysed with a numerical model. The verdict remained the same, namely that the deepest scour holes for a sinusoidal canal formed where Raudkivi (1993) predicted, although it was once again contradicted when the channel width was reduced to 20 m. The 20 m canal scour holes were noticed further downstream. The experiments established that the wider the channel, the further downstream the scour will occur (Brink et al., 2005).

Figure 2.12 provides a mathematical model simulation of two river bends and the location of the deep scour holes that form during a flood.

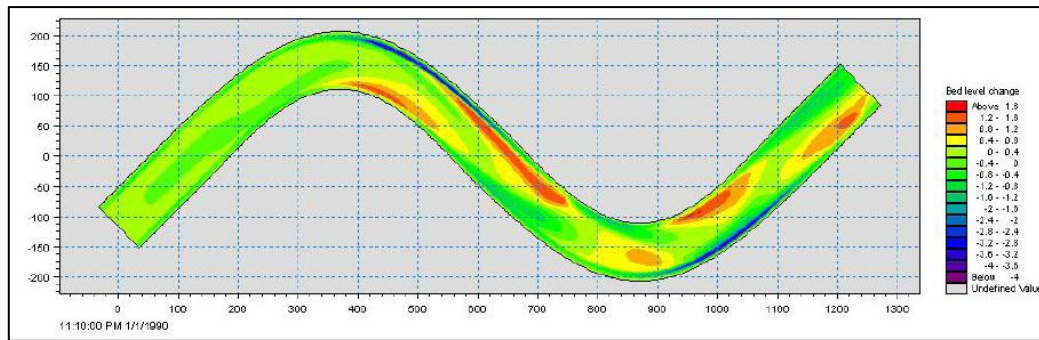


Figure 2.12: Simulated scour and deposition (Brink et al., 2005)

The deepest scour occurred downstream of the vertex of the curve, roughly two breadths after the upstream intersection point. The sand banks that were formed on the bed of the river were due to the large volume of sediment that was scoured at the bends. The deposition and scour indicate that the first bend did not influence the scour observed in the second bend. Figure 2.13 illustrates the helical flow intensity in the channel, which provides proof that there are almost no secondary flows in the centre part between the two curves.

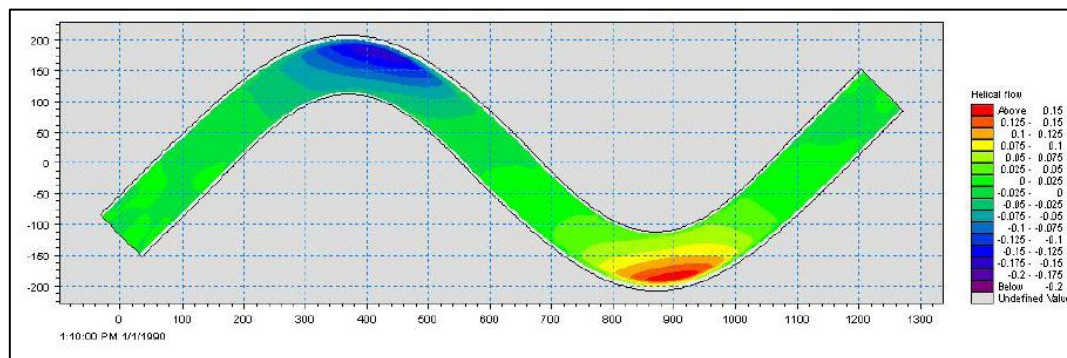


Figure 2.13: Simulated helical flow intensity (Brink et al., 2005)

The next section will entail a discussion of the literature that includes the orientation angle of the intake. Avery (1989) recommended that the angle of the intake should be between 10° and 45° . The angle is measured from the intake centre line to the main direction of river flow. The ideal angle for a particular intake depends on the diverted discharge ratio (DDR), the width of the river and the intake forebay. Avery (1989) also states that diversion angles of less than 45° are favoured, but should be tested in a physical model for better results (Avery, 1989).

Bulle (1926) recommended that there are no optimum diversion angles, since the angle varies with the diversion ratio and the location of the intake; this contradicts Avery's findings. It was discovered that the optimum diversion angle would increase when the diversion discharge ratio (DDR) decreased. Brink et al. (2005) does not agree with this statement, proclaiming that the DDR would increase with the increase in the diversion angle.

2.1.3.1.1 Diverted Discharge Ratio (DDR)

The diverted discharge ratio (DDR) was calculated by the following equation:

$$DDR = \frac{Q_{Diverted}}{Q_{River}} \tag{Equation 2-5}$$

Brink et al. (2005) concluded that the DDR increases as the diversion angle increases, but that it would decrease with an increase in the Froude number. Tan (1996) recommends a DDR from 45% to 50% for Chinese rivers, while Avery (1989) recommends a DDR of 66% to 77% for rivers in England.

2.1.3.1.2 Diverted Sediment Ratio (SDR)

Habermaas (1935) did a series of experiments to measure diverted sediment ratios (SDR) with a constant DDR of 50%. The results were summarised by Mosoyi (1965) and are given in Figure 2.14 below.

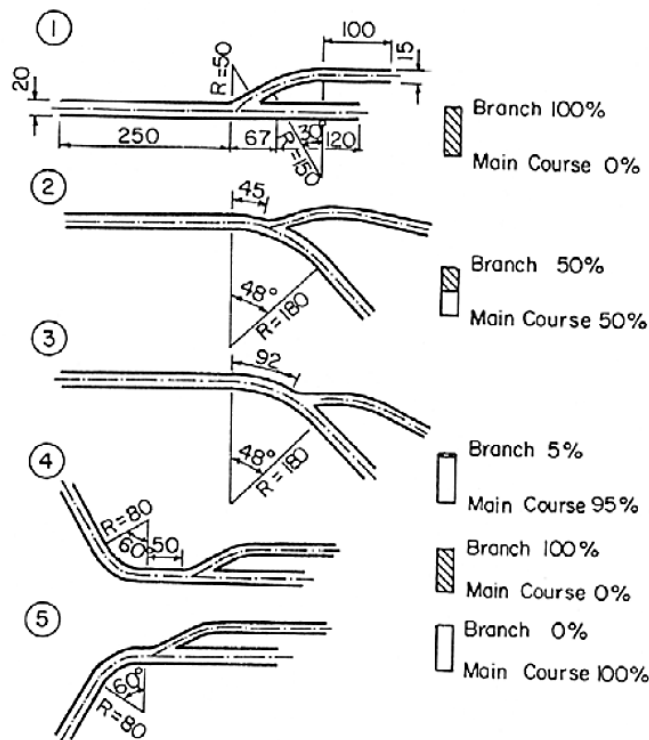


Figure 2.14: Model experiment of diversion structures (Mosoyi, 1965)

The current research aimed mainly to calculate the diverted sediment ratio (SDR), using the following equation:

$$SDR = \frac{Q_{SDiv}}{Q_{SRiv}} \tag{Equation 2-6}$$

where

Q_{SDiv} = diverted sediment load (g/s.m²)

Q_{SRiv} = incoming sediment load from river (g/s.m²)

Using this, the sediment load that was diverted were calculated, after the sediment had been weighed. The sediment was weighed when damp and when dry. The sediment was dried at a temperature of 105⁰C for 24 hours. There were three different formulas, which are given below.

2.1.3.1.3 Diversion Bed Load

$$Q_s \left[\frac{kg}{s.m} \right] = \frac{y[kg]}{L_D[m]} / T[s] \quad \text{Equation 2-7}$$

where

Q_s = sediment load diverted [kg/s.m]

y = dry sediment mass [kg]

L_D = length of diversion structure [m]

T = time of run [seconds]

2.1.3.1.4 Diversion Structure Concentration

$$C_{\text{Sediment}} \left[\frac{kg}{m^3} \right] = C \left[\frac{g}{l} \right] = \frac{y[kg]}{Q[m^3/s]} \times T[s] \quad \text{Equation 2-8}$$

where

C_{Sediment} = concentration of sediment diverted [kg/m³]

y = dry sediment mass [kg]

Q = flow through structure [m³/s]

T = time of run [seconds]

2.1.3.1.5 Diversion Load for Different Intake Areas

$$Q_s \left[\frac{kg}{s.m^2} \right] = \frac{y[g]}{T[s]} / A[m^2] \quad \text{Equation 2-9}$$

where

Q_s = sediment load diverted [kg/sm²]

y = dry sediment mass [g]

A = area of intake structure [m²]

T = time of run [seconds]

The method for calculating the diverted sediment load and the incoming sediment load, used in the SDR ratio, was as follows:

- Q_{SDiv} as diverted sediment load ($g/s.m^2$)

By using Equation 2-5 and the diversion's opening dimensions, the sediment load through the intake could be calculated. The area of the opening was $515 \text{ mm} \times H_2$.

- Q_{SRiv} as incoming sediment load from river ($g/s.m^2$)

By using Equation 2-5 and the channel dimensions, the sediment load in the channel could be calculated. The area of the channel normally is depth dependent.

To summarise the diversion locations:

The radius-to-width (radius of curvature (r_c)/water surface width of canal (w)) ratio is the most commonly used ratio to predict where scour would take place in a river. The ratios to determine where the diversion should be placed are:

- Avery (1989) claims it must be between 3.0 and 5.0,
- Lui et al. (1982) claims it must be between 4.0 and 8.0,
- Shen (1971) claims it must be between 2.5 and 8.0,
- Rzhnitsyn (1960) claims it must be between 10.0 and 14.0.

The Sediment Committee and the Chinese Hydraulic Engineering Society (1992) provided a relationship between the central angle of a bend and the optimal location. This is given in Table 2.2.

To summarise the diversion angles:

The intake angle of orientation should be placed at specific angles to produce sufficient flow through the intake with the least amount of sediment. The orientation also ensures that as little flow as possible is redirected, for the main reason that damming and flow patterns from the diversion structure will ensure different downstream outcomes.

Bulle (1926) stated that the optimum diversion angle decreases as the diversion ratio increases. The diversion angle of the abstraction works that is recommended to be used is as follows (the angle is measured from the centre line of the intake to the main direction of river flow):

- Avery (1989) claims the angle must be between 10° and 45° ,
- Lui et al. (1982) claims the angle must be between 35° and 40° ,
- Hufferd and Watkins (1972) claims the angle must be between 30° and 45° .

2.1.3.2 Site Configuration

The objective of a hydropower scheme is to convert potential energy into electric energy at the lower end of the scheme (Penche and De Minas, 1998). Figure 2.15 illustrates a high head hydropower scheme. The power output of this type of scheme is proportional to the water that flows through the system and to the head (Penche and De Minas, 1998).

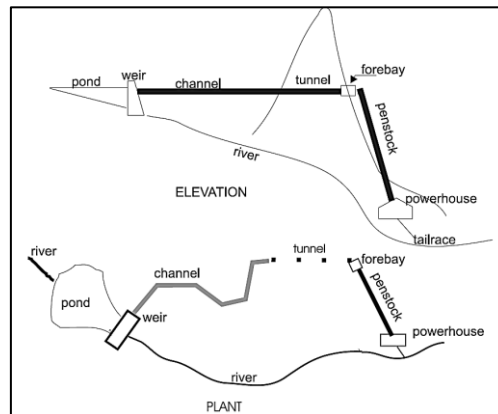


Figure 2.15: High head scheme (Penche and De Minas, 1998)

The research was based mainly on the operation of a RoR scheme without a dam-like structure. The alternative was a small weir with little damming or no weir at all.

The reason for the alternative study was for medium and high head schemes. These schemes use weirs to divert water into the intake. From the intake, which is covered by a trashrack to keep debris out, the water is diverted and conveyed to the turbines via a pressure pipe or penstock. Medium to high head schemes function mainly with penstocks and, as penstocks are a very expensive component, this can be discarded as an option. The alternative to high head penstocks is illustrated in Figure 2.16. Figure 2.16 illustrates that water can be diverted into a short penstock. If the topography and morphology of the terrain does not permit the easy layout of a canal, a low-pressure pipe would be a more economical option (Penche and De Minas, 1998).

At the outlet downstream of the turbines, the water is discharged back into the river. To ensure that rivers keep their natural shape, low head schemes are typically built in river valleys. Two technological options can be selected. Either the water is diverted to a power intake with a short penstock, as shown in Figure 2.16, or the water could be diverted as in high head schemes (Penche and De Minas, 1998).

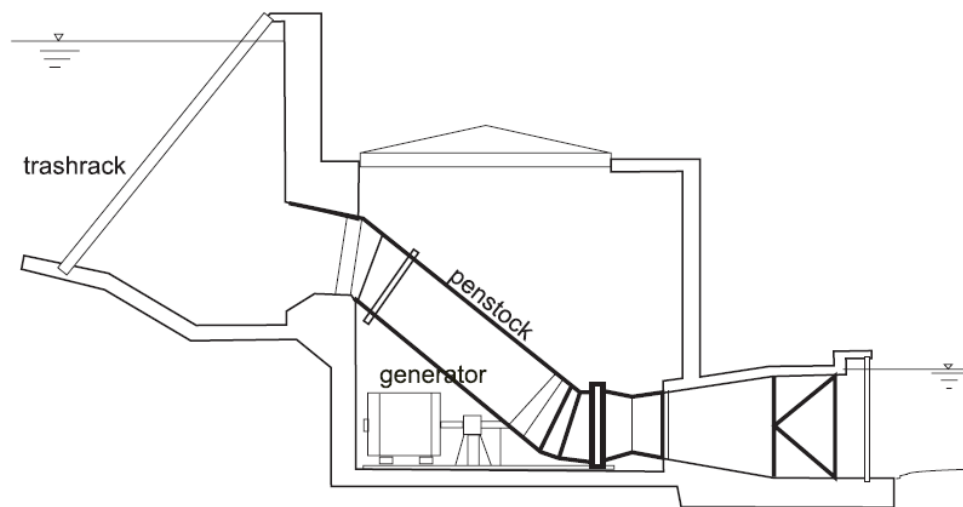


Figure 2.16: Short penstock for low heads (Penche and De Minas, 1998)

2.1.3.3 Intake Structures

2.1.3.3.1 Intake types

The following criteria were clarified by Penche (2004) to distinguish what type of intake is needed for different river abstractions:

- *Power intake*: The intake supplies water directly to the turbine via a penstock. These intakes are often encountered in lakes and reservoirs and transfer the water as pressurised flow.
- *Conveyance intake*: The intake supplies water to other waterways that usually end in a power intake. These are most frequently encountered along rivers and waterways and generally transfer the water as free surface flow.

The suspended load and the type of sediment in the river clarify what type of intake would be more suited for each specific river. Conveyance intakes are frequently found along rivers, as suspended sediment is a common problem in hydropower intakes. All intakes are classified into three different types, namely lateral, frontal and drop intakes. The main characteristics of these three intake types are summarised in Table 2.3.

Table 2.3: Intake characteristics (Penche, 2004)

		River Slope	River Width B	Plan View of River	Sediment Transport
Lateral Intake	In outer river bend	$0.001\% < J < 10\%$	All widths	Curved path is optimal	Strong bedload, small suspended transport
	With gravel deposition canal	$0.01\% < J < 10\%$	$B < 50\text{ m}$	Possible rectilinear path if counter-measures	Strong bedload with continuous flushing, strong suspended load
Frontal Intake	With gravel deposition tunnel	$0.01\% < J < 10\%$	$B < 50\text{ m}$, ($B < 500\text{ m}$ for economical dams/weirs)	Rectilinear is optimal, curved path is possible if counter-measures	Strong bedload with continuous flushing, very strong suspended load
Drop Intake		$J > 10\%$ favourably, possible already at 2.5%	$B < 50\text{ m}$, ($B < 500\text{ m}$ is possible for dams/weirs over part of river width)	Rectilinear	Strong bedload (only large grain sizes)

An intake without any weir will be beneficial to the sediment balance and an economical outcome. Basson (2005) stated that diversion structures without damming structures, which protrude into the flow, could create deep pools upstream of the intake. The following lateral intakes (Avery, 1989) function when rivers bends and gravel deposition channels are used.

2.1.3.3.1.a Bank Intakes

Bank intakes are used with and without weirs. These intakes are generally implemented in rivers where fluctuations in water levels are not extreme. Avery (1989) advises that the maximum abstraction should be 350 Ml/day. A gravel trap with efficient discarding of bed load can be placed upstream of a coarse trashrack.

2.1.3.3.1.b Side Intakes with Cross Weir

Side intakes with the intention of diverting a great proportion of the flow require a cross weir to ensure that water is not lost through the intake at low-level stages. Figure 2.17 illustrates a side intake that allows for screen cleaning when debris becomes stuck. This intake can store 10 m^3 of sediment, which is shovelled manually. The sediment size abstracted is in the range of coarse sand to gravel, plus a few cobblestones (Avery, 1989).

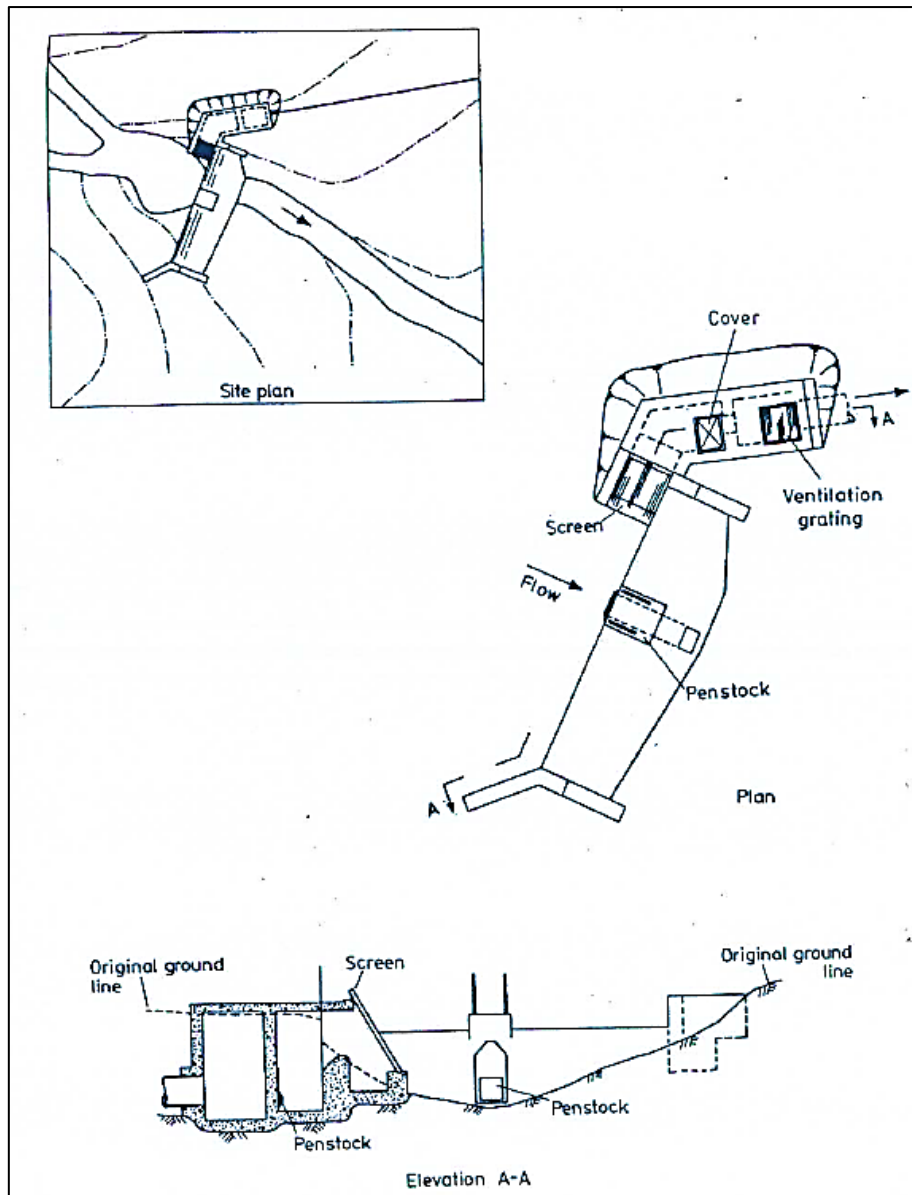


Figure 2.17 : Side intake with cross weir (Avery, 1989)

2.1.3.3.1.c Low Head River or Canal Diversion Works

In the following case, the barrage and associated canal head works are designed to divert water from main watercourses. This leads to the control of sediment entering the diversion canal system. Figure 2.18 illustrates a typical canal diversion for low head rivers.

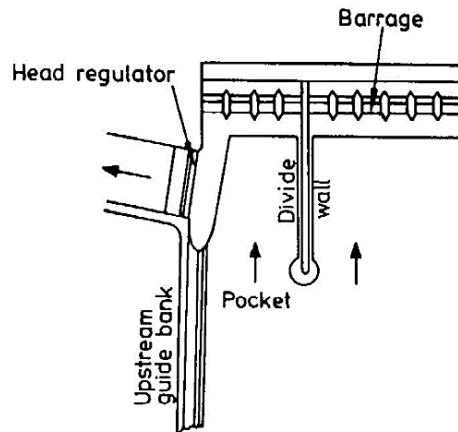


Figure 2.18: Canal diversion works (Avery, 1989)

2.1.3.3.1.d Submerged Intakes

A simple submerged intake comprises a bell mouth set in a block of concrete with a connecting draw-off pipe (Linsley and Franzini, 1979). A similar structure to the submerged intake is known as a shaft spillway (see Figure 2.19; (Penche, 2004)) or submerged shaft intake (Avery, 1989). The submerged intake inlet is protected with a horizontal trashrack. Both the submerged shaft and the simple submerged intake are located nearly at bed level and are used at all water levels. These intakes divert $36 \text{ m}^3/\text{s}$, depending on the river flow.

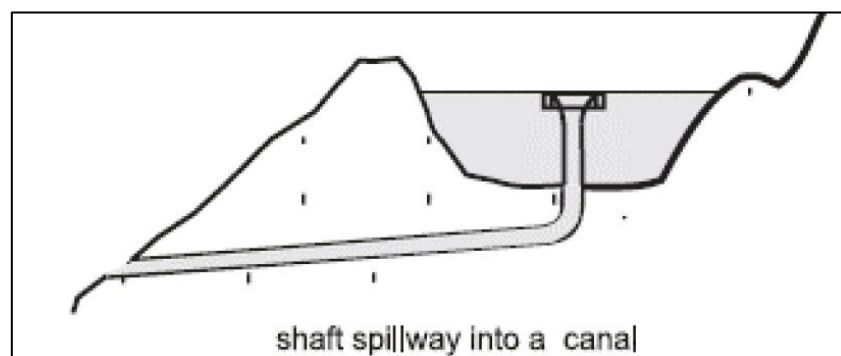


Figure 2.19: Schematic view of a morning glory spillway (Penche, 2004)

2.1.3.3.1.e Tower Intakes

Tower intakes are present in reservoirs with large water levels. Avery (1989) introduced the dry intake tower, but also explained that this process can be a wet intake as well. The dry intake tower has a bottom outlet that is designed to scour out any sediment collected upstream of the intake (Avery, 1989). Figure 2.20 illustrates a wet tower intake, where the bottom intake allows water to flush the bed sediment and provides clean water to the system.

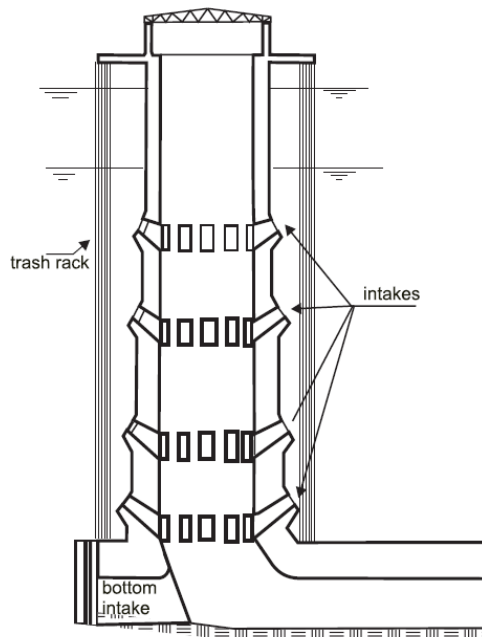


Figure 2.20: Vertical strata scheme (Penche and De Minas, 1998)

The following intake types are frontal intakes. Frontal intake systems are equipped with gravel deposition tunnels known as a sandtraps. These deposition tunnels are flushed continuously. This is where the lateral intake is more improved than the frontal intake. The lateral intake manages larger quantities of sediment, whereas the continuous flushing of deposition channels leads to large losses of energy. Frontal intakes are commonly found in rivers with large beds and suspended load movement, for example in India and Pakistan (Penche, 2004).

The final intake type is the drop intake, also known as bottom intake. Drop intake systems are generally used in steeply sloped rivers. The “French” drop intake in Figure 2.21 is fundamentally a canal built in the streambed, stretching across the width of the river. The drop intake is covered with a trashrack at a slope greater than the stream bed (Penche, 2004).

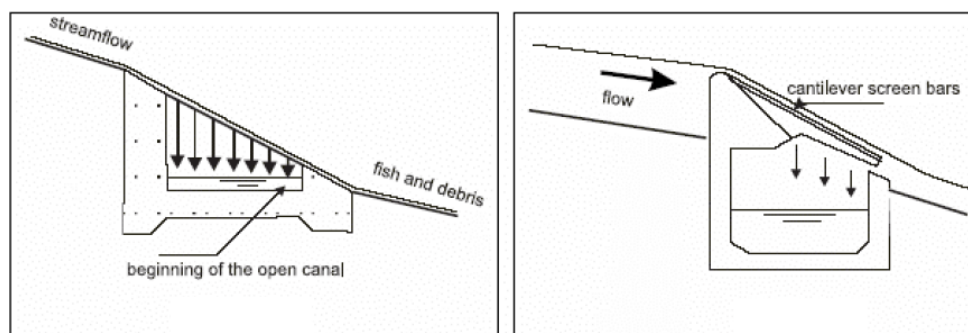


Figure 2.21: Bottom intake across river (Penche, 2004)

Another type of drop intake is the Coanda-type intake. The Coanda intake is known to separate fish and debris from clean water. The intake consists of a weir with a downward sloping, profiled surface

of stainless steel with a flow collection channel below the mesh. The trashrack bars are held horizontal. The trashrack removes 90% of the solids, including sediment smaller than 0.5 mm. As this size sediment can be diverted, a sediment basin and sediment ejection system should be omitted (Penche, 2004).

Figure 2.22 shows a “Tyrolean” intake designed for hydropower schemes in the French Alps (Ract-Madouse et al., 1955).

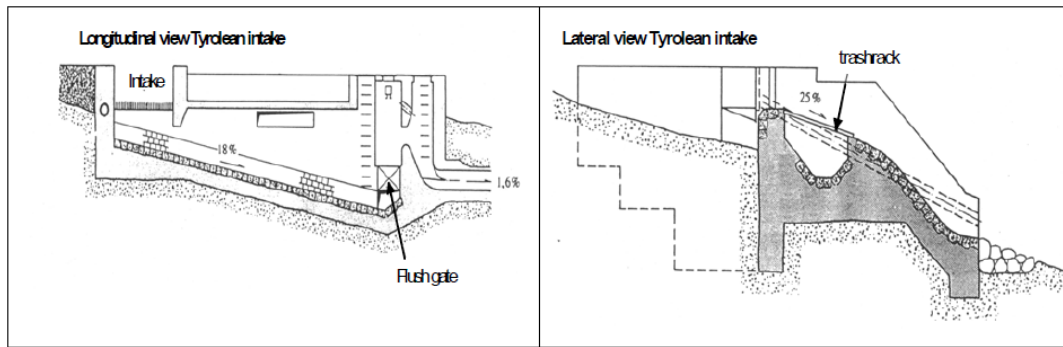


Figure 2.22: “Tyrolean” intake (Penche, 2004)

A few other intake schemes are illustrated in Figures 2.22 to 2.24. These figures demonstrate the curved sluicing flumes (Tan, 1996), the Pressy water intake (Bouvard, 1992) and the bottom outlet (Penche and De Minas, 1998) schemes.

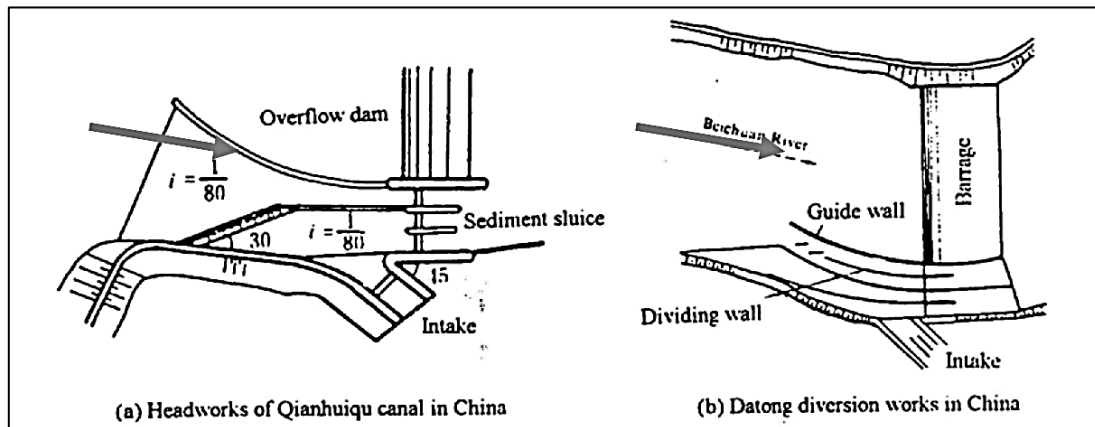


Figure 2.23 : Curved sluicing flumes (Tan, 1996)

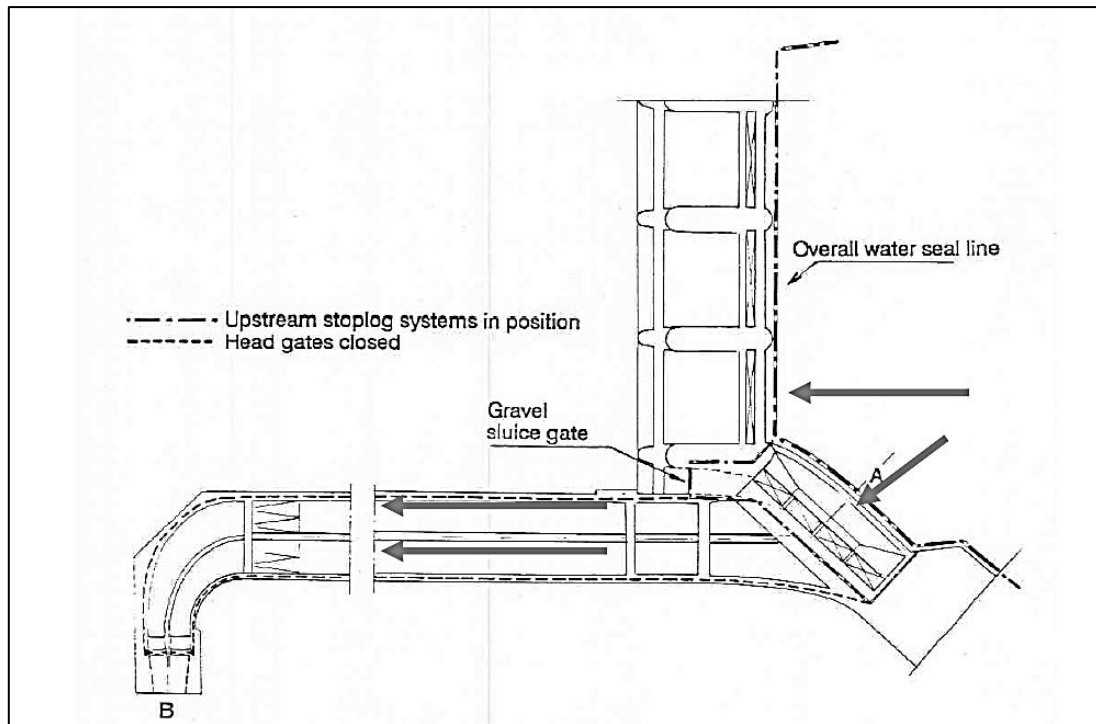


Figure 2.24: Pressy water intake (Bouvard, 1992) (Note: can also be designed as a frontal intake)

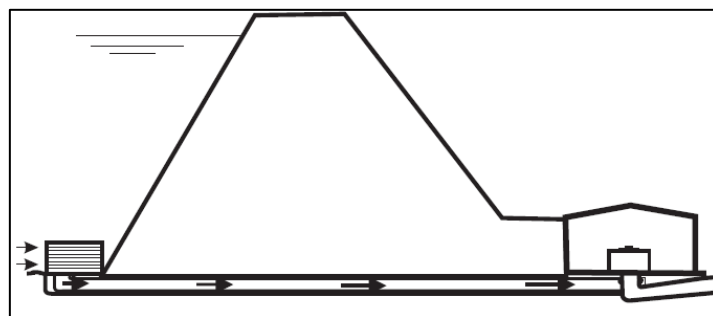


Figure 2.25: Bottom outlet scheme (Penche and De Minas, 1998)

The different types of intakes discussed by Raudkivi (1993) are similar to the lateral, frontal and drop intakes mentioned. Figure 2.26 illustrates the three different design types.

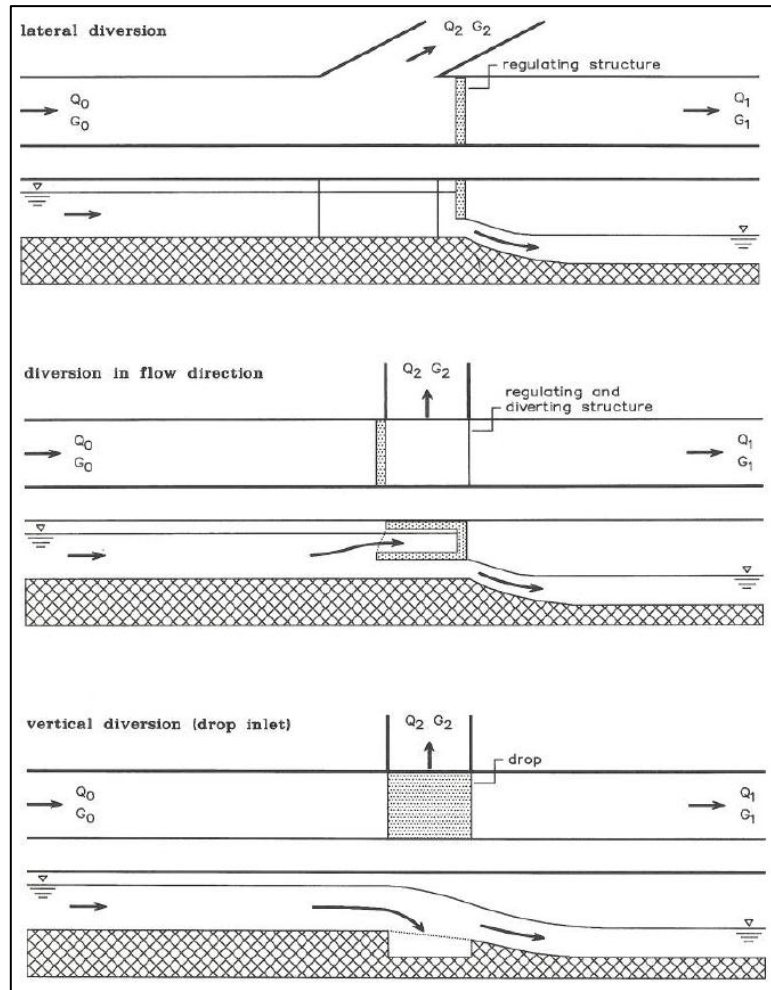


Figure 2.26: Types of intakes (Raudkivi, 1993)

2.1.3.3.2 Sediment control and management at intakes

Open channels deposit sediment on the inside of channel bends and forms scour holes on the outside bend. According to Penche and De Minas (1998), the best location for a hydropower intake is in a relatively straight section of a river.

Penche and De Minas (1998) stated that reducing sediment intake is easier when the intake entrance is placed on a non-erodible riverbed. This is a costlier option, but a very effective method. Figure 2.27 illustrates an intake raised above the riverbed to reduce the sediment intake (Penche and De Minas, 1998).

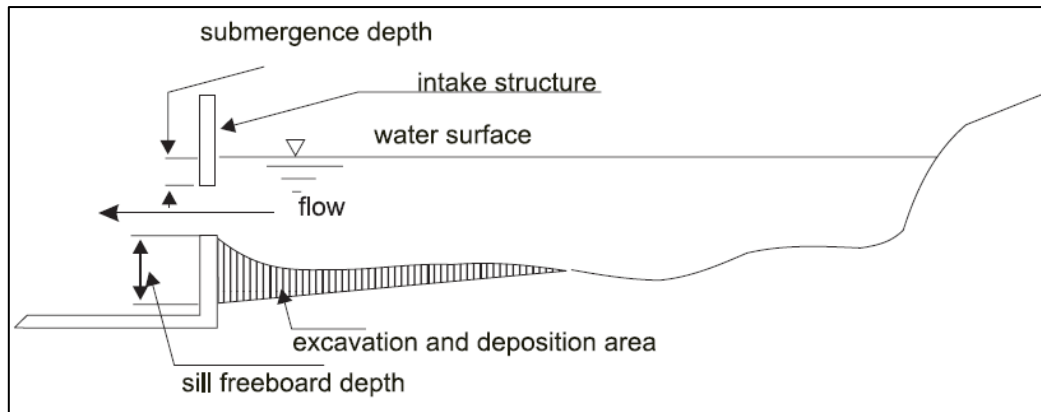


Figure 2.27: Intake raised above the river bottom (Penche and De Minas, 1998)

In some cases a significant quantity of sediment is projected to enter hydropower intakes. In these cases, the large particles are removed by means of a sediment-excluding structure. The sediment trap can be located directly downstream of the intake, where flow velocity is reduced. In some cases the sediment trap or gravel trap is placed upstream of the intake. This has a greater efficiency record. The sediment trap downstream of the intake must be designed to remove all particles larger than 0.2 mm and a considerable portion of the sediment between 0.1 and 0.2 mm (Penche and De Minas, 1998). An example of a sediment trap with an appropriate purging system is illustrated in Figure 2.28.

Recently, new sediment sluicing systems that minimise the sluicing time and the amount of water wasted have appeared in the market. SSSS (Serpent Sediment Sluicing System) is one of these systems (ESHA, 2011).

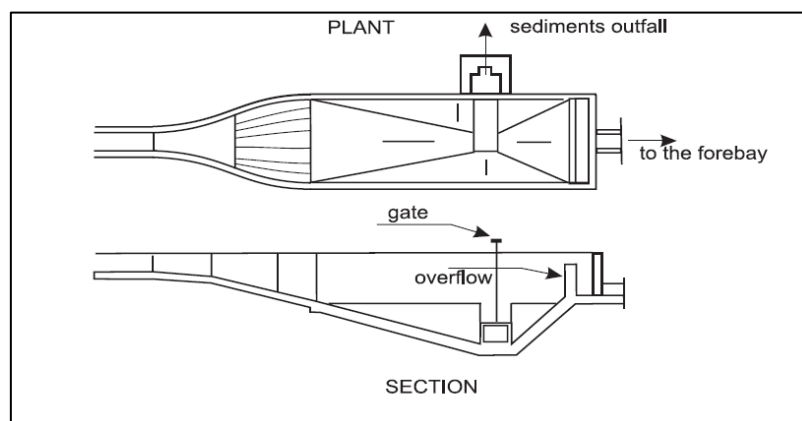


Figure 2.28: Sediment trap (Penche and De Minas, 1998)

2.1.3.3.3 Weirs

Although this study did not include a weir in the laboratory experiments and numerical models, they are still used commonly to obtain the minimum operating levels. If a weir is part of the design, the

following procedure can be applied. The reason a weir was not considered is because weirs tend to accelerate sediment deposition upstream of the intake.

Figure 2.29 illustrates a RoR scheme with a low weir.

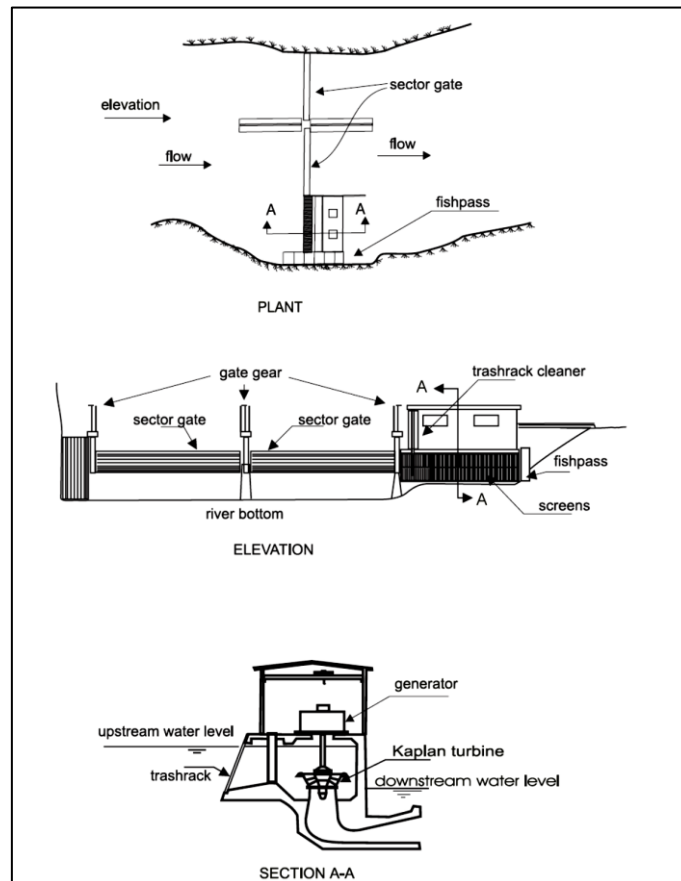


Figure 2.29: Layout of run-of-river power station scheme (Penche and De Minas, 1998)

The Vishnugad Pipalkoti Hydro-Electric Project (VPHEP) is a case study of a RoR project planned for the Alaknanda River in the western Himalayas. The Alaknanda River carries a high sediment load, consisting primarily of quartz, which has a high potential for eroding hydro-mechanical parts. One of the big challenges in developing hydropower potential in the Himalayas is the management of sediment that deposits upstream of the dam. Most rivers arising in the high Himalayas have excessive sediment in the rainy season, resulting in mass deposition upstream of the weir, which reduces energy. This sediment, if not removed from the dam, will cause heavy erosion of the turbine blades and other steel structures in the waterways of RoR hydropower projects (Olesen and Pradhan, 2010).

Another case study was the reduction of dam capacity in the Mbashe Dam in the Eastern Cape. The volume of the dam decreased from 8.8 million m³ to 1.3 million m³. This occurred within three years of the construction date and resulted in the RoR project being discontinued. Problems identified in this RoR were the deposition of sediment upstream of the intake structure, which placed tremendous

strain on the turbines. Another problem was the stability of the weir structure, which had been compromised due to sediment depositing on it. Different approaches to the problem were designed and the conclusions on the final reservoir capacity was that if these designs were not put into work, the volume would reduce to 0.2 million m³.

2.1.3.3.3 a Weir Sedimentation

Weirs in general create a reservoir upstream, which over time fills with sediment and reduces the volume of the reservoir. In most cases the weirs fill up with sediment within the first year to an equilibrium level, which is close to the crest of the weir. The following consequences were identified by Basson (2005):

- The intakes could be covered with sediment and the sediment diversion ratio could increase drastically.
- Flood levels upstream will rise, which could impact on the expropriation of land and the cost of the abstraction works.

Even if the sedimentation rate is slow, the long-term equilibrium conditions must be used to design a sustainable solution. Diversion structures affect the long-term morphology of the river. Thus, to discard weirs, Paish (2002) described a small-scale hydro-scheme as RoR, without any dam or water storage.

A diversion without a weir leads to degradation of the river downstream of the structure. According to Raudkivi (1993), abstraction works without weirs have the main purpose and aim to divert water with as little sediment as possible. Thus, the flow that does not enter the diversion structure will lead to heavy sediment-concentrated water downstream of the hydropower intake. An increase in sediment concentration results in sediment being deposited downstream, which creates a backwater effect. This process continues until the downstream river slope is so steep that the reduced river flow is again capable of transporting the sediment. If the river was eroding before the river diversion was constructed, the reduced flow can be beneficial to the downstream reach of the river.

2.1.3.4 Trashrack

2.1.3.4.1 Trashrack Design and Losses

A trashrack is required at the entrance to hydropower intakes. The reason for the trashrack is to avoid floating debris and large stones from entering the hydropower scheme (Penche and De Minas, 1998). The water flowing through the trashrack experiences head loss and this should be accounted for, as it has an effect on the power output of the RoR system.

Trashracks are made up of panels or metal bars that are evenly spaced. There are two methods available to ensure that trashracks are clear of large debris. The first method is the manual removal of debris and the second is automatic trashrack cleaning equipment (Penche and De Minas, 1998). Figure 2.30 illustrates an automatic type of trashrack cleaning.

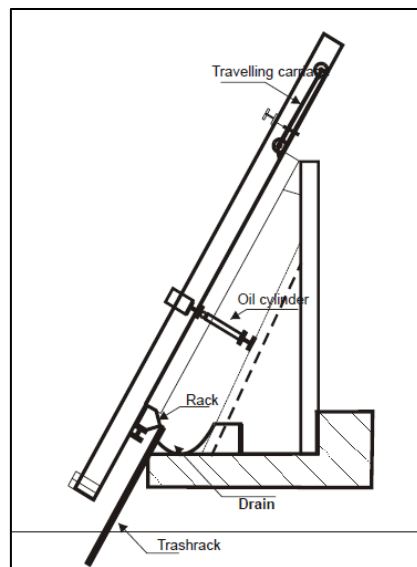


Figure 2.30: Oleo hydraulic cylinders (Penche and De Minas, 1998)

Trashracks are fabricated from stainless steel or plastic bars. The bar spacing of the trashrack varies from 12 mm for small propeller Pelton turbines, to a maximum of 150 mm for large propeller turbines. Trashracks must have a net area (the total area less the bars' frontal area) that reduces the water velocity to 0.75 m/s on small intakes, or 1.5 m/s on larger intakes (Penche, 2004). Basson (2005) stated that 0.3 to 0.5 m/s is the preferred velocity for river abstraction. The reasons for small velocities are to avoid attracting floating debris to the trashrack and to allow fish the opportunity to swim upstream.

Clogged trashracks can also be cleaned manually at depths of up to four metres. On unattended plants, mechanical remote-control rakes are preferred. The mechanical rake was designed to start operation on the basis of a set time or a specific water level. If the trashrack is very long, the rake is placed on a

carriage that can move along the intake (Penche, 2004). Using telescopic hydraulic cylinders, the rake can reach down to a depth of 10 metres.

Another method to intercept heavy debris before it reaches the trashracks is the use of floating booms. An illustration of floating booms is given in Figure 2.31.



Figure 2.31: Prefabricated booms (Penche, 2004)

Figure 2.32 illustrates a complex floating boom layout. The layout does not have to be followed, but it does ensure better prevention of debris entering.

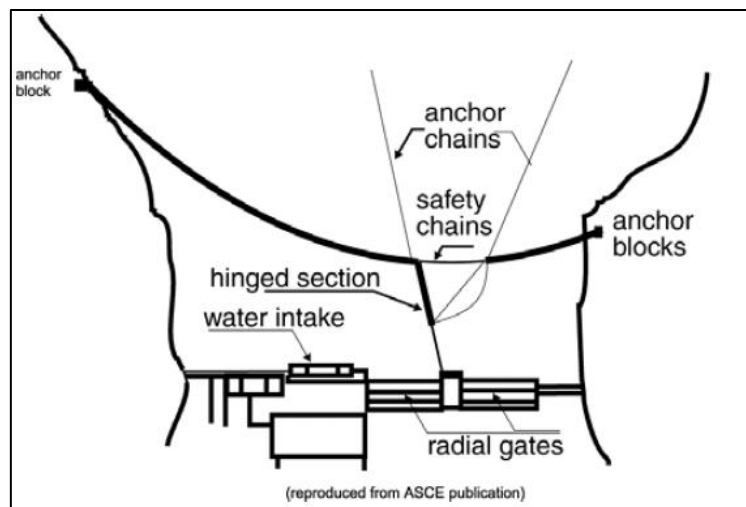


Figure 2.32: Trash boom layout (Penche, 2004)

Even with the booms placed upstream of the intake, the trashrack design should still have an approaching velocity (V_0) of between 0.60 m/s and 1.50 m/s. According to Penche and De Minas (1998), the spacing between the bars is generally specified by the turbine manufacturers. Typical values for Pelton turbines are between 20 and 30 mm, with a spacing of between 40 and 50 mm for Francis turbines and 80 and 100 mm for Kaplan turbines (Penche, 2004).

The spacing between trashrack bars determines head loss. For small hydro plants, *head loss* can be of huge importance to the project outcome and should be minimised as much as possible.

Sources indicate that the velocity profiles of the river influence the trashrack efficiency. This proposes that the velocity profile of the river affects the channel flow, which results in the reduction of head losses.

The research department of Energy, Mines and Resources of Canada (Tung, 1993) commissioned a study of entrance loss coefficients for low-head intake structures. The research (Tung, 1993) was to establish guidelines for selecting the optimum intake geometry. The experiment indicated that the smoother the intake geometry, the greater the economic benefits. Research by Penche and De Minas (1998) indicated that the shorter and more compact the intake, the more costly it will be.

The analysis suggests that the best design is a compact intake with a sloping roof that includes the trashrack and converging walls (see Figure 2.33). The length of the intake is unlikely to be the deciding factor of the overall loss coefficient. Thus, according to the suggested design, a formula was derived that comprises a K coefficient. The K coefficient for this design is 0.19. With the K coefficient known, the head loss in metres for a French drop-type intake is calculated using Equation 2-10:

$$\Delta H = 0.19 \frac{V^2}{2g} \qquad \text{Equation 2-10}$$

where

V = the velocity in the penstock (m/s)

Something to bear in mind with head loss is the spacing between the trashrack bars, the bar size, the bar shape and the orientation of the intake. The effect of debris on the trashrack reduces diverted discharge, which results in the increase of head.

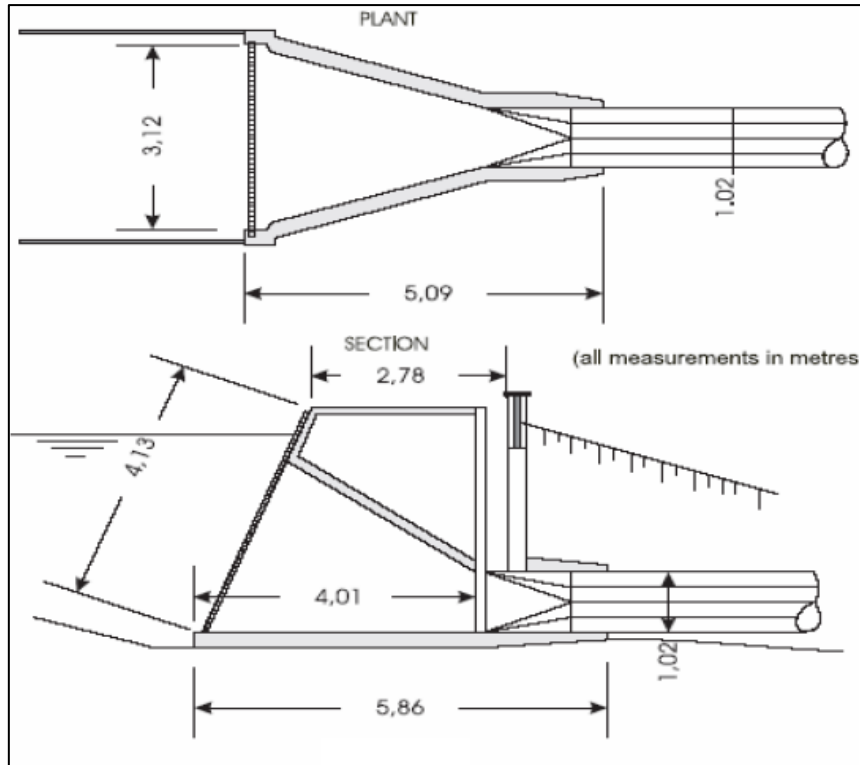


Figure 2.33: French drop intake (Penche, 2004)

The Kirschmer formula is another formula used to determine head loss at trashracks:

$$h_t = Kt \left(\frac{t}{b}\right)^{\frac{4}{3}} \left(\frac{V_0^2}{2g}\right) \sin \Phi \quad \text{Equation 2-11}$$

- where:
- H = head loss (m)
 - t = bar thickness (mm)
 - b = width between bars (mm)
 - V = approach velocity (m/s)
 - g = gravity constant
 - Φ = angle of inclination

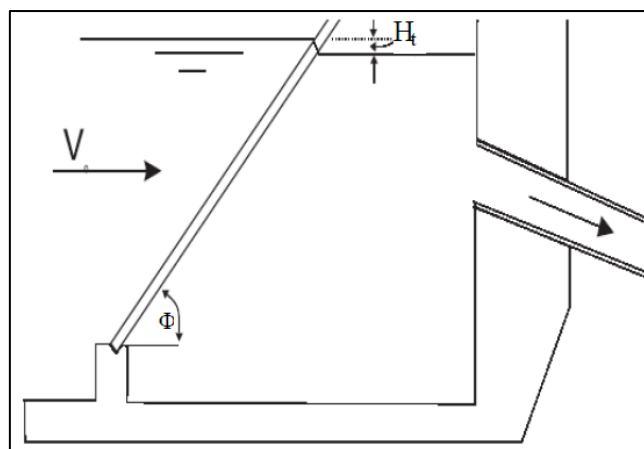


Figure 2.34: Loss coefficient (Penche, 2004)

For structural reasons, the Kirschmer formula is only valid if the length (L) of the trashrack bars is less than five times their diameter (Penche, 2004). If the trashrack is not perpendicular, but placed at an angle Φ with the water flow, there will be an additional head loss. Figure 2.35 provides a table and bar sizes to ensure minimum head loss.

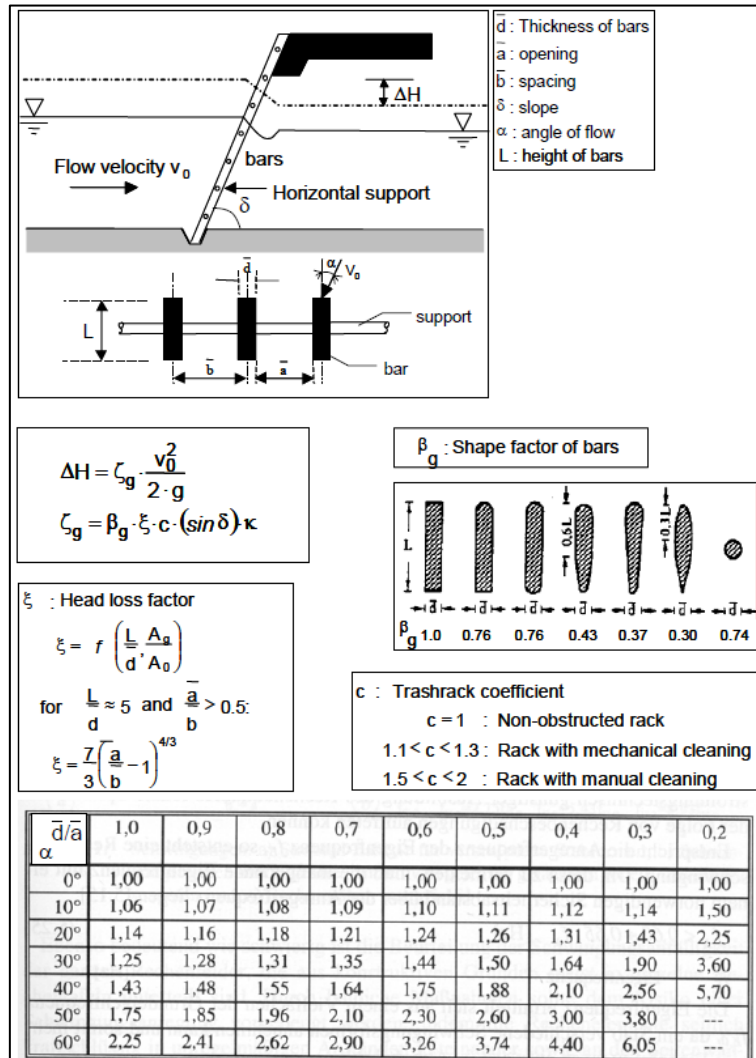


Figure 2.35: Formula for computing head losses (Penche, 2004)

2.1.3.4.2 Turbine Protection

Trashracks provide protection for different turbines against the inflow of solid material. The trashrack is located at the intake of the hydropower station and can be fixed or movable. The trashrack is defined by the space between its bars, a, the length in flow direction, b, the thickness, c, and the total cross section, S.

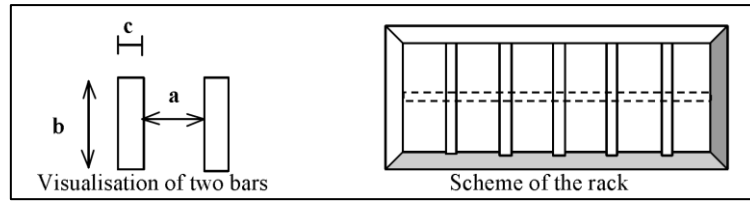


Figure 2.36: Trashrack design according to Ramos (2000)

According to Lencastre and Holmes (1987), the space between the bars, *a*, is a function of the turbine type (see Table 2.4). This provides the information needed to establish the size and dimensions of the trashrack.

Table 2.4: Spacing between bars for different turbine types (Lencastre and Holmes, 1987)

Turbine type	Kaplan	Fast Francis	Slow Francis	Pelton	Small Pumps
a (m)	0.10-0.15	0.08-0.10	0.06-0.09	0.03-0.05	0.02

For a submerged trashrack, the approach velocity of the maximum flow is about 0.80 to 1.00 m/s. This velocity is based on the kinematic law:

$$V = \frac{Q}{A} \tag{Equation 2-12}$$

where *Q* is the turbine discharge value (m³/s), and *A* is the cross section of the trashrack (m²). The flow through the trashrack can induce severe vibrations due to detached swirls, with a frequency, *f_s*. The swirl vibration should be different from the frequency of the bars, *f_b*. In order to avoid oscillation and the collapse of the trashrack, the frequency *f_b* must be a factor greater than the swirl frequency (Ramos, 2000). According to the stability, the following condition should apply:

$$f_b \geq 1.5 f_s \tag{Equation 2-13}$$

The swirl frequency, *f_s* (in Hz):

$$f_s = \frac{S_t V}{c} \tag{Equation 2-14}$$

S_t is the Strouhal number, given in Table 2.5. This Strouhal number depends on the transversal cross section of the bar. The cross section of the bar must be multiplied by the safety factor *F*, according to Table 2.6.

Table 2.5: Strouhal number for different types of bars (Lencastre and Holmes, 1987)

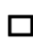





Type of bar	b=c	b=2.8 c	Diameter=c	b=2.8 c	b=2.8 c	b=5 c
						
<i>S_t</i>	0.130	0.155	0.200	0.255	0.265	0.275

Table 2.6: Safety coefficient for Strouhal number (Lencastre and Holmes, 1987)

$\frac{(a+c)}{c}$	1.50	2.00	2.50	3.00	4.00	5.00
F	2.15	1.70	1.40	1.20	1.05	1.01

The calculation of the structural frequency of the bar with fixed boundaries is based on the following equation:

$$f_b = 3.6 \frac{c}{3.46(L_b)} \sqrt{\frac{gE_b}{\gamma_b + \frac{a}{c}\gamma}} \quad \text{Equation 2-15}$$

L_b is the distance between the bar supports (m), g is the gravity acceleration (9.8 m/s^2), E_b is the elasticity modulus (N/m^2), γ_b is the specific weight in N/m^3 of the bar material, where the steel bars' elasticity modulus E_b is equal to $2.1 \times 10^{11} \text{ N/m}^2$ and γ_b is equal to $78\,000 \text{ N/m}^3$ and, lastly, γ is the specific weight of the water, which is $9\,800 \text{ N/m}^3$. In order to guarantee that the trashrack structure remains stable, the dimension H_2 must be reduced until Equation 2.13 is verified (Ramos, 2000). The vibration and frequency of trashrack bars affect the head loss and should be considered during the design.

To summarise trashracks and their relevance for this research:

Turbine choice and trashrack design go hand in hand when designing a hydropower system. A Kaplan turbine was chosen as the optimum turbine. The reason for this choice was that it can endure a head space of between two and twenty metres, with flows from $3 \text{ m}^3/\text{s}$ to $50 \text{ m}^3/\text{s}$.

Trashracks provide diverse protection for different turbines against the inflow of solid material. The trashrack is located at the intake of the hydropower station and can be fixed or movable. Flow through the trashracks should not exceed a velocity of 0.3 to 0.5 m/s, as high velocity could attract floating debris.

Automatic or manual cleaning can be set in place to clean trashracks if needed. Trashracks have to be designed while taking into account head loss, vibration, vortices and sediment.

2.1.3.5 Vortices

Intakes and trashracks should not only minimise head losses but also prevent *vortices*. Vortices can appear in low-head power intakes and should be avoided because they interfere with the performance of turbines. Vortices effectively:

- Produce non-uniform flow conditions.
- Introduce air into the flow, with unfavourable results on the turbines: vibration, cavitation, unbalanced loads, etc.
- Increase head losses and decrease efficiency.

- Draw trash into the intake.

Different types of vortices can occur at the water intake. The following classification of vortices should be borne in mind in any design (see Figure 2.37): Type 1 – developed vortex with a deep nucleus and with drap air; Type 2 - superficial depression, without drag bulb air but with a well-defined nucleus; Type 3 – depression quite neglected, with unstable nucleus; Type 4 – rotational movement without free-surface depression, but with superficial circulation (Ramos, 2000).

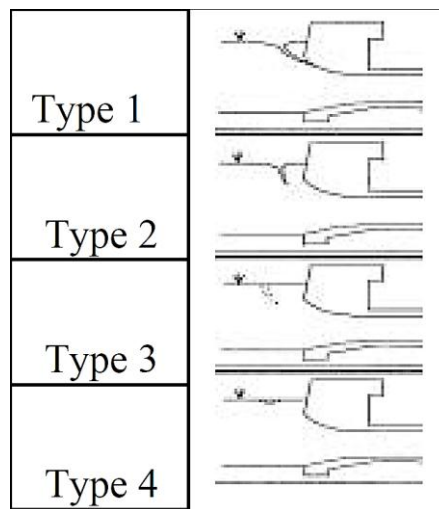


Figure 2.37: Schemes of different types of vortices
(Ramos, 2000)

A procedure to consider when avoiding vortex formation is the approximation of the intake diversion flow. These types of vortices occur at partially open sluice gates.

According to Penche (2004) there is no specific formula to determine the formation of vortices. According to the ASCE Committee on Intakes (1995), disturbances at intakes initiate vortices. These disturbances include:

- Asymmetrical approach conditions.
- Inadequate submergence.
- Flow separation and eddy formation.
- Approach velocities greater than 0.65 m/s.
- Abrupt changes in flow direction.

Empirical formulas with to avoid vortex formation are provided below. These formulas express the minimum degree of submergence (h_i) of the intake. The minimum degree of submergence is illustrated in Figures 2.37 and 2.38.

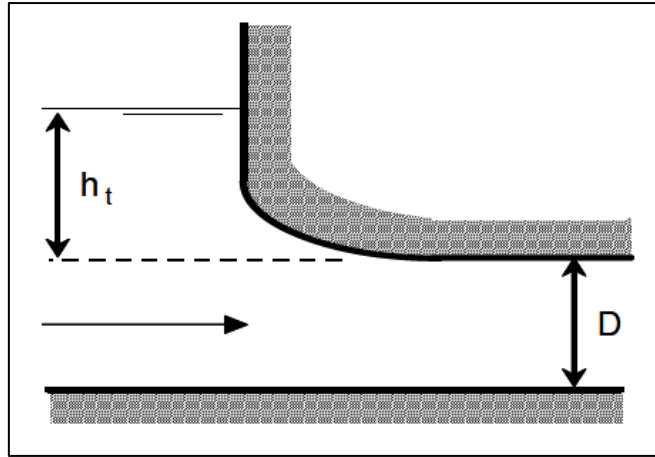


Figure 2.38: Minimum degree of submergence (Penche and De Minas, 1998)

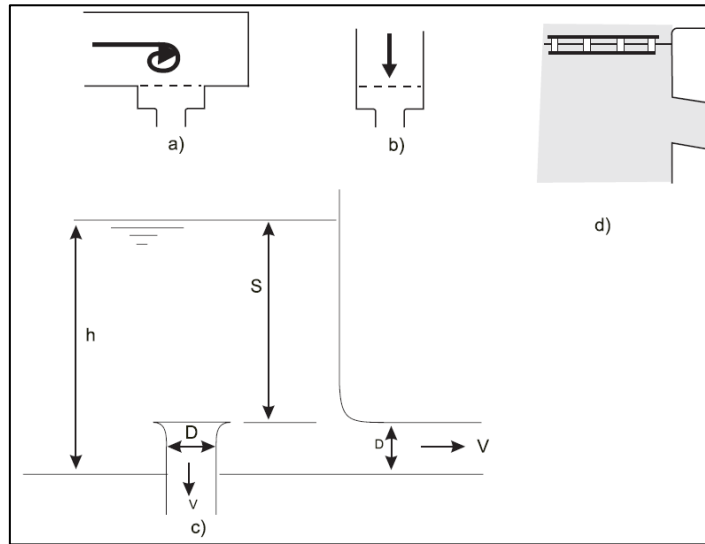


Figure 2.39: Different degrees of submergence (Penche, 2004)

The following formulas express the minimum values for h_t :

$$h_t \geq D \left(1 + 2.3 \frac{V}{\sqrt{gD}} \right) \quad (\text{Knuass, 1987}) \quad \text{Equation 2-16}$$

$$h_t \geq 4.4 (D^{0.50})^{0.54} \quad (\text{Nagarkar in Penche and De Minas (1998)}) \quad \text{Equation 2-17}$$

$$h_t \geq 1.474 V^{0.48} D^{0.76} \quad (\text{Rohan in Penche and De Minas (1998)}) \quad \text{Equation 2-18}$$

$$h_t \geq cV\sqrt{D} \quad (\text{Gordon, 1970}) \quad \text{Equation 2-19}$$

where

$c = 0.7245$ for asymmetrical approach conditions

$c = 0.5434$ for symmetrical approach conditions

It is important to know that V is the velocity inside the downstream conduit in m/s, and D is the hydraulic diameter of the downstream conduit in metres.

Beside a minimum submersion, constructive measures might help to prevent vortex formation. For example, asymmetric flow conditions may be prevented by means of vertical walls, piles, screens and floating rafts, or by the appropriate design of the entrance shape (Penche, 2004).

2.1.3.6 Settlers and Sediment Trap design

2.1.3.6.1 Background

Intakes and trashracks are designed in rivers to eliminate floating debris and bedload transport. However, the intake cannot prevent the entrance of all the sediment into the RoR scheme. For this, a sediment trap is placed downstream of the intake. A sediment trap allows the fine particles to settle over a distance. This settling opportunity delays the wear of turbine components.

The settling of sediment occurs due to gravitational action. Sediment settlers are important for this research, as they provide efficient head and settling capacity. Ramos (2000) states that a settling tank is subdivided into four zones:

- Inlet zone
- Settling zone
- Outlet zone
- Sludge storage zone

The inlet zone should assure a uniform distribution of flow. The reason for a baffle is to ensure that sediment is not disturbed as it is settling in the sludge zone. The settling zone allows for the settling of sediment, with the sole purpose to divert clean water (see Figure 2.40)

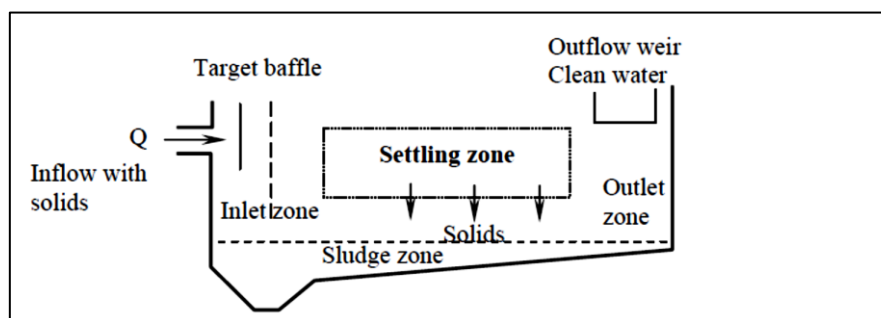


Figure 2.40: Different zones in a sedimentation basin (Ramos, 2000)

2.1.3.6.2 Settlers and Sediment Traps

Penche's (2004) guide for the development of the sediment traps was based on the principle of weakening the flow velocities before water reaches the turbines. Different channels have different situations, which introduce various sediment trap types. These sediment trap types are classified into six categories. The best description of different sediment trap designs has been given by Bouvard (1992) and is discussed in the following section.

2.1.3.6.2.a Traps with Outlet Sediment Scour

In an outlet sediment scour design, the sediment is removed downstream of the turbines. The flow condition in the sediment trap is such that all the sediment in the sediment trap is transported, with the exception of coarse sediment depositing as bed load. A scour outlet is placed at the downstream end of the sediment trap, with the scour gate permanently open (Bouvard, 1992).

2.1.3.6.2.b Traps with Distributed Sediment Excluders

The Dufour sediment trap has an internal sediment excluder. This sediment trap has parallel canals with a sloping bed. The sediment depositing on the side slopes roll down to the centre, prior to removal. The sediment is removed through a scour outlet at a velocity of 2 to 2.5 m/s (Bouvard, 1992). Figure 2.41 provides a sketch of the Dufour system.

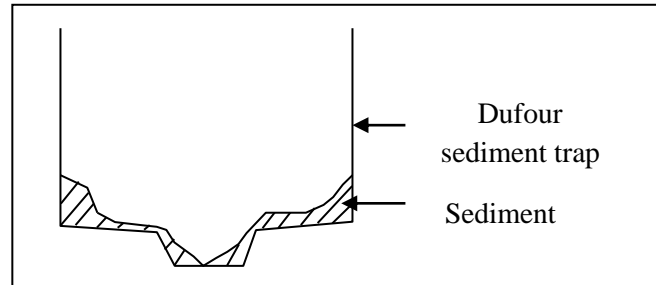


Figure 2.41: Dufour sediment trap (Bouvard, 1992)

According to Basson (2005), sediment traps are typically designed to exclude sediment with diameters of 0.3 mm with an efficiency of 100%. Sediment traps seldom trap sediment smaller than 0.1 mm. Sediment trap flow velocities are preferably in the range of 0.3 m/s to 0.5 m/s.

2.1.3.6.2.c Traps with Intermittent Flushing of Deposited Sediment

Settlers are exclusion systems from which the deposited sediment is removed periodically. Settlers with a typical output of 4 to 6 m³/s, are ideally suited for South African hydropower systems. They operate with a mean flow velocity of 0.1 to 0.2 m/s. Sediment enters the settler upstream and starts depositing in this section of the settler, gradually filling it up.

If the deposited load reaches a critical level, a sluice gate at the downstream end of the settler is opened to force sediment back to the river through scour. During the flushing of the settler, no water can be diverted to the turbines. Settlers are thus operated in two distinct modes, namely deposition and flushing (Basson, 2005).

A settler's volume is based on a general rule. The general rule is that the volume should not exceed 200 times the discharge per second into the settler (Basson, 2005).

Settlers typically cannot exclude sediment particles smaller than 0.1 mm, but can be designed to trap some of the sediment load. Cases that feature such a design are located in the Lebalelo and Vaal Dam (VRESAP) schemes. For design specifications for settlers, Basson's (2005) report on *Considerations for the design of river abstraction works in South Africa* can be consulted.

Hydraulic gates should be placed at the upstream end of a settler to ensure that the flow is controlled. When a downstream gate is placed in the settling basin, the gate should be at the bed level. It should be as wide as the canal and should allow free outflow conditions when flushing takes place (Basson, 2005).

Figure 2.42 provides the essential design of a settling basin according to Bouvard (1992).

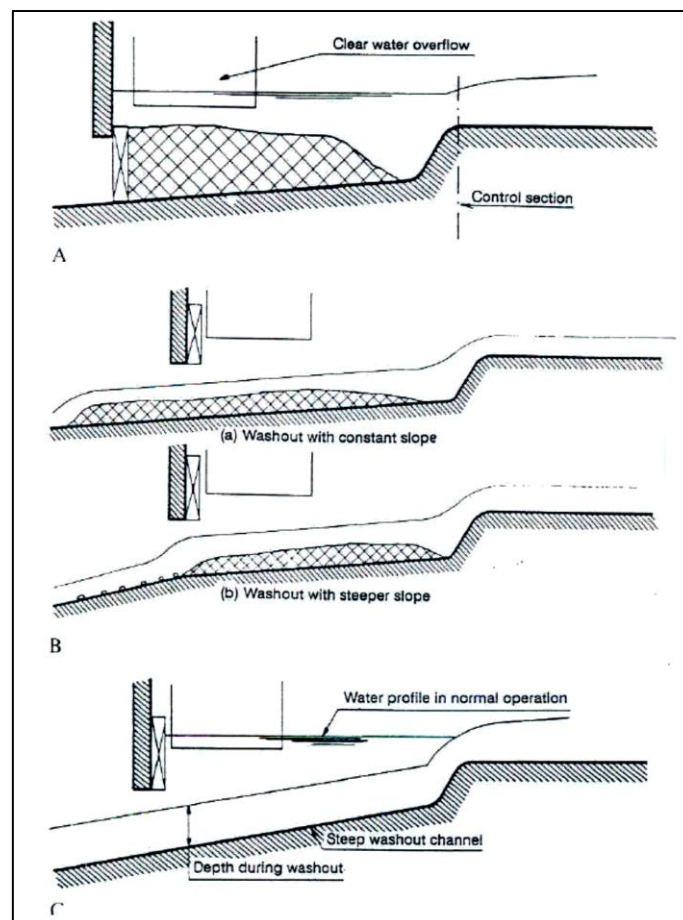


Figure 2.42: Settler design (Bouvard, 1992)

2.1.3.6.2.d Traps with Cones

These excluders originate from water purification technology and include mechanical scrapers. Such systems have been constructed at the Phalaborwa Barrage, Upington, and at the Craighead abstraction works. As this is a RoR hydropower system, this type of excluder was not considered.

2.1.3.6.2.e Curved Channel Sediment Excluder

A curved channel sediment excluder uses the curvature of a channel to reduce the amount of sediment entering the system. This type of sediment excluder is constructed to divert water from the main water course into the hydropower system. This excluder is used mainly in the hydraulic field and was a final design consideration.

Sedimentation on the inside bend of the curved extruder was the main reason for final consideration. The intake into the turbines is placed on the outer convex of the extruder, which reduces the sediment through the hydropower intake.

2.1.3.6.2.f Vortex Tube Sediment Extractor

According to Avery (1989), a vortex tube sediment extractor is a device that is used for the continuous removal of sediment on the channel bed. The vortex tube can be located upstream of the intake, or in the system.

The design of the vortex tube is explained by Avery (1989). Design and performance research on vortex tubes has been carried out by the HRS (Hydraulic Research Station) at Wallingford. The model based on the research results was later confirmed and refined by field measurements of a prototype vortex tube constructed in Indonesia and Nepal. The results estimate that the median bed material sizes extracted were 0.38 mm and 0.2 mm. In a RoR scheme this could be considered as a possible sediment removal method.

2.1.3.6.2.g Hoppers/Deep Sand Trap with Jet Pump

Hoppers are ideal if large quantities of sediment is deposited and transported via jet pump back into the river. Another advantage of a hopper is that the flow velocities into the system are very low. Although a hopper has a large capacity, a jet pump has to be placed at the bottom of the pit to pump the slurry back into the river. A hopper with a side slope of 2:1 (V: H) was considered for the final design review (see Figure 2.43).

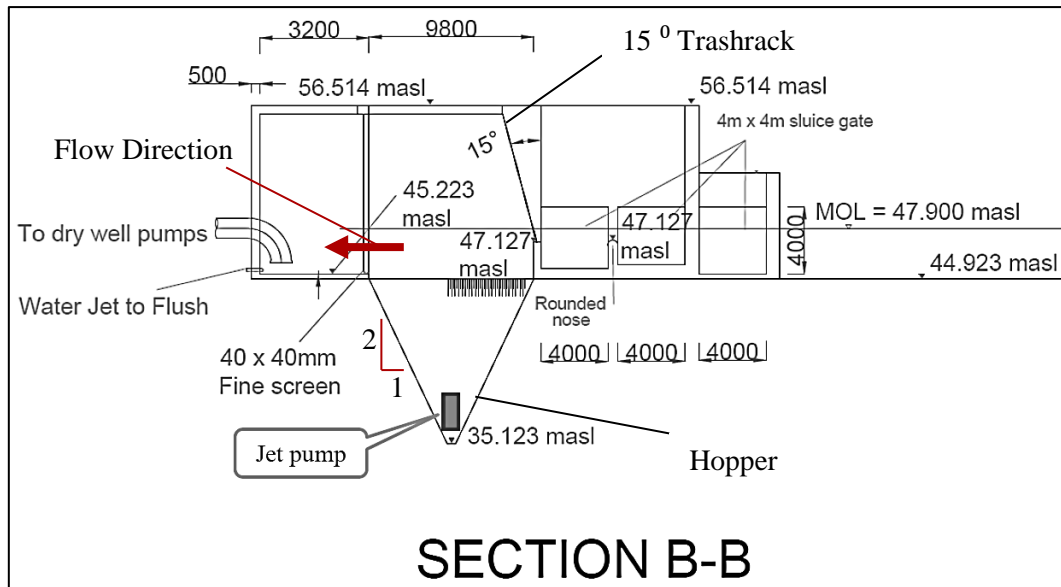


Figure 2.43: Diversion hopper design with jet pump

2.1.3.6.3 Efficiency of a Sediment Trap

The efficiency of the sediment trap estimates the possible suspended sediment passing through the turbines. The choice of efficiency depends on the type of hydro-mechanical equipment and head difference of the power plant. For a Francis turbine, the abrasive power of sediment is expressed as a function of the grain velocity and the operating head (Penche, 2004):

$$P_e = \mu \cdot \nabla \cdot \frac{\rho_s - \rho_E}{R} \cdot V^3 \quad \text{Equation 2-20}$$

where μ is a friction coefficient between the turbine blades and the grains, ∇ is the volume of the sediment, ρ_s and ρ_E are the densities of the sediment and water, R is the radius of the blades and V is the sediment velocity. The volume of the sediment is directly related to the efficiency of the sediment trap (Penche, 2004).

Damage occurs frequently if sediment diversion techniques are not set in place. Francis turbines have lifespans of six to seven years for a sediment trap with an efficiency of 0.2 mm, three to four years for an efficiency of 0.3 mm, and one to two years for an efficiency of only 0.5 mm. According to Penche (2004), the most economical sediment trap efficiency would be around 0.2 mm for severe conditions and around 0.3 mm for normal conditions.

A summary of settlers and sediment traps discussed in the research follows below:

Sediment traps are placed upstream or downstream of hydropower intakes. A sediment trap allows fine particles to settle. This opportunity delays the wear of the turbine components.

Settlers are subdivided into four major sections. These four sections are the inlet zone, the settling zone, the outlet zone and the sludge storage zone. Before water is transported to the settlers, there are many excluders, extractors and sediment traps that ensure maximum sediment deposition.

A hopper with a side slope of 2:1 (V:H) downstream of the trashracks was one of the final considerations. The main reason why a hopper with a jet pump would be efficient is that it does not need a high head to provide water. The other option was sediment traps with low velocity. Although sediment and clay can pass through the turbine with this system, it will still reduce damage to the turbines.

2.1.3.7 Turbine Specifications and Parameters

Additional readings referring to turbines are provided below:

Hydropower

Bishwakarma (2007), Bishwakarma and Stole (2008), ESHA (2011), Central Board of Irrigation & Power and INCOLD (2008), Ramos (2000), Spatial Plans and Local Arrangement for Small Hydro-SPLASH (2005).

2.1.3.7.1 Different Turbines

Different turbines are used at different heads. The following turbines are used in high-head hydropower schemes. The turbine details are discussed briefly according to SPLASH (Spatial Plans and Local Arrangement for Small Hydro, 2005) and the *Guidelines for Micro Hydro Power Development* (ESHA, 2011). Figure 2.44 presents turbines with high head capabilities:

Definition of different heads with reference to different turbines:

- High head: 100 m and above
- Medium head: 30 to 100 m
- Low head: 2 to 30 m

Pelton turbine: This is a typical high-head turbine, which can also be used for medium heads, with power ranging from 5 kW to large sizes (ESHA, 2011).

Cross-flow or Banki Mitchell turbines: These are mainly used at sites where there is low installed power. In general, their overall efficiency (around 75 to 80%) is lower than that of conventional turbines. They have a good response to variations in flow, which makes them appropriate for work where there is a wide range of flows. The turbines are suitable for low to high head sites from 1 m to 200 m, with flows over 100 l/s (ESHA, 2011).

Francis turbines: These are single regulated turbines that are commonly used with higher heads, given their efficiency (ESHA, 2011).

Propeller turbines: These have the advantage of running at high speeds even at low heads. Their response to different ranges of flow conditions is very good (ESHA, 2011).

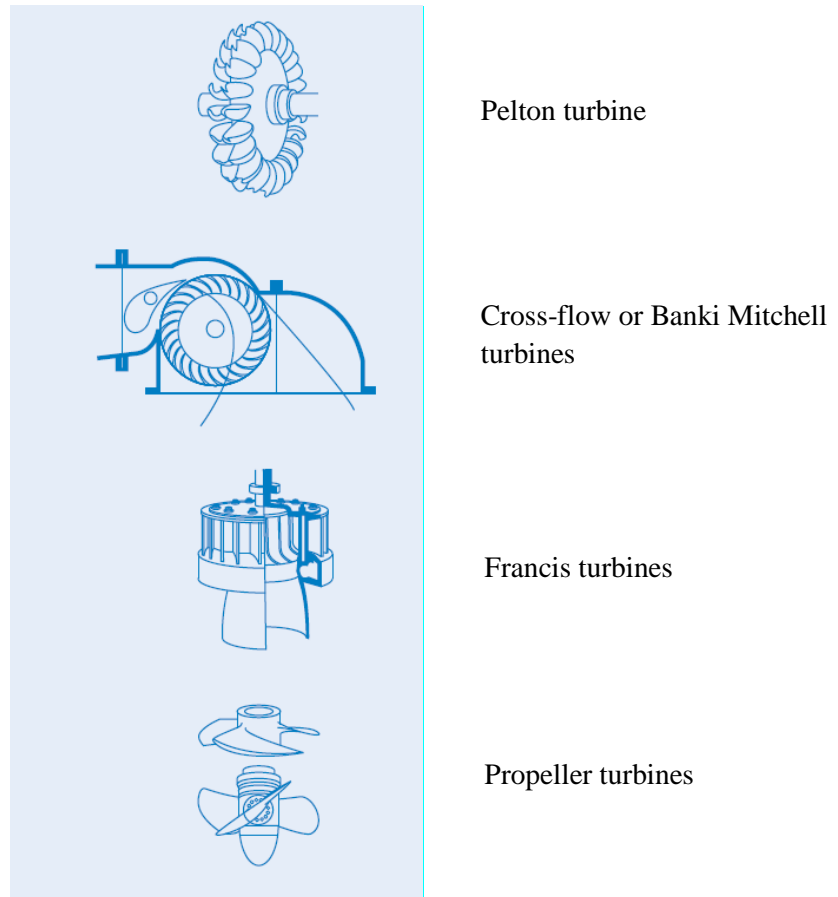


Figure 2.44: High-head turbines

Ramos (2000) provides a brief description of low-head and high-head turbines in Table 2.7.

Table 2.7: Application range of standard turbines and their power output (Ramos, 2000)

Hydraulic Turbines		H (m)	Q (m ³ /s)	P (kW)	N (rpm)
Reaction	Bulb	2-10	3-40	100-2500	200-450
	Kaplan and propeller-axial flow	2-20	3-50	50-5000	250-700
	Francis with high specific speed	10-40	0.7-10	100-5000	100-250
	Francis with low specific speed	40-200	1-20	500-15000	30-100
Impulse	Pelton	60-1000	0.2-5	200-15000	<30
	Turgo	30-200		100-6000	
	Cross-flow	2-50	0.01-0.12	2-15	
	Cross-flow	2-50	0.01-0.12	2-15	

The turbines in Table 2.8 are only used in low-head designs. The different turbine specifications and details are given by SPLASH (2005):

Table 2.8: Low-head turbines

Turbine System	Head Range	Capacity Range	Types of Sites	Cost
Waterwheel-overshot	Up to 5 m	Up to 500 kW	Old mills	High
Waterwheel-undershot	Up to 2 m	Low	Old mills with very low heads	High
Kaplan	0.5-10 m	Wide	Dams and rivers	High
Matrix	3-30 m	200 kW + units in banks	Dams, intakes	Relatively high
Bulb plus impulse turbine on riverbanks	0-0.5 m	Unknown – Small Sites	Structures in rivers, free running rivers	Probably relatively high
Archimedes	0.5-10 m	3-300 kW	Weirs and dams	Unknown
Parallel or modular propeller turbines	0.5-10 m	1.5 kW – 1 MW	Weirs, dams, sluices	Low, but site dependent
Stem pressure turbines	0.5-5 m	20 kW upwards	Weirs, dams	Unknown, but claimed low
Cross flow	1-200 m	Wide	Varied - dams, penstocks, pipeworks	Low

Waterwheels

There are two types of waterwheels: undershot and overshot. Undershot waterwheels have a low efficiency (25%) and are used on sites where there is not enough head for an overshot wheel. Overshot wheels can have relatively high efficiency (60 to 75%).

A new design is claimed to be able to produce hydro-turbines that move paddle wheels and a multiplier mechanism enabling capacities of 20 to 100 kW (ESHA, 2011).

Propeller turbines

The construction and placing of propeller turbines depend on the head rather than the flow. At low head sites, small parallel propeller turbines with a variable speed drive can adapt to the flow by opening and closing individual turbine intakes.

Recently, this concept of the simple modular fixed-flow turbine was taken further. Small modular ‘back-to-back’ reaction turbines have been developed and the dimensions are as follows: They are available in standard diameters ranging from 200 to 600 mm, for heads from 2 to 10 m, with power outputs from 1.6 to 58 kW and for flow rates from 0.095 to 1.7 m³/s (ESHA, 2011).

Archimedes screw

A German firm has adapted the traditional Archimedes screw to generate energy and this has the advantage of letting fish pass through without any problems. A number of examples have been installed in Germany and Switzerland, with heads in the range of 1 to 5 m, and in principle they can use water flows of 0.1 to 5m³/s and heads of up to 10 m, with power capacities from 3 kW to 300 kW (ESHA, 2011).

Bulb turbines

These are traditional modular propeller turbines with an integrated servo-generator. It would be possible to use ultra-low head sites by placing such turbines across a river and using them to drive high-pressure pumps that operate an impulse turbine on the river bank (ESHA, 2011).

Mini Aqua standardised range

Alstom has developed a standardised range of products called Mini Aqua, which integrate a turbine, generator and a control system in a single equipment set. At present these are available only for mini rather than micro hydro (from 300 kW), but they cover a wide range of heads and could theoretically be extended to smaller capacities (ESHA, 2011).

2.1.3.7.2 Turbine Material Coating

Attempts are being made to reduce damage caused by sediment on turbines. Erosion is minimised by reducing the particle velocity, by controlling the particle size and the use of HVOF (high velocity oxygen fuelled) and plasma nitriding (Mann and Arya, 2001).

It has been reported that HVOF-sprayed coatings and boronising provide remarkable improvements of turbine cavitation compared to plasma nitriding. Plasma nitriding as well as HVOF coatings are exploited commercially to overcome the power loss arising due to excessive erosion of hydro turbines (Mann and Arya, 2001).

In recent years, HVOF has been considered as an advantage, especially for materials with melting points below 3000 Kelvin. This coating has environmental advantages compared to chemically formed coatings (Mann and Arya, 2001). The HVOF coating is generally used to combat the erosion and corrosion occurring in hydropower plants.

Plasma nitriding is a modern technique for surface hardening of metallic components. Nitriding processes are based on solid, liquid and gas treatments that traditionally suffer from several drawbacks. Nitriding has replaced most conventional processes in the industry.

Mann and Arya (2001) prepared experiment to establish if the HVOF coating can withstand the erosion and corrosion of slurry. The HVOF was evaluated under both dry particle and slurry erosion conditions with 90° and 20° impingement angles (Mann and Arya, 2001).

The sediment erosion and abrasive wear behaviour of HVOF coating and plasma nitride was observed. These coatings were compared with 13Cr–4Ni steel, which is commonly used in hydro turbines. Angles of incidence, velocity and Reynolds numbers were maintained similar to those used in hydro turbines, simulating low- as well as high-energy particle impingement wear. Two types of sediment erosions were prominent. These erosion types can be controlled by velocity or sediment size on the basis of the equation given below (Mann and Arya, 2001).

$$\text{Impact energy} = \frac{1}{2}mv^2 = \frac{1}{12}\pi\rho d^3v^2 \quad \text{Equation 2-21}$$

where m is the mass, ρ the density, v the velocity and d the diameter of the particle. Sediment erosion resistance at different particle impingement energies is generally correlated with the above equation, although it also depends on a standard equation, given in Equation 2-21 (Mann and Arya, 2001).

$$KtcV^{3.5-4.0} \sum D_i \left(\frac{d}{d_{50}}\right)^{1.5} \left(\frac{H_s}{H_m}\right)^{1.75-2.25} \quad \text{Equation 2-22}$$

where H_s is sediment hardness, c is the concentration, D_i is the distribution, quantity, shape, base material hardness is H_m , K is the wear coefficient and the operating time is t , along with the particle velocity V in m/s, and d , as the particle size, contributes significantly. According to Mann and Arya (2001), there is not much data to compare with regarding the sediment erosion resistance of plasma nitriding and under-simulated hydro-turbine conditions.

After the experiments were completed, it was concluded that the HVOF-coated steel performed much better than that with plasma nitriding (Mann and Arya, 2001).

2.1.3.7.3 Turbine Flow Measurement

To compute the sediment load passing through each of the turbine units, Bishwakama (2007) needed measurements of flow through the turbine. The flow rate was based on the power production, assuming that the supplier provided the efficiency for different flow conditions. In the case of power plants in sediment-loaded rivers, the sediment diversion is critical.

Bishwakama (2007) researched the accurate measuring of flow through a turbine. The various methods developed for measuring total flow through the turbines are not always suitable to measure flow through a single unit. Bishwakama (2007) used ultrasonic flow meters to measure the flow rate through an individual turbine unit, alongside the Winter Kennedy method, the Pitot tube method and the acoustic method.

The easiest method for turbine flow measurement is with the ultrasonic flow meter. The Pitot tube and acoustic methods were used to analyse both the Francis and the Pelton turbines. Excessive sediment concentration altered the results of both the previously mentioned cases. Common problems that occurred with the Winter Kennedy and Pitot tube methods were the clogging of the pipes due to sedimentation and, similarly, the flow measurements were affected in the acoustic method. These methods can be consulted, but physical experiments are recommended for future use.

2.1.3.7.4 Measurement of Turbine Efficiency

Turbine efficiency does not remain constant over time, particularly if one bears in mind that the flow through a turbine changes according to turbine efficiency. The efficiency of a turbine is defined as the ratio of the power that is actually produced to the hydraulic power available upstream of the turbine (Bishwakama, 2007).

Efficiency measurements are done for two purposes. The first purpose would be in relation to new turbines, where the efficiency measurement includes checking contractual compliance. The second purpose would be for old turbines, as the measurement includes the checking of their status in order to qualify their potential for improvement. The efficiency provides the operating status of a turbine, which is linked to its electrical generation output. Periodic measurement of turbine efficiency assists in improving the output potential of existing turbines.

The loss in production results in a loss in revenue for major companies and governments. The reduction in turbine efficiency is largely dependent on sediment-induced erosion. Bishwakarma (2007) indicated that a turbine that operates in sediment-free water, as in Scandinavian countries, could last for several years if operated correctly. In contrast, however, a similar turbine may not endure a single monsoon if exposed to heavily sediment-laden flow in the Himalayan Rivers.

Therefore, the measurement of turbine efficiency, together with sediment concentration and sediment-induced turbine erosion, is vital for RoR schemes. The efficiency testing can help save the turbine from potential irreparable damage, as well as unacceptably high losses in generation.

Chapter 3

3. Physical Model and Data Analysis

3.1 Objectives

A physical model of a RoR intake was designed and tested in the Stellenbosch University Hydraulic Laboratory. The physical model was tested to provide data on the diversion angle and the scouring that takes place in front of the diversion intake.

The purpose of the research was to determine the optimum diversion location in a sinusoidal-curved trapezoidal channel, in order to minimise the abstraction of sediment in RoR systems. For the first physical run, the main objective was a simulation without a diversion structure in the channel flow. The scour pattern in the river was monitored and feedback was given in relation to the findings of Brink et al. (2005).

The second set of test runs was completed to determine the optimum diversion angle for a diversion intake. The bed change results were compared and provide a final orientation of the abstraction. An obstruction was placed in the channel to simulate an abstraction structure, and this will determine the diversion angle. The diversion has a radius of 200 mm on the upstream side and a long section downstream in the configuration of an intake. Figure 3.1 provides the shape of the object used as an obstruction.

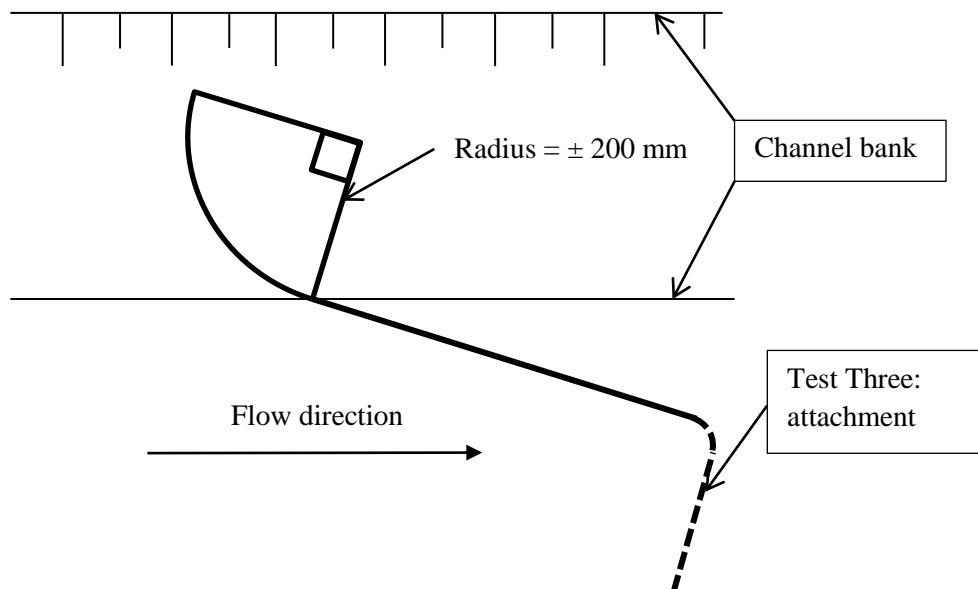


Figure 3.1: Layout plan of diversion intake shape

The third set of tests was similar to the second set of test runs. The difference is the attached section illustrated in Figure 3.1, also see Figure 3.15, will guide flow in a different direction. The reason for this specific L-shape was to observe whether the sediment upstream of the attached area would flush and erode.

The optimum design for all of the above tests was selected and used in the final experiment. The final experiment was to divert sediment and gather information on the volume of sediment diverted at an optimal position and angle. This was tested by observing the depth of scour and placing an intake at a different height. The scour patterns caused by the intake opening and the level of the intake was monitored and the sediment, which was diverted through the intake was weighed.

The bed change of the physical test runs were compared to a calibrated two-dimensional hydrodynamic model of the laboratory model with similar diversion structures. The objective of the numerical modelling was to test the prediction accuracy of the model.

3.2 Physical Hydraulic Model Design

The first step was to construct the river in a sinusoidal shape.

The r_c/w ratio of the laboratory channel was 5.3. The following figures will illustrate the choice of shape and design of the river model and its application in practice (see Figures 3.2, 3.3 and 3.4). The figures below illustrate that water flow in river bends alternates from 90° to 180° . From observation, the physical model was constructed and tested with two 90° bends and had a radius of 4 000 mm.

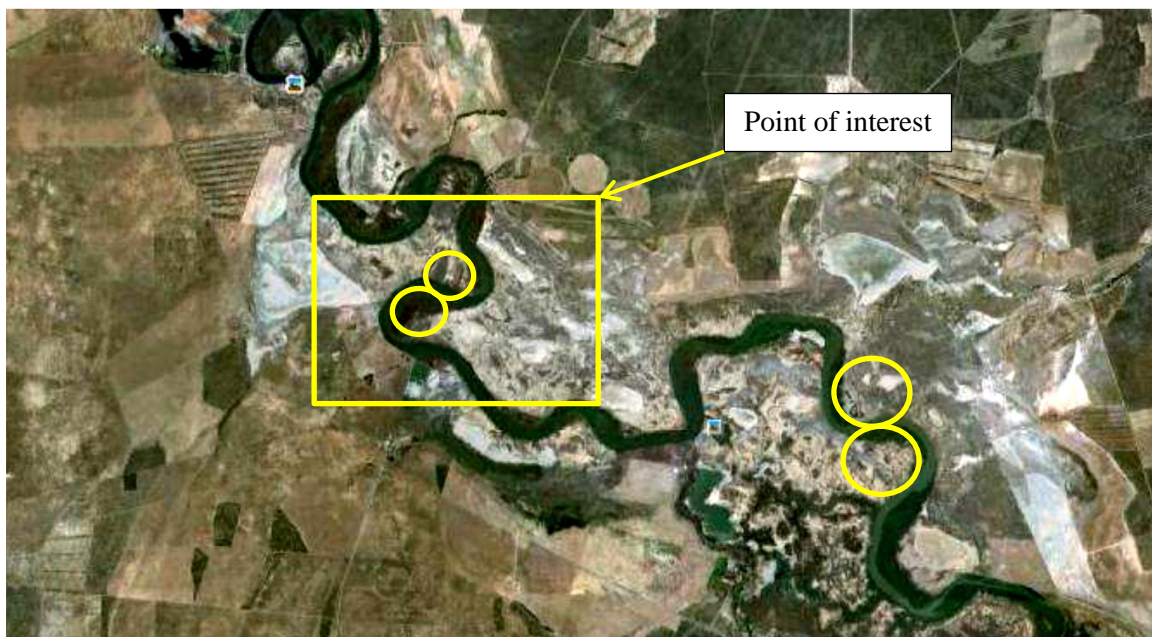


Figure 3.2: Berg River with consecutive 90° bends

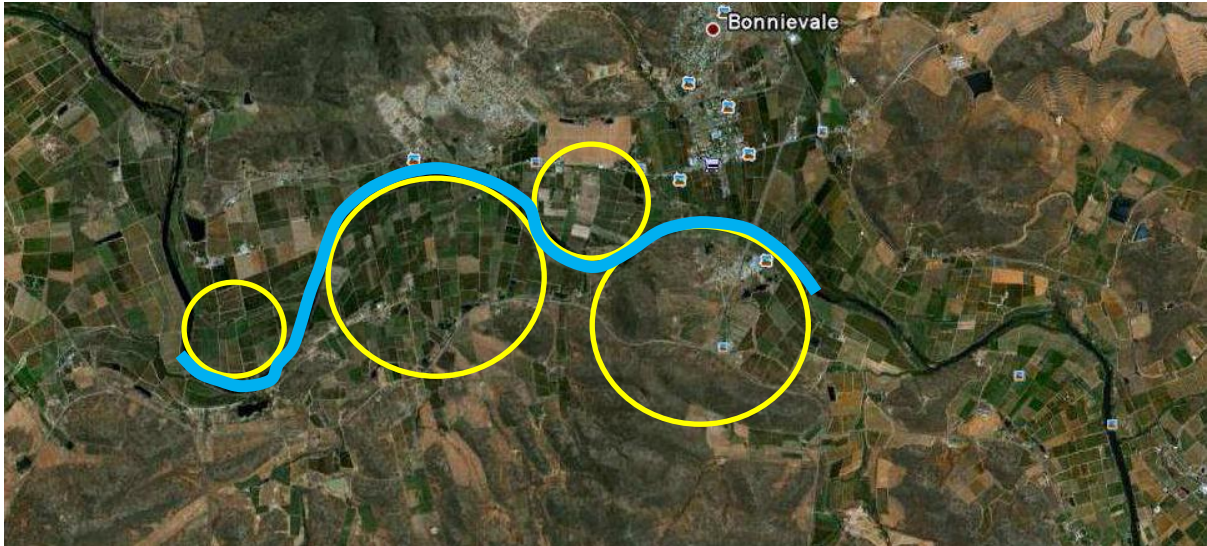


Figure 3.3: Breede River with consecutive 90° bends

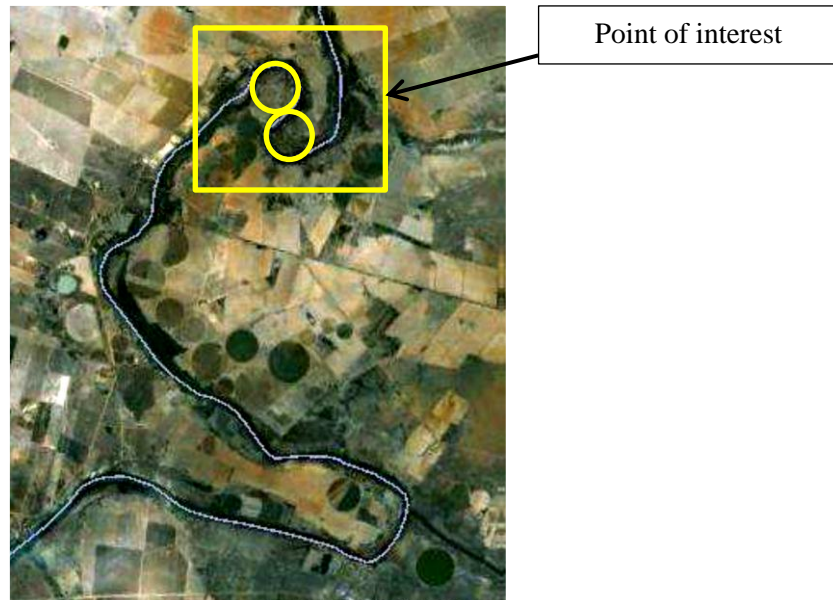


Figure 3.4: Vaal River bends for RoR positioning

The physical model was an erodible boundary experiment, which returned the results of sediment transportation and hydrodynamic movement. An important aspect of the physical model was that the sediment bed was restored to a trapezoidal shape with a bed layer of 100 mm after each test run, as this would provide efficient volumes of sediment for the system. Sediment was not fed in from the upstream river inlet, for the reason that the scour patterns had to be the worst-case scenario. The river was scaled to simulate a RoR abstraction when orientation and diversion were tested. Scale factors were needed to downscale the geometry, kinematics (time and velocity) and dynamics (force) required (Ettema et al., 2000). The following formulas were used to determine the model design. These formulas are based on Froude similarities.

Length:

$$n_l = \frac{L_p}{L_m} \quad \text{Equation 3-1}$$

Velocity:

$$\sqrt{n_v} = \frac{V_p}{V_m} \quad \text{Equation 3-2}$$

Flow:

$$n_Q^{2.5} = \frac{Q_p}{Q_m} \quad \text{Equation 3-3}$$

Time:

$$\sqrt{n_t} = \frac{T_p}{T_m} \quad \text{Equation 3-4}$$

where L_m is the model length (m), L_p is the prototype length (m), Q_m is the model discharge (m^3/s), Q_p is the prototype discharge (m^3/s), V_m is the model velocity (m/s), V_p is the prototype velocity (m/s), T_m is the model time (s), T_p is the prototype time (s), and n_l, n_v, n_Q, n_t is the scale size. The model comprised two 90° bends with a straight intake and outlet channel (see Figure 3.5).

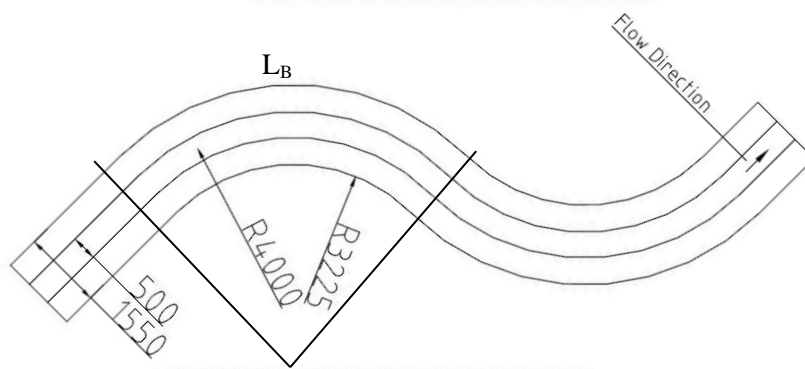


Figure 3.5: Sinusoidal test of 90° bend

$$\frac{r_c}{w} = \frac{4000 \text{ mm}}{755 \text{ mm}} \quad \text{Equation 3-5}$$

$$= 5.3 \quad \text{Which is acceptable } (2.5 < \frac{r_c}{w} < 8.0)$$

The straight intake channel of the river was 3 000 mm long, while the straight outlet channel was 1 500 mm. The river was a trapezoidal channel with a bottom width of 500 mm and a depth of 350 mm. The side slope of the channel bank was chosen at 1:1.5 as it provided a more natural and cohesive channel. The sediment slide angle (Section 3.3.1., p. 3-7) was tested and provided an angle of 1:5, but would not simulate correctly, as it would not be the main channel flow in natural rivers.

The reason for main channel flow experiments was to ensure constant diversion of water through the diversion intake.

As the channel bank was designed with a slope of 1:1.5 the banks of the channel could collapse causing possible inaccuracy in the results. The channel banks that collapsed during the experiment deposited directly on the toe of the channel bank. This collapsing action had no effect on the downstream sediment load.

The water was supplied from a constant pressure head tank through a 250 mm diameter pipe to ensure a constant discharge. Flow directors were placed upstream of the narrowed channel to dampen turbulence and to ensure uniform flow conditions. The downstream end of the settling basin contained a sluice gate that controlled the downstream water level. By ensuring that the downstream water level was controlled, the sediment in the channel could be saturated by damming the water to the specific downstream water level. Figure 3.6 provides a layout plan of the river model in the Stellenbosch University Hydraulics Laboratory.

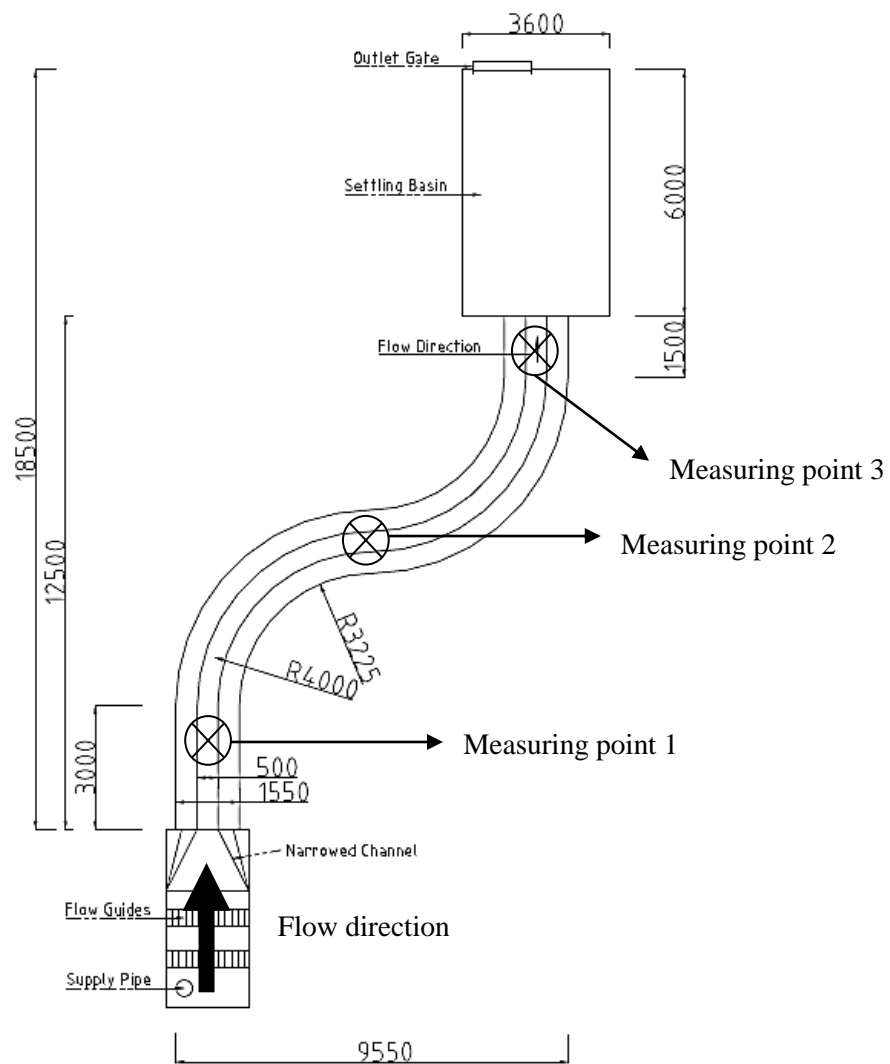


Figure 3.6: Layout plan of physical model to determine diversion position and angle

The trapezoidal channel contained a 100 mm sediment layer. The aggregate was a combination of two size classes of crushed peach pips. The two different sized aggregates have the same relative density of 1.3 and had a d_{50} of 0.4 mm and 0.8 mm, with a d_{90} of 0.6 mm and 1.28 mm respectively. The two sediment sizes were mixed fifty-fifty and provided a combined d_{50} of 0.56 mm, which represents coarse sand in the field.

Channel flow calibration was done using the Chezy formula (Chadwick, Morfett and Borthwick, 2004), with a k_s (surface roughness) value of 0.56 mm, the Manning formula (Chadwick, Morfett and Borthwick, 2004) with a Manning n value of 0.025 and a bed slope of 1 in 300. The reason for calibration was to observe if the Manning n value was selected correctly before the experiments could start. The slope was derived from Beck and Basson (2003) river data.

Using Chadwick et al. (2004), the following calculation was done to ensure that the sediment moved in the river model:

For model ($n = 0.025$)

$$\text{Velocity } V = \frac{R^{2/3} S^{1/2}}{n} \quad \text{Equation 3-6}$$

Let the depth, $y = 0.085$ m

With the flood depth known, the uniform flow velocity, area and flow through the system could be calculated. With the known values, the Froude number was calculated to see whether the water flow was subcritical or supercritical.

$$V = 0.375 \text{ m/s}$$

$$A = (0.5 + 1.5 \times 0.085)0.085 = 0.053 \text{ m}^2$$

$$B = 0.5 + 2(1.5)(0.085) = 0.755 \text{ m}$$

$$Q = VA \quad \text{Equation 3-7}$$

$$F_r = \left[\frac{Q^2 B}{g A^3} \right]^{0.5} \quad \text{Equation 3-8}$$

The flow value for Equation 3-7 is $0.02 \text{ m}^3/\text{s}$, which was the chosen flow for the model. The Froude number was calculated as 0.45, which is smaller than 1, and thus illustrates that the flow in the channel was subcritical.

The following tests had to be done to ensure that the sediment placed in the model could be transported with the experiment channel flow. The Modified Lui Diagram (Rooseboom et al., 1983) provides the relationship for incipient sediment movement. The settling velocity was measured by calculating the distance a particle drops over a set distance in water.

The sediment was dropped over a distance of 300 mm for each sediment size. The distance was divided by the time for each sediment size, where 50 tests were prepared in each size class. The three sediment sizes were 0.4 mm to 0.7 mm, 0.7 mm to 1.6 mm and 1.0 mm to 2.5 mm.

The model's sediment had a d_{50} of 0.56 mm, with a measured V_{ss} (settling velocity) of 0.033 m/s. The kinematic viscosity of the water (ν) was $1.14 \times 10^{-6} \text{ m}^2/\text{s}$ at 15°C .

Table 3.1: Sediment movement in laboratory model

Description	Model	Reference
Normal depth	$D = 0.085 \text{ m}$	Equation 3.2
Shear velocity equation	$V_* = \sqrt{gDS}$ $= 0.053 \text{ m/s}$	Equation 2.1 (Rooseboom et al., 1983)
Boundary between laminar and turbulent flow: $\frac{V_* d_{50}}{\nu} = 13$	$\frac{V_* d_{50}}{\nu} = 25.9$ > 13	(Rooseboom et al., 1983)
Flow region	Turbulent	Lui Diagram, Figure 8.10, Drainage Manual (Rooseboom et al., 1983)
Sediment movement value for turbulent flow	$\frac{V_*}{V_{ss}} = 1.6$ > 0.12	Equation 2.2 (Rooseboom et al., 1983)
Sediment movement	Takes place	Outcome in sediment movement section in Lui Diagram

3.2.1. Sediment Slide Angle

There were two sets of tests to decide what the sediment slide angle would be. Each test is described briefly, followed by the angle chosen to scrape the sediment in front of the intake. The reason for this scraped section was to ensure that the sediment did not fall into the intake when a test run was set in place. In hydraulic practice, the sediment was scraped and removed at the intake.

Test 1 was started by placing two thin plates in a flume of water. The plates were then placed parallel to each other at a distance apart. Sediment from the river model was laid in between the parallel plates until the sediment broke the water surface. With one motion, one plate was pulled up and away, and the sediment collapsed, as illustrated in Figure 3.7. The ratio of slip for test 1 was 1:4.4.

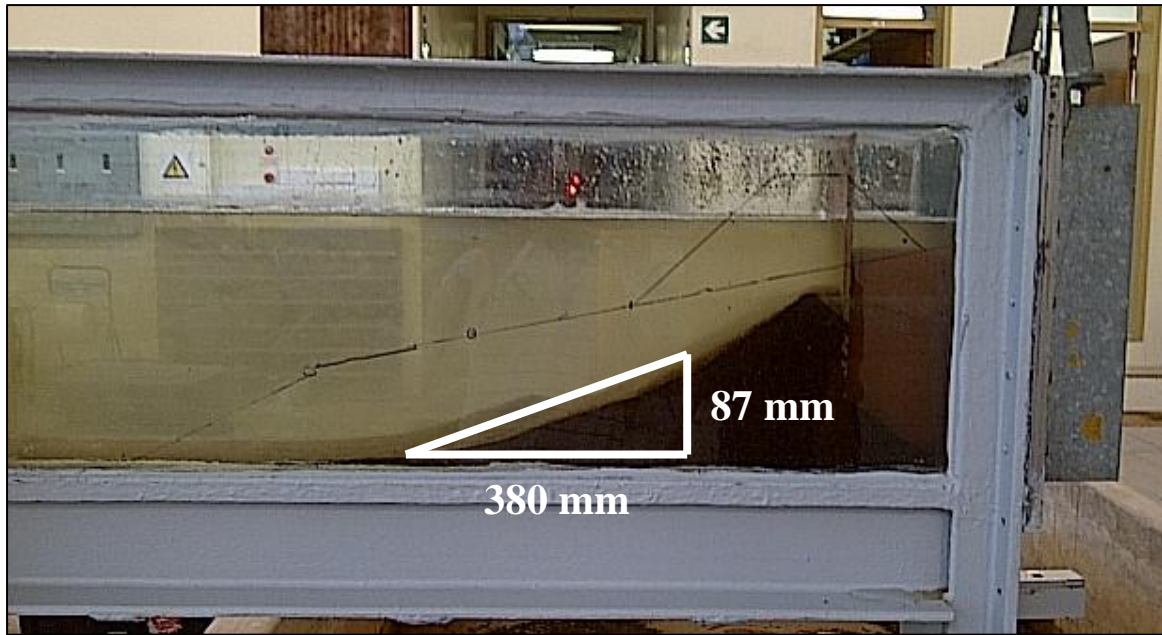


Figure 3.7: Test 1 for sediment slide angle

Test 2 was completely: was accomplished by placing the model sediment into the flume by hand. The objective was to create a pyramid shape to see when the sediment would stop sliding.

Test 2 had two results and they were as follows (see Figure 3.8):

- Pyramid A: ratio of 1:4.2
- Pyramid B: ratio of 1:3.2

The final ratio chosen for the scraped angle was 1:5 (V: H), which would insure that the sediment did not flush into the intake before the test started.

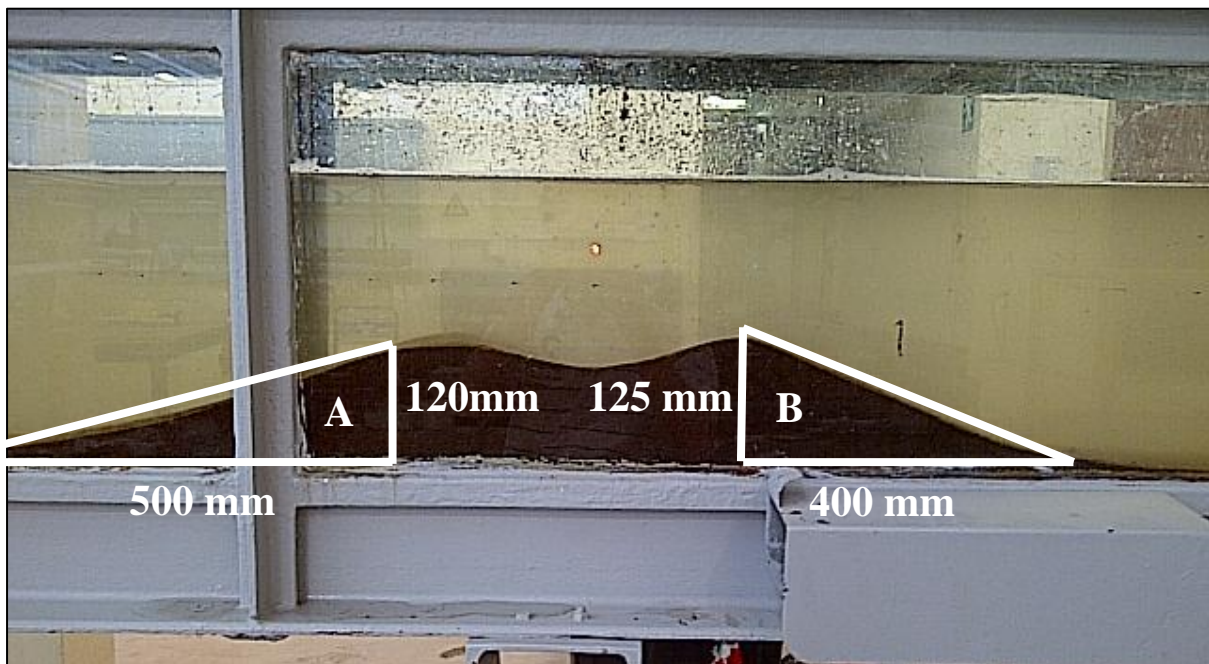


Figure 3.8: Test 2 for sediment slide angle

3.3 Laboratory Test Procedure

3.3.1 Experiment 1: Maximum scour location without structure

The first simulation and experiment was a full system run without any constrains and diversions. The sediment was placed in the channel evenly, at a thickness of 100 mm, before water was pumped into the channel. The reason for this experiment was to observe where the sediment deposition would take place and where the scouring in the river channel bend would occur. A study of the topic has been done by Brink et al. (2005), who also tested for the placing of the intake in different bends.

The measuring of the water levels was done with a needle gauge and the measuring of the sediment elevation levels was identified with a Leica total station. The following upstream and downstream sections were possible measurement sections. Measurements were taken between cross sections 7 and 13 (see Figure 3.9).

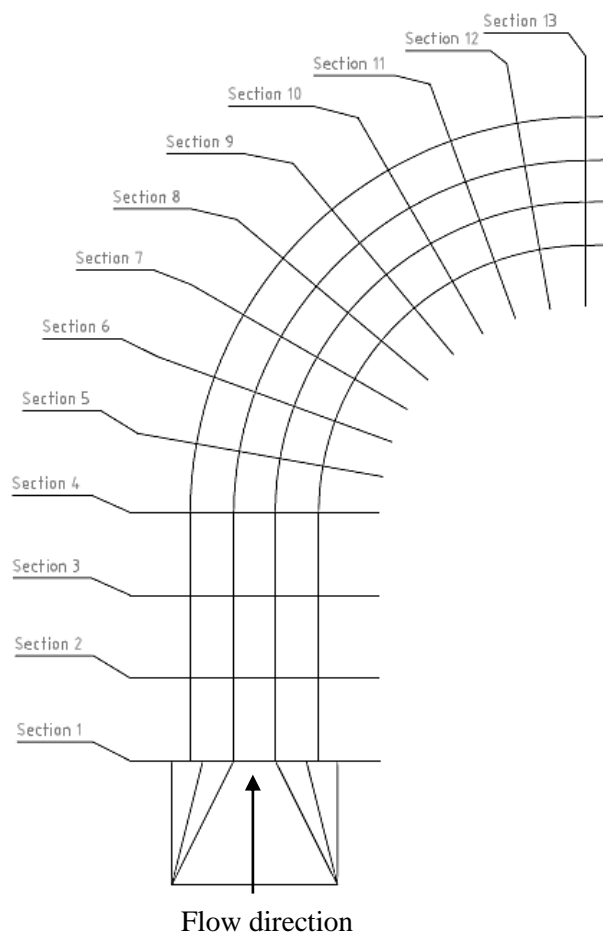


Figure 3.9: Cross section layout of physical model

Typical test procedure summarised:

- The model was filled with sediment to a level of 100 mm above the model bed and sides.
- The downstream sluice gate was closed to allow ponding of the water to ensure that excessive scouring in the bend was prevented.
- The needle gauge was set to the required level.
- The downstream sluice gate was closed until the calculated depth was reached and the sand was fully saturated.
- The next step was to simultaneously lift the downstream sluice gate, very slow, and to open the valve until it reached the required discharge.
- After the test had been done, the sluice gate and the valve were again closed simultaneously.
- The valve was fully closed, whereas the sluice gate was left slightly open to ensure that the water in the model flowed out with as little disturbance as possible to the scouring.
- The measuring of the sediment levels was done after all the water had drained.
- The process was repeated until the bed of the model was exposed.

As the placing of the structure in the river is important, the same importance is placed on the alignment, also known as the orientation, of the intake.

3.3.2 Experiments 2 to 9: Angle of diversion structure

The following experiments were set up as a prototype of a RoR intake. The diversion angle in relation to the flow direction was changed to observe what effect the intake angle would have on scouring patterns upstream and downstream. The following figure illustrates the measuring angle for the experiments (see Figure 3.10).

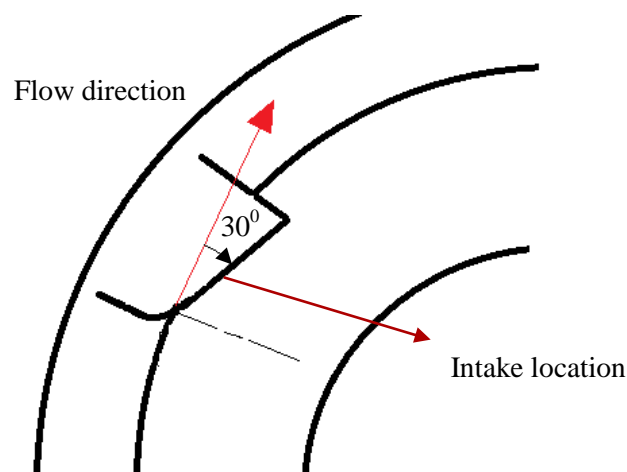


Figure 3.10: Orientation of structure with reference to flow direction

The following angles of the diversion intakes were tested: 0° , 30° , 45° and 60° . The scouring depth and deposited elevations were measured upstream and downstream of the structure for each diversion angle.

Avery (1989) argues in his book on sediment control at intakes that the angle recommended for the intake should be between 10° and 45° . The angle was measured from the centre line of the intake to the main direction of river flow. The ideal angle for a particular intake depends on the ratio of abstraction to river flow, the width of the river and the intake forebay. Avery (1989) declares that diversion angles of less than 45° are favoured, but should be tested with a physical model for better results. Other recommendations were:

- Lui et al. (1982) recommended an angle between 35° and 40° ,
- Hufferd and Watkins (1972) recommended an angle between 30° and 45° .

The difference between the thesis terminology and practice terminology is provided below in Table 3.2. As the terminology differs, a table is provided to illustrate the difference between the thesis angles and what they are in practice.

Table 3.2: Difference in terminology

Angle of orientation in thesis (measured according to illustration in Figure 3.10)	Angle of thesis orientation in practice (measured from intake centre line to river flow direction)
0°	90°
30°	60°
45°	45°
60°	30°

The design of the diversion position and angle are given in Figures 3.11 to 3.14. The structures tested in the physical model were high enough to ensure that water did not overflow the diversion. Experiments 2 to 9 did not abstract water during the physical model runs.

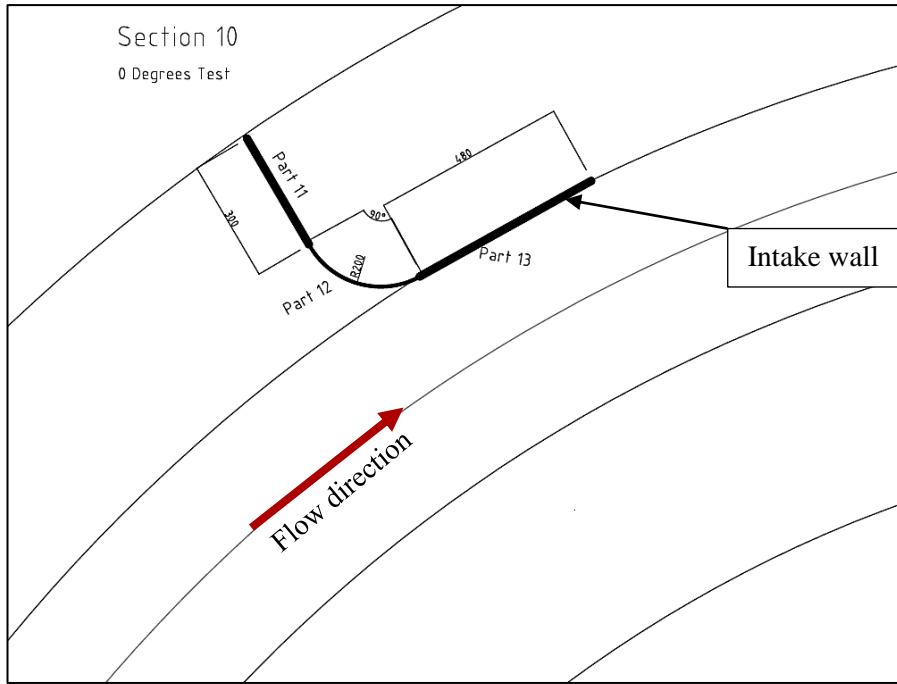


Figure 3.11: Diversion angle with 0° orientation to channel flow

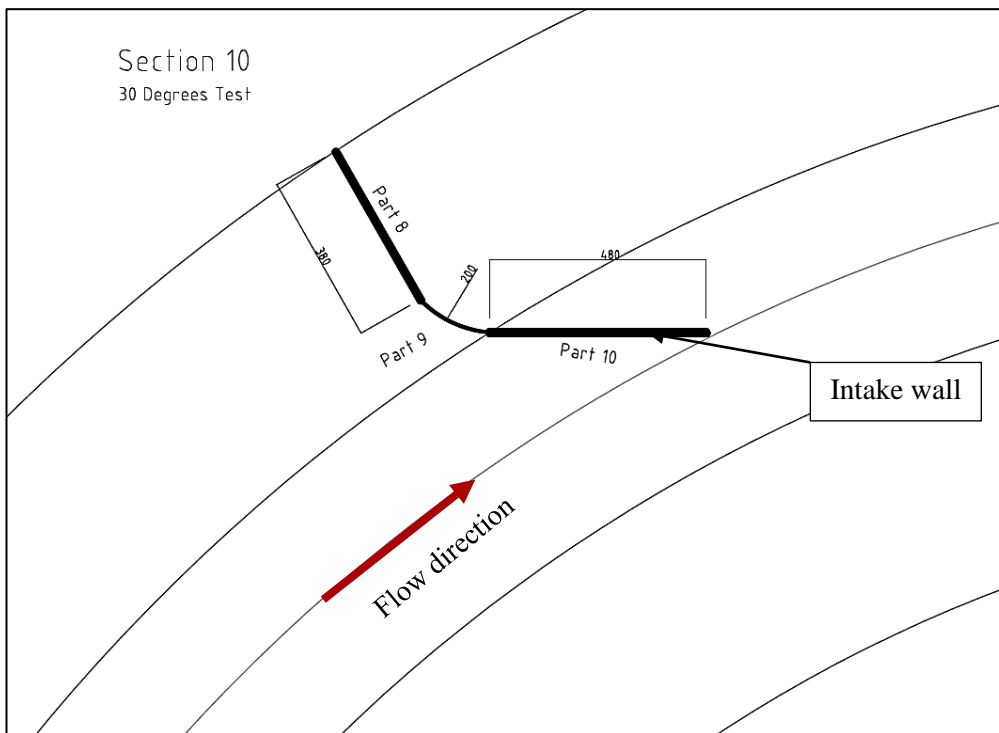


Figure 3.12: Diversion angle with 30° orientation to channel flow

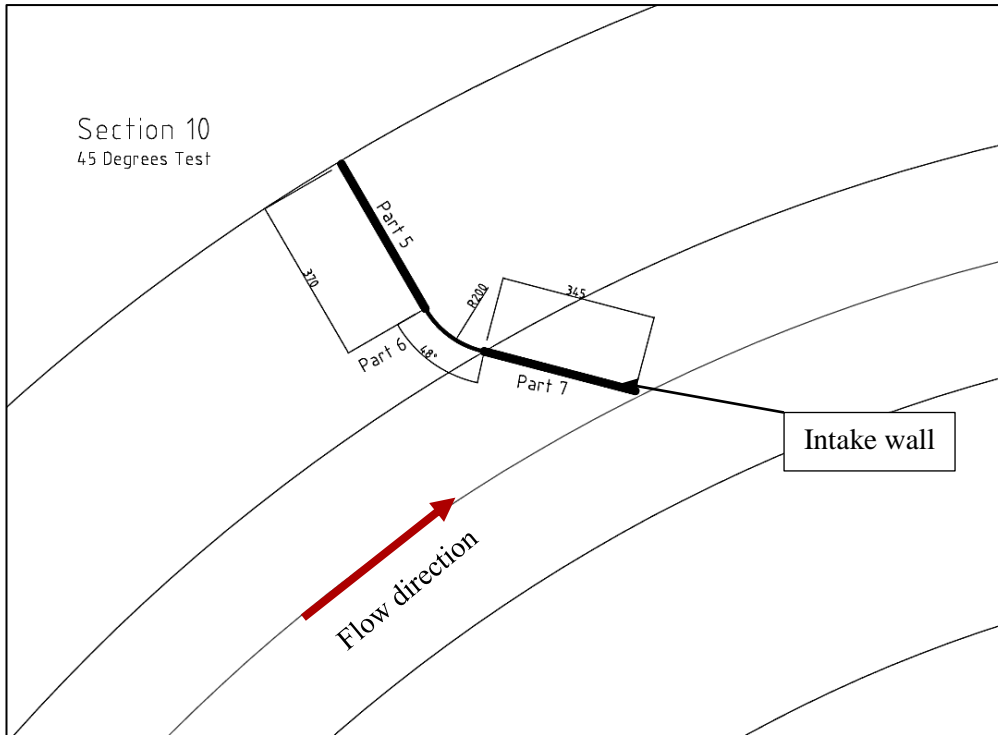


Figure 3.13: Diversion angle with 45° orientation to channel flow

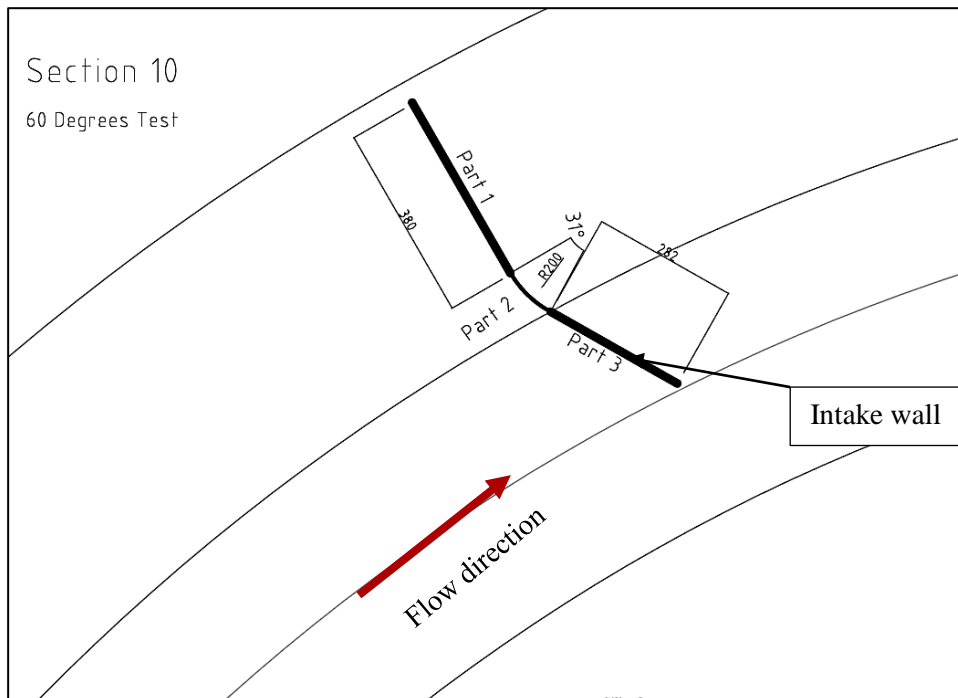


Figure 3.14: Diversion angle with 60° orientation to channel flow

3.3.3 Experiment 10

The final experiment was to choose the optimum angle of all the previously tested diversion angles. The diversion with the deepest and longest scour in front of the diversion structure was used. The 30° and 60° diversion angles had similar scour results, which led to an additional study with a wider bottom width (1 m wide) being simulated numerically. The size of the scour, the position of the deepest scour and the minimal effect of the structure on the opposite river bank led to the selection of the diversion structure used in this experiments

This experiment started off by observing what the scour depth was and moved on to analysing what the intake height should be. From analysing the results of previous physical test runs, and according to numerical simulation runs, as explained later, an opening was inserted into the diversion structure to determine what the sediment load and the concentration of the sediment diverted would be. A few scenarios were tested and are discussed in detail.

The opening of the diversion intake was determined as follows:

According to the literature, a Kaplan turbine should have a trashrack spacing of 0.1 to 0.15 m, but this was not the final choice for the design, as a 100 mm particle of sediment would cause damage to the hydropower station. Thus a spacing of 40 mm with a bar 10 mm in diameter was chosen as the prototype trashrack design. Four Kaplan turbines would provide a total flow of 12 m³/s (3 m³/s per turbine). By scaling the diverted flow needed (scale 1:40) and choosing an opening height of 61.5 mm, 515 mm was provided.

Figure 3.17 below illustrates the shape of the model. Appendix A and B provides the figures that explain each test, with physical test photos of the diversion scour.



Figure 3.17: Model abstraction structure (scale 1:40)

The method was as follows:

- The volume of the aggregate placed in the river was at a depth of 100 mm.
- The system was set in motion and the system and flow were stopped after the experiment.
- Sediment was diverted through an intake with a length of 515 mm (see Appendix B and Table 3.5)
- The diverted sediment-laden water was pumped while sediment was trapped in an internal filter.
- The flow at the inlet pipe and at the diverted end of the pump was monitored with a V-notch weir.
- The volume of the sediment diverted was weighed when wet and when dry.
- The mass diverted was in m_m (kg).
- The weight of sediment diverted was also divided by the running time (s) of the physical test to produce the sediment load (mg/s.m) and concentration (g/l) diverted. This was compared to different parameters of the structure and different flows.

V-notch weirs were placed where needed, to ensure that the experiments had the correct flow (see Figure 3.18). They were placed upstream at the pipe inlet, as there were different river flows, and downstream of the pump, as the diversion discharges had to be very precise. These flows and results are summarised in Table 3.5. The V-notch equation is as follows:

$$Q = \frac{8}{15} C_d \sqrt{2g} \tan\left(\frac{\theta}{2}\right) H^{\frac{5}{2}} \quad \text{Equation 3-9}$$

where

H = water level above V-notch

$\theta = 60^\circ$

$C_d = 0.59$ (British Standards Institution, 1965)



Figure 3.18: V-notch weir at inlet of river and outlet of intake structure

3.4 Analysis and Results of Physical Experiment

The following section of analysis begins by providing the literature on each experiment and comparing these literature results with the physical experiments at hand. The experimental results are also compared to the numerical results found in Chapter 4, in order to be able to decide which of the results will be used as the optimal design.

The radius-to-width (r_c/w) ratio found in the literature was the comparative factor in this experiment. Experiment 1 was compared to the following ratios to determine whether the diversion location is as expected:

1. Current experiment has a ratio of 5.3
2. Avery (1989) claims it must be between 3.0 and 5.0
3. Lui et al. (1982) claims it must be between 4.0 and 8.0
4. Shen (1971) claims it must be between 2.5 and 8.0
5. Rzhnitsyn (1960) claims it must be between 10.0 and 14.0

The diversion angle of the abstraction works was compared to the following literature:

1. Current research says the angle is between 0° and 60°
2. Avery (1989) says it is between 10° and 45°
3. Lui et al. (1982) say it is between 35° and 40°
4. Hufferd and Watkins (1972) say the angle is between 30° and 45°

After the location and angle of diversion had been optimised and compared to the numerical results given in Chapter 4, the concentration of sediment (DS – diverted sediment) moving through the intake was tested. According to Scheuerlein (1984) the diverted discharge should be kept below 50% of the total river flow, as this will reduce the chances of experiencing bedload problems.

Table 3.4 and Table 3.5 provide a full summary of the experiments and their reference pages.

3.4.1 Experiment 1 (without diversion structure, 20 l/s)

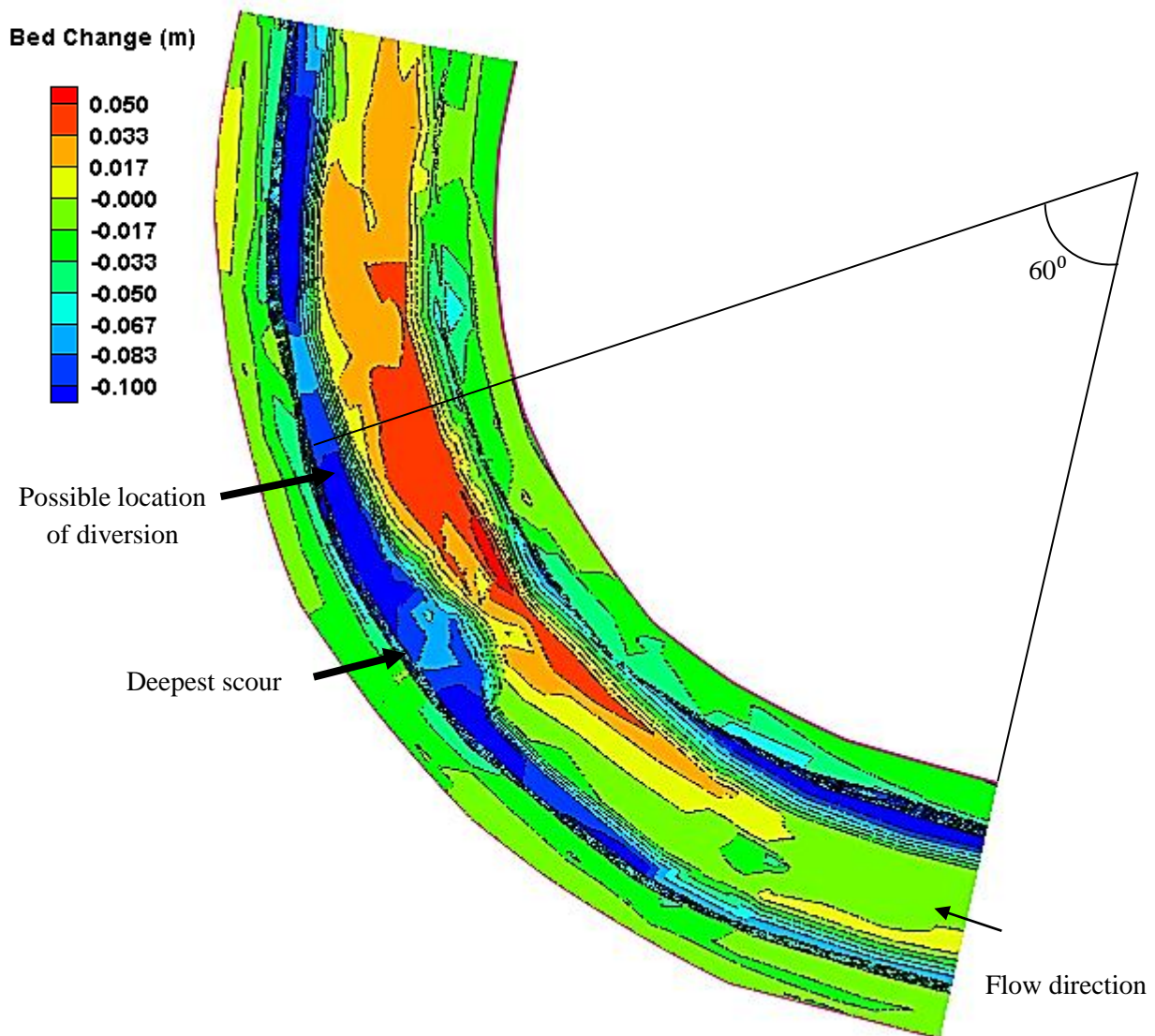


Figure 3.19: Bed change result for physical experiment 1 (without diversion structure, $Q = 20$ l/s)

The total discharge during the test was 20.0 l/s, with water depths of 98 mm, 105 mm and 110 mm for the measuring points 1, 2 and 3 respectively (see Figure 3.6). A Manning n value of 0.025 was used for the calibration against tailwater depth. The calibration test revealed that a Manning n value of 0.03 had to be used in the subsequent test to obtain the correct water depths. The reason for the higher Manning n value was a result of the sediment ripples that formed on the river bed during the test run.

The scouring started five minutes after the start of the test. The test had a run time of 9 min and 30 seconds. Table 3.4 provides the page numbers of the photos taken of the sediment elevation results of the experiment in Appendix A.

In Figure 3.19 there is visual proof of deposition on the inside of the bend. Figure 3.19 also illustrates unusual scour at the downstream end of the section. Although the downstream water level was maintained at the desired water level at all times, the scouring still occurred. The scouring starts 40° into the channel bend and end approximately 60° into the bend. As time and channel flow can have an effect on the maximum scouring position the following investigation was prepared.

Thus further investigation had to be prepared. The length from the start of the bend to the scour at the possible abstraction position was 55° into the bend. As this test could not whether the location was correct, later test proved that the possible location of abstraction was, in fact, correct. The combination of figures below illustrates the change in position of the scour as the flow depth increased (see Figure 3.20).

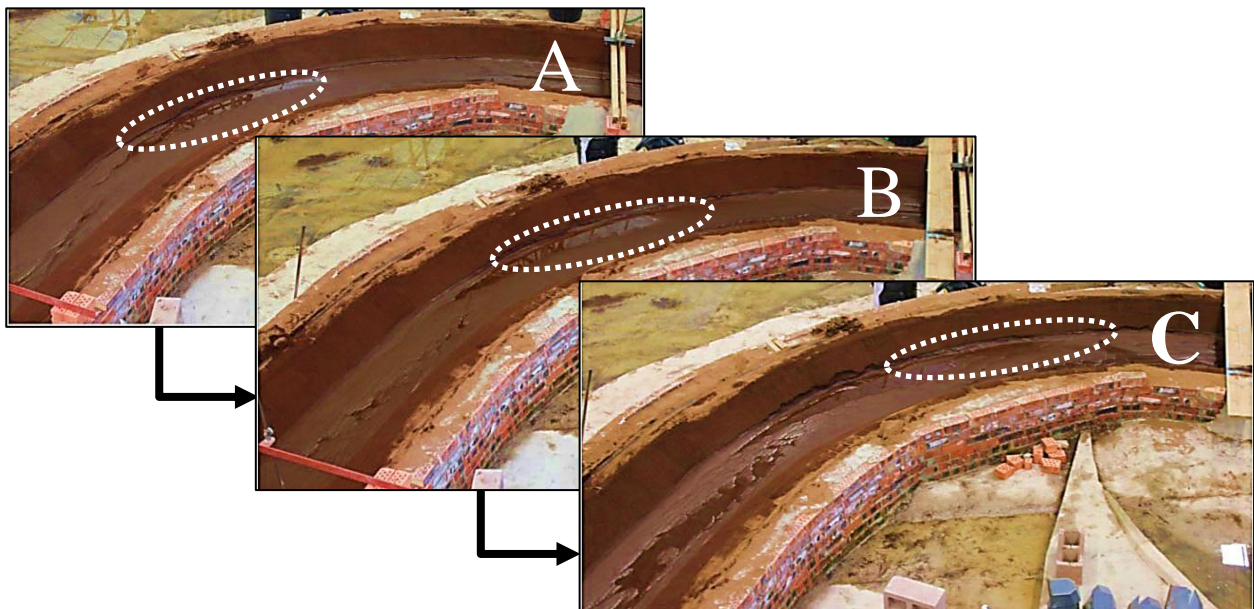


Figure 3.20: Change in location of maximum diversion from low to high flow

Figure 3.20 A had a flow of 1.4 l/s, B was 1.9 l/s and C was 2.4 l/s. Figures A, B and C above provide the change of position as the flow increased. As the secondary currents had not fully develop with flows less than 2.4 l/s the position of maximum scour could not be established. This was not measured physically, but was derived mainly from observation. A better illustration is provided in Figure 3.21, which shows how the change in position was occurring.

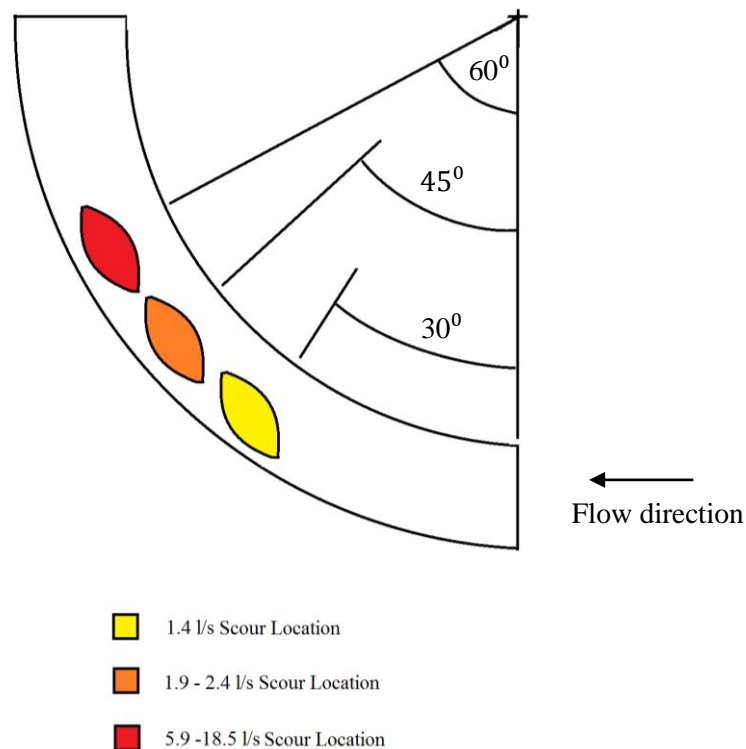


Figure 3.21: Change in scour location due to different river flows (see Experiment 10A)

The test confirmed that the zone of maximum velocity was on the outside of the bend and that slower velocities were found on the inside. This could be observed by watching sediment movement during the tests, and by inspecting scour and deposition after the test. A possible reason for the change of scour position is that secondary currents occurred at full bank flow and these should be accounted for when designing the river. As the low flows were well under full bank flow, the forces of the water on the banks of the river would change until a near full bank river flow was attained. As the low flow water depths were small, they ensured that full river bank flow and secondary flow in this model only occurred at 5.9 l/s and higher. The final location of maximum scour occurred 60° into the channel bend (see Figure 3.22).

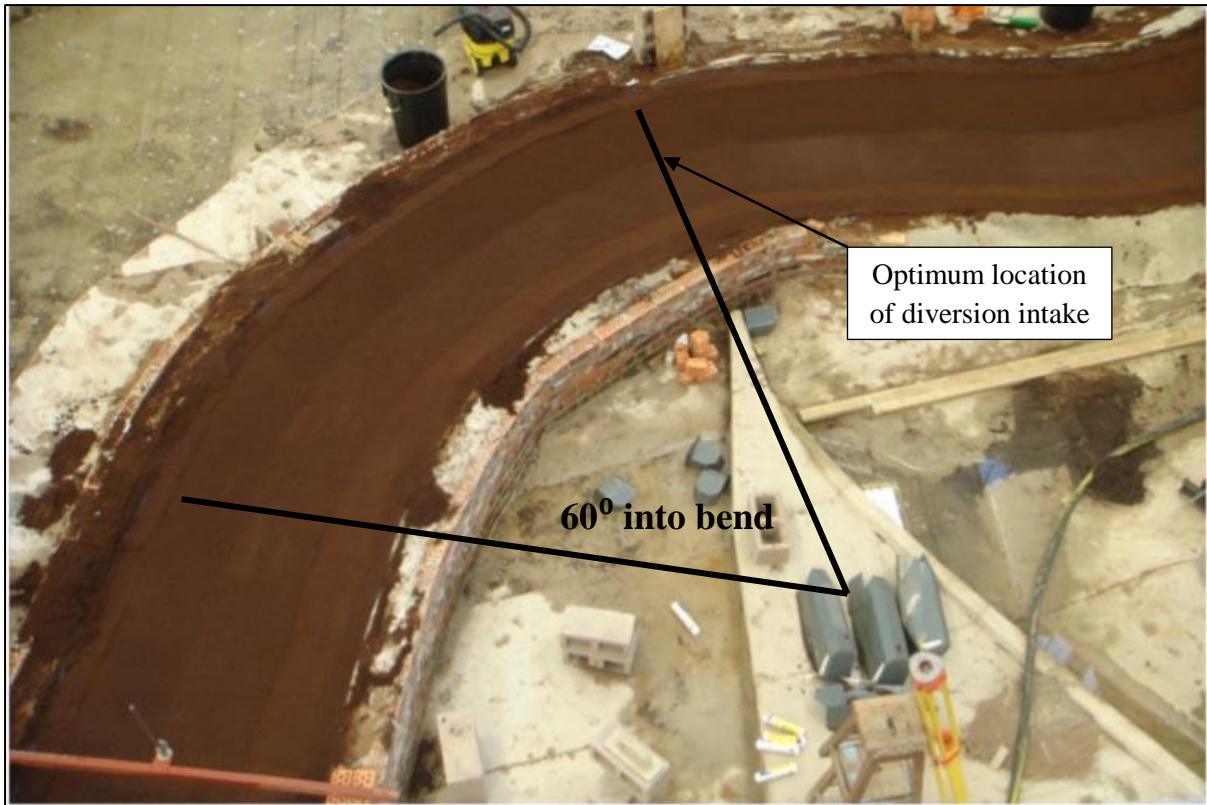


Figure 3.22: Location of optimum diversion in channel bend

3.4.2 Experiment 2 (0° with flow, 17.5 l/s)

Figure 3.23 illustrates the result of Experiment 2.

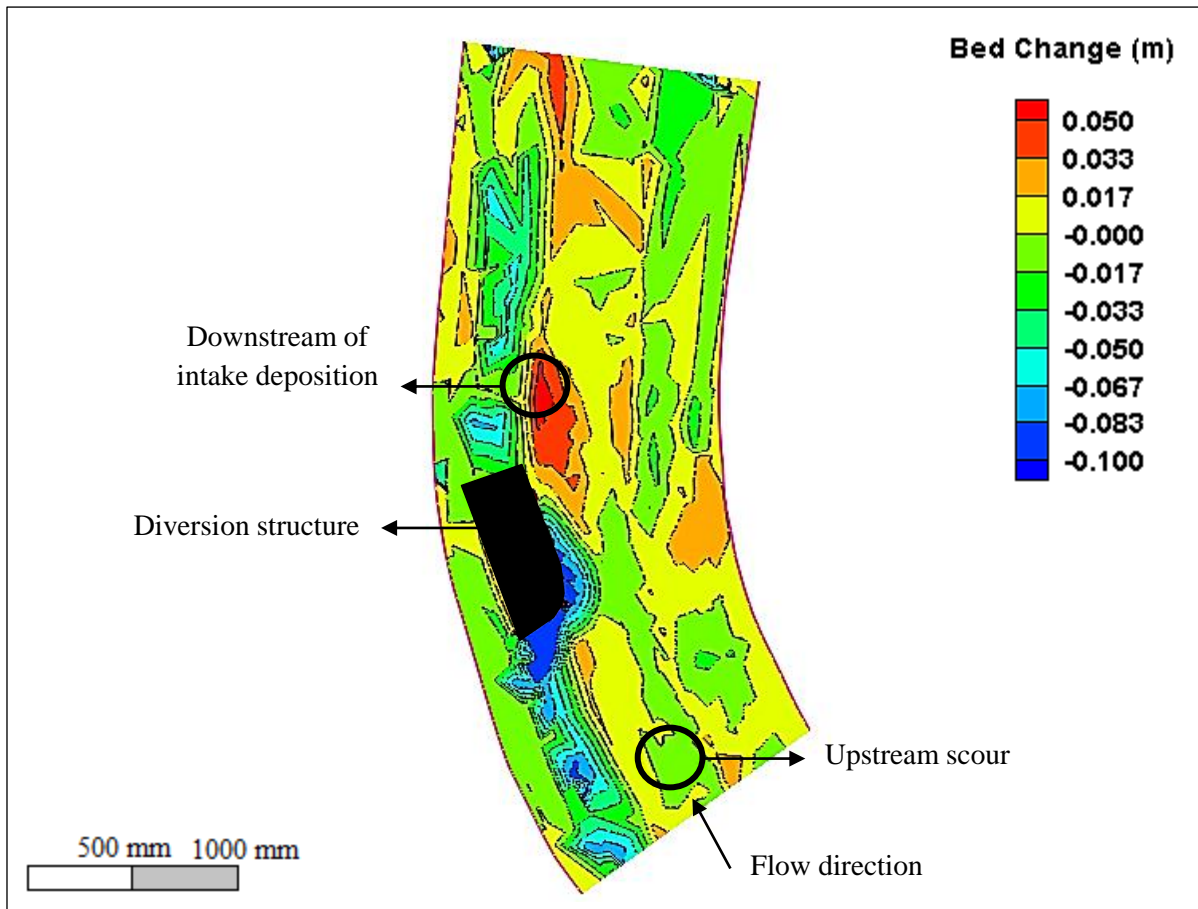


Figure 3.23: Bed change result for physical experiment 2 (0° with flow, $Q = 17.5$ l/s)

The total discharge during the test was 17.5 l/s, with water depths of 87 mm, 78 mm and 101 mm for the measuring points 1, 2 and 3 respectively (see Figure 3.6). The Manning n value was chosen as 0.03.

The experiment had been in progress three minutes in total when the scouring reached the bed of the river. Table 3.4 provides the page numbers in the Appendix of the photos taken of the sediment elevation results of the experiment.

An observation was made that the structure with this specific angle did not cause a disruptive action on the opposite river bank and at the downstream end of the section. The deposition of sediment occurred downstream of the intake, as expected.

On examining the scour upstream of the structure it was detected that the scouring had reached the river bed, providing assurance that the length of the trashrack could stretch across the structure bend towards the side bank of the river. Although this was a positive point, the negative point was greater

than the positive, as only three quarters of the diversion structure was scoured. As the trashrack is across the full length of the diversion structure, it can be assumed that this orientation, although showing great results, would not be sufficient for this research to accept as conclusion.

3.4.3 Experiment 3 (0° L-shape with flow, 14.5 l/s)

Figure 3.24 illustrates the result of Experiment 3.

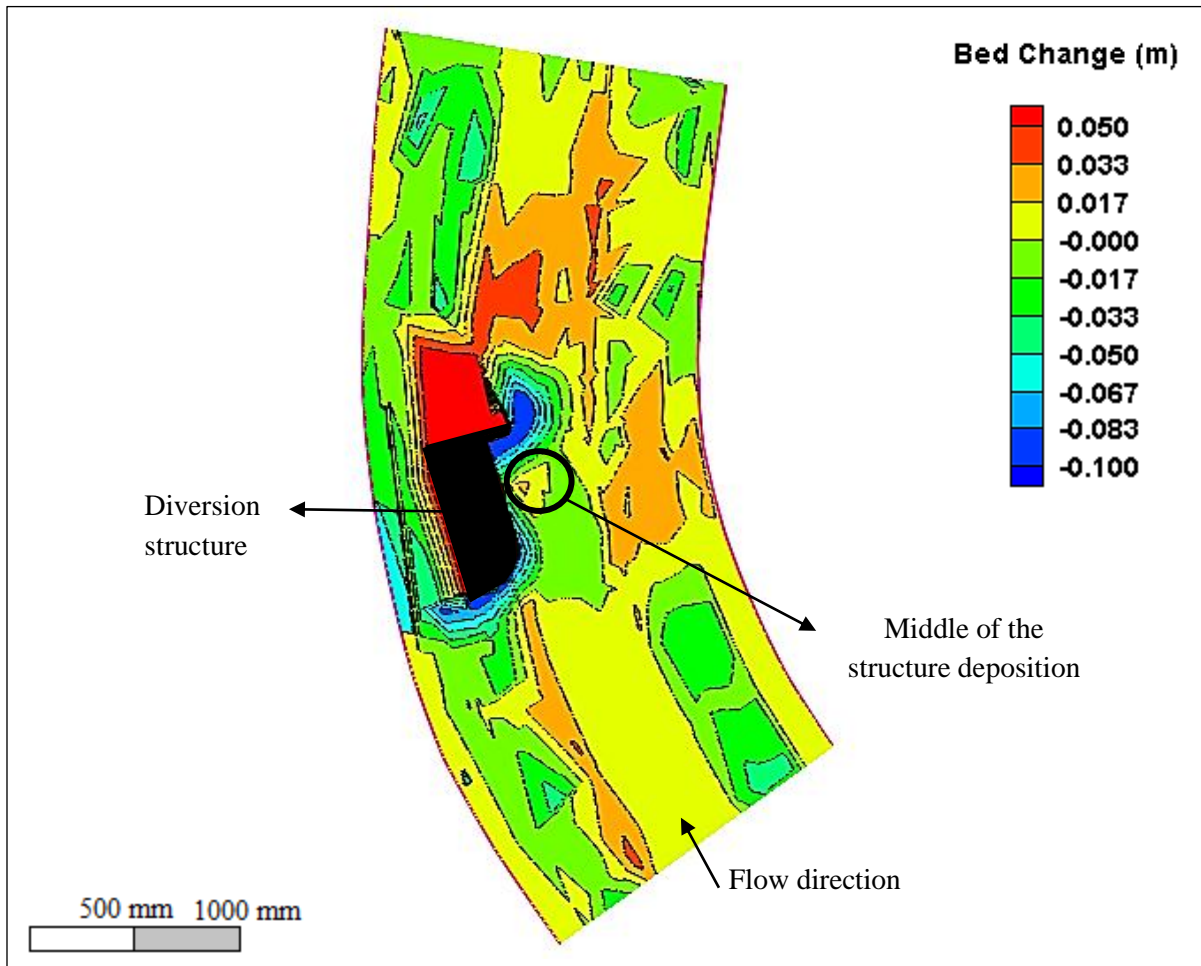


Figure 3.24: Bed change result for physical experiment 3 (0° L-shape structure, $Q = 14.5$ l/s)

The total discharge during this test was 14.5 l/s, with water depths of 76 mm, 88 mm and 95 mm for the measuring points 1, 2 and 3 respectively. The Manning n value was 0.03. The experiment had lasted three minutes and one second in total when the scouring reached the bed of the river. Table 3.4 provides the page numbers in Appendix A of the photos taken of the sediment elevation results of the experiment.

Although this specific angle did not cause a disruptive action on the opposite river bank, it did cause slight scouring on the upstream side and deposition on the downstream side. The deposition of sediment occurring downstream of the intake was as expected.

On examining the scour upstream of the structure it was detected that the scouring had reached the river bed, but this was not reassuring as the scour was very close to the structure. It was observed (see Appendix A photos 1 to 3, page A-f) that the sediment was not scoured or flushed in the centre of the structure. The reason for this is that the downstream L-shaped attachment reduced flow velocity upstream of the attachment, ensuring that less sediment was transported. This L-shaped attachment is common in abstraction works with weirs. This would not be a suitable structure with the specific orientation used here.

3.4.4 Experiment 4 (30° with flow, 18.8 l/s)

Figure 3.25 illustrates the result of Experiment 4.

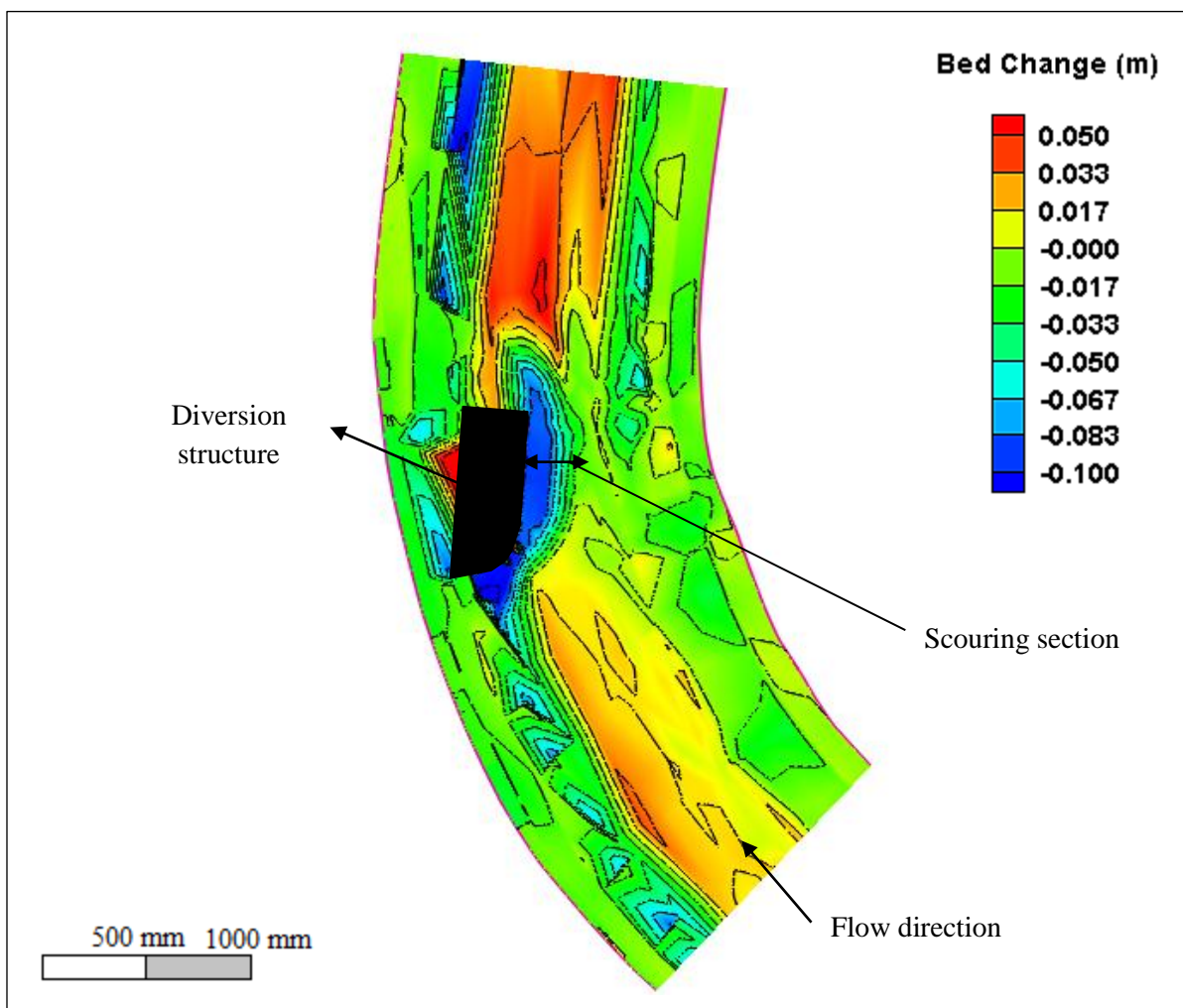


Figure 3.25: Bed change result for physical experiment 4 (30° with flow, $Q = 18.8$ l/s)

The total discharge during the test was 18.8 l/s, with water depths of 89 mm, 47 mm and 100 mm for the measuring points 1, 2 and 3 respectively. A Manning n value of 0.03 was used for this model. The reason for the shallow water at measuring point 2 was because of the drastic deposition of 34 mm of sediment.

The experiment had been in progress three minutes and thirty-six seconds in total when the scouring reached the bed of the river. Table 3.4 provides the page numbers in Appendix A of sediment elevation results of the experiment.

It was observed that the structure with this specific angle did not cause a disruptive action on the opposite river bank and the downstream end of the river. Great quantities of sediment was deposited downstream of the intake. The deposition downstream could ensure that water levels would stay constant, with less turbulent flow of water, thus creating a natural damming. As water damming took place, the sediment scouring would be less, but great quantities of sediment were scoured on the outside of the bend (in front of the intake), in contrast to approximately 30 mm scouring on the inside of the bend.

Scouring occurs everywhere along the structure, thus providing assurance that the length of the trashrack can extend from far downstream on the structure, across the structure bend towards the side bank of the river. The structure and orientation of experiment 4 provided the best results thus far and was considered as an optimal design.

3.4.5 Experiment 5 (30° L-shape with flow, 17.8 l/s)

Figure 3.26 illustrates the result of Experiment 5.

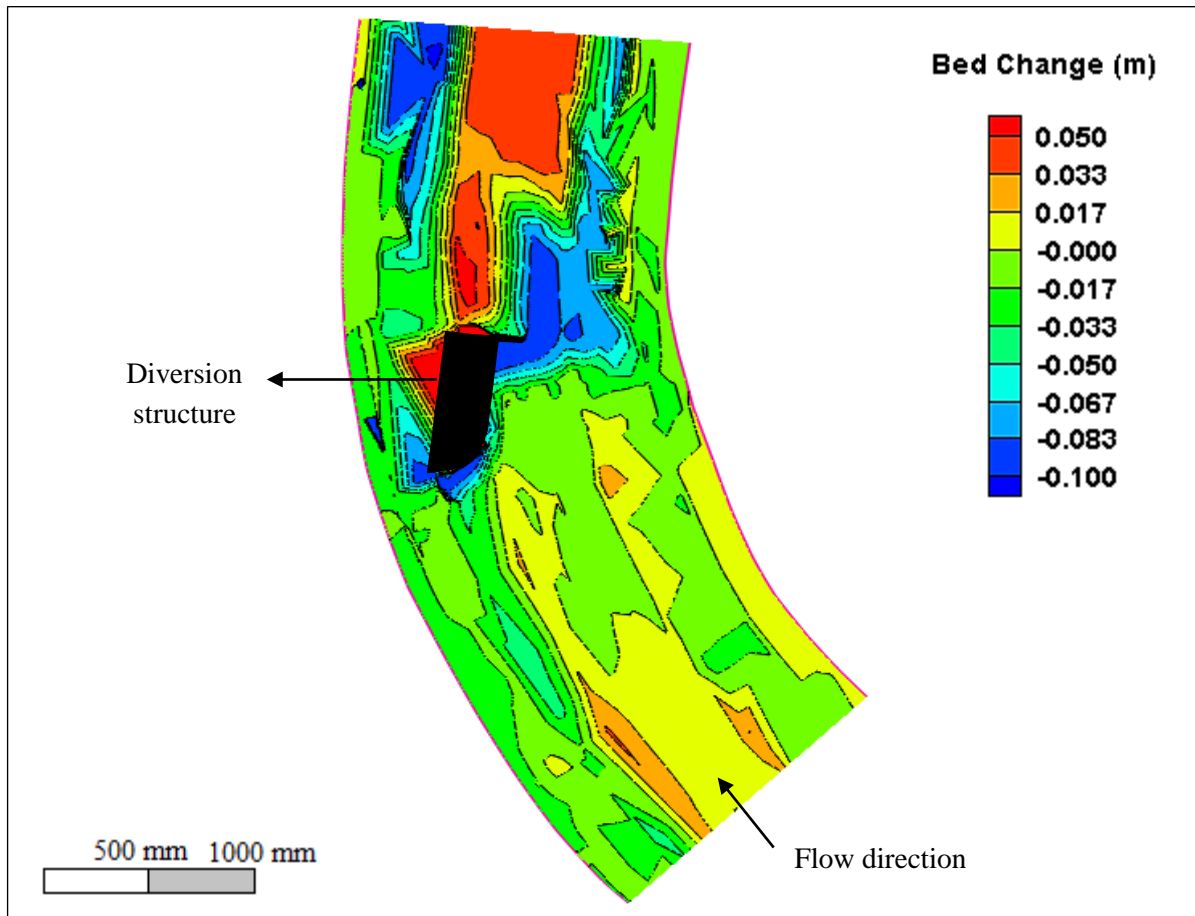


Figure 3.26: Bed change result for physical experiment 5 (30° L-shape structure, $Q = 17.8$ l/s)

The total discharge during this test was 17.8 l/s, with water depths of 94 mm, 35 mm and 101 mm for the measuring points 1, 2 and 3 respectively. A Manning n value of 0.03 was used in this river model. The shallow water at measuring point 2 had a deposition of 43 mm of sediment.

The experiment had lasted three minutes and thirty-eight seconds in total when the scouring reached the bed of the river. Table 3.4 provides the page numbers in Appendix A of the photos taken of the sediment elevation results of the experiment.

This specific angle caused a disruptive action on the opposite river bank. The side slope collapsed as vortices formed around the attachment, causing the inner river bank to deteriorate. This was assumed to occur because the area of flow was narrowing with the attachment, although the vortices and the side slope of the river bed could have caused the sediment slide, as the sediment was scouring at the

toe of the side slope. The deposition of sediment occurring downstream of the intake was as in the previous experiment.

It was observed (see Appendix A photos) that, once again, sediment was not scoured in the centre of the structure. The reason for this must be the downstream L-shaped attachment, which reduces flow velocity upstream of the attachment, ensuring that less sediment is transported. Scouring took place around the attachment and downstream of the attachment, as seen in Figure 3.26, but there was very little scouring in front of the intake. This structure would not be suitable with this specific orientation.

3.4.6 Experiment 6 (45° with flow, 17.2 l/s)

Figure 3.27 illustrates the result of Experiment 6.

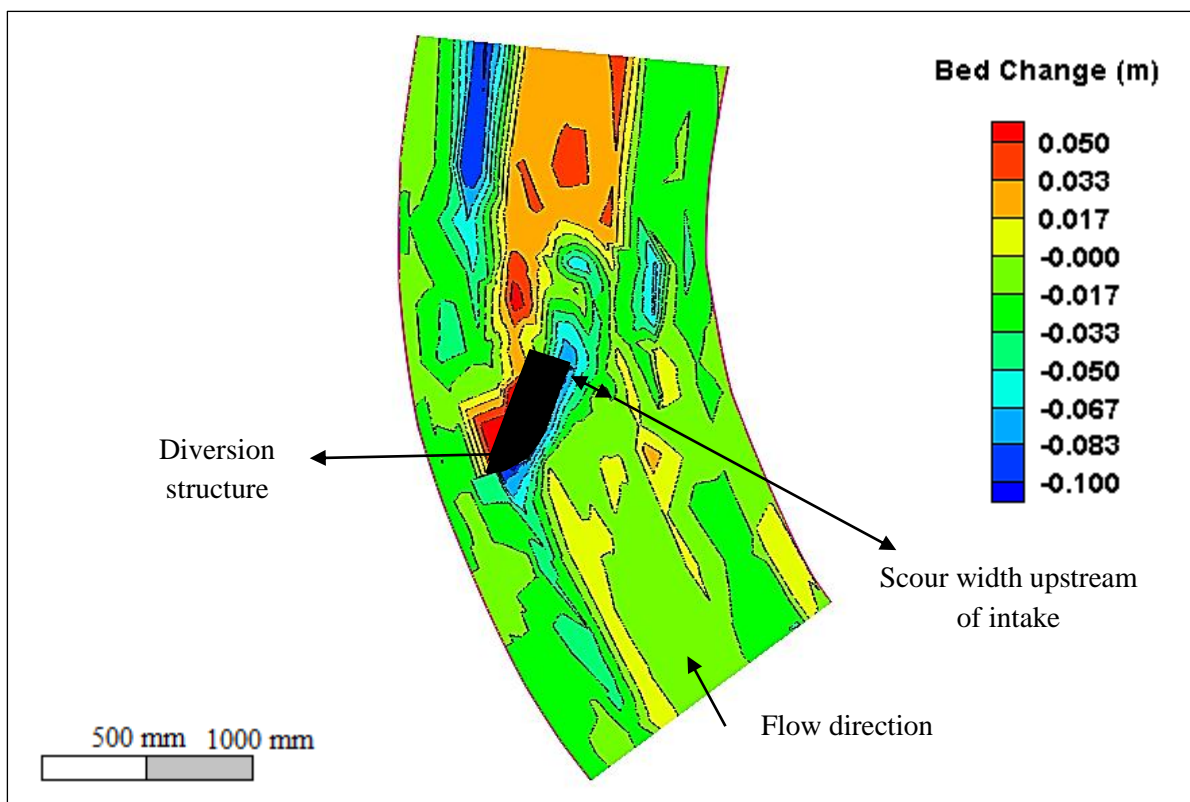


Figure 3.27: Bed change result for physical experiment 6 (45° with flow, $Q = 17.2$ l/s)

The total discharge during the test was 17.2 l/s, with water depths of 74 mm, 43 mm and 100 mm for the measuring points 1, 2 and 3 respectively. A Manning n value of 0.03 was used in this river model. The shallow water at measuring point 2 had a deposition of 27 mm of sediment.

The experiment had lasted four minutes and twenty-eight seconds in total when the scouring reached the bed of the river. Table 3.4 provides the page numbers of the sediment elevation results of the experiment in Appendix A.

It was observed that the structure with this specific angle did not cause a disruptive action on the opposite river bank and the downstream end of the river. Deposition downstream of the structure was to the minimum and would have little, if any, effects on river flow.

Scouring occurs everywhere along the structure, thus providing assurance that the length of the trashrack can stretch from far downstream on the structure, across the structure bend towards the side bank of the river. The problem with the width of scour, as illustrated above, was that there was less scouring in 268 seconds than in experiment 4, thus making the result of experiment 4 the better the two.

3.4.7 Experiment 7 (45° L-shape with flow, 15.5 l/s)

Figure 3.28 illustrates the result of Experiment 7.

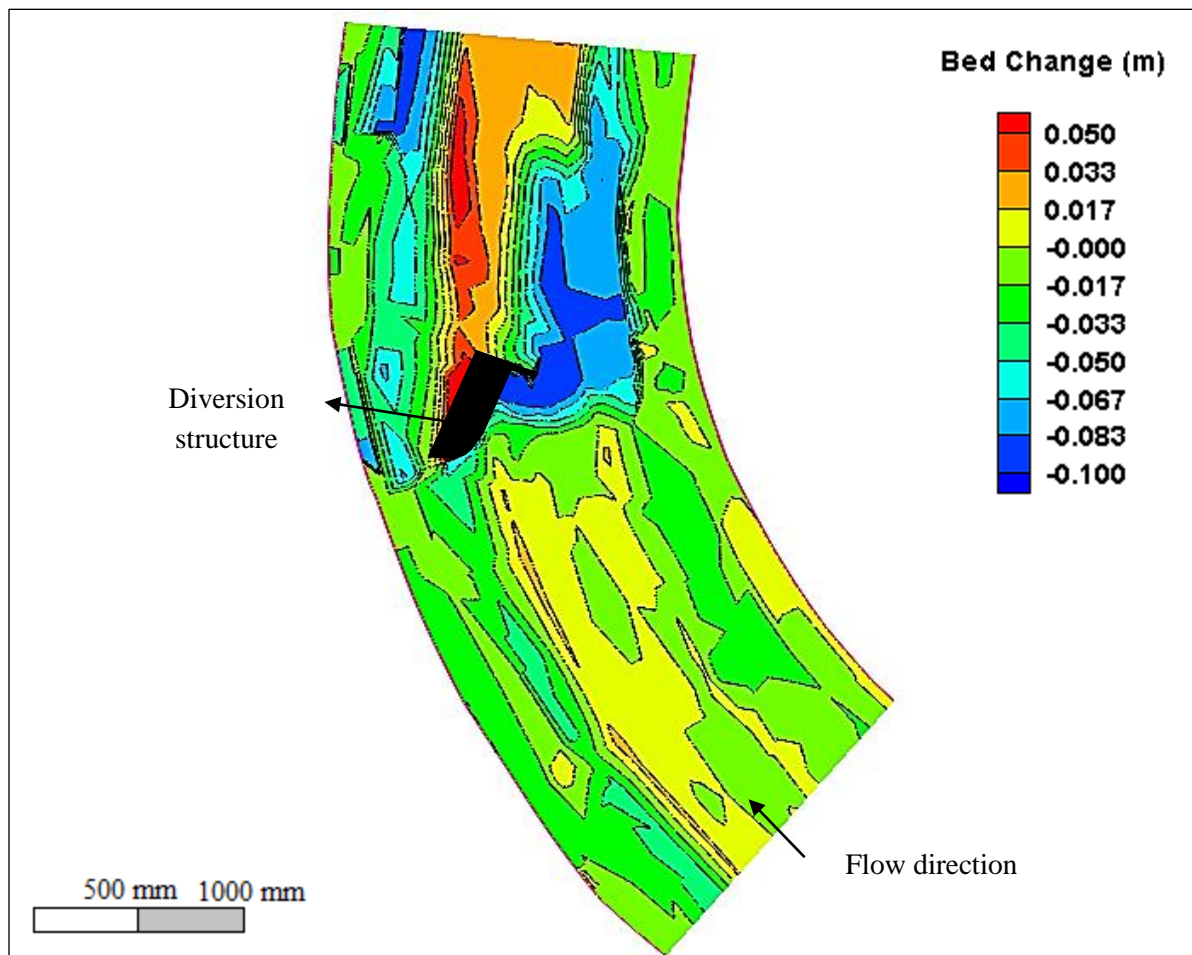


Figure 3.28: Bed change result for physical experiment 7 (45° L-shape structure, $Q = 15.5$ l/s)

The total discharge during this test was 15.5 l/s, with water depths of 78 mm, 60 mm and 100 mm for the measuring points 1, 2 and 3 respectively. The shallow water at measuring point 2 had a deposition of 19 mm of sediment.

The experiment had lasted three minutes and twenty-three seconds in total when the scouring reached the bed of the river. Table 3.4 provides the page numbers in Appendix A of the photos taken of the sediment elevation results of the experiment.

This specific angle caused a disruptive action on the opposite river bank. The side slope collapsed once again, which could have been for the same reason as stated in experiment 5. The deposition of sediment occurring downstream of the intake was as in the previous experiment.

It was observed (see Appendix A photos) that sediment was scoured only around the attachment and downstream of the structure. The reason for this was the L-shaped attachment, which created local scouring around the downstream end of the structure. Another problematic observation was that the scouring was ± 20 mm in front of the intake and for three quarters of the intake length (see Figure 3.28). This would not be a suitable structure with this specific orientation.

3.4.8 Experiment 8 (60° with flow, 18.4 l/s)

Figure 3.29 illustrates the result of Experiment 8.

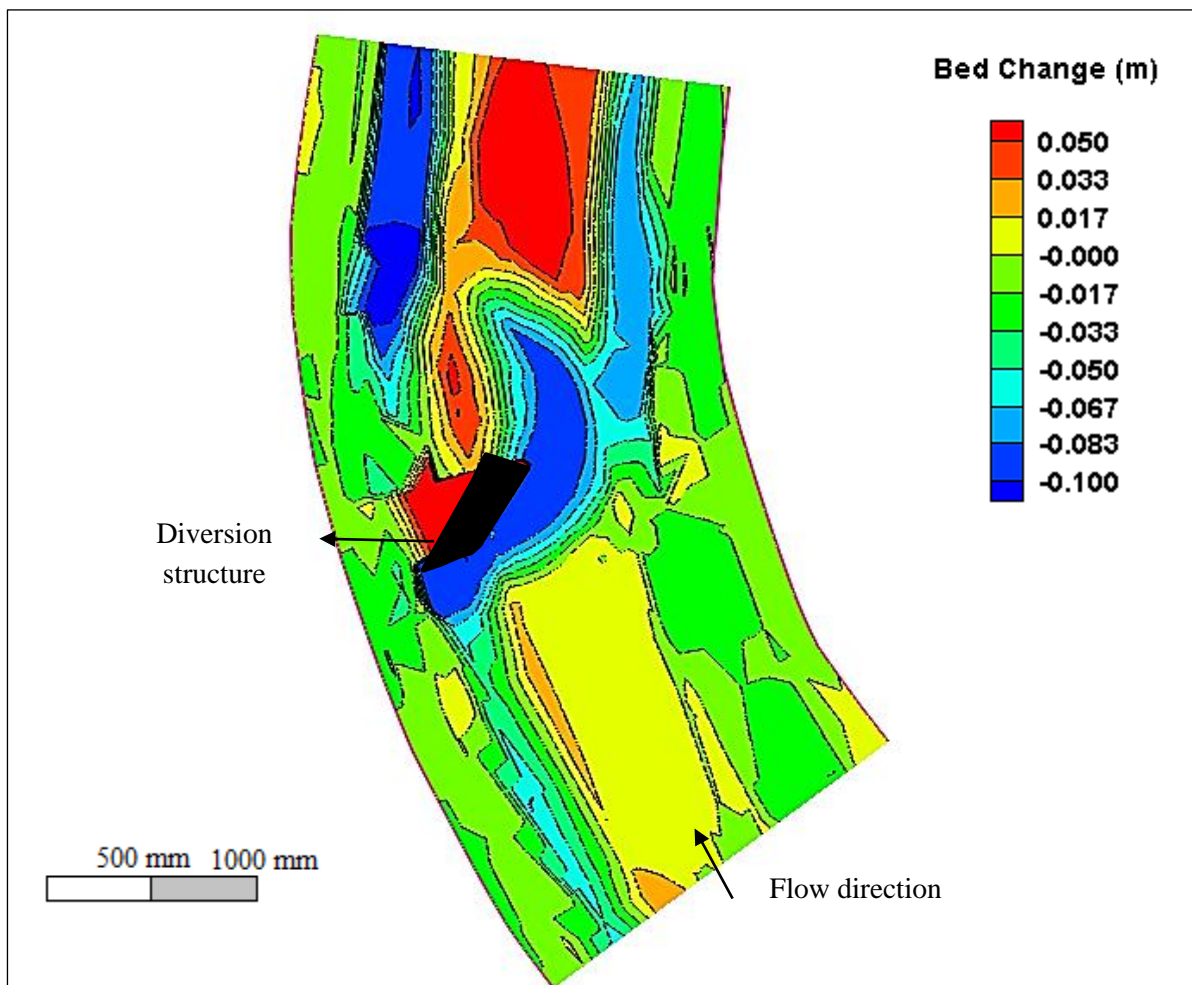


Figure 3.29: Bed change result for physical experiment 8 (60° with flow, $Q = 18.4$ l/s)

The total discharge during the test was 18.4 l/s, with water depths of 80 mm, 31 mm and 100 mm for the measuring points 1, 2 and 3 respectively. A Manning n value of 0.03 was used in this river model. The reason for the shallow water at measuring point 2 was the drastic deposition of 57 mm of sediment.

The experiment had lasted three minutes and forty-three seconds in total when the scouring reached the bed of the river. Table 3.4 provides the page numbers in Appendix A of sediment elevation results of the experiment.

This structure caused the opposite river bank to erode slightly. This would not occur with a wider channel. Deposition in great quantities took place downstream of the intake.

Scouring occurred everywhere along the structure, thus providing the assurance that the length of the trashrack could stretch from far downstream on the structure, across the structure bend towards the side bank of the river. Scouring occurred along the entire bottom width of the river bed and thus provided a great area of erosion to ensure clean water upstream of the intake.

This structure also provided a slight damming of water upstream of the structure, which was observed during the physical run. This will provide efficient head, as a weir is not present in this design. This structure and orientation provided excellent results and would be considered as an optimal design.

3.4.9 Experiment 9 (60° L-shape with flow, 15.5 l/s)

Figure 3.30 illustrates the result of Experiment 9.

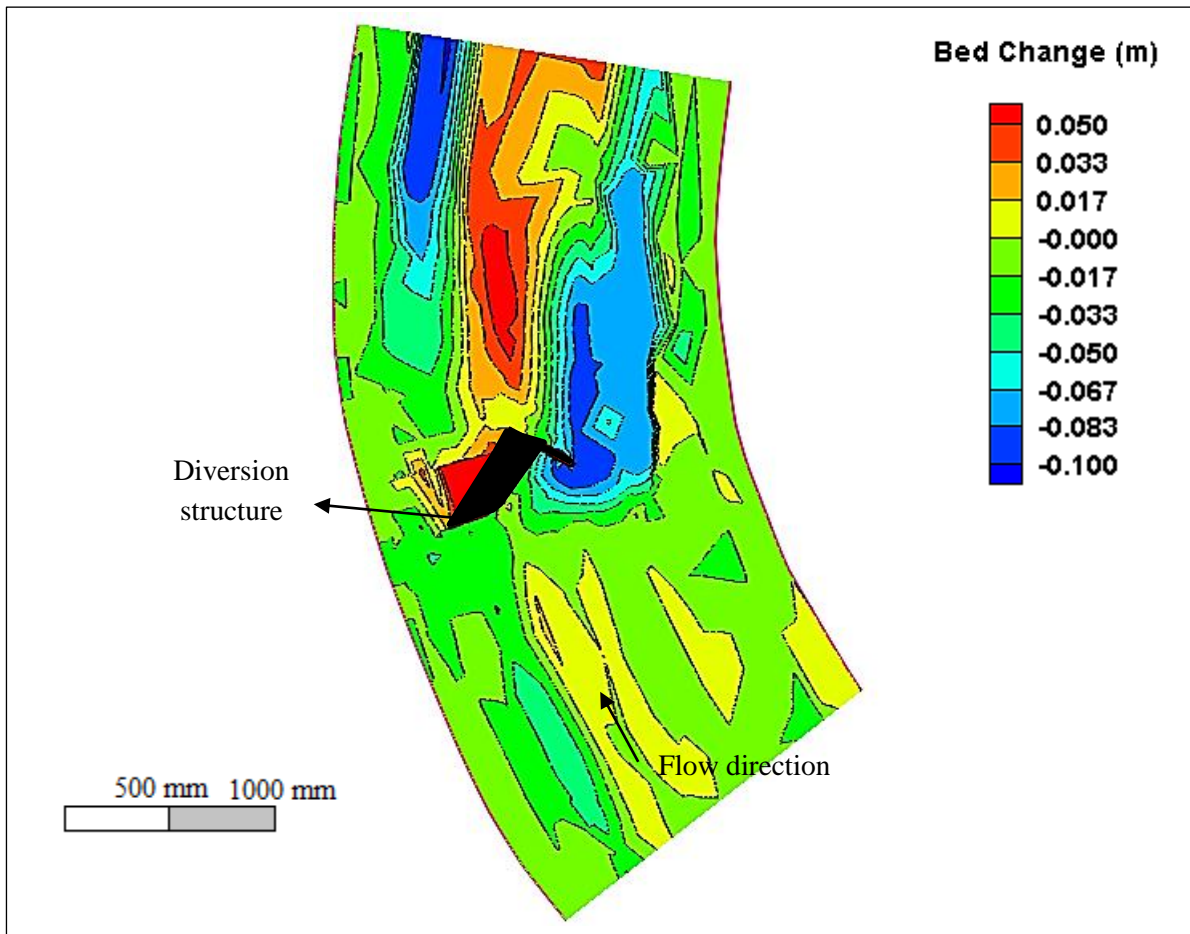


Figure 3.30: Bed change result for physical experiment 9 (60° L-shape structure, $Q = 15.5$ l/s)

The total discharge during this test was 15.5 l/s, with water depths of 86 mm, 41 mm and 99 mm for the measuring points 1, 2 and 3 respectively. The shallow water at measuring point 2 had a deposition of 46 mm of sediment.

The experiment had been in progress three minutes and fifteen seconds in total when the scouring reached the bed of the river. Table 3.4 provides the page numbers in Appendix A of the photos taken of the sediment elevation results of the experiment.

This specific angle caused a disruptive action on the opposite river bank. The side slope collapsed, possibly for the same reason as that stated in experiments 5 and 7. The side slope collapsed for the length of the scour downstream of the attachment.

It was observed (see Appendix A photos) that sediment was scoured only around the toe of the downstream point of the L-shaped structure. The reason for this was the L-shaped attachment, which created local scouring around the downstream end of the structure. A problematic observation was

that scouring was not taking place (see Figure 3.28). This would not be a suitable structure with this specific orientation.

3.4.10 Experiment 10

The experiments that follow are dependent on the diverted discharge ratio (DDR). Figure 3.31 illustrates what heads (H) were measured at which section of the diversion model. The length of the intake was 515 mm at different intake opening heights (H2). Experiment 10 was an optimised experiment, with the best possible diversion location and diversion angle according to the physical results from Chapter 3 and the numerical results from Chapter 4.

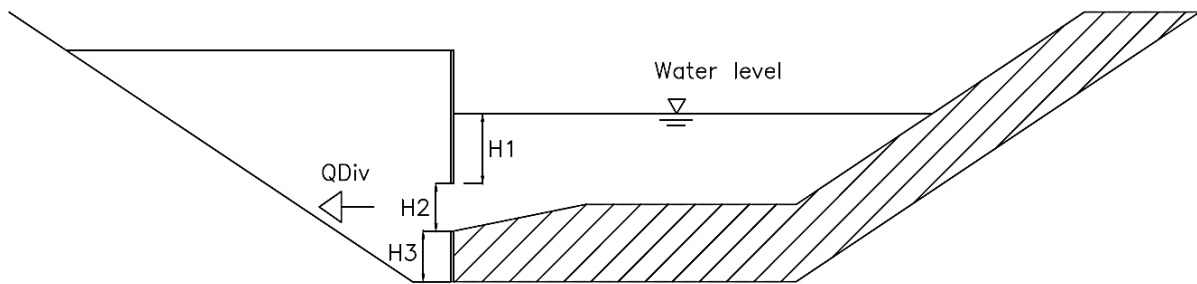


Figure 3.31: Head details of experiment 10 series

These concentrations and DDRs are compared at different river flows and intake positions. All the experiments used the same pump, which had a maximum pump discharge flow of 5 l/s. Not all the sediment was able to pass through the pump during the physical test. The sediment would settle and clog in some sections and this had to be accounted for. Possible sediment losses were:

- Sediment was immovable or clogging in piping
- Sediment passing the filter or settling in the pump
- Not accumulating all the sediment in the structure

Thus, to ensure that the sediment lost during the test runs was not a problem, a filter was placed on the downstream end of the pump. After each test run, river flow or diversion flow, the pump was flushed with clean water. This would ensure that, if there was a loss of sediment, it could be accounted for and added to each experiment as needed. On average, the sediment loss factor was 5.24% and this was added to all the sediment sample weights. Table 3.3 provides the adjusted weight of each test.

Table 3.3: Weight adjustment

Avg. Factor	5.24%	
Test	Weight (g)	New weight (g)
10A1	4.94	5.20
10A2	6.93	7.29
10A3	2.51	2.64
10A4	53.75	56.57
10A5	13.10	13.79
10B1	592.26	623.30
10B2	1353.10	1424.02
10B3	561.23	590.64
10C1	640.31	673.87
10C2	634.01	667.24
10C3	529.67	557.43
10C4	410.97	432.51
10C5	385.27	405.46
10D1	640.31	673.87
10D2	335.13	352.69
10D3	592.26	623.30

3.4.10.1 Experiment 10A (Sediment Load Test without Structure)

The 10A series of experiments was mainly sediment load tests where only the sediment load of the bed load movement was measured. Equation 2-7 in section 2.1.3.1.3 was used to calculate the sediment load in the river. Equation 2-7 was derived to provide the load per metre width and thus offer a result on any river width.

This experiment was executed with a filter bag, 500 mm long, connected to a 100 mm by 100 mm square frame rod (see Appendix B, pp. B-b). This structure was placed on the sediment bed and kept at a constant depth during the test run. A brief description of each individual experiment is provided below, followed by the results and result details. For any specific details, consult Table 3.5.

3.5.10.1.1 Experiment 10A 1 (DDR = 0.0)

Using a 1.4 l/s river flow, the sediment started to move only after 10 minutes of run time. With this in mind, the total sediment load was mainly washed-up bed load in the filter bag, while most of the bed load sediment scoured around the square frame. This test resulted in a 68.14 mg/s.m sediment transport load with a physical depth of 0.025 m.

As ripples on the channel bed did not form with this low flow, it led to the difference in water depths (see Table 3.5). As far as the secondary flow is concerned, it could not be developed fully, as this depth of flow was very shallow. An observation was made that the location of maximum scour was 30° into the turn.

3.5.10.1.2 Experiment 10A 2 (DDR = 0.0)

Using a 1.9 l/s river flow in this experiment, the sediment movement was fair and more than that of experiment 10A 1. Once again the ripples did not form with this low flow and it was concluded that the Manning n value had been chosen incorrectly. As far as the secondary flow was concerned, it was not yet fully developed in this case, possibly because of the shallow depth of flow. This test resulted in a 182.33 mg/s.m sediment transport load.

The location of scour was over a distance in this experiment. This was observed to be between 30° and 60° , with the location of maximum scour at $\pm 45^{\circ}$ into the turn. According to the literature, this is a relevant distribution of scour location.

3.5.10.1.3 Experiment 10A 3(DDR = 0.0)

The 2.4 l/s river flow in this experiment led to little sediment movement. The sediment that moved started moving fast on the outside bend and very slowly on the inside, forming wave-like actions scouring the outside bend and depositing sediment on the inside bend. This could be the changing point between no secondary flows and pre-secondary flow. This test resulted in a 31.33 mg/s.m sediment transport load.

The location of scour was at two distinct positions in this experiment. It was observed to be between 45° and 55° , but with the location of maximum scour at $\pm 55^{\circ}$ into the turn. This could be proof that the location of scour changes accordingly as the flood or flow increases.

3.5.10.1.4 Experiment 10A 4 and 10A 5 (DDR = 0.0)

The river flow in this experiment was 5.9 l/s and 18.5 l/s. Sediment movement was very visible and secondary current was easily spotted. This was near fully developed secondary flow, as it was not yet full bank flow in the river. These tests resulted in a 741.4 mg/s.m and a 653.4 mg/s.m sediment transport load.

The maximum scour was at 60° into the turn. SC and CHES (1992) were correct in this case, and this could be used when river flows are fully developed.

3.5.10.1.5 Results

The figure below starts with the lowest flow of 1.4 l/s on the left (A1) and ends with the highest flow of 18.5 l/s (A5) on the right. The graphs of experiment series 10A are as follows:

- Figure 3.32: Load of sediment diverted (mg/s.m) at different river flows (m^3/s)

According to Figure 3.32, the river flow results between 1.4 and 2.4 l/s can be very unpredictable, as the secondary flow has not developed fully. What is understood from the rest of the graph is that the sediment load will reach a maximum after a flow of 5.9 l/s and level out as the flow increases. Thus, as the flow increases the secondary flow increases, ensuring that the sediment moves past the possible position of abstraction, minimising bed sediment for abstraction.

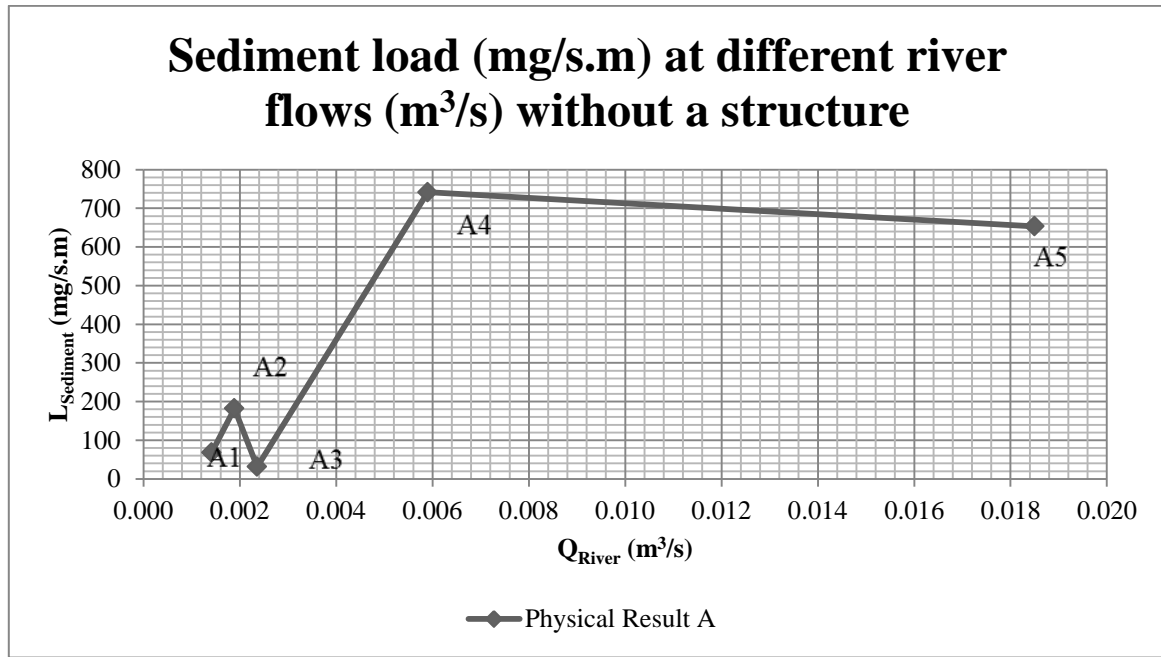


Figure 3.32: Sediment loads (mg/s.m) at different river flows (m³/s) without a structure on the outside of the channel bend

The final conclusion for this experiment series is that the sediment load will reach equilibrium after 5.9 l/s.

3.4.10.2 Experiment 10B (Concentration Test with Greater Diversion Flows)

The 10B series of experiments is mainly concentration tests in which the intake area was increased, leading to an increase in diverted discharge. Equation 2-8 in section 2.1.3.1.4 was used to calculate the sediment concentration through the intake opening. Equation 2-8 was derived to provide the concentration for different diversion discharge ratios (DDR) and sediment diversion ratios (SDR).

This experiment was executed with a pump that was forced to divert 0.7 l/s, 0.9 l/s and 1.2 l/s. The dimensions and details of each experiment can be found in Appendix B, pp. B-d. The structure was placed 60° into the bend. A brief description of each individual experiment is provided below, which is followed by the results and a discussion. For any specific details, consult Table 3.5.

3.5.10.2.1 Experiment 10B 1 (DDR = 0.3)

Using a constant channel flow of 2.4 l/s, the sediment movement occurred as expected. The 1:5 slope in front of the intake ensured that less sediment was flushed into the intake (see Figure 3.33). After the experiment was completed, a large volume of sediment deposited in front of the intake (see Figure B-8). This deposition could cause constant sediment inflow into the inlet and should be a major concern. If the 1:5 prevention slope in front of the intake had not been prepared, the sediment load could have been more.

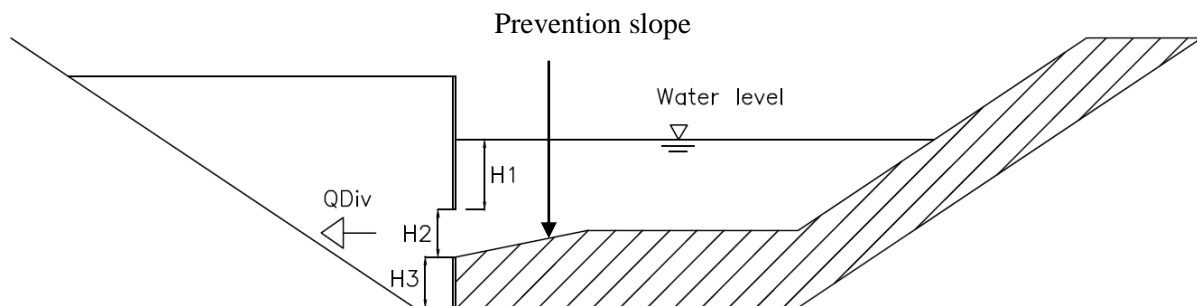


Figure 3.33: Prevention slope of 1:5 in front of diversion intake

Secondary flow occurred at a small scale, as expected. The water depth at measuring point 2 was 31 mm, because a constant flow of 0.7 l/s was diverted, ensuring that the downstream river flow decreased. The sediment diversion ratio (SDR) for the specific DDR was 17.7%. At measuring point 2, the sediment deposited was 14 mm thick and this could be the cause of all the sediment being flushed away from the intake.

3.5.10.2.2 Experiment 10B 2 (DDR = 0.4)

The experiment had a 2.4 l/s river flow and a diversion flow of 0.9 l/s. The sediment in front of the intake was scraped at a slope of 1:5 to ensure that less sediment would be flushed into the intake.

After the experiment was completed it was once again obvious that the sediment would not scour away, as the sediment settled at the intake level (see Figure B-12). The upstream end of the structure scoured flawlessly, ensuring sediment free water at the bend of the structure.

The water depth at measuring point 2 was 17 mm and could have been caused by the DDR increasing. At measuring point 2, the sediment deposited was 4 mm thick. The deposition was so little because the water level was so shallow and 40% of the river flow was diverted. Scouring at the intake was at a bare minimum and this should be considered when recommendations are made. The sediment diversion ratio (SDR) for the specific DDR was 18.4%.

3.5.10.2.3 Experiment 10B 3 (DDR = 0.5)

This experiment had a 2.4 l/s river flow and a diversion flow of 1.2 l/s. During the experiment the sediment rushed through the intake and never reached equilibrium. The sediment scour at the intake was similar to that of experiment 10B 2. After the experiment had been completed, a small flow through the river illustrated that the scour hole in front of the intake would fill and the sediment level increased to the intake level (see Figure B-16).

The water depth at measuring point 2 was 16 mm and this was caused by the DDR increasing. At measuring point 2, the sediment deposit was 10 mm thick. The deposition was more than that in 10B 2, but still had the same result of the water level decreasing as the DDR was 50%. Scouring at the intake was at a bare minimum, and closed up very fast. The sediment diversion ratio (SDR) for the specific DDR was 18.4%.

3.5.10.2.4 Results

The figures below starts with the lowest diversion flow of 0.7 l/s on the left (B1) and ends with the largest diversion flow of 1.2 l/s (B3) on the right. The graphs of experiment series 10B are as follows:

- Figure 3.34: Concentration of sediment diverted (g/l) at different DDRs, and
- Figure 3.35; Concentration of sediment diverted (g/l) at different intake level heights (m).

Figure 3.34 illustrates that the concentration will increase until equilibrium is reached, when the concentration will level out or decrease as the diversion flow or DDR keeps on increasing. The rule of diversion should always set the environment first and bear in mind that not more than 50% should be diverted at any time. What we can understand from the rest of the graph is that the curvilinear effect and secondary flow will occur and have an effect, even when the diversion rate is increased, although on a smaller scale.

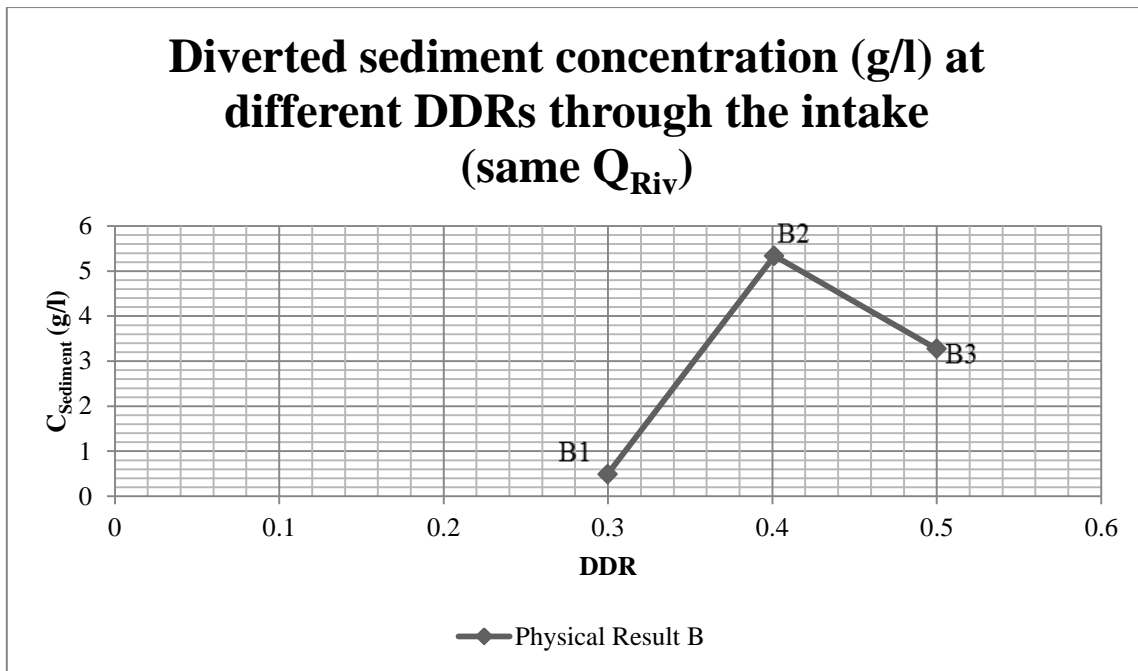


Figure 3.34: Diverted sediment concentration (g/l) at different DDRs through the intake (same Q_{Riv})

Appendix B (p. B-d, p. B-f and p. B-h) illustrates how the intake level changes for each experiment. Figure 3.35 illustrates that the closer the intake level is towards the river bed, the greater the chances are of sediment flowing into the intake. One thing that can be concluded is that, if the intake height level measured from the concrete channel bed (H_3) in front of the intake is very small, there is an assured possibility that the sediment would be flushed into the intake, which will provide a greater amount of sediment through the intake.

This is proved to be an accurate assumption when observing Figure 3.35, and the result that sediment concentration increased when the intake level has dropped. Thus, when the intake level was 37 mm above the river bed (Figure 3.35), the concentration was greater than when the level was at 78 mm.

This was also only possible with the 1:5 (V:H) slope scraping in front of the intake. This should be a set standard in this operation, in order to ensure that the sediment does not drop into the intake when the water is stagnant.

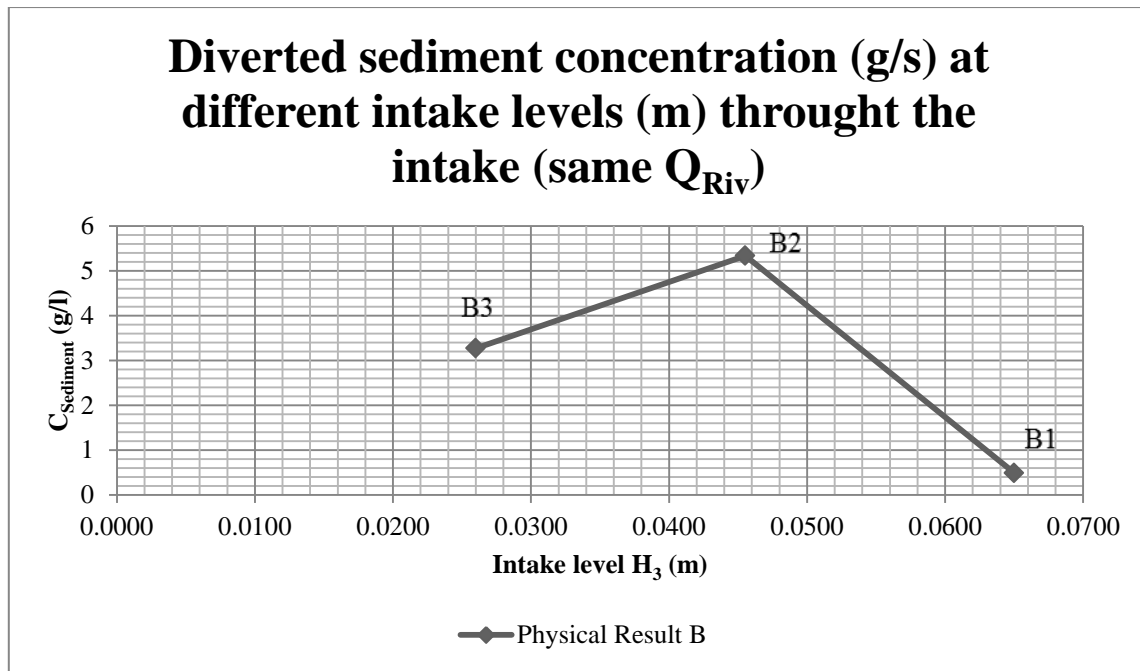


Figure 3.35: Diverted sediment concentration (g/l) at different intake levels (m) through the intake (same Q_{Riv})

3.4.10.3 Experiment 10C (Concentration Test with Greater Flows)

The 10C series of experiments is mainly concentration tests in which the water flow was increased, leading to an increased water level. Equation 2-8 in section 2.1.3.1.4 was used to calculate the sediment concentration of sediment diverted through the intake opening

This experiment was executed with a pump that was forced to divert a constant 0.7 l/s. The dimensions and details of each experiment can be found in Appendix B, pp. B-j. The structure was held in place at 60° into the bend. A brief description of each individual experiment is provided below, then will follow the results and discussion. For any specific details, consult Table 3.5.

3.5.10.3.1 Experiment 10C 1 (DDR = 0.5)

The river flow in this experiment was 1.4 l/s and this provided sufficient sediment movement. The 1:5 slope into the intake ensured that less sediment was flushed into the intake. Although methods of provision were enforced (see Figure 3.33), this still did not prevent sediment from rushing into the intake. One could see that, as the DDR reached 50%, it attracted the sediment that should flush past and deposited it in front of the intake (see Figure B-19). A sediment diversion ratio (SDR) of 24.9% was diverted through the intake. The SDR was calculated with Equation 2-6, where the sediment load diverted was calculated with Equation 2-9 and provided a result of 51.3 g/s.m^2 .

Secondary flow occurred on a small scale and caused minimum scour in front of the intake. The run was too short to see any river deposition and formation of river topography, but it could not continue as the intake was attracting too much sediment. An observation was that no deposition occurred at measuring point 2, and could be because of very little sediment scouring in the river.

3.5.10.3.2 Experiment 10C 2 (DDR = 0.375)

This experiment had a river flow of 1.9 l/s. In this experiment the head above the intake (H1) increased to 13.9 mm. This head above the intake could lead to more clean water being forced into the intake. The sediment diverted in the eleven minute and fifty-nine second test run was very low. The DDR in this test looks a lot better than that of experiment 10C 1. A SDR of 20.8% with a load of 29.3 g/s.m² was diverted, which confirms the statement above of a better DDR result.

Secondary flow started to occur, but it could not develop as fully as one would want and expect. This was the case in experiment 10C 1 as well. The scouring in front of the intake was along the whole intake (see Figure B-23). The water depth at measuring point 2 was 21 mm which was caused by a lower tail water level. At measuring point 2, the sediment deposit was 5 mm thick.

3.5.10.3.3 Experiment 10C 3 (DDR = 0.30)

This experiment had the best concentration to DDR ratio in this series, with a 2.4 l/s river flow. The scour at the bend of the intake was very good, but again led to a dune formation in front of the intake (see Figure B-27). The SDR was 18.9%. Secondary flows occurred perfectly and sediment movement was as expected.

The water depth at measuring point 2 was 42 mm which deeper than the normal flow depth. This was not caused by deposition downstream of the intake, as the sediment deposition at measuring point 2 was only 5 mm thick. It could have been caused by difficulties with the downstream sluice, which did not allow the correct amount of water through. Other than that the experiment was a success.

3.5.10.3.4 Experiment 10C 4 (DDR = 0.12)

This experiment was very successful in the sense that scouring occurred along the whole intake at an acceptable depth (see Figure B-31). As the river reached normal flow there was clean water running through the intake, with only suspended sediment depositing in the intake.

Ripples that determined the Manning value were established and caused no effect on the water depth. The water depth at measuring point 2 was 63 mm, with a deposit of 19 mm thick. Thus, for such a DDR and flow, it can be assumed that the downstream water depth at measuring point 2 was correct. The sediment diversion ratio (SDR) was 13.9%.

3.5.10.3.5 Experiment 10C 5 (DDR = 0.04)

This experiment had an 18.5 l/s river flow and proved that, during a high flow or flood, there would be sufficient scour in front of the intake without the opposite bank sliding or giving way. The section of scour directly in front of the intake was astonishing and proved that, even though slight scouring occurs during small flows, there will always be a bigger flow to clean the whole section once again. This flow and orientation of the structure provided a SDR of 7.4%, which was the best result.

A deposition of 40 mm took place at measuring point 2. This supplies an efficient river bank downstream to ensure that the flow velocity is reduced, which decreases sediment movement upstream of the bank. This bank was formed after the section in front of the intake has been scoured clean. This bank was formed from the sediment scoured and flushed away from the intake, thus providing a clean water dam effect in front of the intake.

3.5.10.3.6 Results

The figure below starts with the lowest river flow of 1.4 l/s on the right (C1), with a DDR of 50%, and ends with the biggest river flow of 18.5 l/s (C5), with a DDR of 3.8%. The graphs of experiment series 10C are as follows:

- Figure 3.36: Concentration of sediment diverted (g/l) at different DDRs, and
- Figure 3.37: Sediment concentration (g/l) at different heads above intake (m),

In this series of experiments, the diversion flow rate was kept at a constant 0.7 l/s. The river flow was thus increased, with the water level as explained in Table 3.5. The figure above has the greatest flood, C5, at the left of the graph, with an 18.5 l/s river flow and a DDR of 3.8%. This is then followed by a river flow of 5.9 l/s, with a DDR of 12%, and ends on the right with a river flow of 1.4 l/s and a DDR of 50% (C1).

Figure 3.36 illustrates that the concentration increases as the DDR increases. C1 on the graph had such a high concentration for the reason that secondary flow had not yet developed and sediment was being attracted to the intake, as the DDR was 50%. The graph then illustrates exactly what is expected and the concentration decreases as the DDR reduces. C4 has a much smaller DDR of 12% and, as the secondary currents are fully developed, this could mean that the suspended sediment was forced into the intake and not flushed past on the inside of the river.

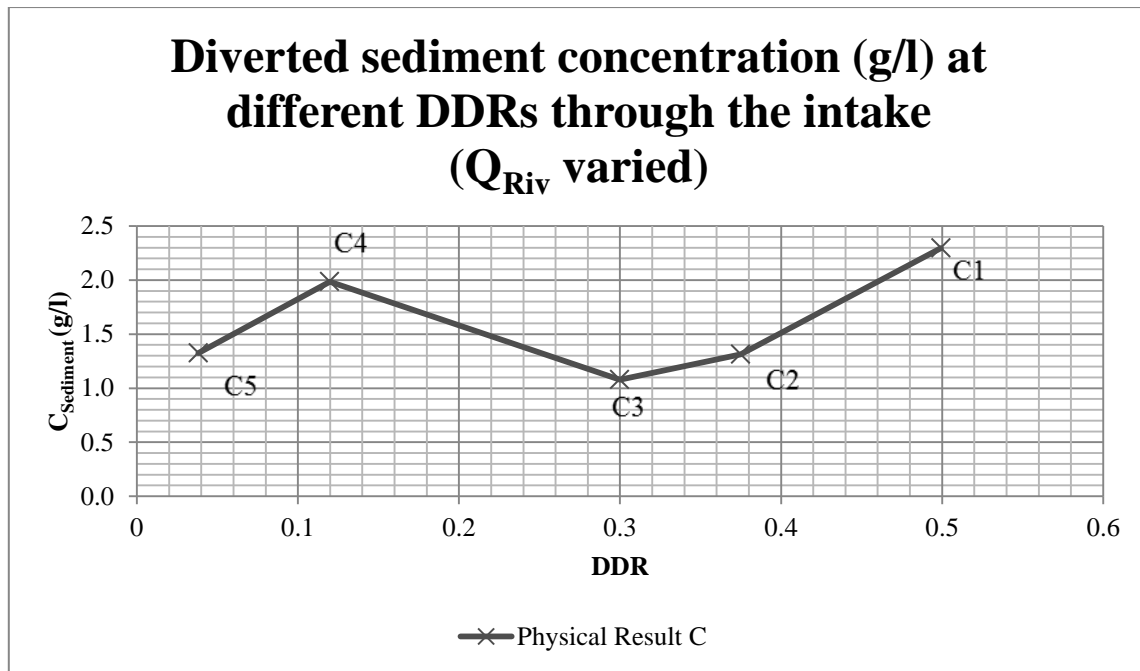


Figure 3.36: Diverted sediment concentration (g/l) at different DDRs through the intake (Q_{Riv} varied)

Experiment C4's channel flow could not flush sediment away in front of the model intake. The sediment upstream of the intake was transported past the diversion intake, which caused a deposition of sediment downstream of the intake. This caused a damming effect, which could be the reason for larger quantities of sediment being diverted.

Experiment C5's channel flow flushed all the sediment away in front of the model intake. The final conclusion was that the concentration at different DDRs is a very important aspect during the change phase of river flow to possible floods and should be considered at all times during the design of RoRs.

From Figure 3.37 the flow depth at C1 to C2 was very shallow and had a small sediment-to-water ratio. The secondary flow current had not developed at all and this proves that more sediment will flush into the intake instead of washing past. That is why the sediment concentration peaked at C1 and then dropped to 1.08 g/l at C3, where the secondary current started coming into play (see Figures 3.39 and 3.40).

From C3 to C5 there was a slight peak in concentration at C4, followed by reduction at C5 once again. As the water head above the intake grew, it was observed that the concentration would keep on growing until a secondary flow was fully developed, not only partially as in C4, although one would expect fully developed secondary currents at C4. From this it can be assumed that the greater the head in front of the intake, the less sediment was abstracted, while the secondary flow will force the sediment past the intake.

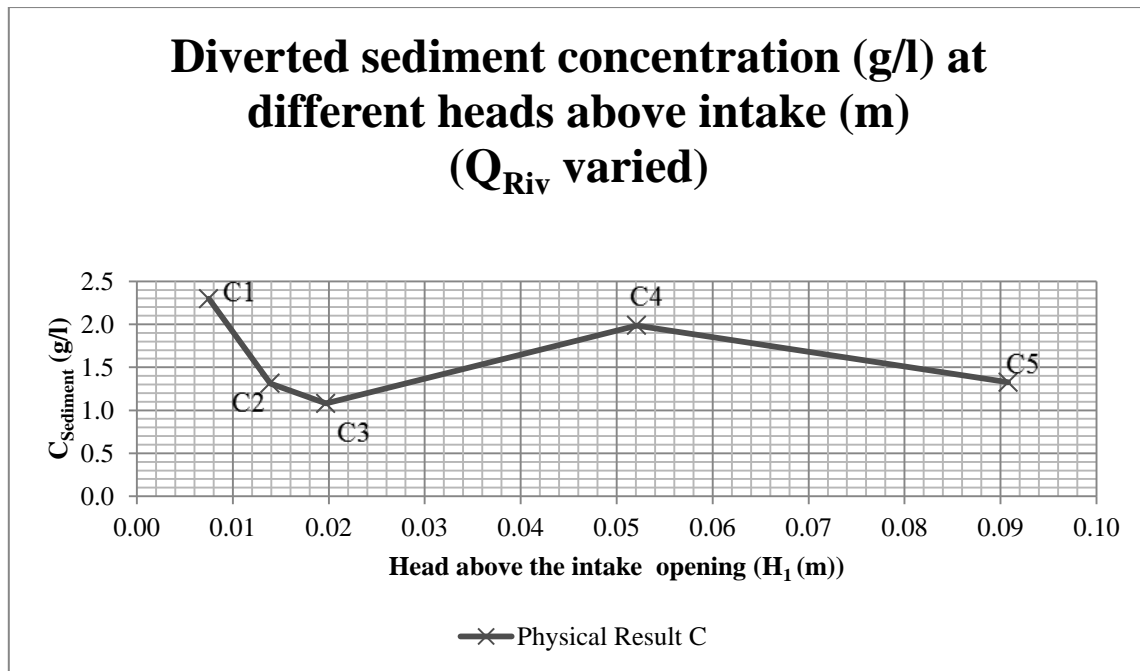


Figure 3.37: Diverted sediment concentration (g/l) at different heads above intake (m) (Q_{Riv} varied)

3.4.10.4 Experiment 10D (Concentration Test, Change of Intake Level)

The 10D series of experiments comprised mainly out of concentration tests in which the intake level was increased away from the bed. The experiment started by testing the furthest away intake level and by cutting out sections the intake level moved closer to the channel concrete bed. Experiment D1, had an intake level of 65.6 mm above the channel bed and had a DDR of 50 %. This DDR attracted the sediment into the intake enforcing a greater concentration. The experiment that followed was D2 with an intake level of 72.0 mm above the channel bed, which ends with experiment D3 at an intake level of 77.8 mm above the concrete channel bed. Equation 2-8 in section 2.1.3.1.4 was used to calculate the sediment concentration through the intake opening

This experiment was executed with a pump that was forced to divert a constant 0.7 l/s. The dimensions and details of each experiment can be found in Appendix B, pp. B-t. A brief description of each individual experiment is provided below. Table 3.5 can be consulted for any specific details.

3.5.10.4.1 Experiment 10D 1 (DDR = 0.5, H_3 = 65.6 mm above channel bed)

The river flow in this experiment was 1.4 l/s and provided efficient sediment movement. A sediment diversion ratio (SDR) of 24.9% was the result. As this test had the same dimensions and outcome as Experiment 10C 1, these two tests were combined in one test to retrieve the same results (see Figure B-39). Thus, all the problems, results and sediment concentrations from Experiment 10C 1 can be consulted on page 3-39.

3.5.10.4.2 Experiment 10D 2 ($DDR = 0.375$, $H_3 = 72.0$ mm above channel bed)

This experiment had a 1.9 l/s river flow. The sediment moved gradually into the intake. The sediment diverted was 335.13 g, but with the loss factor of 5.24% the weight increased to 352.69 g. A sediment diversion ratio (SDR) of 20.0% was the final result. A dune formed in the middle of the intake in this experiment (see Figure B-42) and could have caused the future consistent sediment flow into the intake.

Secondary flow forced the deposition to continue occurring on the opposite side of the intake. If this form of deposition occurred on the opposite bank from the intake, it would force the clean water needed into the intake and attract the sediment to be deposited on that specific side. This is true, as this was the result in Figure 3.37.

3.5.10.4.3 Experiment 10D 3 ($DDR = 0.3$, $H_3 = 77.8$ mm above channel bed)

Using a constant river flow of 2.4 l/s the sediment movement occurred as expected. A sediment diversion ratio (SDR) of 17.7% was the result. As this test had the same dimensions and outcome as Experiment 10B 1, they were combined into one test to obtain the same results (see Figure B-46). All the results from Experiment 10B 1 can be consulted on page 3-36.

3.5.10.4.4 Results

The figure below starts with the lowest river flow of 2.4 l/s on the right (D1) with a DDR of 50 % and ends with the biggest river flow of 18.5 l/s (D3) with a DDR of 30 %. The graphs of experiment series 10D are as follow:

- Figure 3.38: Concentration of sediment diverted (g/l) at different DDRs, and
- Figure 3.39: Sediment concentration (g/l) at different intake level heights (m).

The head above the intake level (H_1) was kept at a constant height of 7.5 mm below the water level. Due to this constant height H_1 the water level had to increase when the intake level increased. Figure 3.38 illustrates that the further the intake level moved away from the river bed the less sediment would flow through the intake. Thus the conclusion was that a greater discharge flow and a higher intake level should be considered during the design of an abstraction structure.

Experiment 10D 1 to 10D 3 had a constant diversion flow with higher intake levels (see Figure 3.39). Thus it was concluded that one would design for an intake level position as far above the river bed as possible.

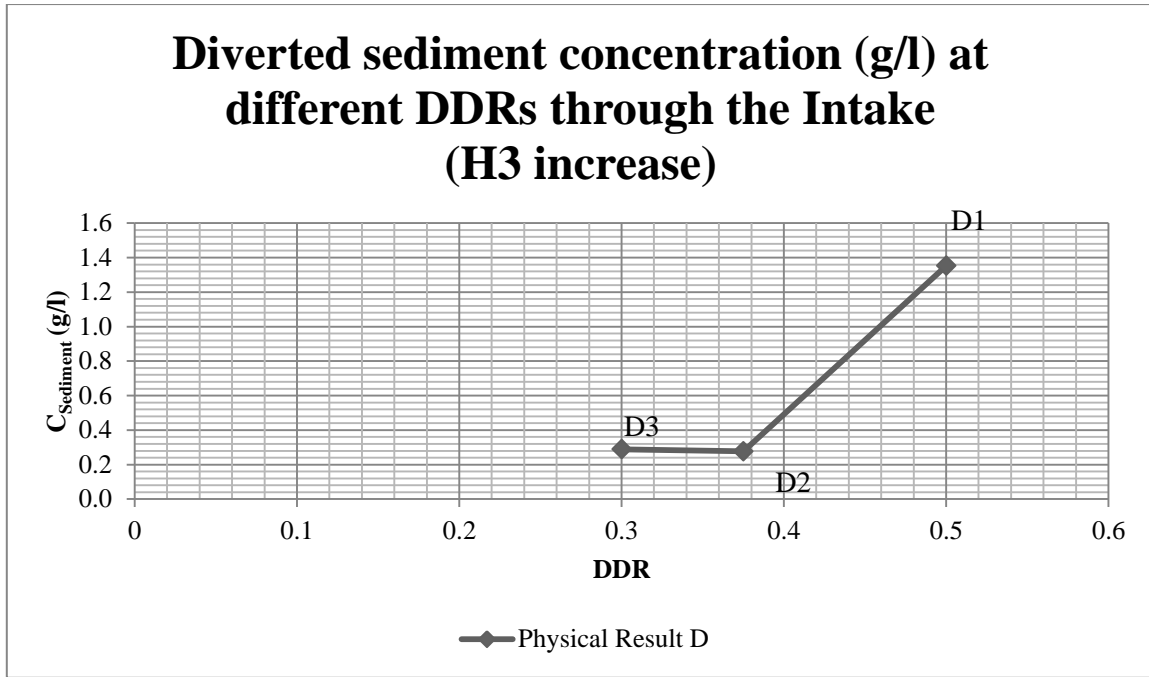


Figure 3.38: Diverted sediment concentration (g/l) at different DDRs through the intake (H3 increase)

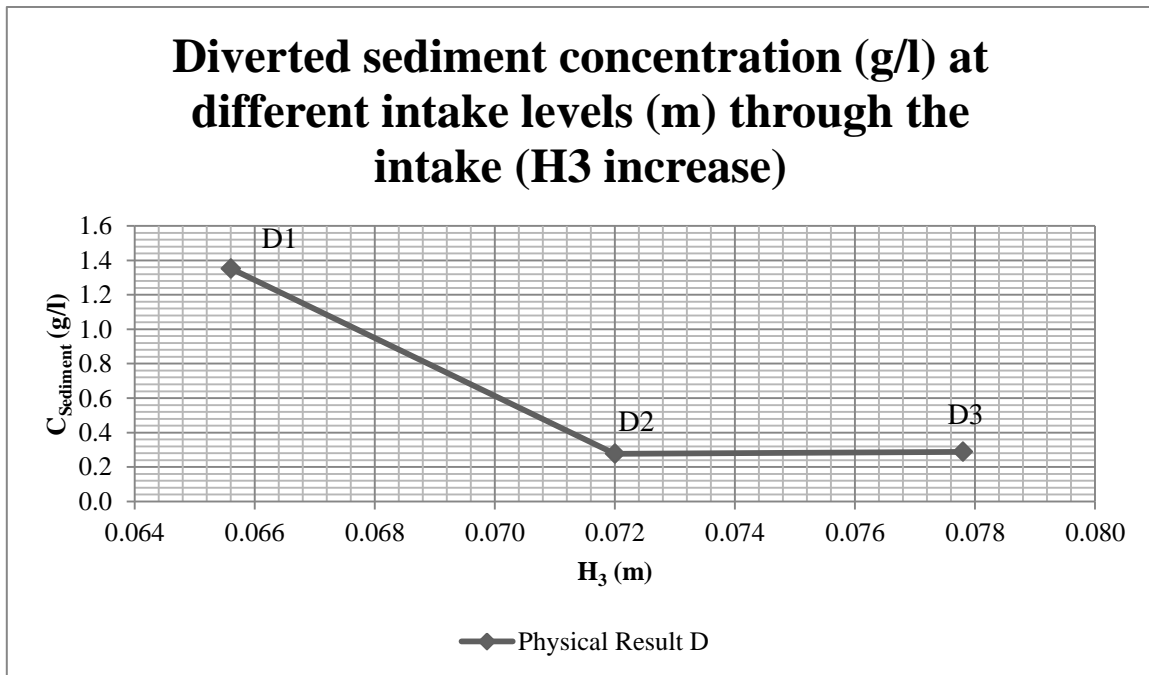


Figure 3.39: Diverted sediment concentration (g/l) at different intake levels (m) through the intake (H3 increase)

Table 3.4: Summary of results of physical experiments 1 to 9

Physical Experiment	Run Time	Flow Q (l/s)	Physical Water Depth (mm)			Note	Page Number		
			Upstream (Measuring Point 1)	Measuring Point 2	Downstream (Measuring Point 3)		Chapter 3	App. A	
1	Without Diversion Structure	570 s	20.0	98 mm	105 mm	110 mm	Manning n = 0.03 Damming of 110 mm downstream	3-18	A-b
2	0° Structure with Flow	180 s	17.5	87 mm	78 mm	101 mm	Manning n = 0.03 Damming of 100 mm downstream	3-22	A-d
3	0° Structure with Flow (L-Shape)	181 s	14.5	76 mm	88 mm	95 mm	Manning changed to n = 0.03	3-23	A-f
4	30° Structure with Flow	216 s	18.8	89 mm	47 mm	100 mm	Sediment deposited 34 mm at Measuring Point 2	3-24	A-h
5	30° Structure with Flow (L-Shape)	218 s	17.8	94 mm	35 mm	101 mm	Deposited 43 mm	3-26	A-j
6	45° Structure with Flow	268 s	17.2	74 mm	43 mm	100 mm	Deposited 27 mm	3-27	A-l
7	45° Structure with Flow (L-Shape)	203 s	15.5	78 mm	60 mm	100 mm	Deposited 19 mm	3-28	A-o
8	60° Structure with Flow	223 s	18.4	80 mm	31 mm	100 mm	Deposited 57 mm	3-29	A-r
9	60° Structure with Flow (L-Shape)	195 s	15.5	86 mm	41 mm	99 mm	Deposited 46 mm	3-31	A-u

Table 3.5: Summary of results of physical experiments 10 A to 10 D

Physical Test	Run Time (s)	Flow Q_{River} (l/s)	Flow Q_{Diverted} (l/s)	Upstream V-notch Head (mm)	Diversion V-notch Head (mm)	DDR	SDR	Physical Values			Page Number	
								Water Depth (mm)			Chapter 3	App. B
								Upstream (Measuring Point 1)	Measuring Point 2	Downstream (Measuring Point 3)		
10A1	763	1.4	0.0	79.1 mm	0 mm	0%	0.00	25.0	40.0	40.0	3-33	B-b
10A2	400	1.9	0.0	88.7 mm	0 mm	0%	0.00	32.0	38.0	42.0	3-33	B-b
10A3	843	2.4	0.0	97.0 mm	0 mm	0%	0.00	42.0	39.0	50.0	3-33	B-b
10A4	763	5.9	0.0	140.0 mm	0 mm	0%	0.00	56.0	88.0	88.0	3-33	B-c
10A5	211	18.5	0.0	221.1 mm	0 mm	0%	0.00	84.0	106.0	118.0	3-33	B-c
10B1	1800	2.4	0.7	97.0 mm	59.9 mm	30%	0.18	34.0	31.0	40.0	3-36	B-d
10B2	282	2.4	0.9	97.0 mm	67.3 mm	40%	0.18	35.0	17.0	35.0	3-36	B-f
10B3	153	2.4	1.2	97.0 mm	73.5 mm	50%	0.19	36.0	16.0	31.0	3-36	B-h
10C1	415	1.4	0.7	79.1 mm	59.9 mm	50%	0.25	29.0	27.0	27.0	3-39	B-j
10C2	719	1.9	0.7	88.7 mm	59.9 mm	37%	0.21	32.0	21.0	21.0	3-39	B-l
10C3	731	2.4	0.7	97.0 mm	59.9 mm	30%	0.19	36.0	42.0	42.0	3-39	B-n
10C4	308	5.9	0.7	140.0 mm	59.9 mm	12%	0.14	62.0	63.0	75.0	3-39	B-p
10C5	433	18.5	0.7	221.1 mm	59.9 mm	4%	0.07	95.0	55.0	113.0	3-39	B-r
10D1	415	1.4	0.7	79.1 mm	59.9 mm	50%	0.25	29.0	27.0	27.0	3-43	B-t
10D2	1061	1.9	0.7	88.7 mm	59.9 mm	37%	0.20	31.0	31.0	31.0	3-43	B-u
10D3	1800	2.4	0.7	97.0 mm	59.9 mm	30%	0.18	34.0	31.0	40.0	3-43	B-w

3.5 Summarised discussion of results

A number of experiments and numerical simulations provided results to establish in what manner a RoR micro-hydropower station should be designed on a river to minimise sediment diversion through the intake.

3.5.1 Sediment diversion

The sediment load and sediment concentration results were determined by diverting water through a designed intake. This design was completed with different outcomes and can be defined as follows:

- Load of bed load in a sinusoidal river without a structure
- Sediment load and concentration at a diversion structure with increasing diversion flows
- Sediment load and concentration at a diversion structure with increasing river flows
- Sediment load and concentration at a diversion structure with change of intake levels

Figure 3.40 shows the SDR versus the DDR. The SDR cannot exceed 1, as the maximum sediment diverted cannot exceed 100%. As the structure was placed in the river to ensure that sediment load intake be kept to a minimum, one can conclude that this structure accomplished this result. The results for physical result B to D illustrate that the greater the flow, the smaller the DDR, and the smaller the DDR, the smaller the SDR.

In Figure 3.40 the physical model results have B, C and D notations.

- Physical Results B; had greater diversion discharges with the same river flows.
- Physical Results C; had a constant diversion discharges, but had different river discharges.
- Physical Results D; was a constant diversion discharges with an increasing height above river the river bed.

The data for SDR and DDR calculations are given in Table 3.6 and are presented in Figure 3.40.

Table 3.6: Sediment data for SDRs at specific DDRs

Experiment number	Q_{sDiv} (g/s.m ²)	Q_{sRiv} (g/s.m ²)	$Q_{Diverted}$ (l/s)	Q_{River} (l/s)	DDR	SDR
10 A1	0.00	13.63	0.00	1.42	0%	0.00
10 A2	0.00	28.49	0.00	1.89	0%	0.00
10 A3	0.00	3.73	0.00	2.36	0%	0.00
10 A4	0.00	66.19	0.00	5.90	0%	0.00
10 A5	0.00	38.89	0.00	18.50	0%	0.00
10 B1	10.94	61.65	0.71	2.36	30%	0.18
10 B2	119.67	650.91	0.95	2.36	40%	0.18
10 B3	73.17	387.13	1.18	2.36	50%	0.19
10 C1	51.30	206.34	0.71	1.42	50%	0.25
10 C2	29.32	141.17	0.71	1.89	37%	0.21
10 C3	24.09	127.52	0.71	2.36	30%	0.19
10 C4	44.36	318.80	0.71	5.90	12%	0.14
10 C5	29.58	401.44	0.71	18.50	4%	0.07
10 D1	51.30	206.34	0.71	1.42	50%	0.25
10 D2	10.50	52.34	0.71	1.89	37%	0.20
10 D3	10.94	61.65	0.71	2.36	30%	0.18

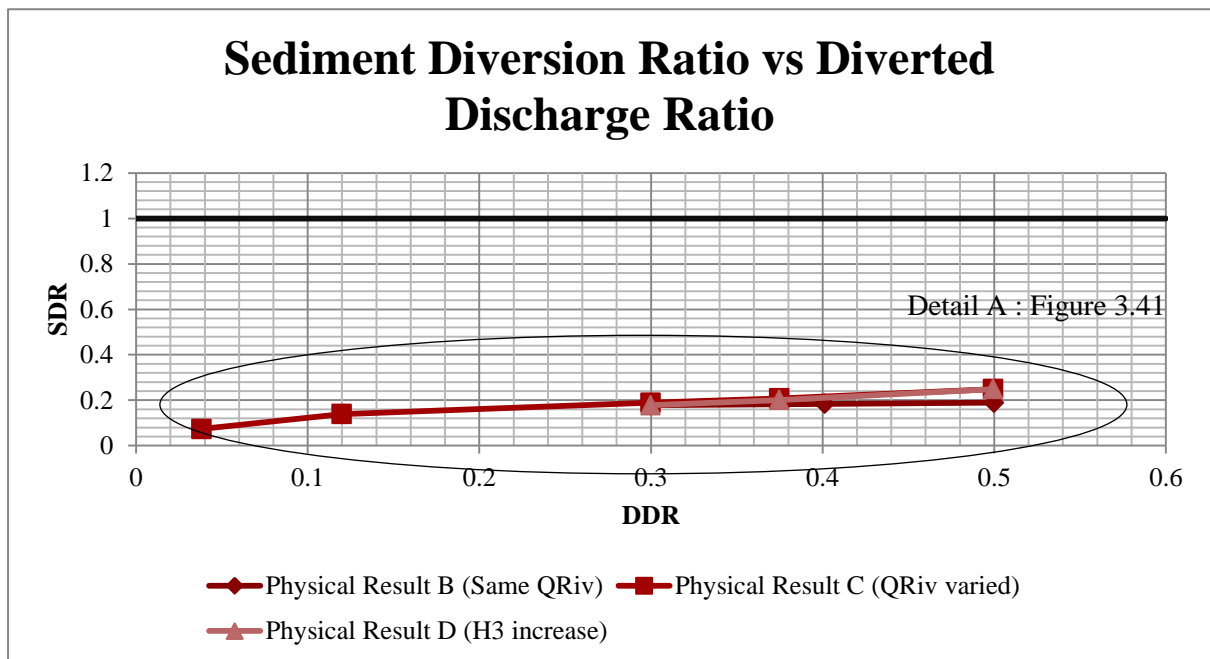


Figure 3.40: Graph of SDR versus DDR

Figure 3.41 illustrates the detailed section A of Figure 3.40. Figure 3.41 illustrates that the further the intake level was from the river bed, the slighter the chance were of that sediment being diverted into the intake. Physical result C5 had the largest flow with the smallest SDR.

The interrelationship between SDR, DF_rR and DDR was illustrated. SDR decreases with decreasing DF_rR and DDR, but is less sensitive compared to the changes in DF_rR and DDR.

Tan (1996) recommended that a DDR of 45% to 50% should be used for rivers in China, whereas Avery (1989) recommended that a DDR of 66% to 77% should be used for rivers in England. Bulle (1926) stated that the optimum diversion angle decreases as the diversion discharge ratio (DDR) increases. Brink et al. (2005) disagree, and concluded that the optimum diversion angle should increase as the DDR increases.

The DDR as a discharge relationship does not provide sufficient evidence of secondary currents developing, or its effect on the SDR result. The DF_rR (diverted Froude ratio) was implemented, as it accounts for more parameters of the channel and includes secondary current as a result. The DF_rR was calculated by the following equations:

$$F_r = \sqrt{\frac{Q^2 B}{g A^3}} \quad \text{Equation 3-10}$$

The Froude number was calculated for the channel and the diversion opening. The opening's Froude number was the discharge flow, as Q (m^3/s), the length of the opening as B (m) and the area of the opening as A (m^2).

The Froude number for the channel is calculated with Chadwick et al.'s (2004) trapezoidal dimension equations. The DF_rR equation is as follows:

$$DF_rR = \frac{F_{r \text{ Diversion}}}{F_{r \text{ River}}} \quad \text{Equation 3-11}$$

where $F_{r \text{ Diversion}}$ = Froude number through intake diversion
 $F_{r \text{ River}}$ = Froude number of river

Figure 3.42 illustrates the SDR vs. equation 3-10's diverted Froude ratio with reference to the DDRs of physical experiments. The DDR values of an individual experiment were observed and linked to the same DDR result of other experiments. This was accomplished for all cases and resulted in parallel lines, as illustrated in Figure 3.42. Although only a small number of experiments were tested and presented, the results in Figure 3.42 showed correlation and provided sufficient evidence to prove that the SDR will decrease as the DDR and the DF_rR decreases.

Figure 3.42 provides the results of a very particular diversion design. The result details are as follows:

- The sediment d_{50} was 0.56 mm
- The angle of orientation for the diversion was 30°
- The flow velocity through the intake was 0.3 m/s
- A radius-to-width ratio of 5.3 was used
- The channel size
- The channel slope was 1:300

Figure 3.42 adapts to detailed changes of the river. For example, if the d_{50} was greater than 0.56 mm, it would result in less sediment movement in the river and less sediment diversion. The SDR would decrease and the whole figure would move closer to the x-axes. If larger river flows are present during a design, the $F_{r \text{ River}}$ could increase and sediment movement could occur more rapidly. Depending on the $F_{r \text{ Diversion}}$ and the DDR, the result would be the figure moving along the x and y-axes.

An example to demonstrate the use of Figure 3.42 was illustrated on the figure. If a design requires a DDR of 0.375 with a specific $F_{r \text{ River}}$, the diverted discharge can be calculated. The general rule of the DDR not exceeding 50% should be satisfied. With the diverted discharge known, the area and Froude of the diversion intake can be calculated. Using equation 3-10, the $D F_r R$ would be calculated. Illustrated on Figure 3.42 the example $D F_r R = 0.15$ and by following the arrow to the DDR, it reflects to the SDR, which resulted in a SDR value of 0.215.

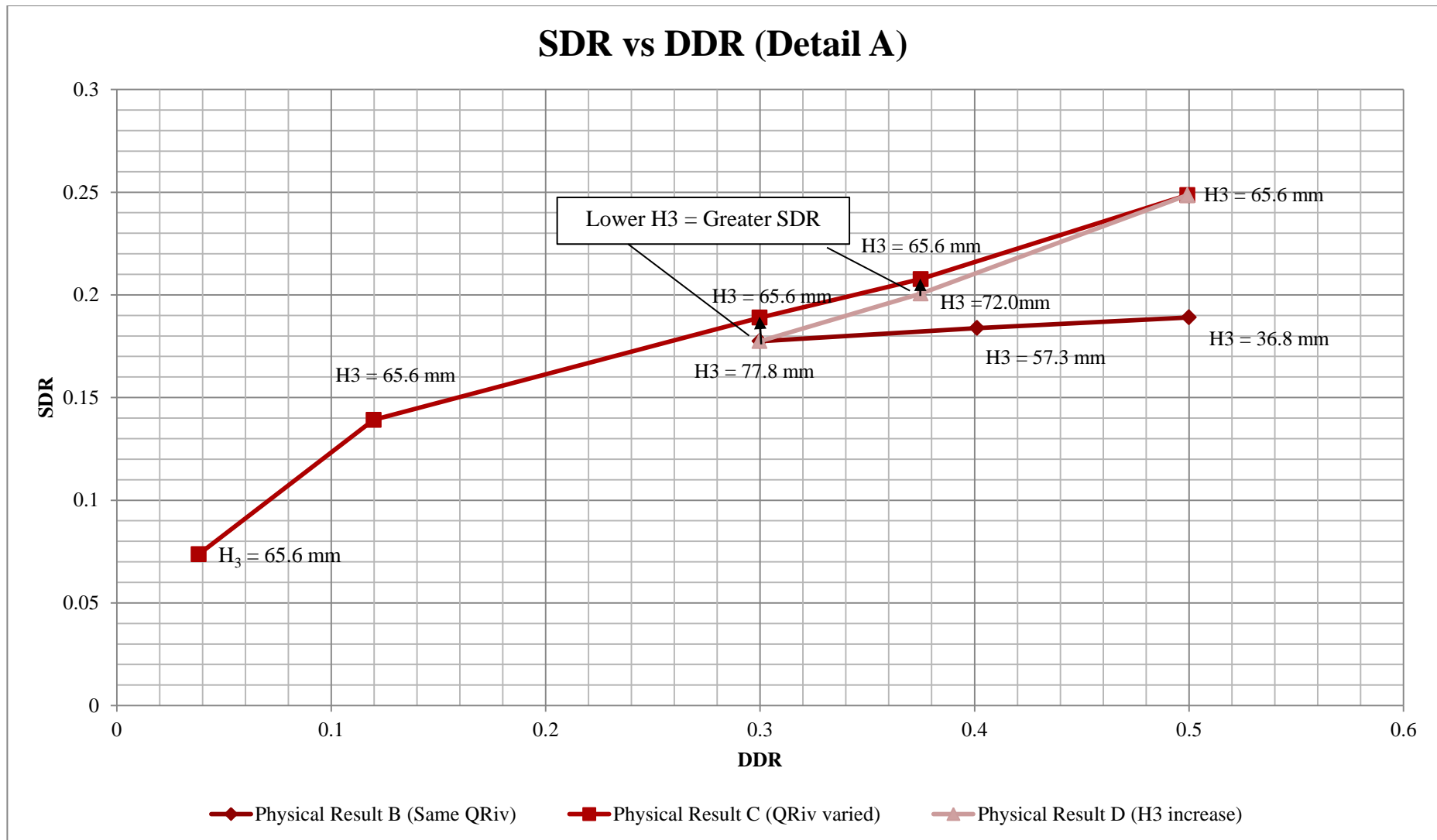


Figure 3.41: Detail A of SDR versus DDR graph

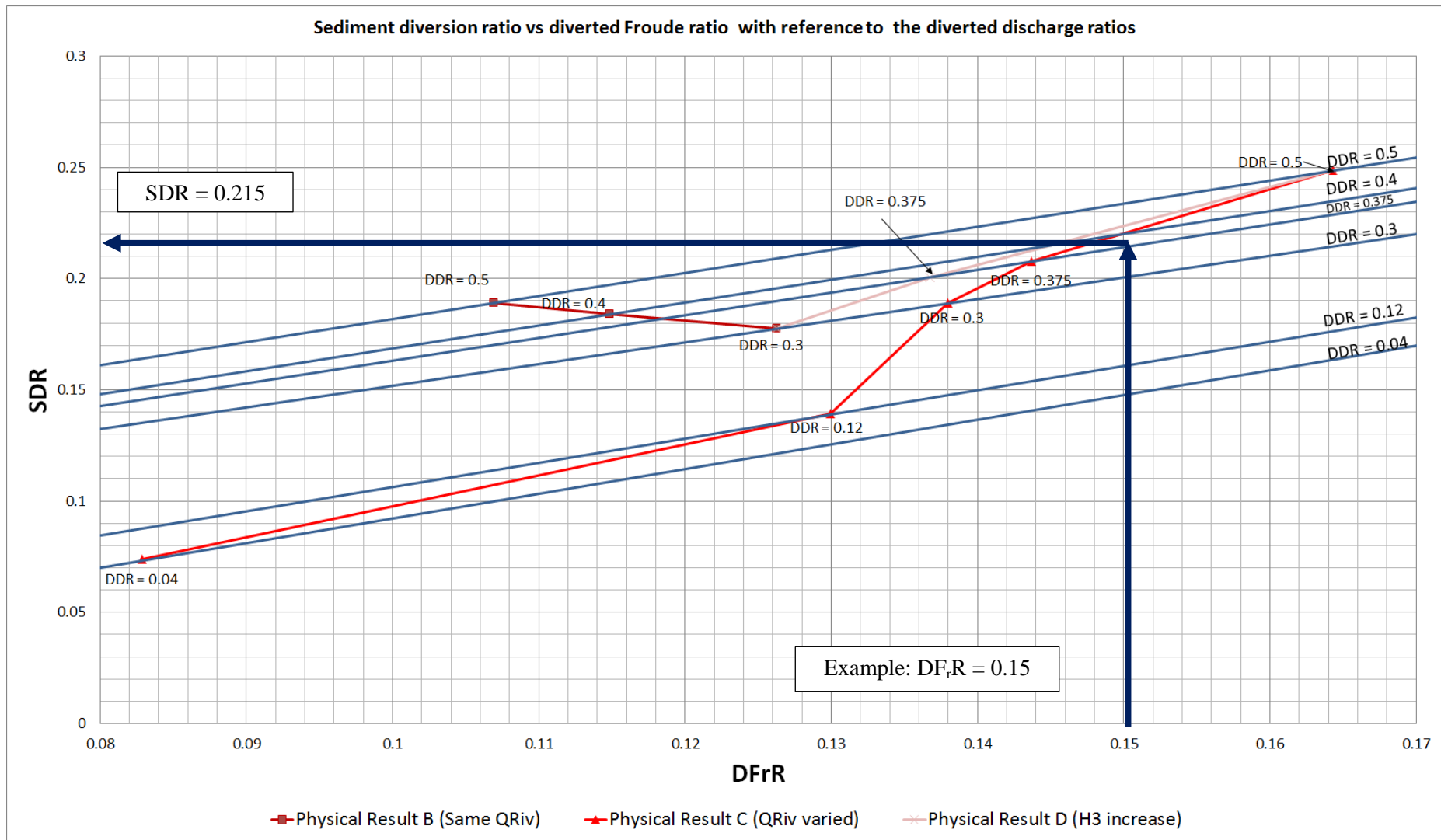


Figure 3.42: Sediment diversion ratio vs. diverted Froude ratio with reference to the diverted discharge ratios

Chapter 4

4. Numerical Model and Data Analysis

4.1 CCHE 2D

The National Centre for Computational Hydroscience and Engineering (NCCHE) makes use of two programs, CCHE-GUI 3.0 and CCHE-MESH 3.0, which are depth-integrated two-dimensional hydrodynamic and sediment transport models: CCHE 2D.

These models can be used for steady and unsteady river flows, and also provide sediment transport functions for hydraulic engineers. The formulations, equations and considerations will be discussed in the chapter describing the 2D model. All the basic mathematics, numerical techniques, hydraulics and sediment transport approaches in CCHE will be discussed in full. For readers interested in reading or understanding the numerical implementation in full detail, the manuals describing CCHE, as well as the following reports, can be consulted:

- CCHE 2D User Manual: Technical Report No. NCCHE-TR-2001-1 (Feb, 2001), Reference: (Jia and Wang, 2001)
- CCHE-GUI User Manual: Technical Report No. NCCHE-TR-2006-02 (Feb, 2001), Reference: (Zhang, 2006)
- CCHE-MESH User Manual: Technical Report No. NCCHE-TR-2009-01 (Feb, 2001), Reference: (Zhang and Jia, 2009)
- CCHE 2D Sediment Transport Model User Manual: Technical Report No. NCCHE-TR-2001-3 (Feb, 2001), Reference: (Wu, 2001)

Users who intent practising and using CCHE can download the software from <http://www.ncche.olemiss.edu/software>.

4.1.1 Numerical Description of 2D Mesh Generator

The mesh referred to is a representation of a computational domain and should be approached carefully. A domain consists of two kinds of boundaries: the outer boundaries and the inner boundaries. The CCHE-MESH generator is a two-dimensional method combined with a multi-block scheme and is used to generate algebraic meshes.

There are three basic steps involved in the generation of a two-boundary algebraic mesh, (Zhan (2006), Zhang and Jia (2009)).

- Defining the outer boundaries and the inner boundaries by placing the boundary control points.
- Distributing an equal number of boundary points along the top and bottom boundaries. Each pair of boundary points forms a control line (referred to as Jmax nodes) in the y-direction.
- Distributing the internal mesh nodes along the control lines (referred to as Imax nodes) in the x-direction.

The nodal distribution was controlled by using an RL (Ryskin and Leal Method, Zhang and Jia (2009)) orthogonal mesh with smoothness controls, and the bed was interpolated triangularly.

4.1.2 Description of Hydrodynamics

The depth-integrated two-dimensional equations are solved in the CCHE2D model.

Continuity equation:

$$\frac{\partial Z}{\partial t} + \frac{\partial(hu)}{\partial x} + \frac{\partial(hv)}{\partial y} = 0 \quad \text{Equation 4-1}$$

Conservation of momentum in the x-direction:

$$\frac{\partial u}{\partial t} + \mathbf{u} \frac{\partial u}{\partial x} + \mathbf{v} \frac{\partial u}{\partial y} = -g \frac{\partial Z}{\partial x} + \frac{1}{h} \left[\frac{\partial(h\tau_{xx})}{\partial x} + \frac{\partial(h\tau_{xy})}{\partial y} \right] - \frac{\tau_{bx}}{\rho h} + f_{Cor} \mathbf{v} \quad \text{Equation 4-2}$$

Conservation of momentum in the y-direction:

$$\frac{\partial v}{\partial t} + \mathbf{u} \frac{\partial v}{\partial x} + \mathbf{v} \frac{\partial v}{\partial y} = -g \frac{\partial Z}{\partial y} + \frac{1}{h} \left[\frac{\partial(h\tau_{yx})}{\partial x} + \frac{\partial(h\tau_{yy})}{\partial y} \right] - \frac{\tau_{by}}{\rho h} + f_{Cor} \mathbf{u} \quad \text{Equation 4-3}$$

where u and v are the depth-integrated velocity components in the x and y directions respectively; g is the gravitational acceleration; Z is the water surface elevation; ρ is water density; h is the local water depth; f_{Cor} is the Coriolis parameter; τ_{xx} , τ_{xy} , τ_{yx} and τ_{yy} are the depth-integrated Reynolds stresses; and τ_{bx} and τ_{by} are shear stresses on the bed surface (Zhang, 2006).

4.1.2.1 Flow Parameters for Diversion Model

Table 4.3 can be consulted for simulation time(s), time steps(s) and flow parameters for the mesh generated for each specific simulation.

4.1.3 Sediment Transport Description

A brief introduction to CCHE 2D sediment transport is presented here. For details, please refer to the technical report by Wu (2001). Sediment transport modelling in CCHE 2D is based on the equilibrium bed load transport of uniform materials. Non-uniform sediment, non-equilibrium transport and suspended transport will be added to a later version of CCHE. Bed form change which is due to bed

load transport can be calculated with this version of CCHE, while the influence of the secondary flow on sediment motion in a curved channel has been included in the calculations.

4.1.3.1 Total Load

According to the CCHE convention classification, moving sediment is divided into suspended load and bed load along the vertical direction. Bed load is the part of the sediment moving on or near the bed, while the suspended load moves in suspension, which physically occupies the water column along the flow depth above the bed load layer (Zhang, 2006).

The equation used to govern bed load transport is given below:

$$\phi_{bk} = 0.0053 \left[\left(\frac{n'}{n} \right)^{3/2} \frac{\tau_b}{\tau_{ck}} - 1 \right]^{2.2} \quad \text{Equation 4-4}$$

where ϕ_{bk} is the non-dimensional bed load transport capacity, n is the Manning n roughness coefficient for the channel bed, n' is the Manning n coefficient corresponding to the grain size roughness, τ_b is the bed shear and τ_{ck} is the critical shear stress.

4.1.3.2 Initial Conditions

To ensure that a full, detailed result was provided, the complete information necessary for the simulation of sediment transport must be added to the model: information on the sediment properties, sediment transport capacity, non-equilibrium adaptation length and movable bed roughness. The sediment properties include the sediment grain size, specific gravity, grain shape factor (default value: 0.7) and bed material porosity. The sediment transport capacity, non-equilibrium adaptation length and the movable roughness are determined by empirical formulas.

4.1.3.3 Empirical Formulas

Formulas are available for fractional non-cohesive sediment transport. The CCHE model provides five modules capable of accounting for the hiding and exposure effect. The sediment transport capacity that is available to determine the transport formulation includes Van Rijn's formula, Wu et al.'s formula, the SEDTRA module, the modified Ackers and White formula, and the modified Engelund and Hansen formula (Wu, 2001). The effects of secondary flow on the main flow and sediment transport in curved channels have also been considered. The Wu et al. method was chosen as it accommodates more than one particle size.

Wu et al. (2001) provided the transport formulation used in the current diversion model and this can be found on pages 17 to 19 in the CCHE 2D Sediment Transport Manual.

4.1.3.4 Sediment Parameters for Diversion Model

Table 4.1 introduces the sediment parameters and properties used in all numerical simulations of the diversion structure.

Table 4.1: CCHE 2D properties for all simulations

CCHE sediment parameter	Description	Value assigned
Modelling period	Length of simulation	Table 4.3
Time step	Length of calculation iteration	0.1 seconds
Boundaries	Water levels and discharge	Table 4.3 and discharge level was 100 mm deep
d_{50} of sediment	Size of sediment	d_{50} of 0.56 mm was used
Transport mode	Type of sediment movement	Total load as bed load model
Empirical formula used	Theory behind sediment movement	Wu et al. method (Wu, 2001)
Specific gravity		1.3
Manning n value	Roughness of channel	0.03 s/m ^{1/3} for simulation tests 1 to 9 and 0.045 s/m ^{1/3} for simulation tests 10S 1 and 2

4.2 Objective

The objective of the numerical simulation and results was to compare them with the physical results. This will provide sufficient evidence of the agreement between the numerical models and the physical models and give conclusions in relation to the future use of this numerical simulation program.

The most optimal result/s was placed into a wider channel to observe what the flow will do to the sediment movement when the area of flow past the diversion is increased. This will only be tested numerically and will result in concentration experiments, which are explained in full in Chapter 3. Finally, a professional conclusion and recommendation in relation to the specific results and comparisons was provided.

4.3 Numerical Model Calibration

The calibration of the numerical model was prepared with regard to the following aspects. The numerical parameters were changed to ensure that the physical model was represented correctly. Each aspect is explained with relevance to the current numerical model.

- Manning n value

The Manning n value for all the numerical runs was selected as 0.03. Factor differences in the numerical water levels over the physical water levels were 0.96 and 0.94 for measuring points 1 and 2 respectively.

Thus, with the calibration of Manning n values of 0.03 the correct water levels were achieved.

- Water levels

The downstream water level was held at a constant depth for each individual channel flow to ensure that normal flow would occur in the numerical model. By calibrating the downstream water level (see Table 4.2) of the physical model against the numerical model with one another, it was concluded that the Manning n value had been selected correctly.

The water levels deviated with 4%, 6% and 0% for measuring points 1, 2 and 3. Thus the numerical model can be used with 100% certainty for these parameters.

Table 4.2: Water level comparison at measuring points 1, 2 and 3

Test number	Physical Model			Numerical Model			Factor Difference	
	Point 1 (mm)	Point 2 (mm)	Point 3 (mm)	Point 1 (mm)	Point 2 (mm)	Point 3 (mm)	Point 1	Point 2
1	571.9	546	532.9	573.9	551	532.9	2.04%	4.76%
2	560.9	519	523.9	561.07	524.1	523.9	0.20%	6.54%
3	549.9	529	517.9	553.4	524	517.9	4.61%	-5.68%
4	562.9	526	522.9	564.57	534.7	522.9	1.88%	10.24%
5	567.9	519	523.9	570.57	523	523.9	2.84%	5.13%
6	547.9	511	522.9	555.1	515.9	522.9	9.73%	7.00%
7	551.9	520	522.9	557.27	528.4	522.9	6.88%	10.63%
8	553.9	529	522.9	553.9	536	522.9	0.00%	7.95%
9	559.9	528	521.9	558.2	525	521.9	-1.98%	-3.45%

Note: The target water level at Measuring Point 3 was 522.3 metres above the laboratory floor.

4.4 Numerical Results

The parameters used in the simulations are shown in Table 4.1. Appendix C contains the results of all the simulation tests and provides the following images of the results:

- Model bathymetry,
- Water depth(m) with velocity vectors,
- Velocity magnitude(m/s) with velocity vectors,

- Bed load transport rate (kg/s),
- Bed change(m),
- Scoured bed elevation.

To compare the results with the physical experiments, a more localised image is presented below. Table 4.3 provides the page numbers in Chapter 4 and Appendix C for each specific simulation test. These localised bed change results and velocity magnitude results was discussed and summarised in full. Figure 4.1 illustrates the mesh used in the numerical channel setup.

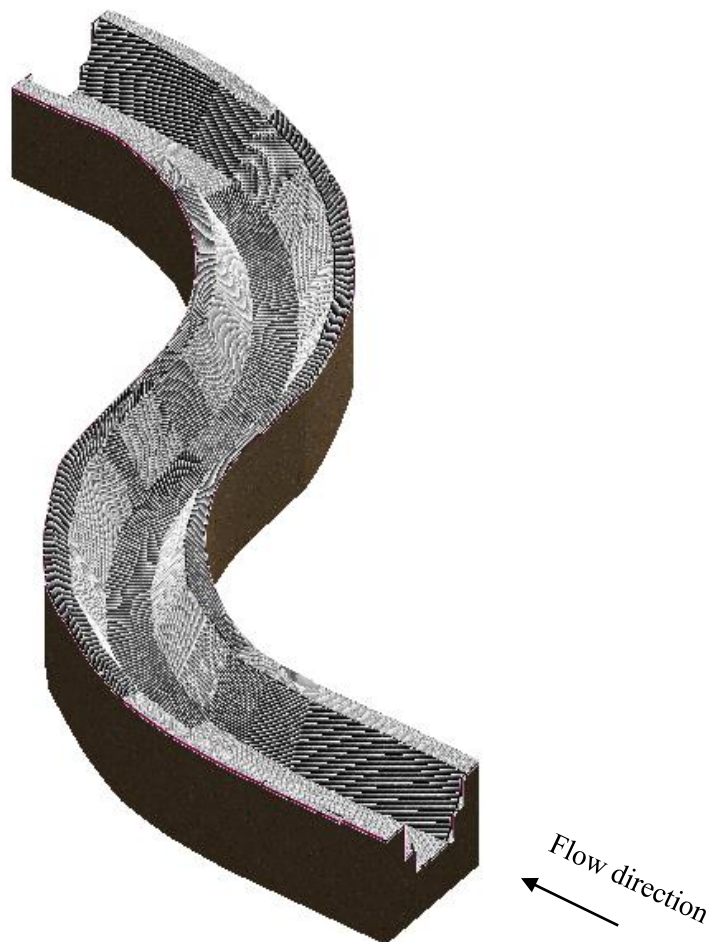


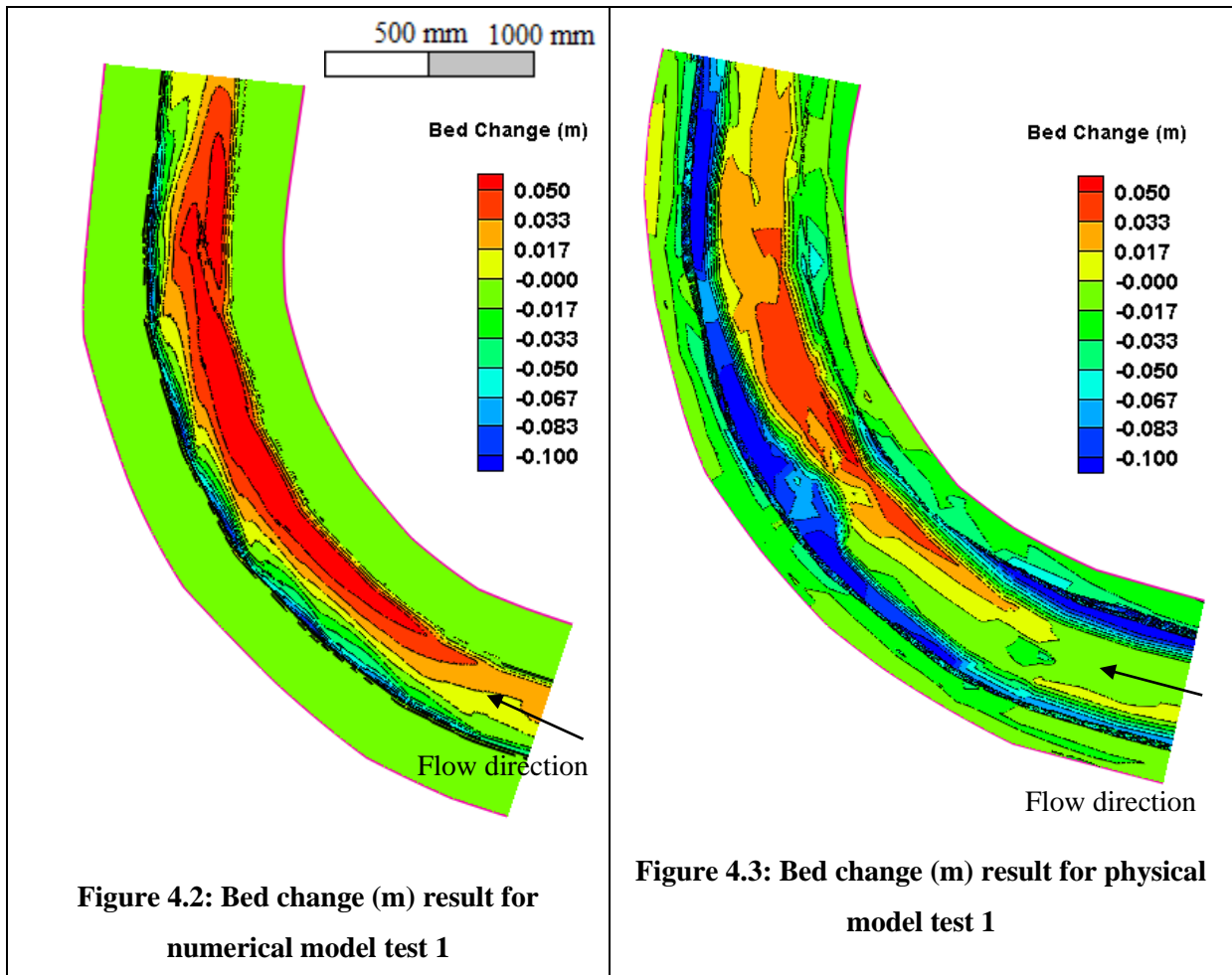
Figure 4.1: River mesh generated from numerical model

Table 4.3: Summary of numerical model setup

Simulation Test		Simulation Time	Flow Q (l/s)	Mesh Size		Cell Length (mm)				Time Step (s)	Manning n	Page Number	
				I _{max}	J _{max}	Minimum I Direction	Maximum I Direction	Minimum J Direction	Maximum J Direction			Chapter 4	App. C
1	Without Diversion Structure	570 s	20.0	400	800	3.4	4.9	12.8	25.9	0.1	0.03	4-9	C-b
2	0° Structure with Flow	180 s	17.5	200	600	6.9	10.0	17.2	34.5	0.1	0.03	4-11	C-g
3	0° Structure with Flow (L-Shape)	181 s	14.5	200	1000	7.0	10.0	10.3	20.7	0.1	0.03	4-13	C-m
4	30° Structure with Flow	216 s	18.8	200	600	6.9	10.0	17.2	34.5	0.1	0.03	4-15	C-s
5	30° Structure with Flow (L-Shape)	218 s	17.8	200	1000	6.7	10.4	10.3	20.7	0.1	0.03	4-17	C-y
6	45° Structure with Flow	268 s	17.2	200	700	6.9	10.0	14.9	30.1	0.1	0.03	4-19	C-ee
7	45° Structure with Flow (L-Shape)	203 s	15.5	200	1000	6.7	10.4	10.3	20.7	0.1	0.03	4-21	C-kk
8	60° Structure with Flow	223 s	18.4	200	800	6.9	10.0	12.9	25.9	0.1	0.03	4-23	C-qq
9	60° Structure with Flow (L-Shape)	195 s	15.5	200	1000	6.7	10.4	10.3	20.7	0.1	0.03	4-25	C-ww
10S1	30° with Flow Structure (1 Metre Wide Bottom Width)	216 s	37.6	300	800	5.6	8.7	11.1	27.7	0.1	0.03	4-28	C-ccc
10S2	60° with Flow Structure (1 Metre Wide Bottom Width)	223 s	36.9	300	900	5.6	8.7	10.0	25.0	0.1	0.03	4-29	C-iii

4.4.1 Simulation Test 1 (Without Diversion Structure, $Q = 20$ l/s)

Figures 4.2 and 4.3 illustrate the validation results of simulation test 1.



The total discharge during this simulation test was 20.0 l/s, with water depths of ± 100 mm, 110 mm and 110 mm for the measuring points 1, 2 and 3 respectively (see Figure 3.6). A Manning n value of 0.03 was used in the simulation test. The physical water depths were 98 mm, 105 mm and 110 mm.

The simulation lasted five minutes in total, which is the exact run time of physical experiment 1. Table 4.3 provides the page numbers in Appendix C of the images taken of the sediment elevation results.

The scour depth of the simulated channel compared to the physical scour depth is underestimated by 2.0%. The scour of the simulation was on the outside of the river bend, as suspected in the literature, whereas the physical experiment outside channel bank collapsed (see Figure 3.19). The deposition of the numerical simulation on the inside channel bend correlates to that of the physical model. The numerical models scouring size was not as wide as that of the physical model, but did occur between 45° and 60° into the channel bend.

The velocity profile in Figure 4.4 was exactly as expected and showed no unusual flow patterns. The flow velocity was slow on the inside bend and fast on the outside, hence the deposition on the inside bend and scour on the outside bend.

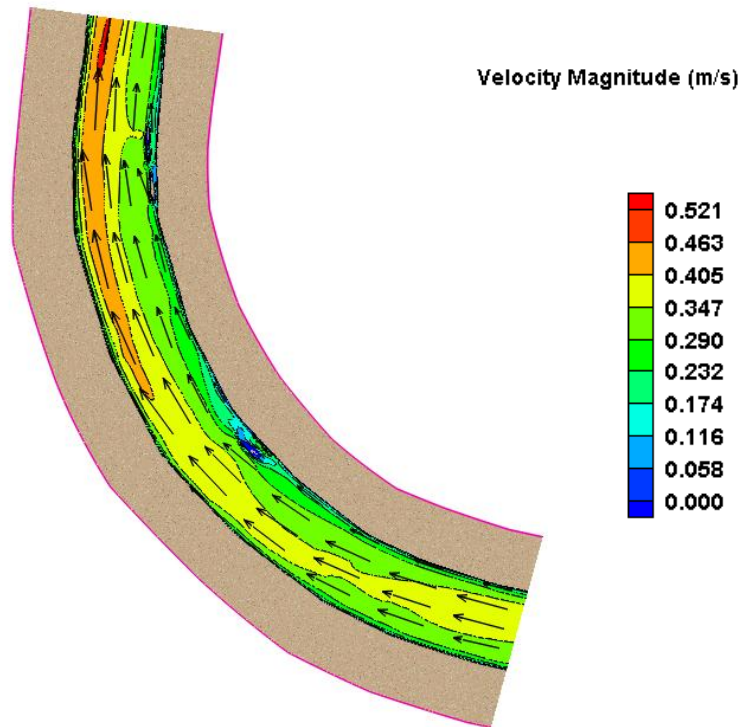
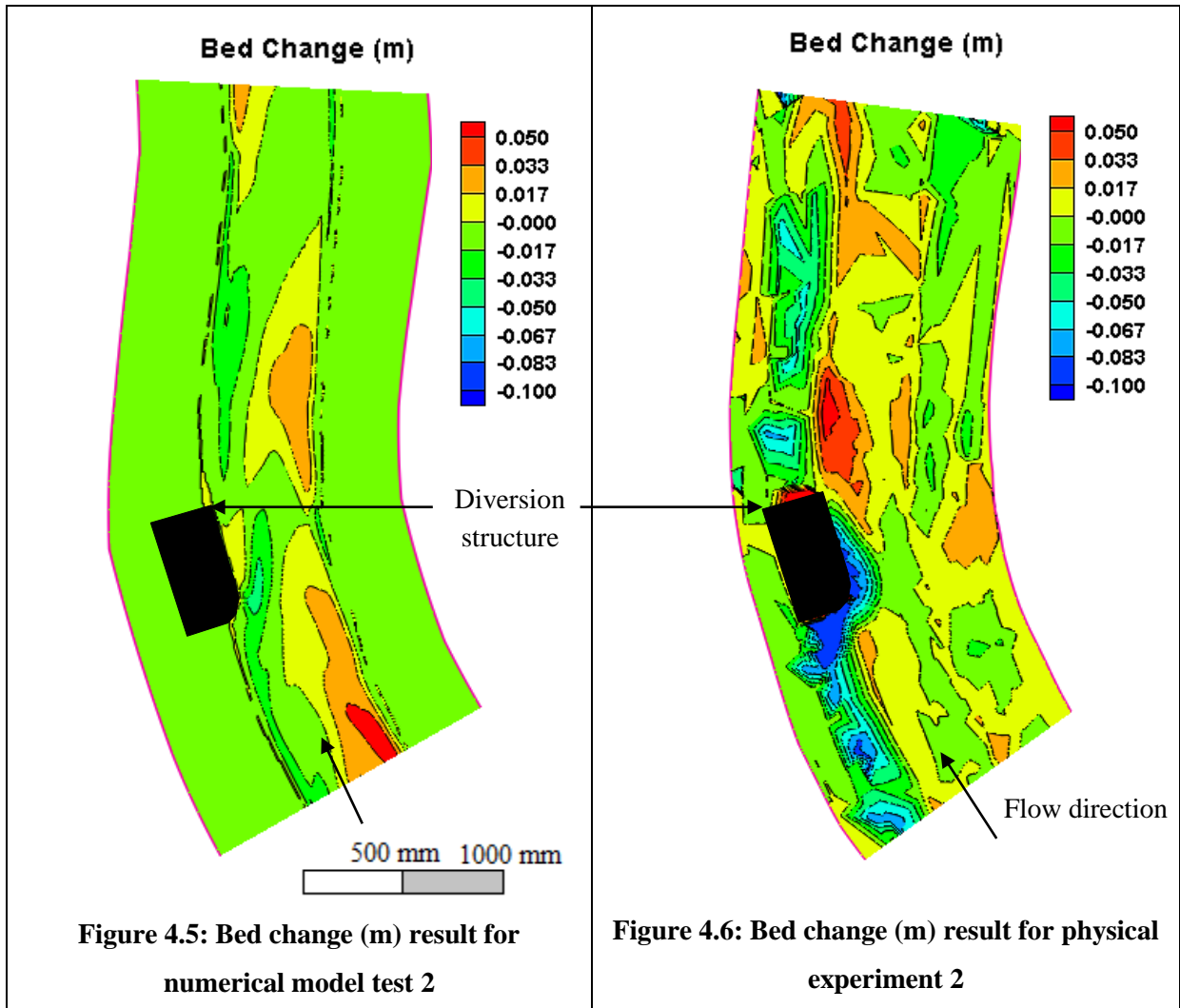


Figure 4.4: Velocity magnitude (m/s) result for numerical model test 1

Empirically, numerically and physically the maximum scour position was similar, thus concluding the numerical model with literature is sufficient when establishing the maximum scour location in a 90⁰ channel bend.

4.4.2 Simulation Test 2 (0° with flow, Q = 17.5 l/s)

Figures 4.4 and 4.5 illustrate the validation results of simulation test 2.



The total discharge during this simulation test was 17.5 l/s, with water depths of ± 87 mm, 83 mm and 101 mm for the measuring points 1, 2 and 3 respectively. A Manning n value of 0.03 was used in the simulation test. The physical water depths were 87 mm, 78 mm and 101 mm.

The simulation lasted three minutes in total, which is the exact run time of physical experiment 2. Table 4.3 provides the page numbers in Appendix C of the images taken of the sediment elevation results of the experiment.

The scour depth of the simulated channel compared to the physical scour depth is underestimated by 38.0%. The scour of the simulation starts on the structure bend and will ensure that full scour in front of the structure face would take place if the simulation run were longer. The other reason for this inconsistency could be that the model is a two-dimensional model simulator. It therefore provides

velocity vectors only in the x and y-direction, whereas modelling the z-direction velocity would ensure that flat surface sediment movement could be shown to take place close to the structure. The velocity profile in Figure 4.7 was exactly as expected and showed no unusual flow patterns.

The flow velocity was slow on the inside bend and fast on the outside, thus deposition would occur on the inside bend and scour would occur on the outside bend. Large velocities were present in the middle of the channel.

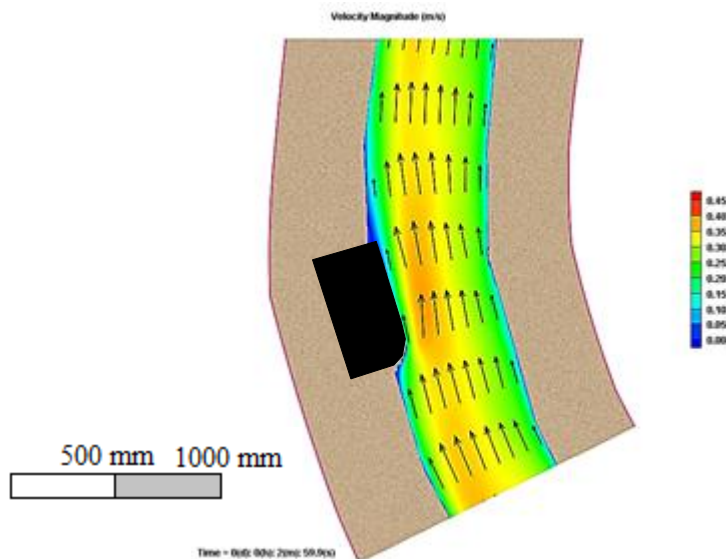
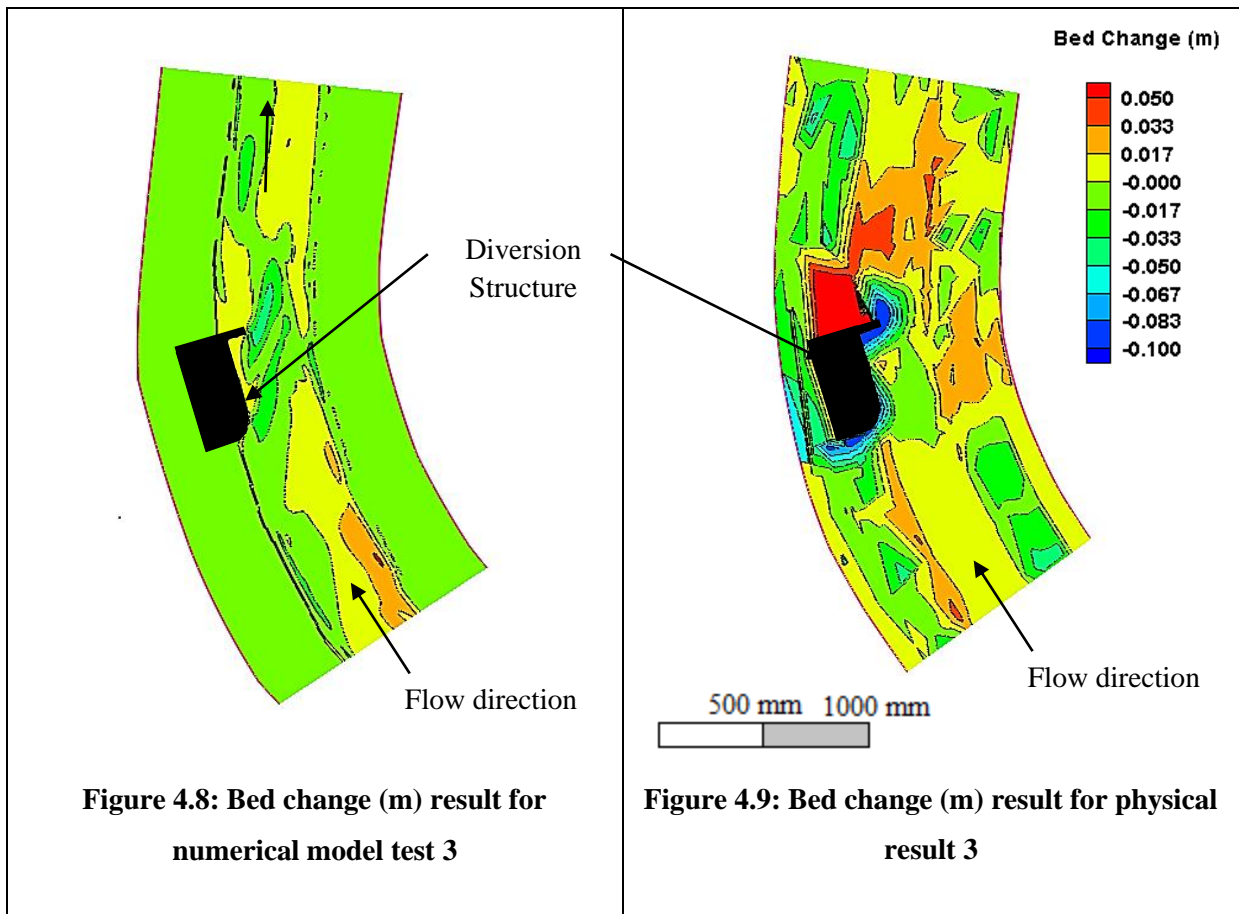


Figure 4.7: Velocity magnitude (m/s) result for numerical model test 2

The deepest scour hole achieved during the simulation was ± 62 mm below the original bed level, compared to the physically measured scour depth of 100 mm.

4.4.3 Simulation Test 3 (0° L-shape with flow, Q = 14.5 l/s)

Figures 4.7 and 4.8 illustrate the validation results of simulation test 3.



The total discharge during this simulation test was 14.5 l/s, with water depths of ± 80 mm, 83 mm and 95 mm for the measuring points 1, 2 and 3 respectively. A Manning n value of 0.03 was used in the simulation test. The physical water depths were 76 mm, 88 mm and 95 mm. These simulated water depths are very similar to the actual depths.

The simulation lasted three minutes and one second in total, which is the exact run time of physical experiment 3. Table 4.3 provides the page numbers in Appendix C of the images taken of the sediment elevation results of the experiment.

The scour depth of the simulated channel compared to the physical scour depth is underestimated by 47.0%. The corner of the attached section caused disturbance to the flow and resulted in the deepest scour for the simulation at that point. The scour patterns differ only in depth of scour, but resemble each other in shape and position of scour. The middle of the intake in the simulation also provides evidence that an island of sediment will form, which resembles the physical experiment closely. The reason for this inconsistency could be that the model is a two-dimensional model simulator and not

three-dimensional. The velocity profile in Figure 4.10 was exactly as expected and had no unusual flow patterns. The flow velocity was the same on the inside bend and on the outside.

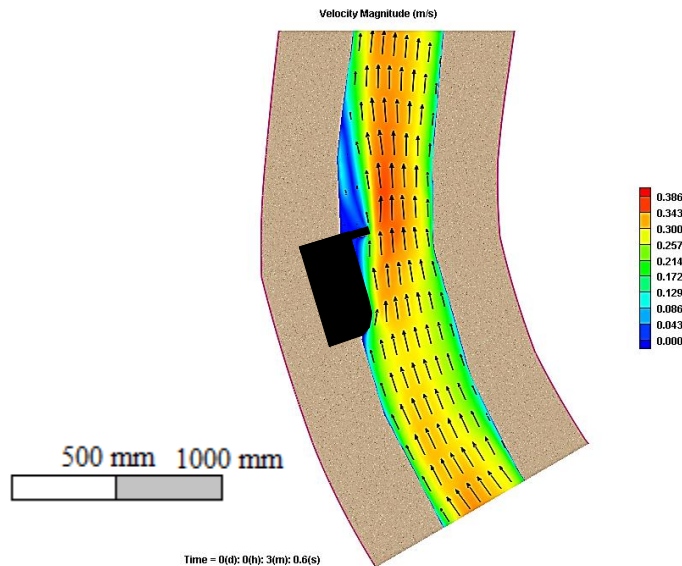
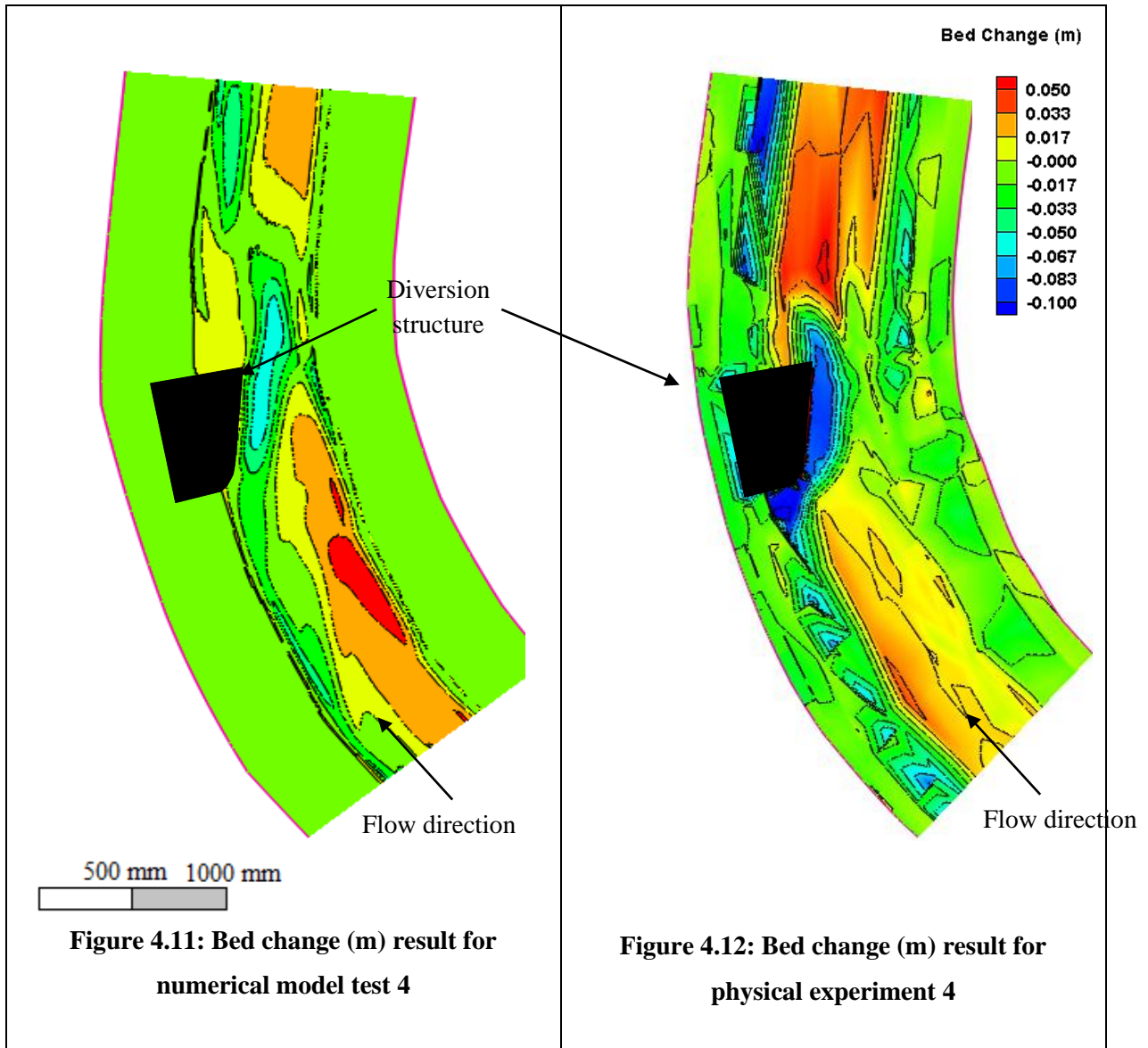


Figure 4.10: Velocity magnitude (m/s) result for numerical model test 3

The deepest scour hole achieved during the simulation was ± 53 mm below the original bed level, compared to the physically measured scour depth of 100 mm below the original bed. The simulation produced an accurate prediction of the observed bed level.

4.4.4 Simulation Test 4 (30° with flow, Q = 18.8 l/s)

Figures 4.10 and 4.11 illustrate the validation results of simulation test 4.



The total discharge during this simulation test was 18.8 l/s, with water depths of ± 90 mm, 93 mm and 100 mm for the measuring points 1, 2 and 3 respectively. A Manning n value of 0.03 was used in the simulation test. The physical water depths were 89 mm, 47 mm and 100 mm. The water depths were similar to the real depths. The location of measuring point 2 had 34 mm deposition as a physical result, but 21 mm as simulated result. This could have resulted in the different water depths at measuring point 2.

The simulation lasted three minutes and thirty-six seconds in total, which is the exact run time of physical experiment 4. Table 4.3 provides the page numbers in Appendix C of the images taken of the sediment elevation results of the experiment.

The scour depth of the simulated channel compared to the physical scour depth is underestimated by 37.0%. The scour of the simulation starts on the structure bend and scours across the face of the structure to the downstream end (see Figure 4.11). The scour patterns differ only slightly in depth of scour, but resemble each other accurately in shape and position of scour. The reason for the slight inconsistency in scour position could be that the model is a two-dimensional model simulator and not three-dimensional. The velocity profile in Figure 4.13 was exactly as expected and showed no unusual flow patterns. The flow velocity was slow on the inside bend and fast on the outside, thus deposition would occur on the inside bend and scour on the outside bend. Large velocities were present in the middle of the channel and at the face of the diversion.

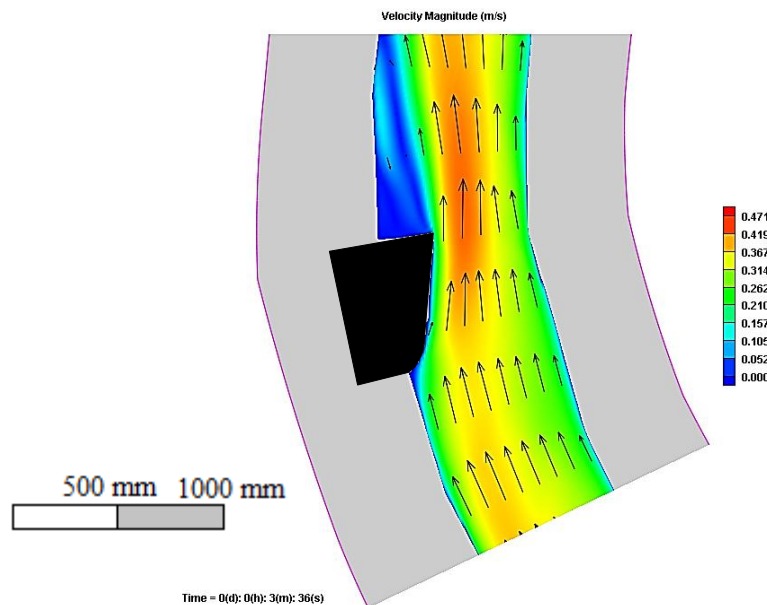
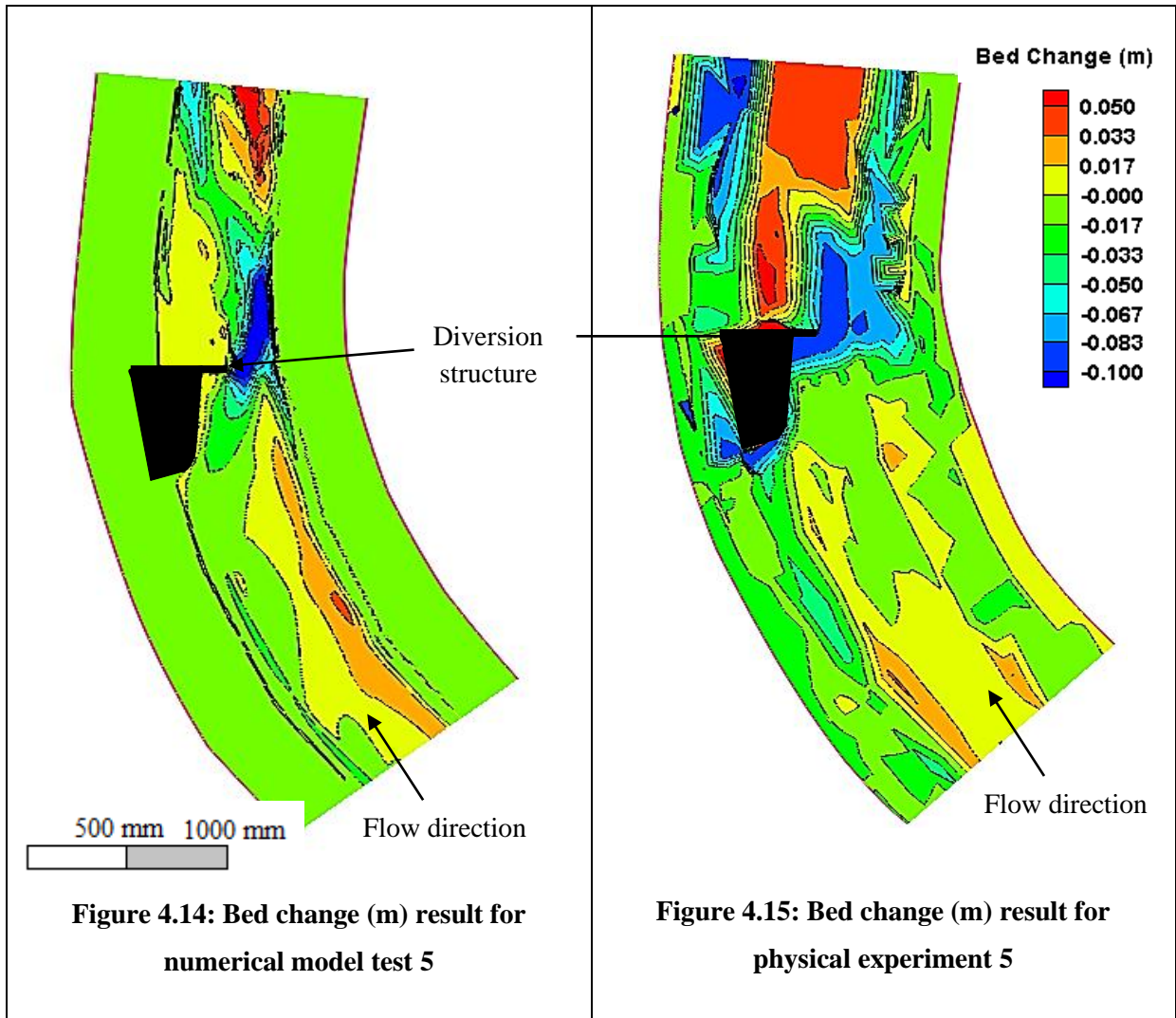


Figure 4.13: Velocity magnitude (m/s) result for numerical model test 4

The deepest scour hole achieved during the simulation was ± 63 mm below the original bed level, compared to the physical measured scour depth of 100 mm below the original bed. The simulation also produced an accurate prediction of the observed bed level.

4.4.5. Simulation Test 5 (30° L-shape with flow, Q = 17.8 l/s)

Figures 4.13 and 4.14 illustrate the validation results of simulation test 5.



The total discharge during this simulation test was 17.8 l/s, with water depths of ± 97 mm, 40 mm and 101 mm for measuring points 1, 2 and 3 respectively. A Manning n value of 0.03 was used in the simulation test. The physical water depths were 94 mm, 35 mm and 101 mm. The simulated water depths were similar to the real depths. The location of measuring point 2 had 43 mm deposition as a physical result, but 42 mm as simulated result. This could have resulted in the different water depths at measuring point 2.

The simulation lasted three minutes and thirty-eight seconds in total, which is the exact run time of physical experiment 5. Table 4.3 provides the page numbers in Appendix C of the images taken of the sediment elevation results of the experiment.

The scour depth of the simulated channel compared to the physical scour depth is overestimated by 41.0%. The corner of the attached section caused disturbance to the flow and resulted in the deepest

scour for the simulation at that point. The scour pattern appears to be moving upstream of the origin of scour towards the bend of the structure upstream. The scour patterns do not differ in depth of scour, but in shape and position of scour. An island of deposited sediment was evidence that the attachment reduced the flow velocity, compared to the simulation test where the sediment deposited upstream of the attachment.

The reason for this inconsistency is that the model is a two-dimensional model simulator and not three-dimensional. The velocity profile in Figure 4.16 was exactly as expected and did not force the velocity into the opposite bank, as in the physical model. The velocity profile shows that the velocity becomes greater as this area between the opposite bank and the attachment gets smaller. The flow velocity was slow on the inside bend and on the outside upstream of the diversion, thus deposition would occur gradually. High velocities were present in the middle of the channel and at the downstream end of the diversion. The velocity vectors show that no scour would occur at the face of the diversion, because the L-shape is obstructing the flow.

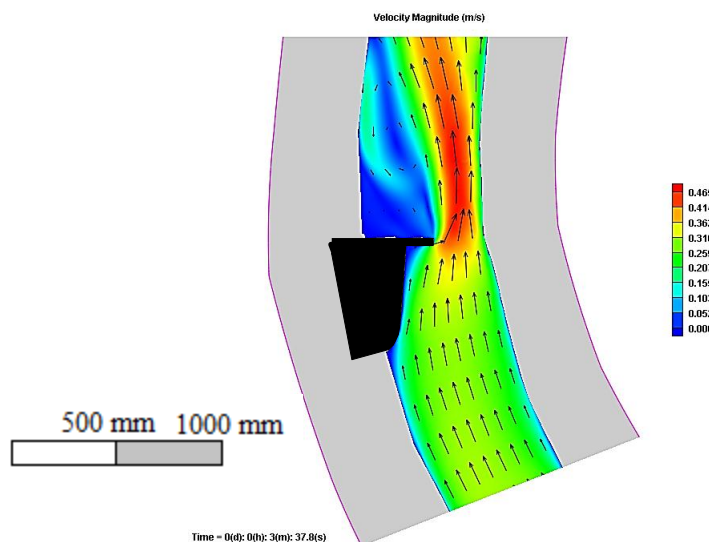
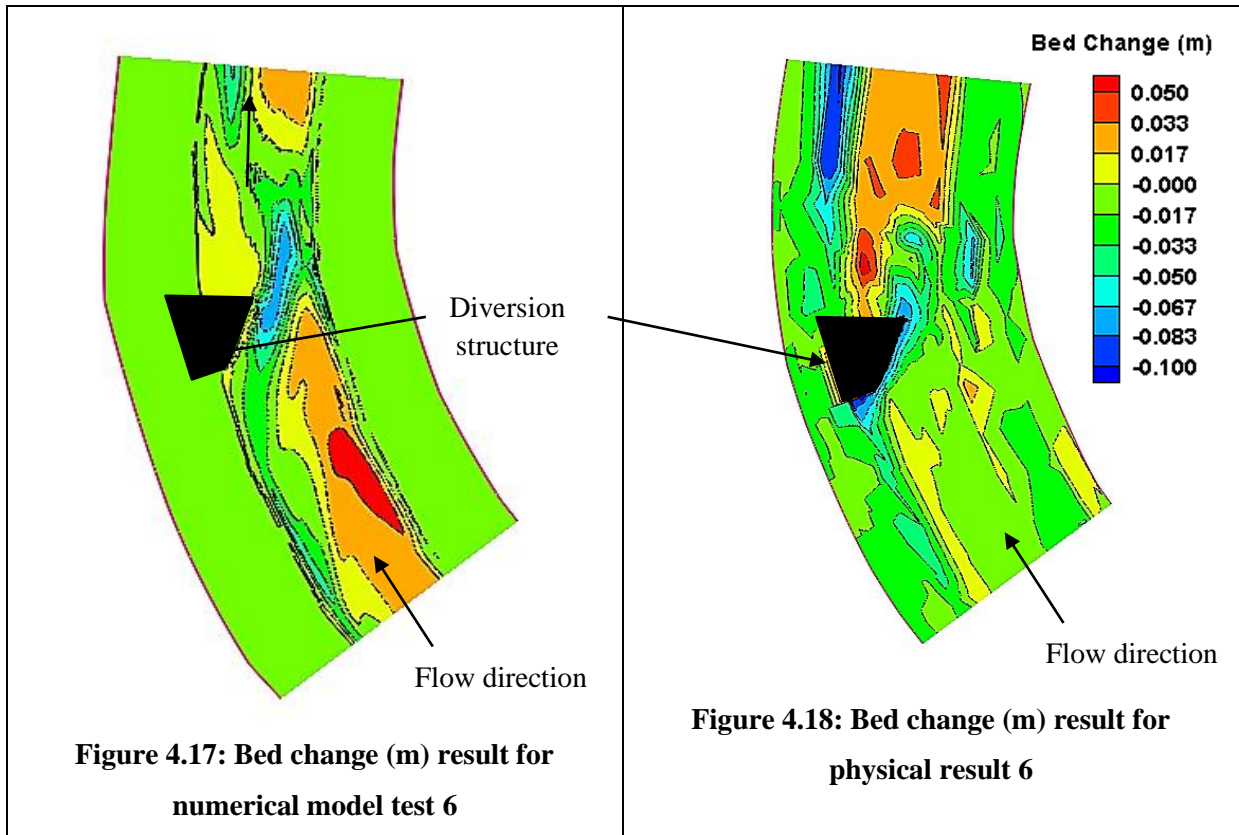


Figure 4.16: Velocity magnitude (m/s) result for numerical model test 5

The deepest scour hole achieved during the simulation was 141 mm below the original bed level, compared to the physically measured scour depth of 100 mm below the original bed. This is impossible, as the present bed of the channel is limited by a concrete channel bed 100 mm below the top layer of sediment. The simulation produced the most accurate prediction of the observed bed level.

4.4.6. Simulation Test 6 (45° with flow, Q = 17.2 l/s)

Figures 4.16 and 4.17 illustrate the validation results of simulation test 6.



The total discharge during this simulation test was 17.2 l/s, with water depths of ± 81 mm, 40 mm and 100 mm for measuring points 1, 2 and 3 respectively. A Manning n value of 0.03 was used in the simulation test. The physical water depths were 74 mm, 43 mm and 100 mm. The water depths were similar to the real depths. The location of measuring point 2 had 27 mm deposition as a physical result, but 34 mm as simulated result. This could have been because of the different water depths at measuring point 2.

The simulation lasted four minutes and twenty-eight seconds in total, which is the exact run time of physical experiment 6. Table 4.3 provides the page numbers in Appendix C of the images taken of the sediment elevation results of the experiment.

The scour depth of the simulated channel compared to the physical scour depth is underestimated by 19.0%. The scour of the simulation starts upstream of the structure bend and scours across the face of the structure to the downstream end (see Figure 4.17). The scour patterns do not differ in depth of scour, but slightly in shape and position. The velocity profile in Figure 4.19 was exactly as expected, although the highest flow velocity was downstream of the structure. The hydraulic conditions at the

test section were simulated very accurately. The flow velocity was slow on the inside bend and fast on the outside upstream of the diversion, thus deposition would occur gradually from the inside out. High velocities were present in the middle of the diversion face to the downstream end. The velocity vectors show that no scour would occur at the upstream side of the diversion.

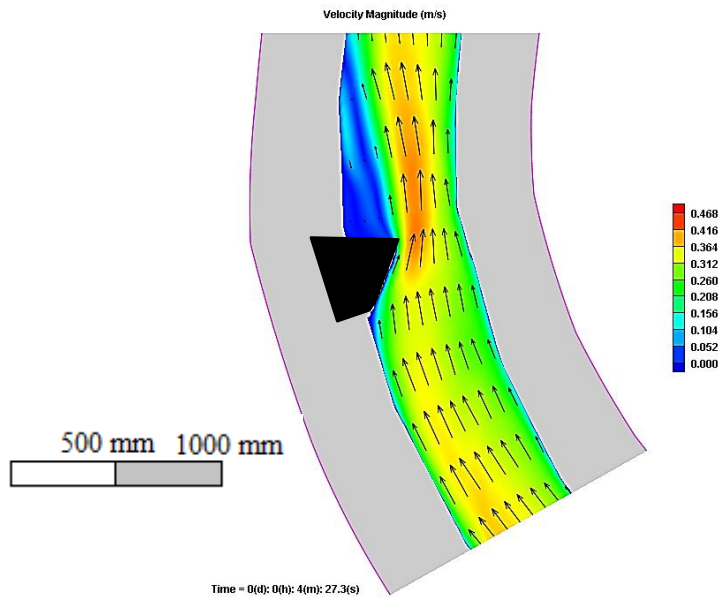
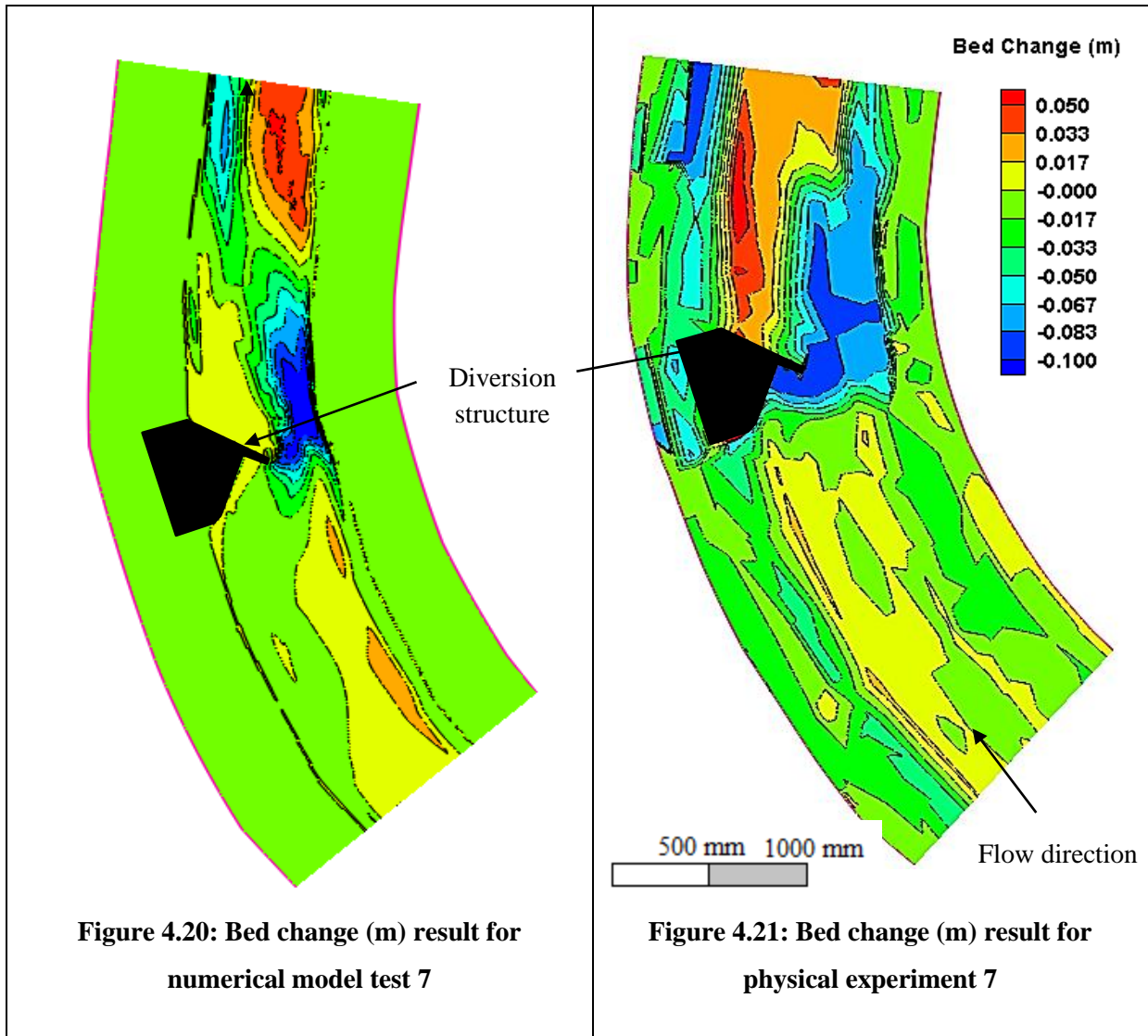


Figure 4.19: Velocity magnitude (m/s) result for numerical model test 6

The deepest scour hole achieved during the simulation was 81 mm below the original bed level, compared to the physically measured scour depth of 100 mm below the original bed. The simulation produced an accurate prediction of the observed bed level.

4.4.7. Simulation Test 7 (45° L-shape with flow, Q = 15.5 l/s)

Figures 4.19 and 4.20 illustrate the validation results of simulation test 7.



The total discharge during this simulation test was 15.5 l/s, with water depths of \pm 83 mm, 62 mm and 100 mm for measuring points 1, 2 and 3 respectively. A Manning n value of 0.03 was used in the simulation test. The physical water depths were 78 mm, 60 mm and 100 mm. The water depths were similar to the real depths. The location of measuring point 2 had 19 mm deposition as a physical result and 25 mm as simulated result. This is a very respectable outcome for this comparison.

The simulation lasted three minutes and twenty-three seconds in total, which is the exact run time of physical experiment 7. Table 4.3 provides the page numbers in Appendix C of the images taken of the sediment elevation results of the experiment.

The scour depth of the simulated channel compared to the physical scour depth is overestimated by 72.0%. The corner of the attached section caused disturbance to the flow and resulted in the deepest scour for the simulation at that point. The scour pattern appeared to be moving around and downstream of the origin. The scour pattern did not differ in depth of scour, in shape or position of scour.

The velocity profile in Figure 4.22 was exactly as expected and forced the flow into the opposite bank. As the velocity vectors move into the bank it can be assumed that the river would need to be wider to ensure that the opposite bank did not disappear. Thus the orientation and shape of the structure would not be sufficient, according to the simulation results. The flow velocity was slow on the inside bend and on the outside upstream of the diversion, thus deposition would occur gradually. High velocities were present in the middle of the channel and at the downstream end of the diversion. The velocity vectors show that no scour would occur at the face of the diversion, because the L-shape is obstructing the flow.

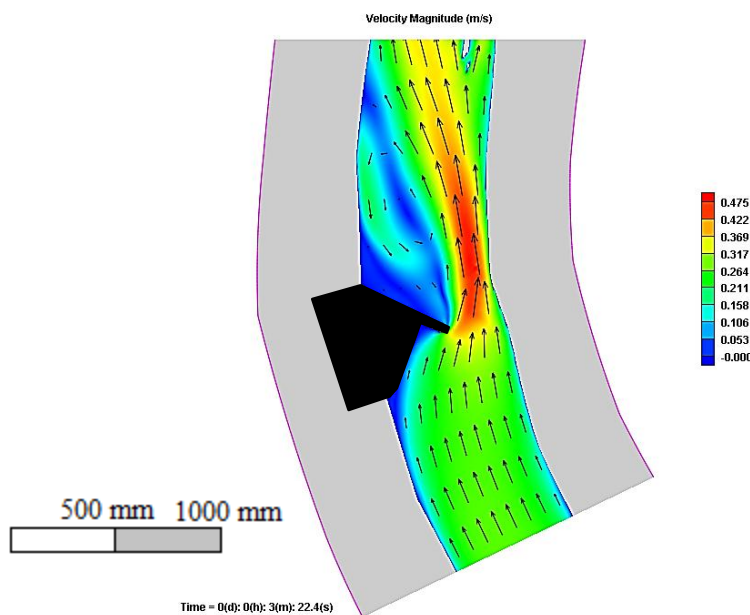
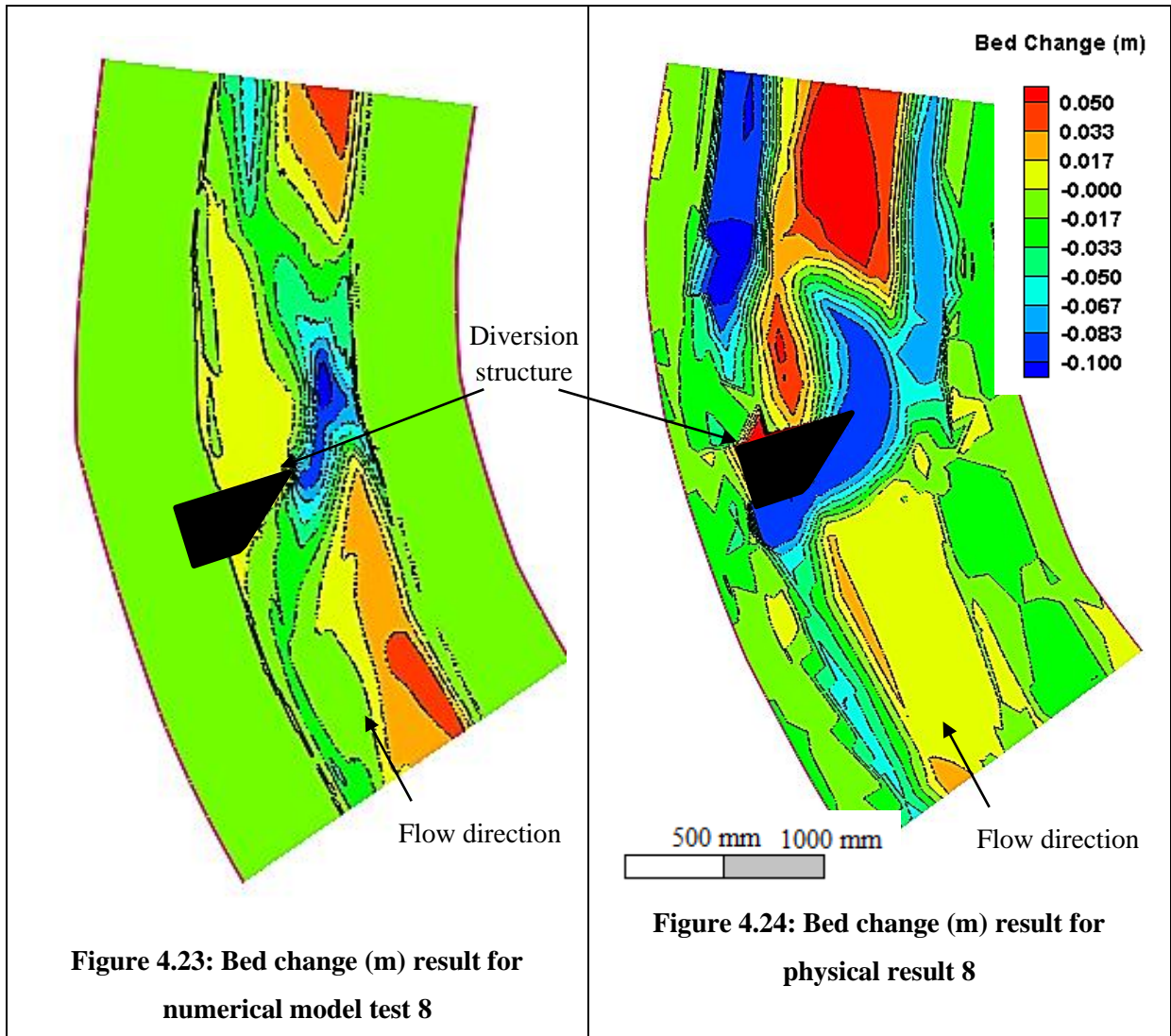


Figure 4.22: Velocity magnitude (m/s) result for numerical model test 7

The deepest scour hole achieved during the simulation was ± 172 mm below the original bed level, compared to the physically measured scour depth of 100 mm below the original bed. This is impossible, as the present bed of the channel is limited by a concrete channel bed 100 mm below the top layer of sediment. The simulation produced a very accurate prediction of the observed bed level.

4.4.8. Simulation Test 8 (60° with flow, Q = 18.4 l/s)

Figures 4.22 and 4.23 illustrate the validation results of simulation test 8.



The total discharge during this simulation test was 18.4 l/s, with water depths of ± 80 mm, 42 mm and 100 mm for the measuring points 1, 2 and 3 respectively. A Manning n value of 0.03 was used in the simulation test. The physical water depths were 80 mm, 31 mm and 100 mm. The water depths were proximate to the real depths. The location of measuring point 2 had 57 mm deposition as a physical result, but 53 mm as simulated result. This could have been because of the different water depths at measuring point 2.

The simulation lasted three minutes and forty-three seconds in total, which is the exact run time of physical experiment 8. Table 4.3 provides the page numbers in Appendix C of the images taken of the sediment elevation results of the experiment.

The scour depth of the simulated channel compared to the physical scour depth is overestimated by 11.0%. The scour of the simulation moves more downstream, but there was some scouring taking place in front of the structure (see Figure 4.23). The scour patterns do not differ in depth of scour, but have a different shape and position. The velocity profile in Figure 4.25 was exactly as expected, although the bank on the opposite side collapsed in the physical run. It could therefore be concluded that the velocity at the toe of the side slope could have been more that illustrated. The flow velocity was slow on the inside bend and fast on the outside upstream of the diversion, thus deposition would occur gradually from the inside out. Large velocities were present in the centre of the diversion face to the downstream end. The velocity vectors show that no scour would occur at the upstream side of the diversion.

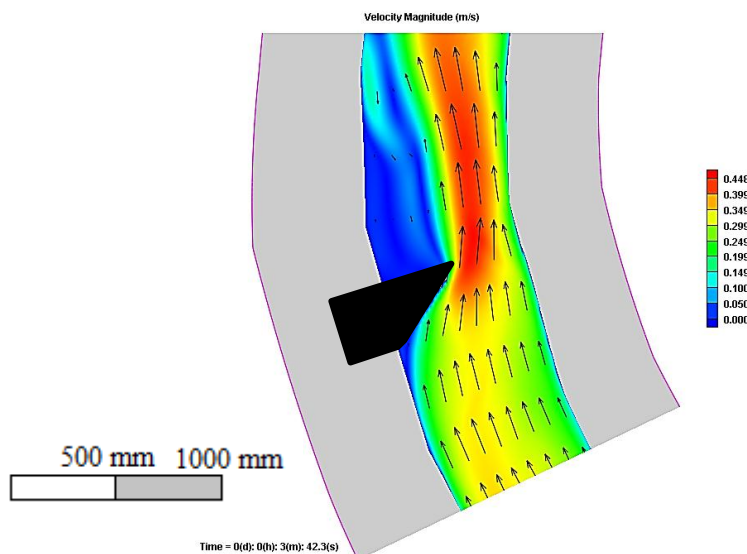
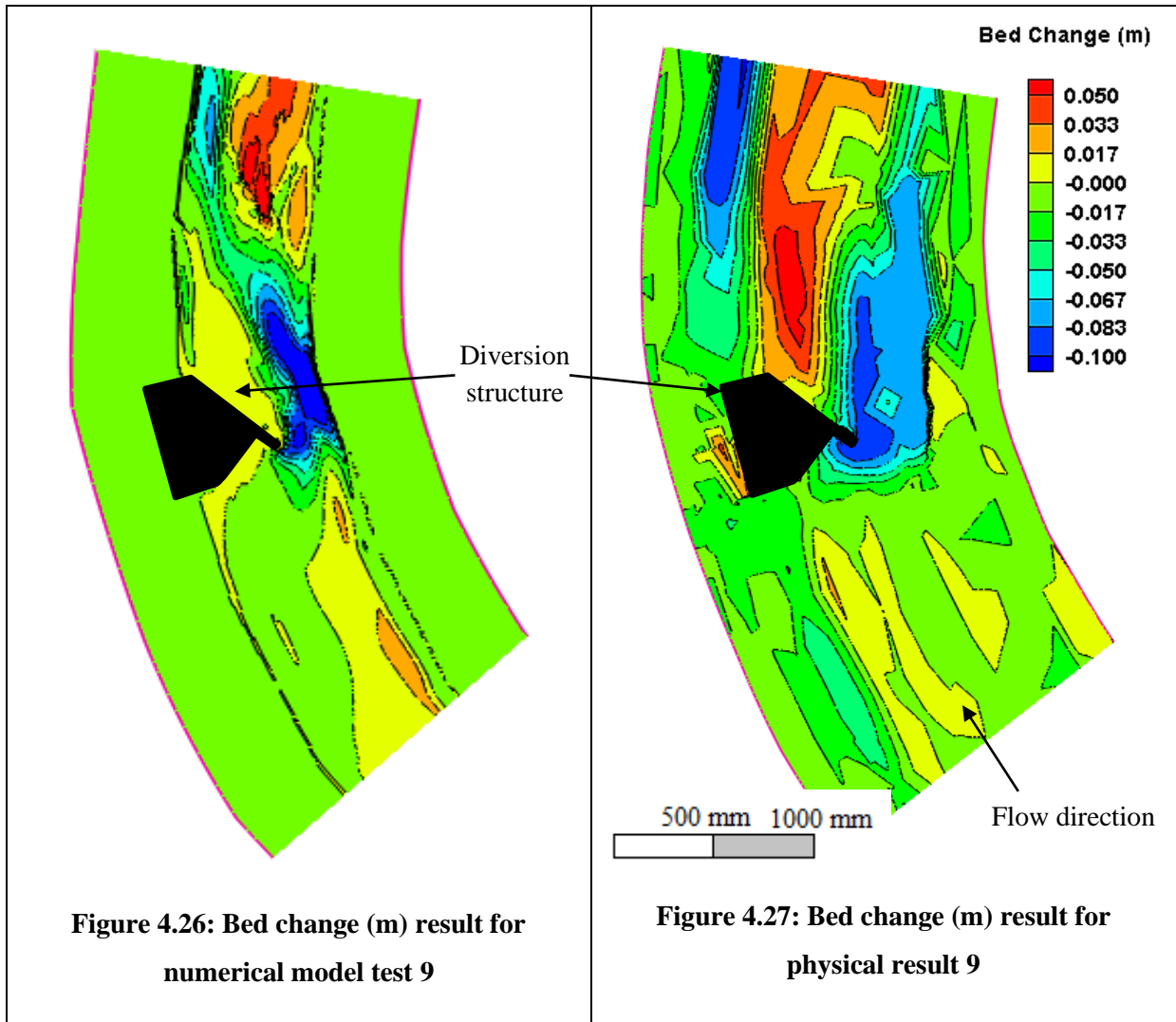


Figure 4.25: Velocity magnitude (m/s) result for numerical model test 8

The deepest scour hole achieved during the simulation was 111 mm below the original bed level, compared to the physically measured scour depth of 100 mm below the original bed. This is impossible, as the present bed of the channel is limited by a concrete channel bed 100 mm below the top layer of sediment. The simulation otherwise produced an accurate prediction of the observed bed level.

4.4.9. Simulation Test 9 (60° L-shape with flow, Q = 15.5 l/s)

Figures 4.25 and 4.26 illustrate the validation results of simulation test 9.



The total discharge during this simulation test was 15.5 l/s, with water depths of ± 84 mm, 34 mm and 99 mm for measuring points 1, 2 and 3 respectively. A Manning n value of 0.03 was used in the simulation test. The physical water depths were 86 mm, 41 mm and 99 mm. The water depths were similar to the real depths. The location of measuring point 2 had 46 mm deposition as a physical result and 50 mm as simulated result. The upstream water depth could be different for the reason that the damming of the water upstream of the structure affected the outflow to the right of the structure. As the flow was constricted in flowing past, the level downstream in the simulation could be wrong, as the physical river has a fixed bed which forces the water through a specific area. This is a very acceptable outcome for this comparison.

The simulation lasted three minutes and fifteen seconds in total, which is the exact run time of physical experiment 9. Table 4.3 provides the page numbers of the images taken of the sediment elevation results of the experiment in Appendix C.

The scour depth of the simulated channel compared to the physical scour depth is overestimated by 56.0%. The corner of the attached section caused disturbance to the flow and resulted in the deepest scour for the simulation at that point. This led to a high flow velocity, which was diverted into the opposite bank (see Figure 4.27), resulting on the collapsing of the right bank. The scour pattern appears to be moving around and downstream of the intake attachment. The scour patterns did not differ in depth of scour, in shape or in position.

The velocity profile in Figure 4.28 was exactly as expected and formed a depositing vortex downstream of the structure. As the velocity vectors move into the bank it can be assumed that the river would need to be wider to ensure that the opposite bank does not disappear. Thus this orientation and shape of the structure would not be sufficient, according to the simulation results. The flow velocity was slow on the inside bend and on the outside upstream of the diversion, thus deposition would occur gradually. Large velocities were present in the middle of the channel and at the downstream end of the diversion. The velocity vectors show that no scour would occur at the face of the diversion, because the L-shape is obstructing the flow.

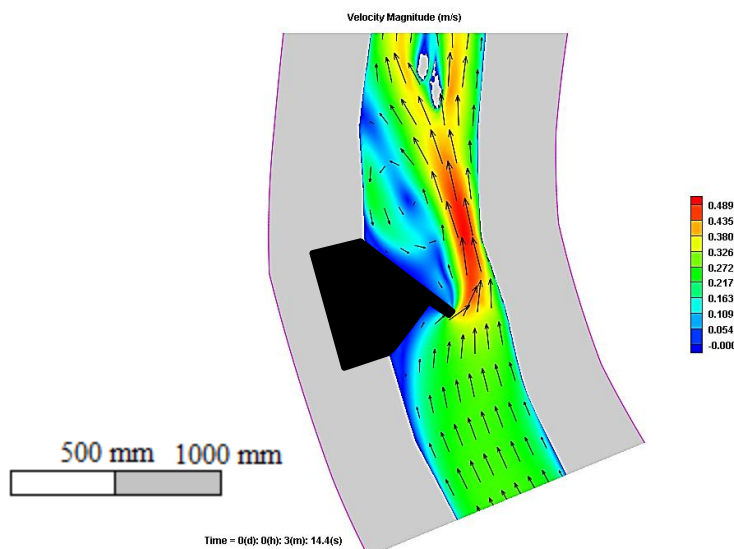


Figure 4.28: Velocity magnitude (m/s) result for numerical model test 9

The deepest scour hole achieved during the simulation was ± 156 mm below the original bed level, compared to the physically measured scour depth of 100 mm below the original bed. This is impossible, as the present bed of the channel is limited by a concrete channel bed 100 mm below the top layer of sediment. The simulation produced a very accurate prediction of the observed bed level.

4.4.10. Simulation Test 10S 1 (30° 1 metre wide, Q = 37.6 l/s)

The structures angled at 30° and 60° presented similar physical results, with long and wide scour holes along the diversion structure. To finalise the angle of orientation, a 1 m wide channel was numerically simulated with a hydrodynamic sediment model (CCHE 2D).

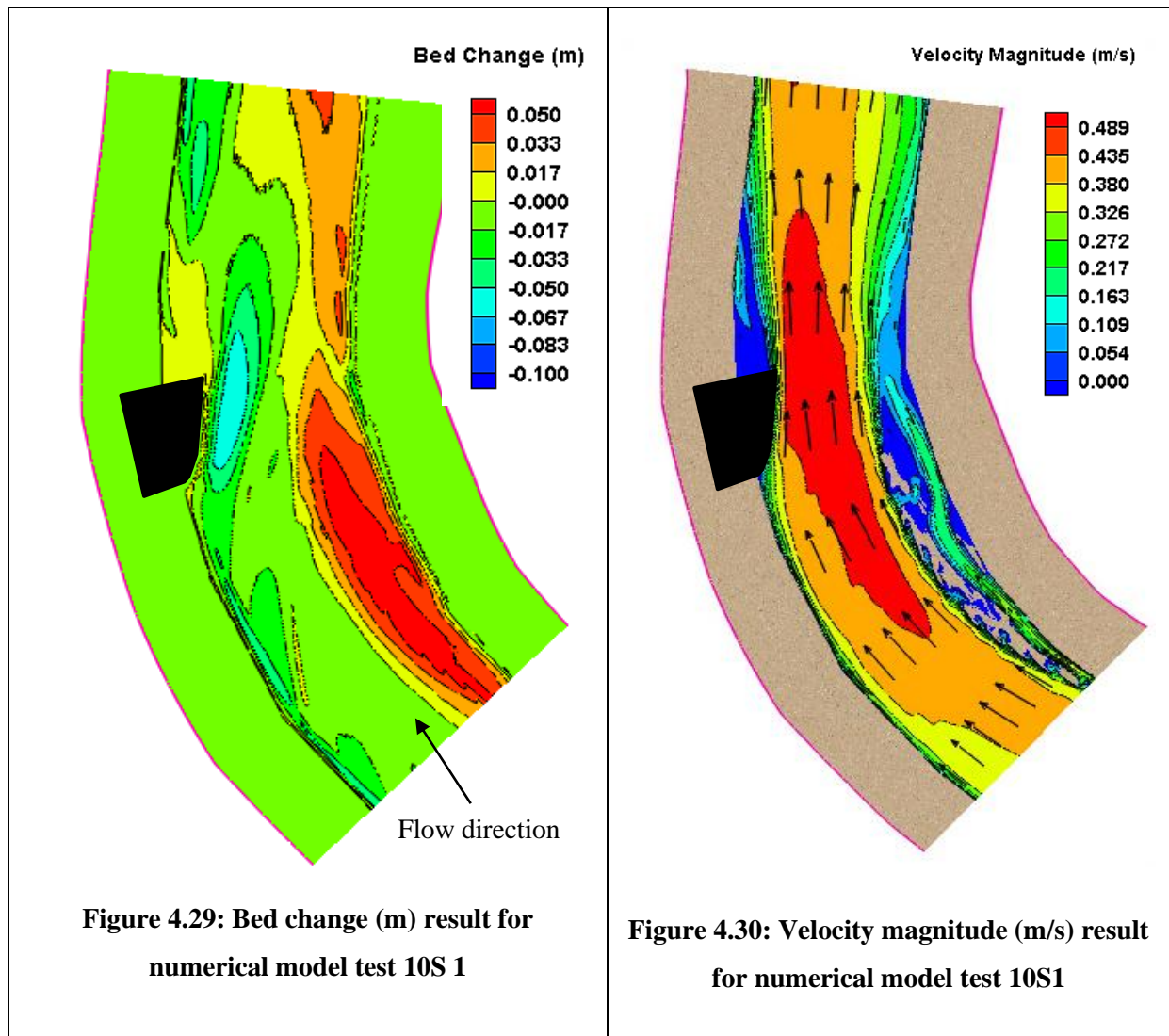
One reason for these two simulations was to observe the differences between a narrow and a wider channel. Another reason was to observe the bed change, scour hole position, scour hole size and main channel formation with a structure. Numerical simulation 10S 1 with a structure angled at 30° follows.

The total discharge during this simulation test was 37.6 l/s, with water depths of ± 92 mm, 73 mm and 101 mm for measuring points 1, 2 and 3 respectively. A Manning n value of 0.045 was used in the simulation test. The location of measuring point 2 had 30 mm of deposited sediment for the simulated result. The reason for the greater water depth, which is very close to the water depths in simulation test 4, is that the Manning n value is greater and the channel is wider with a larger flow.

The simulation lasted three minutes and thirty-six seconds in total, which is the exact run time of physical experiment 4 and simulation test 4. Table 4.3 provides the page numbers in Appendix C of the images taken of the sediment elevation results of the experiment.

The bed change profile from simulation test 4 and simulation 10S 1 therefore resemble each other. The scour of the simulation starts on the structure bend and scours across the face of the structure to the downstream end (see Figure 4.11 compared to Figure 4.29). The scour patterns differ only slightly in depth of scour, but resemble each other accurately in shape and position of scour. The deposition on the inside of the river bend is considerable and forces the water towards the structure.

Flow velocity was larger on the outside bend where the structure was placed compared to the low flow velocities on the inside bend. The low flow velocities led to deposition, as shown by the vectors in Figure 4.30.



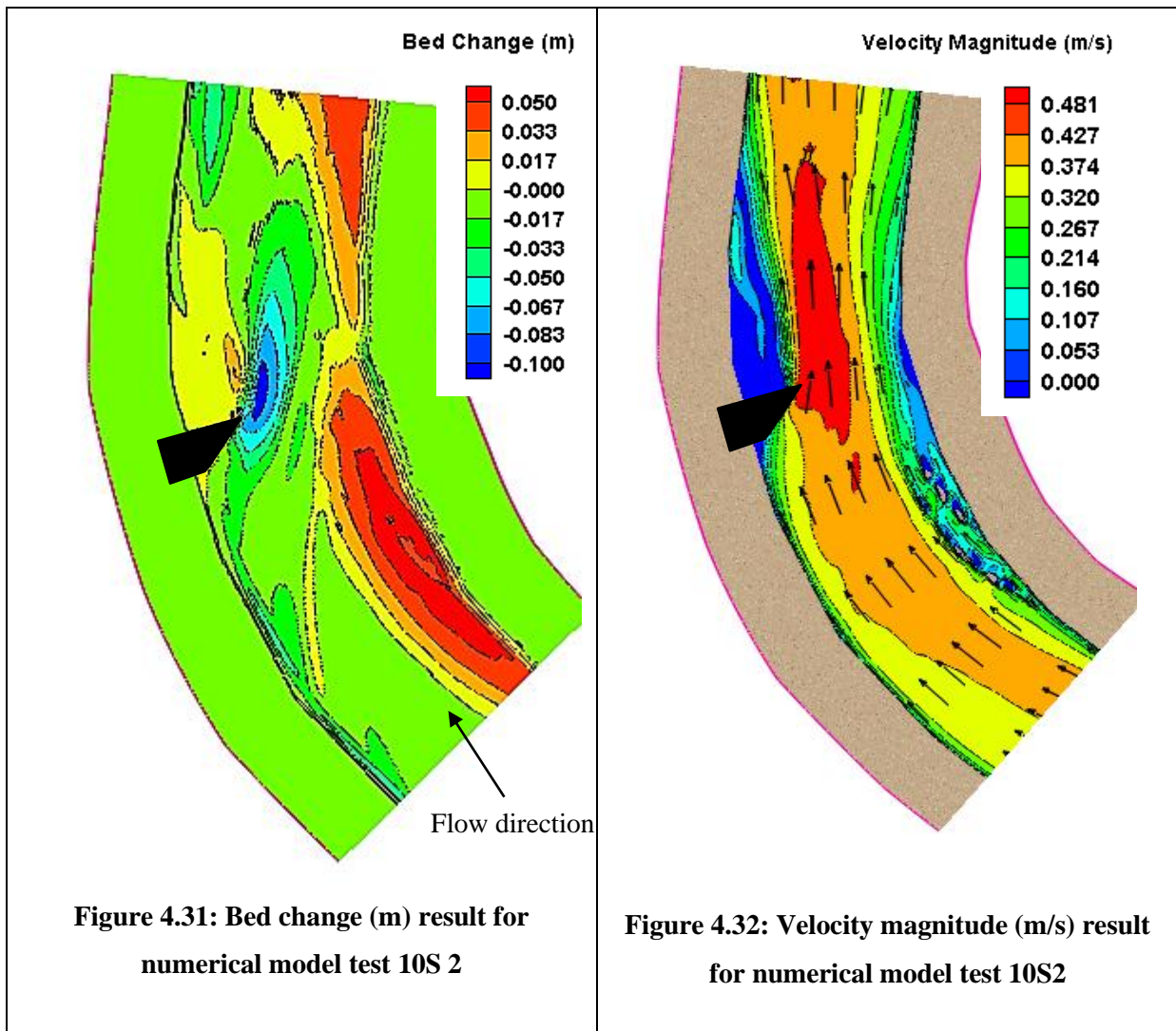
The deepest scour hole achieved during simulation 10S 1 was ± 74 mm below the original bed level, compared to measured scour depth in simulation 4 of 63 mm below the original bed. The simulation also produced an accurate prediction of the observed bed level.

4.4.11. Simulation Test 10S 2 (60° 1 metre wide, $Q = 36.9$ l/s)

The total discharge during this simulation test was 36.9 l/s, with water depths of ± 98 mm, 70 mm and 108 mm for measuring points 1, 2 and 3 respectively. A Manning n value of 0.045 was used in the simulation test. The location of measuring point 2 had 27 mm of deposited sediment for the simulated result. The reason for the greater water depth, which is not near to the water depths of simulation test 8, is that the Manning n value is greater and the channel is wider with a larger flow.

The simulation lasted three minutes and forty-three seconds in total, which is the exact run time of physical experiment 8 and simulation test 8. Table 4.3 provides the page numbers in Appendix C of the images taken of the sediment elevation results of the experiment.

The bed change profile from simulation test 8 and simulation 10S 2 do not resemble each other. The scour of the simulation 10S 2 scours a lot more across the face of the structure to the downstream end (see Figure 4.23 compared to Figure 4.31), but does not scour as deeply as in the narrower channel. The scour patterns differ only slightly in depth of scour, in shape and in position of scour. The deposition on the inside of the river bend is considerable and forces the water towards the structure, but does also ensure that the flow does not collapse the river banks. The hydraulic conditions at the test section were simulated very accurately.



The deepest scour hole achieved during simulation 10S 2 was ± 92 mm below the original bed level compared to the measured scour depth of simulation 8 of 111 mm below the original bed. The simulation also produced an accurate prediction of the observed bed level.

4.5. Summarised discussion of results

To ensure that the comparisons between the physical and numerical results were correct, a percentage error table was set up between the maximum scour depths of the physical and numerical tests. The numerical simulations were calibrated against the physical models Manning n value, water levels and individual parameters. By comparing the maximum scour depths in Table 4.4, the reliability of the use of this numerical model was set in place.

Table 4.4: Percentage error between the maximum scour depths (mm) of the numerical and physical tests (60° into the channel bend)

Test number	Run Time (s)	Flow (l/s)	Physical experiment maximum scour depth (mm)	Numerical simulation maximum scour depth (mm)	%Error
1	570	20	100	98	-2.00%
2	180	17.5	100	62	-38.00%
3	181	14.5	100	53	-47.00%
4	216	18.8	100	63	-37.00%
5	218	17.8	100	141	41.00%
6	268	17.2	100	81	-19.00%
7	203	15.5	100	172	72.00%
8	223	18.4	100	111	11.00%
9	195	15.5	100	156	56.00%
10S 1 compared to numerical simulation 4	216	37.6	60	63	3.00%
10S 2 compared to numerical simulation 8	223	36.9	100	111	11.00%
				Percentage error between numerical and physical results 1 to 9	43.81%

Note: Physical experiments ended when scouring reached the channel bed. The sediment bed was 100 mm above the channel bed.

The average percentage error was 43.81%. According to Basson and Rooseboom (1997) the discrepancy ratio for the following methods were calculated according to average laboratory data compared to numerical data:

- Van Rijn method had a 41% error
- Engelund-Hansen formula had a 46% error
- Ackers-White formula had a 52% error
- Yang formula had a 59% error

The result of the Wu et al. (200) method had a discrepancy of 43.81% in Table 4.4. According to Basson and Rooseboom (1997) this discrepancy was acceptable, as the percentage of error was in the range of the other methods.

Chapter 5

5. Case Study

5.1 Background

South Africa has various river pumping stations and Run-of-river (RoR) hydropower stations that work on the principle of an abstraction works diverting water. A few examples of Eskom RoR hydropower stations in South Africa are known as Colley Wobbles on the Mbashe River, First and Second Falls and the Ncora hydropower scheme. The following case study was prepared on an abstraction works with the main purpose of predicting the maximum scour location and the optimum orientation of the structure in the Berg River, at the proposed site location. The same concept used in pump station abstraction works could be used in the run-of-river hydropower schemes in this study, with the modification of using hydropower principles to ensure that the system can function fully after development.

During 2012, a hydraulic design was carried out on a proposed river abstraction works on the Berg River at Voëlvlei Dam. A possible site for the abstraction works was identified on the left bank at a bend in the Berg River during the pre-feasibility study. A topographical survey of the site and geological information were obtained during this study. The literature above and the processes proposed were used to ensure optimal design of the Berg River abstraction works.

5.2 Case Studies on Scope of Work

The work completed on the project involved the following:

- a) Field work to obtain sediment samples for grading analysis
- b) Flood hydrology
- c) Analysis of the river hydraulics to determine the most suitable site

Figure 5.1 shows satellite images of the river bend on the Berg River where the abstraction works were proposed to be built. According to the literature, the abstraction works had to be on the left bank (outside of the river bend) to make best use of secondary currents during floods to scour the intake area and to keep coarse sediment away from the intake.

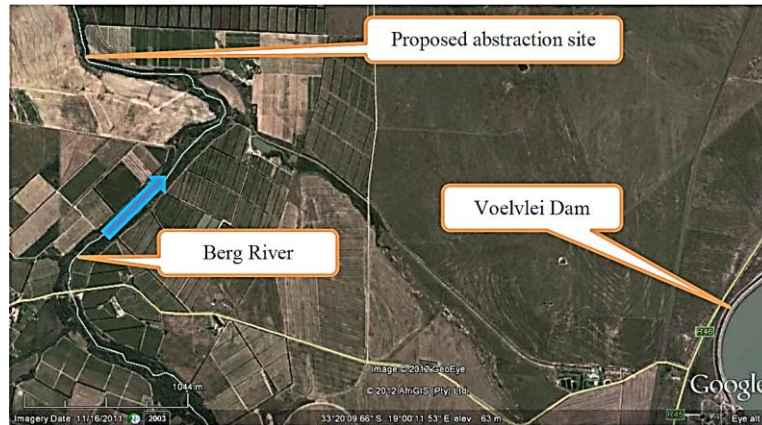


Figure 5.1: Satellite image of the Berg River near Voelvlei Dam

5.3 Site Visit

Field work was carried out during April 2012 to obtain river bed sediment for grading analysis. This is required for the mathematical modelling of the fluvial morphology. The results of the grading analysis, with photographs taken at each specific sampling location, can be viewed in Basson (2012). Figure 5.2 shows the bathymetry of the proposed abstraction site. The sediment sample positions are given in Figure 5.3, with their coordinates in Table 5.1. The grading analysis is based on sieve and hydrometer tests.

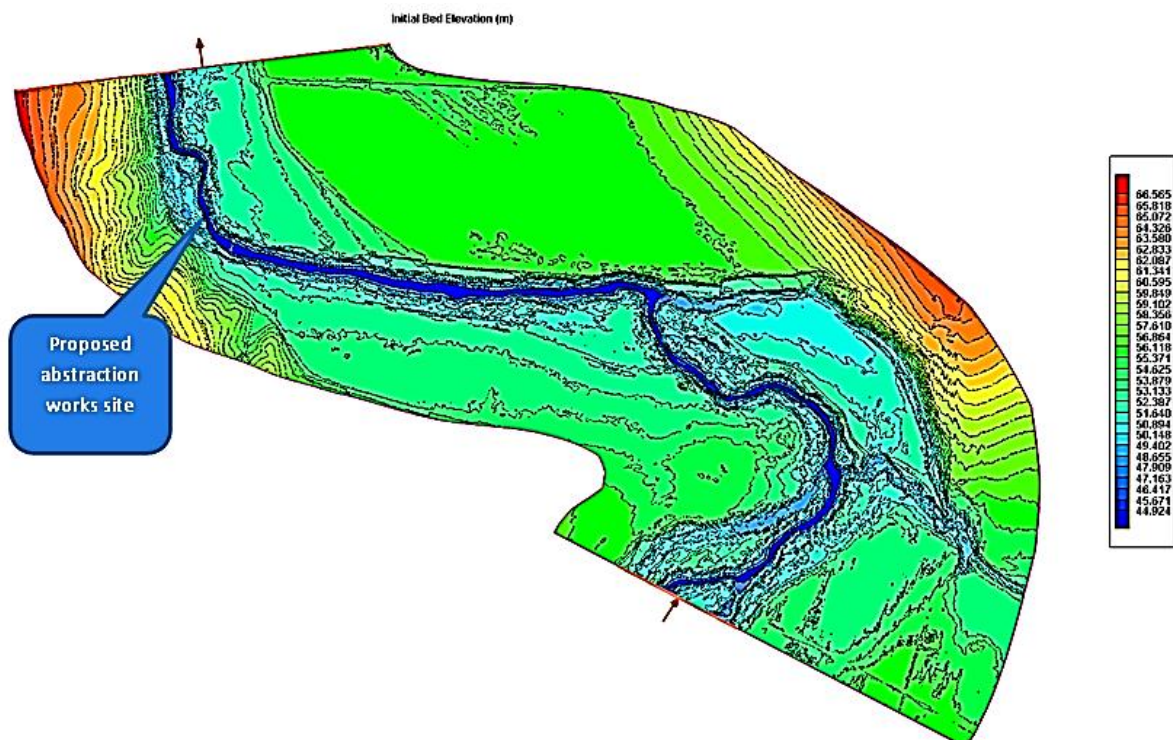


Figure 5.2: 2D model bathymetry of Berg River abstraction works (elevation based on survey data as masl)

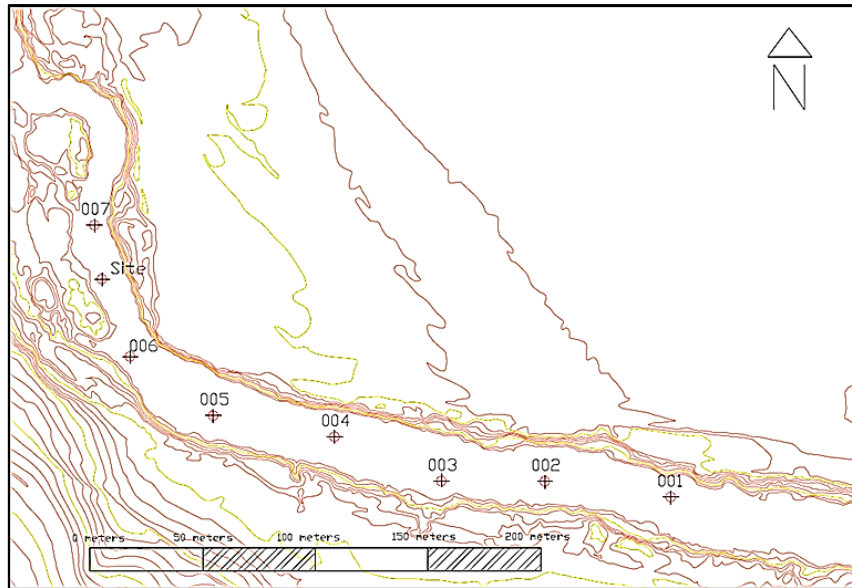


Figure 5.3: Sediment sampling locations

Table 5.1: Site visit sample coordinates

Description	South Coordinates			East Coordinates		
	Degrees	Minutes	Seconds	Degrees	Minutes	Seconds
Measuring Point 001	33°	19'	45.26"S	18°	58'	0.30"E
Measuring Point 002	33°	19'	44.80"S	18°	58'	56.95"E
Measuring Point 003	33°	19'	44.70"S	18°	58'	55.14"E
Measuring Point 004	33°	19'	44.23"S	18°	58'	53.48"E
Measuring Point 005	33°	19'	44.01"S	18°	58'	51.30"E
Measuring Point 006	33°	19'	43.56"S	18°	58'	49.32"E
Measuring Point 007	33°	19'	41.49"S	18°	58'	48.89"E
Abstraction Works Site	33°	19'	42.14"S	18°	58'	48.82"E

After retrieving the sediment samples on site and sending the sediment for grading analysis, the samples sieve analysis and hydrometer results were placed in Table 5.2. Table 5.2 provides a summary of the sediment fractions obtained from the grading analysis. The average d_{50} value was 0.4 mm (sand) if data from sites 001 to 006 were used. The sample at site 007 was affected by bedrock and was therefore not used. Bedrock was visible on the left bank of the river bend during the field visit.

Table 5.2: Summary of sediment grading results

		Unit	Sample 001	Sample 002	Sample 003	Sample 004	Sample 005	Sample 006	Sample 007	Average d_{50}^* Used (CCHE)
Class 1	0-20%	mm	0.01	0.031	0.18	0.06	0.14	0.075	19.00	0.083
Class 2	20-40%	mm	0.05	0.07	0.37	0.33	0.40	0.26	30.00	0.247
Class 3	40-60%	mm	0.13	0.15	0.54	0.50	0.64	0.42	39.00	0.397
Class 4	60-80%	mm	0.23	0.30	0.84	0.80	1.00	0.65	42.00	0.637
Class 5	80-100%	mm	0.44	0.54	1.50	1.70	2.20	1.20	47.00	1.263

5.4 Hydraulics of the proposed abstraction works site

A two-dimensional fully hydrodynamic model (CCHE 2D: Chapter 4) was used to simulate the flow patterns and sediment dynamics in the Berg River to aid in the design of the abstraction works.

The bathymetry (masl) in Figure 5.2 was set up based on the survey data. The survey data consisted of a LIDAR survey and three river cross sections. Based on the geotechnical report, the possible weir location is as indicated and is based on a proposed site from the pre-feasibility study (DWA, 2011). The left river bank is quite steep, while the right bank floodplain is wide. The main channel bed is relatively low compared to the floodplain levels at the proposed site. The average river bed gradient is hydraulically small, at 1:1282.

The following assumptions were made in the mathematical modelling:

- Main channel hydraulic roughness Manning $n = 0.045 \text{ s/m}^{0.333}$
- Floodplain roughness Manning $n = 0.060 \text{ s/m}^{0.333}$
- Tailwater levels based on normal flow calculations and applied at the downstream end of the model, about 80 m from the abstraction works site, and at coordinates X : -1831.591, Y : -3689108.659

Using CCHE 2D sediment modelling as the numerical simulation program, the following results were obtained. The two-, 10- and 100-year flood peaks (Table 5.3) for the specific area were calculated respectively and placed into the numerical simulator.

Table 5.3: Flood peaks

Flood recurrence interval (years)	Flood peak (m ³ /s)
2	376
10	560
100	1493

Figure 5.4 shows the simulation results of the water depth for a two-year flood. The highest flow velocity is on the outside of the main river bend (left bank), where the abstraction works is proposed. This bend effect will therefore limit the abstraction of coarse sediment. The flow stays mainly in the main river channel during this flood. The flood width at the site is much narrower than at the upstream bend. The flow depth at the site is about 7.6 m.

Figure 5.5 indicates that the flow velocity during the two-year flood at the proposed site is about 2.11 m/s. The flow velocities at the upstream bend are much smaller in comparison. Figures 5.6 and 5.7 indicate the same as Figures 5.4 and 5.5, for the 10-year flood. During the 100-year flood, the right floodplain flow is wide, but the velocities at the left bank remain high.

The proposed site on the left bank seems to be ideally located. The flow depth is about 10.39 m during the 100-year flood, with a flow velocity of ± 2 m/s. The floodplain of the right bank is under water, with low flow velocities and shallow water. For this reason it should be possible to construct a weir/embankment on the floodplain without significantly increasing the major flood levels upstream.

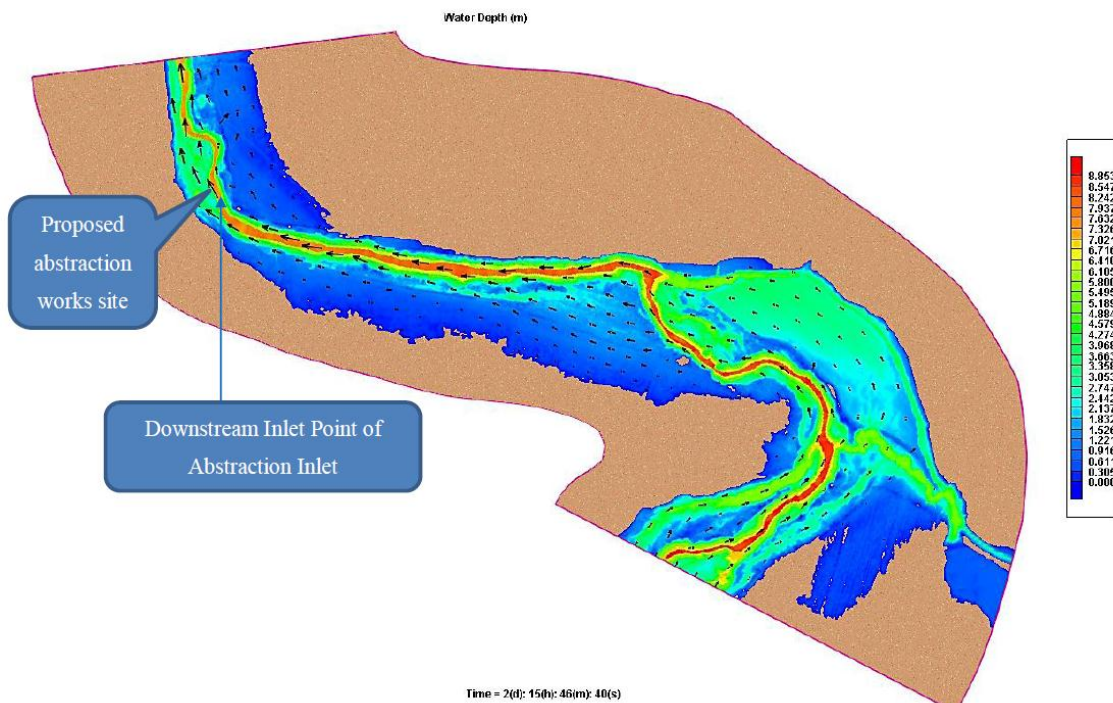


Figure 5.4: Two-year flood water depth (m) with velocity vectors

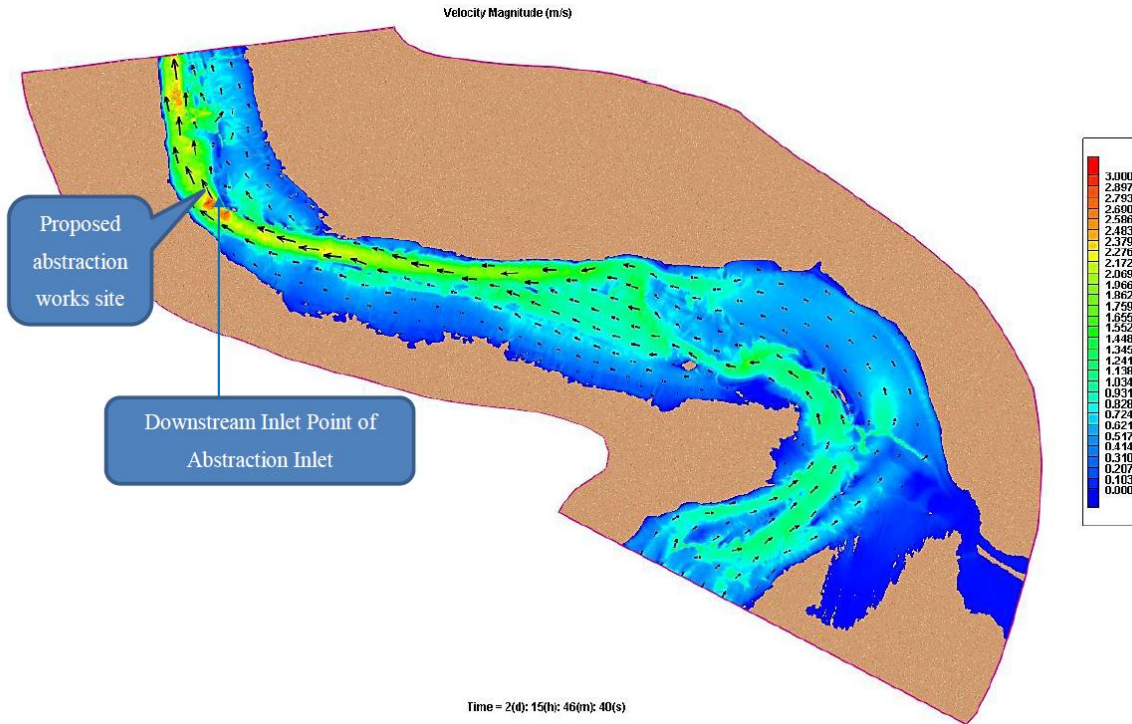


Figure 5.5: Two-year flood velocity magnitude (m/s) with velocity vectors

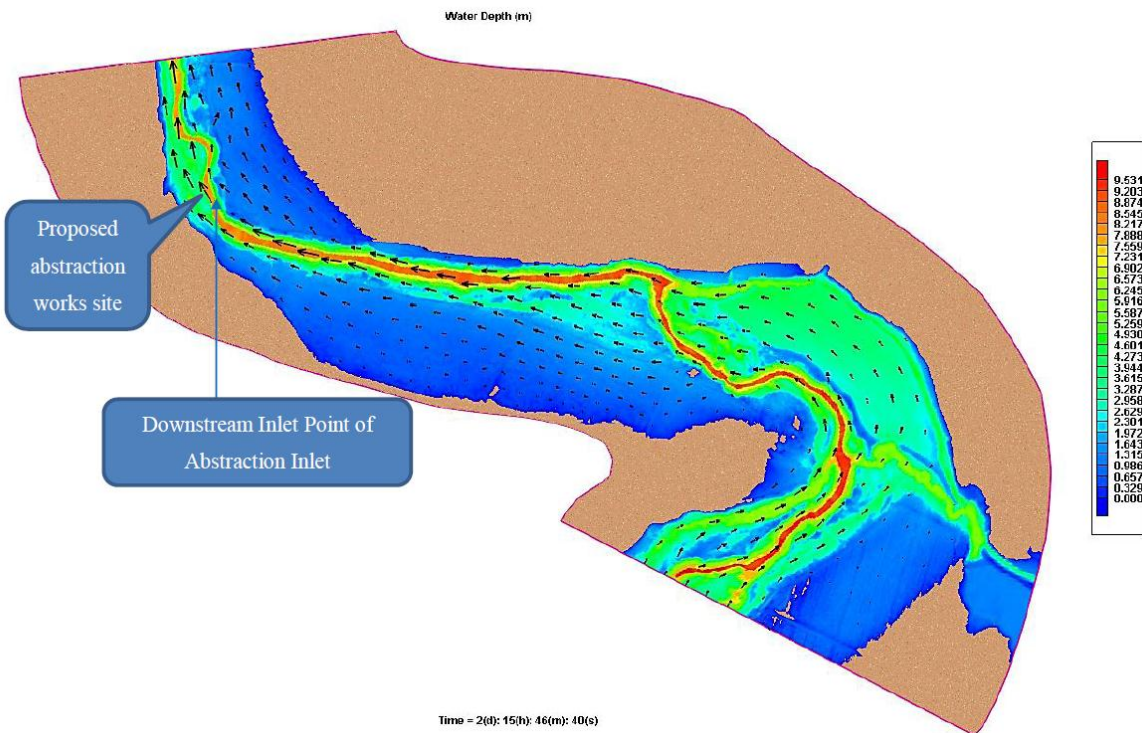


Figure 5.6: Ten-year flood (water depth) with velocity vectors

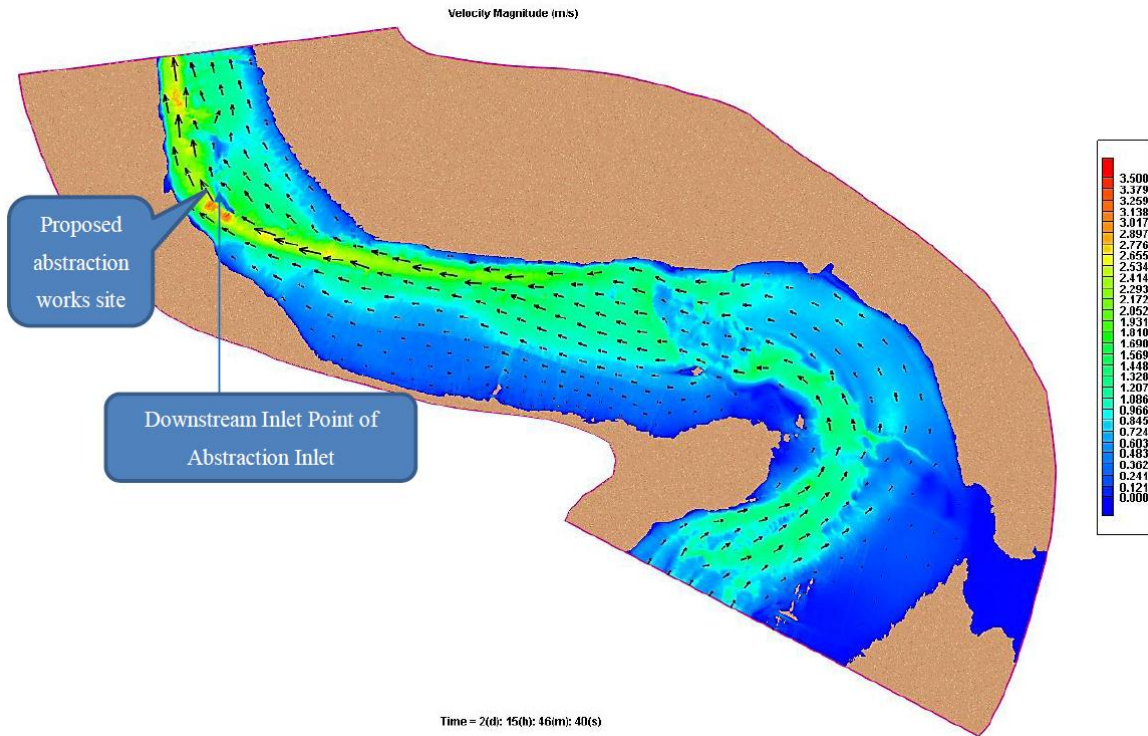


Figure 5.7: Ten-year flood (velocity magnitude) with velocity vectors

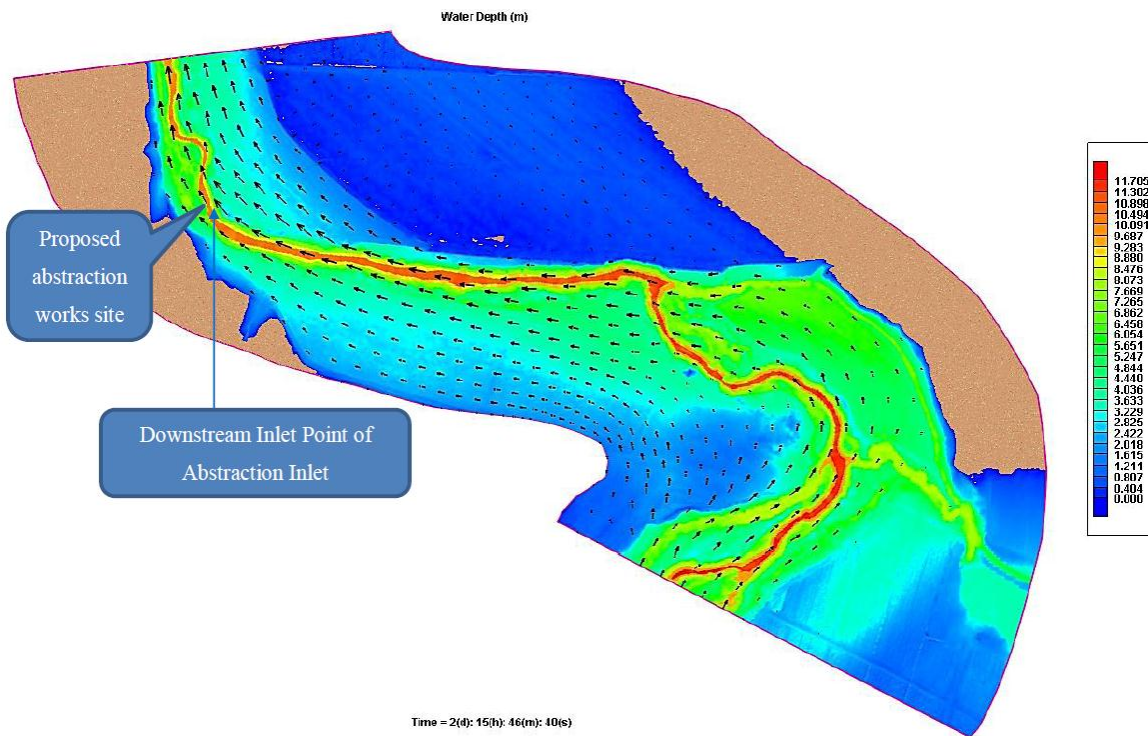


Figure 5.8: Hundred-year flood (water depth) with velocity vectors

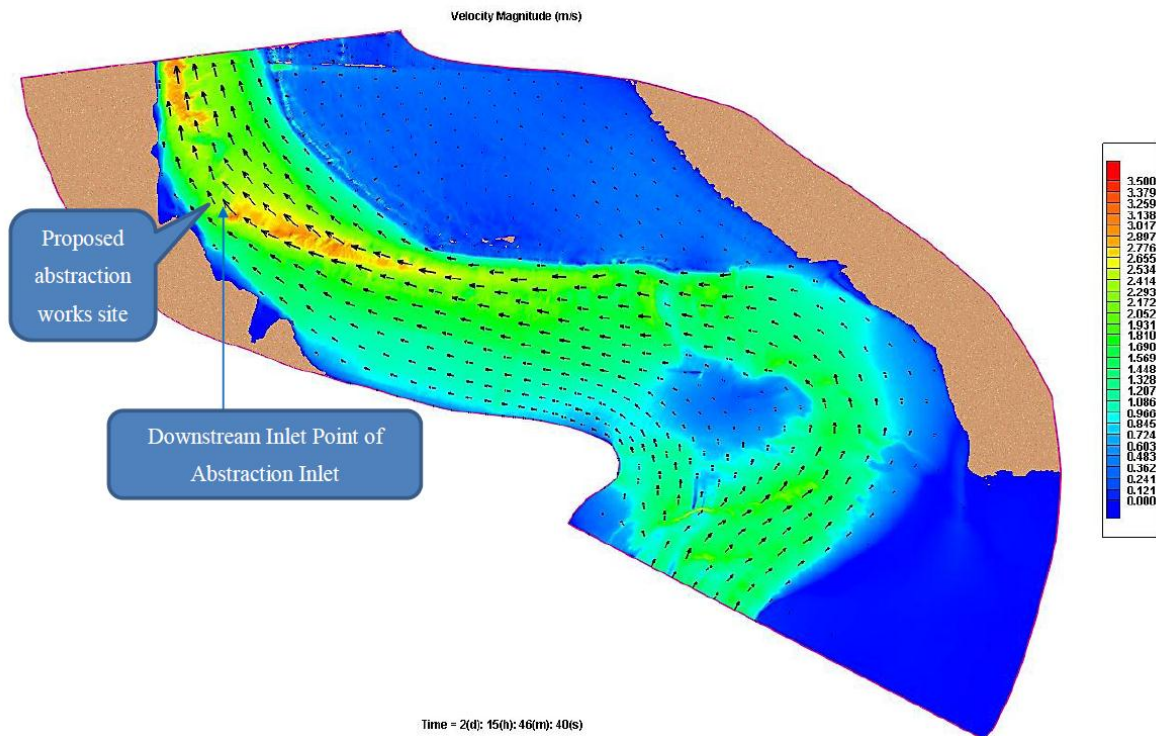


Figure 5.9: Hundred-year flood (velocity magnitude) with velocity vectors

Figures 5.10 to 5.12 show the bed erosion and scour as bed change from the original survey. The results that follow are the two-year, 10-year and 100-year bed changes respectively.

After studying the bed change figures, the finding was made that, during the two-year flood, when the flow was confined more to the main channel, scour was in the order of 3.5 m, whereas the scour depth was about 4.7 m during the 100-year flood.

It was also observed that sediment build-up during the 100-year flood occurs in mass volumes where the structure will be placed. Nevertheless, during a two-year flood the scour does take place at the position specified in Figure 5.12. Thus it is assumed that, during a 100-year flood, there will be sediment build-up in the gravel trap as seen, but that the gravel and sediment will be flushed from the gravel trap during a two-year flood, thus ensuring that the intake of the abstraction works and the upstream area of the intake will be sediment free.

Scour was simulated at the outside of the bend in the river. No bedrock was specified in the model.

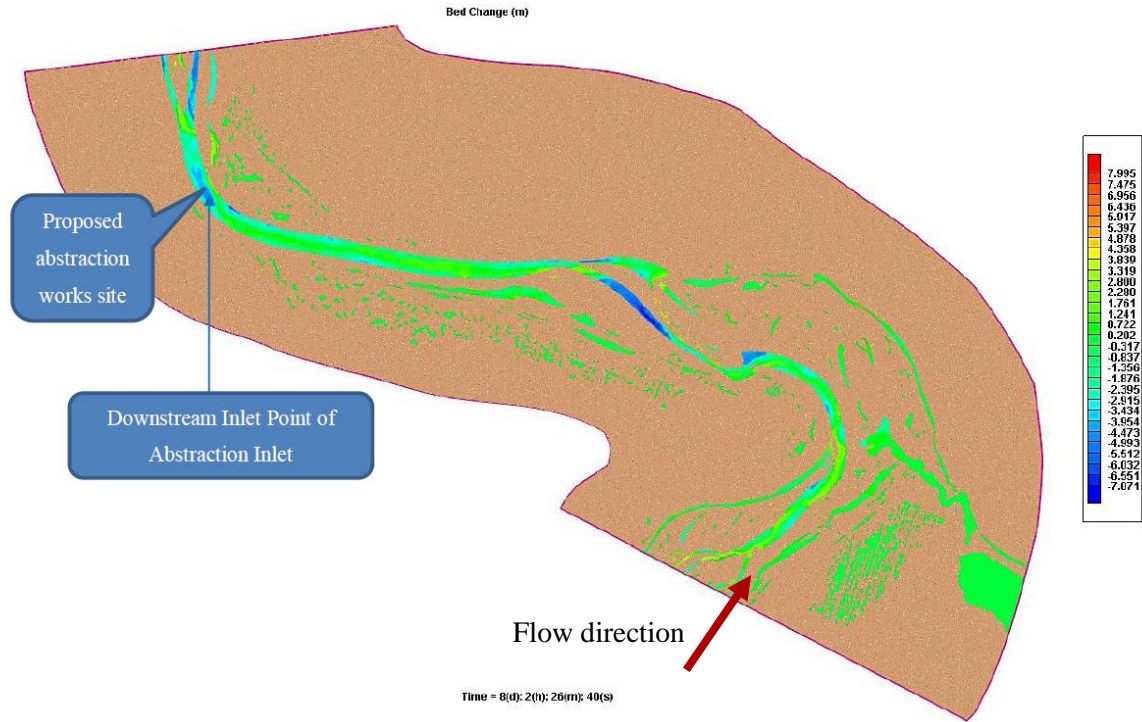


Figure 5.10: Two-year flood (bed change)

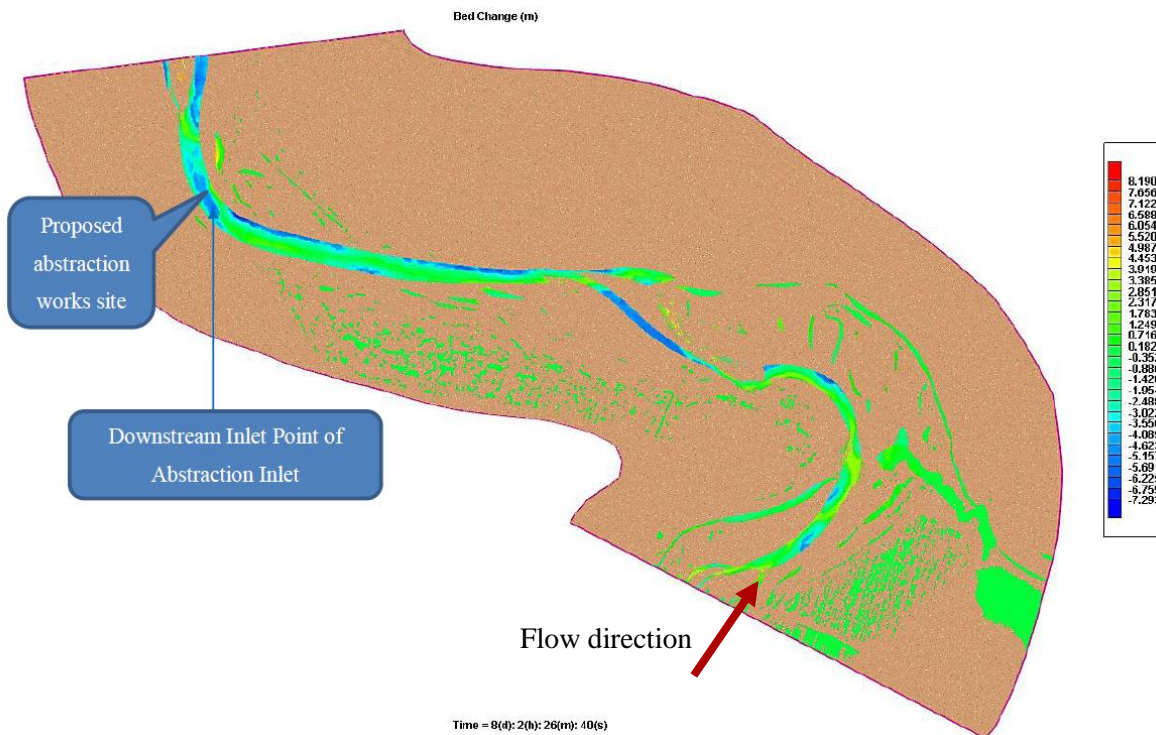


Figure 5.11: Ten-year flood (bed change)

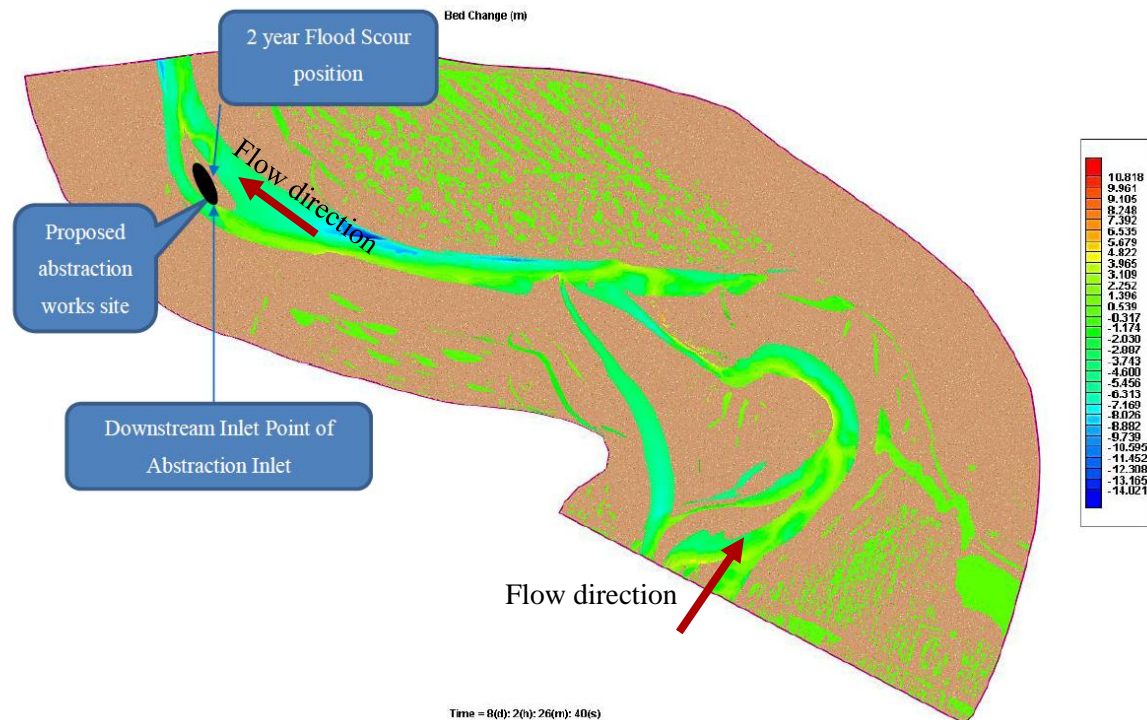


Figure 5.12: Hundred-year flood (bed change)

The position of the abstraction works was finalised at $\pm 30^\circ$ in the bend direction relative to the local flow direction. The reason for the specific orientation was that the intake leads to sediment traps, before reaching the trashrack. The intake was placed at this angle to ensure that efficient momentum was reached to flush the sediment settling systems.

Figure 5.13 illustrates the 30° angle of orientation compared to the flow direction in the Berg River's main channel. Figure 5.13 also provides the hydraulic structures of the abstraction works, with a low crump weir on the right bank. The position of the abstraction works was as far as possible into the main river canal on the toe of the left river bank. The reason for the placement of the structure was that the river width was limited and needed an optimum location for abstraction. This was where the most continuous river flow would occur and was the main purpose of this thesis study.

The angle of the intake in the Berg River abstraction works was chosen in terms of the terminology of this thesis study's orientation (Figure 1.3). Chapters 3 and 4 illustrated through physical and numerical model results that a 30° orientation provided the least obstruction in the river.

As a weir was required in the design of the Berg River abstraction works, the result was related more to the 30° L-shaped laboratory experiment (see p 3-26). According to the experiment, local scouring occurred upstream of the radial gate of the boulder trap. In the case where the boulder trap was flushed during operation, the minimum operating level was provided by the weir and the area along the underwater intake opening flushed clear.

The sediment and debris that pass through the intake will deposit in the gravel trap or be stopped by the trashrack before passing through the trashrack. As a final measure to reduce sediment from being abstracted to the pumps, four hoppers with jet pumps were placed downstream of the trashrack. The total volume of the hoppers should not exceed 200 times the discharge per second into the hopper (Basson, 2005).

To ensure that all the sediment diversion structures work correctly, it would be recommended that a physical model of the Berg River abstraction works be built.

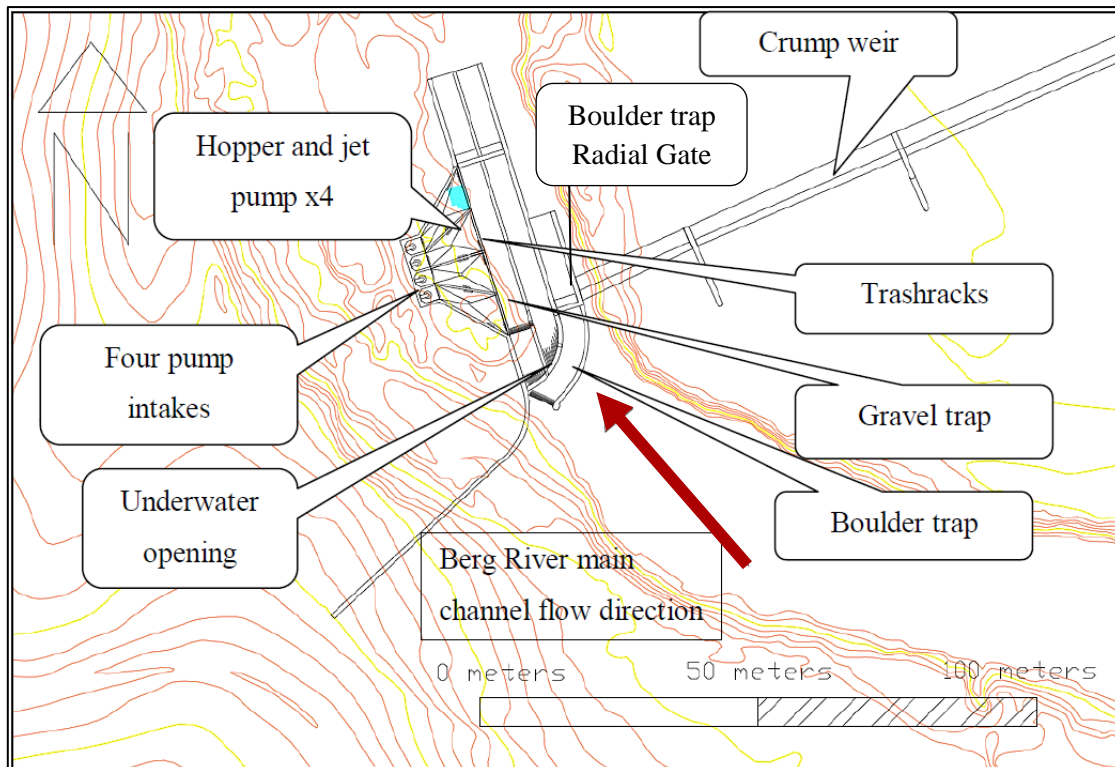


Figure 5.13: Plan view of layout of proposed abstraction works

Chapter 6

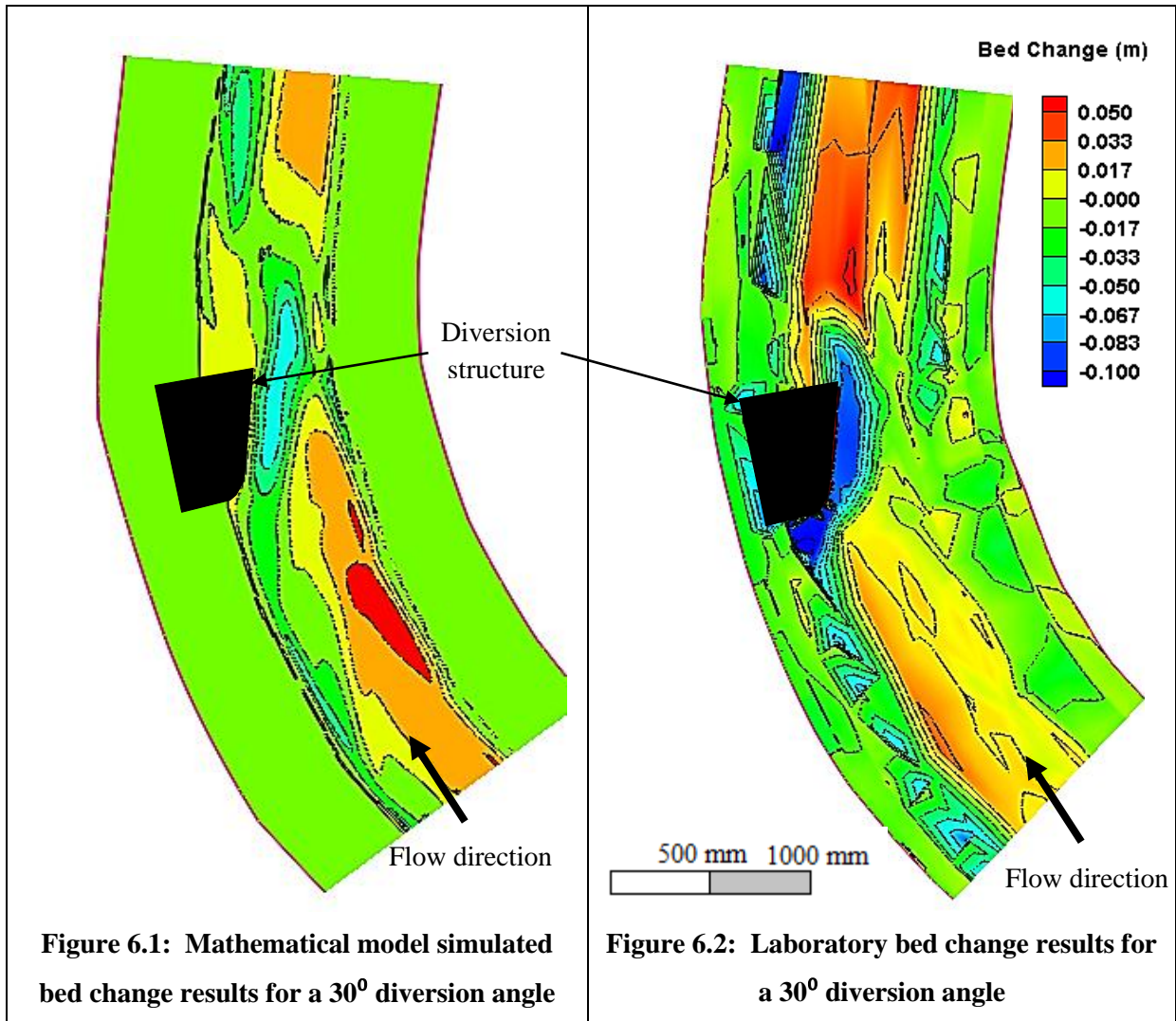
6. Conclusions and Recommendations

Regarding the diversion location, Lui et al. (1982) and Shen (1971) claimed that radius-to-width ratios of 4.0 to 8.0 and 2.5 to 8.0 respectively, will provide fully developed secondary flow and supply the optimum scour in the river bend. The deepest scour in the physical experiments carried out during this study occurred as stated in the literature, which was shown to be correct. The above ratios in the literature can be used, as they will ensure that secondary currents are developed and that scour will take place in the channel on the outside of the bend.

For planning purposes it is recommended that the empirical relationship of Table 2.2 (SC and CHES, 1992) be used in predicting the optimum diversion location, as it extends over a wide range of radius-to-width ratios and hydraulic conditions.

The orientation of the diversion structure to limit sediment diversion follows from the results in Figures 6.1 and 6.2, which provide the physical model bed change and the numerical model simulated bed change of a 30° diversion angle. The L-shaped structure was not considered, as it caused damming upstream of the intake, resulting in slower velocity flow and in general deposition of sediment. The 30° angled diversion structure had the least effect on the opposite channel bank scour due to deflection, with the best positioned and size of scour.

A percentage error of 37 % was present between the numerical and physical model scour depth results for the 30° angle of orientation test. Thus the bed change results were in relatively good agreement with one another, considering that the model only simulated 2D depth averaged flows. The position of scour was along the structure face, where the intake would be located. The only difference in scour was the size, and this specific detail can only be achieved accurately with three-dimensional simulation modelling.



Figures 6.3 to 6.6 illustrate the sediment levels before and after the physical and numerical test runs. Avery (1989), with Hufferd and Watkins (1972), explained that an ideal diversion angle is between 10° and 45°. This angle was measured from the centre line of the intake to the main direction of river flow. The final recommendation is that a 30° angle of orientation be used, with reference to the terminology of this thesis regarding angle of orientation (see section 3.3.2), for RoR hydropower generation.

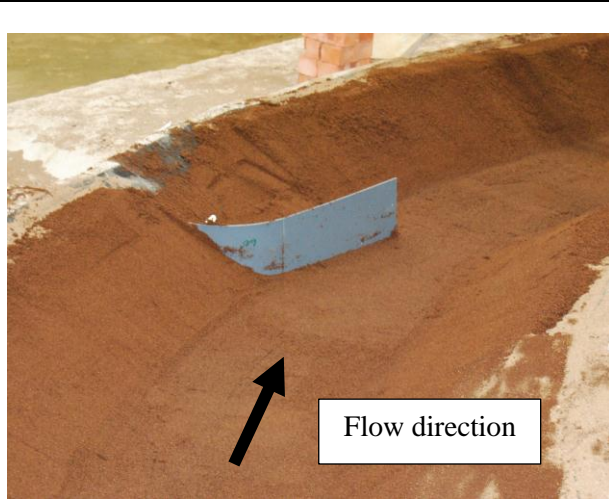


Figure 6.3: Sediment level of physical model before experiment run

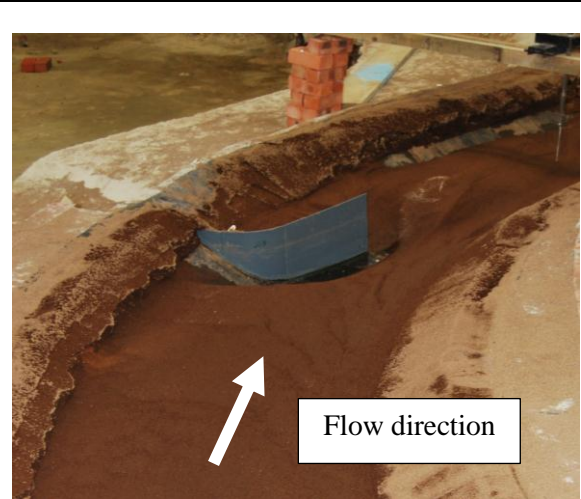


Figure 6.4: Sediment bed level of physical model after experiment run

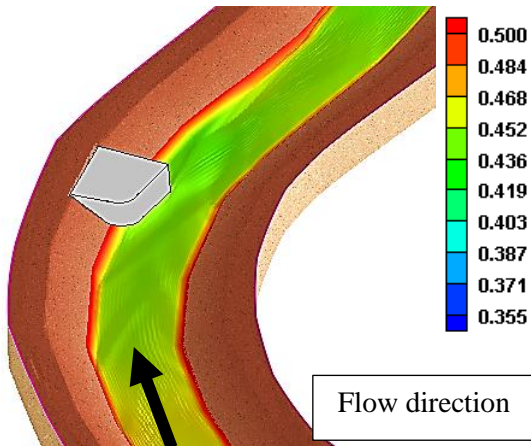


Figure 6.5: Sediment level of numerical model before simulation

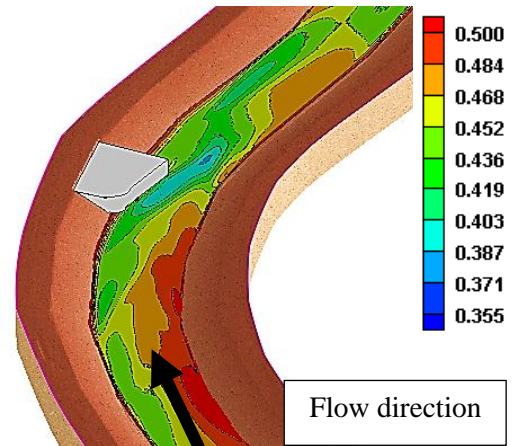


Figure 6.6: Sediment level of numerical simulation after test run

According to this thesis and Figure 6.7, the DDR recommended for RoR hydropower stations should not exceed 50%. Figure 6.8 originated from the results of Figure 6.7's results and provided an SDR according to calculated DF_rR and DDRs. Figure 6.8 can be used in practice with relevance to this thesis study's specific parameters and outcome.

In RoR hydropower stations the smaller the SDR ratio, the less the hydro damage. According to Figure 6.8 the best operating DDR would occur during floods or in large rivers with small diversion discharges.

Sand traps or hoppers with jet pumps are ideal to deposit coarse sediment and to limit mechanical wear on the turbines and are recommended for RoR hydropower schemes. As the RoR hydropower in this thesis was only for low head power generation, a Kaplan turbine with an HVOF protection layer

is recommended. Plasma nitriding does not provide sufficient protection, according to Mann and Arya (2001).

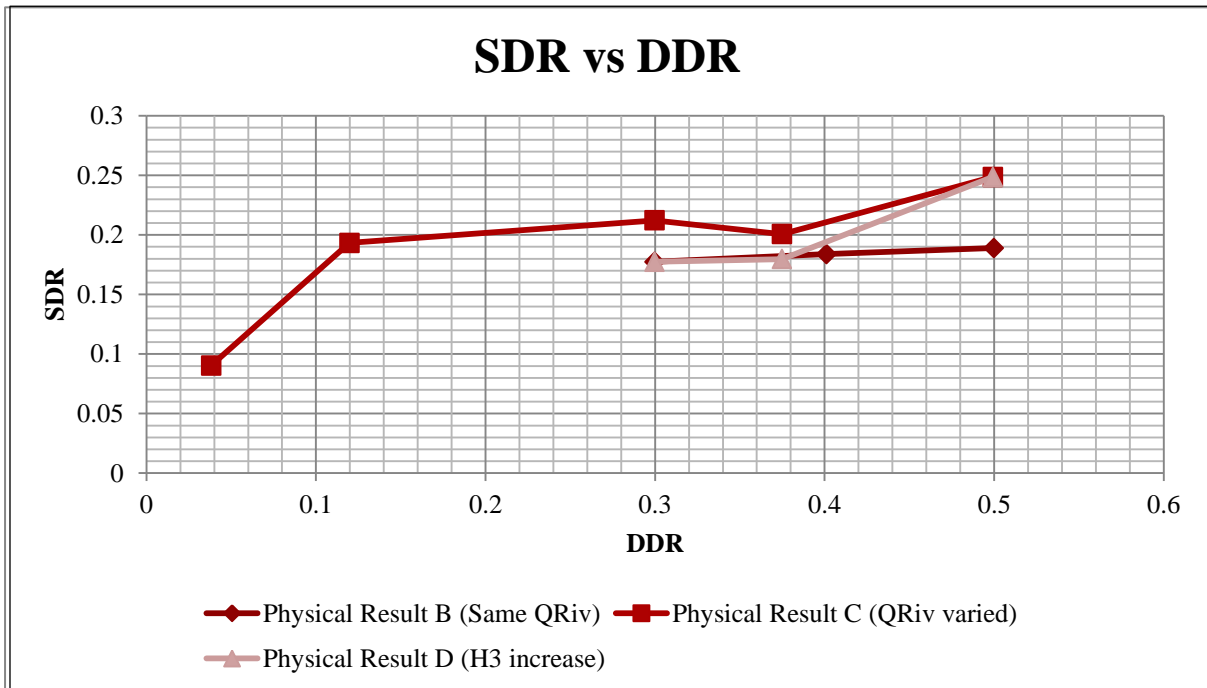


Figure 6.7: SDR versus DDR for RoR hydropower generation

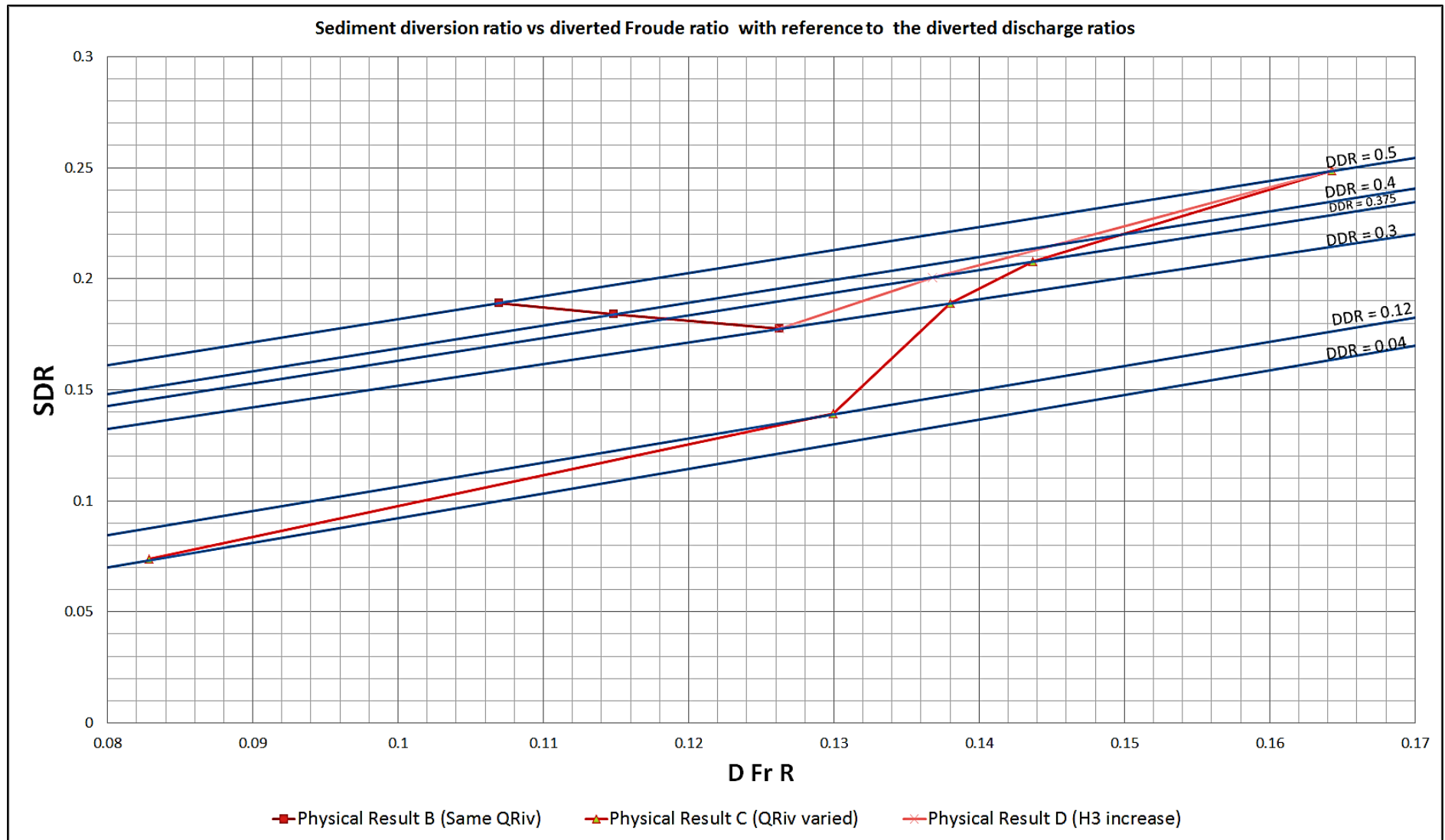


Figure 6.8: Sediment diversion ratio vs. diverted Froude ratio with reference to the diverted discharge ratios

Recommendations to improve RoR hydropower schemes and suggestions for future research are provided below:

- Different river shapes/bends and topographies with different width-to-depth ratios can be investigated, as the maximum scour position can differ in the channel bend.
- The river width can be increased to observe what the angle and the effect of the diversion structures will be.
- Sediment needs to be fed into the river to establish whether the scour hole, according to curvilinear effects, will occur as described and whether sediment ingress into the intake opening will increase.
- Three-dimensional numerical modelling can be attempted as opposed to a two-dimensional modelling system used here.
- Physical models and numerical models of the sediment diversion effects on settling basins, settlers, forebays and penstocks can be investigated.
- Sediment flushing in the diversion structure can be studied to determine whether flushing will occur effectively.
- The diversion of sediment in straight channels can be researched in order to compare with the results of research on curved channels.
- Further studies on channel flows are recommended, with Froude numbers smaller or equal to 0.8. These studies can include different sediment d_{50} 's, angles of diversion orientation, channel bend angles, channel size and different slopes.

References

- ASCE Committee on Intakes (1995) *Guidelines for the Design of Intakes for Hydroelectric Plants*”, ASCE.
- Atkins, W.A. (2003) *Hydroelectric Power*.
- Avery, P. (1989). *Sediment Control at Intakes- A Design Guide*, Bedford: BHRA.
- Basson, G.R. (2005). *Consideration for the Design of River Abstraction Works in South Africa*, Stellenbosch: Stellenbosch University.
- Basson, G.R. (2012). *Western Cape Future Schemes: Hydraulic Design of the proposed Berg River Abstraction Works at Voëlvllei Dam*, Stellenbosch.
- Basson, G.R. and Rooseboom, A. (1997). *Dealing with Reservoir Sedimentation: WRC Report No. TT 91/97*, Pretoria: Water Research Commission.
- Beck, J.S. and Basson, G.R. (2003) *The hydraulics of the impacts of dams development on the river morphology*, WRC.
- Bishwakama, M.B. (2007) 'Concept Paper for Research on Optimum Sediment Handling in Run-Of-River Hydropower Plants', International Conference on Small Hydropower, Sri Lanka, pp. 1-9.
- Bishwakarma, M.B. and Stole, H. (2008) 'Real-time Sediment Monitoring in Hydropower Plants', *Journal of Hydraulic Research*, vol. 46, no. 2, pp. 282-288.
- Bouvard, M. (1992). *Mobile Barrages and Intakes on Sediment Transporting Rivers*, Brookfield: A.A. Balkema.
- Brink, C.J., Basson, G.R. and Denys, F. (2005). *Bend Diversion to minimise sediment intake*, Stellenbosch: Stellenbosch University.
- British Standards Institution (1965). *BS 3680.- Methods of measurement of liquid flow in open channels*, 44th edition, London: BSI.
- Bulle, H. (1926). *Reduction of Sediment Entrainment: Diversion Angle*, Littleton, USA: Water Resource Publication.
- Central Board of Irrigation & Power and INCOLD (2008). *Silting Problems in Hydropower Projects*, New Delhi: Central Board of Irrigation & Power and INCOLD.
- Chadwick, A., Morfett, J. and Borthwick, M. (2004). *Hydraulics in Civil and Environmental Engineering*, London: Spon.
- De Belidor, B.F. (2010). *Encyclopædia Britannica*, Encyclopædia Britannica.
- Department of Environmental Affairs and Tourism (1999) *National State of the Environment Report-South Africa: Freshwater Systems and Resources: State #4*, October, [Online], Available: <http://www.ngo.grida.no/soesa/nsoer/issues/water/state4.htm> [18 September 2012].

- Donegan, E., Falzone, K., Fox, S. and Siodmak, C. (2002). *History of Hydropower*.
- DWA (2011) *Berg River Abstraction Works at Voëlvlei Dam*, Aurocon.
- ESHA (2011) 'Guidelines for Micro Hydro Power Development', *Spatial Plans and Local Arrangement for Small Hydro*, pp. 1-46.
- Ettema, R., Arndt, R., Robert, P. and Wahl, T. (2000). *Hydraulic Modeling: Concepts and practice*, VA: ASCE.
- Gordon, J.L. (1970) 'Vortices at intakes', *Water Power*, vol. 22, April, pp. 137-138.
- Habermaas, F. (1935). *Cited in Shen (1971)*.
- Henderson, F.M. (1967). *Open Channel Flow*, New York: The Macmillan Company.
- Hufferd, J.A. and Watkins, J.S. (1972). *Sediment Control Methods: Chapter V - Control of Sediment in Canals*, New York: American Soc. Civil Engineering Task Committee for the Preparation of the Manual of Sedimentation.
- Jia, Y. and Wang, S.S.Y. (2001). *CCHE2D: Two-dimensional Hydrodynamic and Sediment Transport Model For Unsteady Open Channel Flows Over Loose Bed*, Mississippi: National Center for Computational Hydroscience and Engineering.
- Karimi, A. and Schmid, R.K. (1992) 'Ripple formation in solid-liquid erosion', *Wear*, no. 156, pp. 33-47.
- Knauss, J. (1987) 'Swirling flow problems at intakes', *Hydrological Science*, vol. 33, no. 3, June.
- Kuun, G.F. (2009). *The Construction of Dams to Ensure Water Security in South Africa*, Pretoria: University of Pretoria.
- Lane, E.W. (1955). *Cited in Shen (1971)*.
- Lencastre, A. and Holmes, P. (1987). *Handbook of Hydraulic Engineering*, Harlow: Prentice Hall Europe, Ellis Horwood Ltd.
- Library of Congress *The World's First Hydroelectric Power Plant Began Operation September 30, 1882*, [Online], Available: http://www.americaslibrary.gov/jb/gilded/jb_gilded_hydro_2.html [8 May 2012].
- Linsley, R.K. and Franzini, J.B. (1979). *Water-Resources Engineering*, 3rd edition, Tokyo: McGraw-Hill Kogakusha Ltd.
- Lui et al. (1982). *Cited in Tan (1996)*.
- Mann, B.S. and Arya, V. (2001) 'Abrasive and erosive wear characteristics of plasma nitriding and HVOF coatings: their application in hydro turbines', *Elsevier*, February, pp. 354-360.
- Mosoyi, E. (1957). *Water Power Development*, 1st edition, Budapest: Hungarian Academy of Science.
- Mosoyi, E. (1965). *Cited is Shen (1971)*.

Murray, A.J. and Watermeyer, C.F. (2011). *The provision of a detail study and investigation for the desiltation of dam weir in Mbashe Dam in the Southern Region*, East London: Eskom Holding - Southern Region.

Naidu, B.K.S. (1996) 'Silt Erosion problems in hydropower stations and their possible solutions', in *Proc. Silt damages on equipment in hydropower stations and remedial measures*, New Delhi.

O'Connor, J.J. and Roberson, E.F. (2004). *Johann Andreas von Segner*, <http://www-history.mcs.st-and.ac.uk/Biographies/Segner.html> edition.

Olesen, K.W. and Pradhan, A. (2010). *Sediment Handling optimization for a Himalyan run-of-river scheme*, India.

Paish, O. (2002) 'Small Hydro power: Technology and current status', *Pergamon-Renewable and Sustainable Energy Reviews*, vol. 6, February, pp. 537-556.

Penche, C. (2004). *Guide on How to Develop a Small Hydropower Plant*, ESHA.

Penche, C. and De Minas, D.I. (1998). *Layman's Handbook on How to Develop a Small Hydro Site*, 2nd edition, ESHA.

Philo of Byzantium. *Multilingual Archive*, [Online], Available: http://www.worldlingo.com/ma/enwiki/en/Philo_of_Byzantium [8 May 2012].

Pruess, M. (2010). *History of Hydropower*.

Ract-Madouse et al. (1955) 'Some recently build high altitude bottom intakes', *La houille Blanche*, Dec, p. 853.

Ramos, H. (ed.) (2000). *Guideline for Design of Small Hydropower plant*, Belfast: WREAN and DED.

Raudkivi, A.J. (1993). *Sedimentation: Exclusion and Removal of Sediment from diverted water*, Rotterdam: A.A. Balkema.

Rooseboom et al. (1983). *National Transport Commission road drainage manual*, 2nd edition, Pretoria: South African National Roads Agenct Ltd.

Rzhanitsyn, N.A. (1960). *Cited in Shen (1971)*.

SC and CHES (1992). *Sedimentation Handbook (In Chinese)*, Beijing: Environment Science Press.

Scheuerlein, H. (1984) *Die Wasserentnahme aus geschiebeführenden Flüssen (In German)*, Berlin, Germany.

Shen, H.D. (1971). *River Mechanics: Volume 2*, USA.

Simons, D.B. and Senturk, F. (1992). *Sediment Transport Technology: Water and Sediment Dynamics*, Littleton, Colorado: Water Resource Publication.

SPLASH (2005). *Guideline for Micro Hydro power Development*, SPLASH.

Tan, Y. (1996) 'Design of silt related hydraulic structures', International Conference on reservoir sedimentation.

The Thomas Edison Papers (2012), [Online], Available: <http://edison.rutgers.edu/generator.htm> [8 May 2012].

Thompson, J. (1876). *Cited in Vanoni (1977)*.

Tung, T.P. (1993). *Evaluation of Alternative Intake Configuration for Small Hydro*, Munich: Actas de HIDROENERGIA 93.

Vanoni, V.A. (1977). *Sedimentation Engineering*, New York: Am. Soc. Civ Engineers Task Committee for the Preperation of the Sediment Manual.

Wu, W. (2001). *CCHE 2D Sediment Transport Model*, Mississippi: National Centre for Computational Hydroscience and Engineering.

Yen, C. and Lee, K.T. (1995) 'Bed topography and sediment sorting in channel bend with unsteady flow', *Journal for Hydr. Eng.*, vol. 121, no. 8, pp. 591-599.

Zhang, Y. (2006). *CCHE-GUI – Graphical Users Interface for NCCHE Model*, Mississippi: National Centre for Computational Hydroscience and Engineering.

Zhang, Y. and Jia, Y. (2009). *CCHE-MESH: 2D Structured Mesh Generator*, Mississippi: National Centre for Computational Hydroscience and Engineering.

Appendix A

Physical Results

Physical Experiment 1 - Without Diversion Structure



Figure A-1: Photo 1 of river flow without diversion structure



Figure A-2: Photo 2 of river flow without diversion structure



Figure A-3: Photo 3 of river flow without diversion structure



Figure A-4: Photo 4 of river flow without diversion structure

Physical Experiment 2 - 0° Structure with Flow



Figure A-5: Photo 1 of 0° structure



Figure A-6: Photo 2 of 0° structure

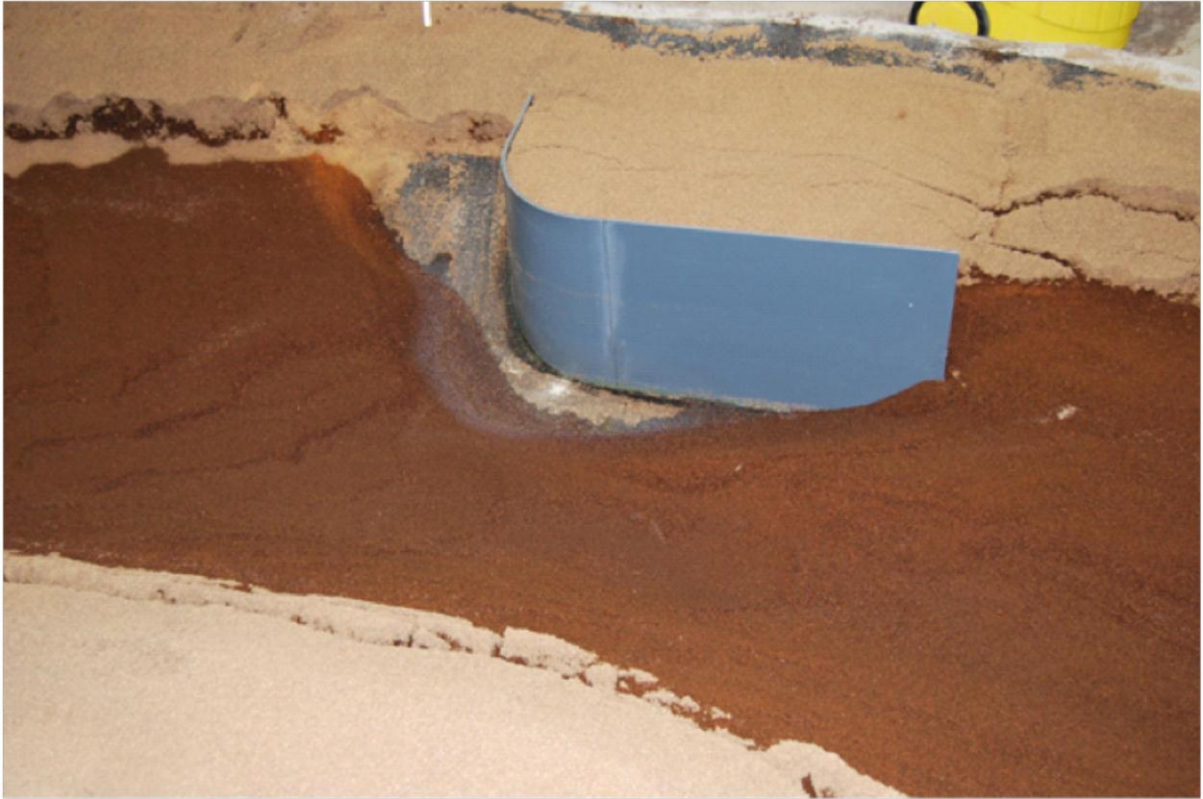


Figure A-7: Photo 3 of 0° structure

Physical Experiment 3 - 0° with Flow (L-Shaped Structure)



Figure A-8: Photo 1 of 0° structure with L-shaped attachment



Figure A-9: Photo 2 of 0° structure with L-shaped attachment



Figure A-10: Photo 3 of 0° structure with L-shaped attachment

Physical Experiment 4 - 30° Structure with Flow



Figure A-11: Photo 1 of 30° structure



Figure A-12: Photo 2 of 30° structure



Figure A-13: Photo 3 of 30⁰ structure



Figure A-14: Photo 4 of 30⁰ structure

Physical Experiment 5 - 30° with Flow (L-Shaped Structure)



Figure A-15: Photo 1 of 30° structure with L-shaped attachment

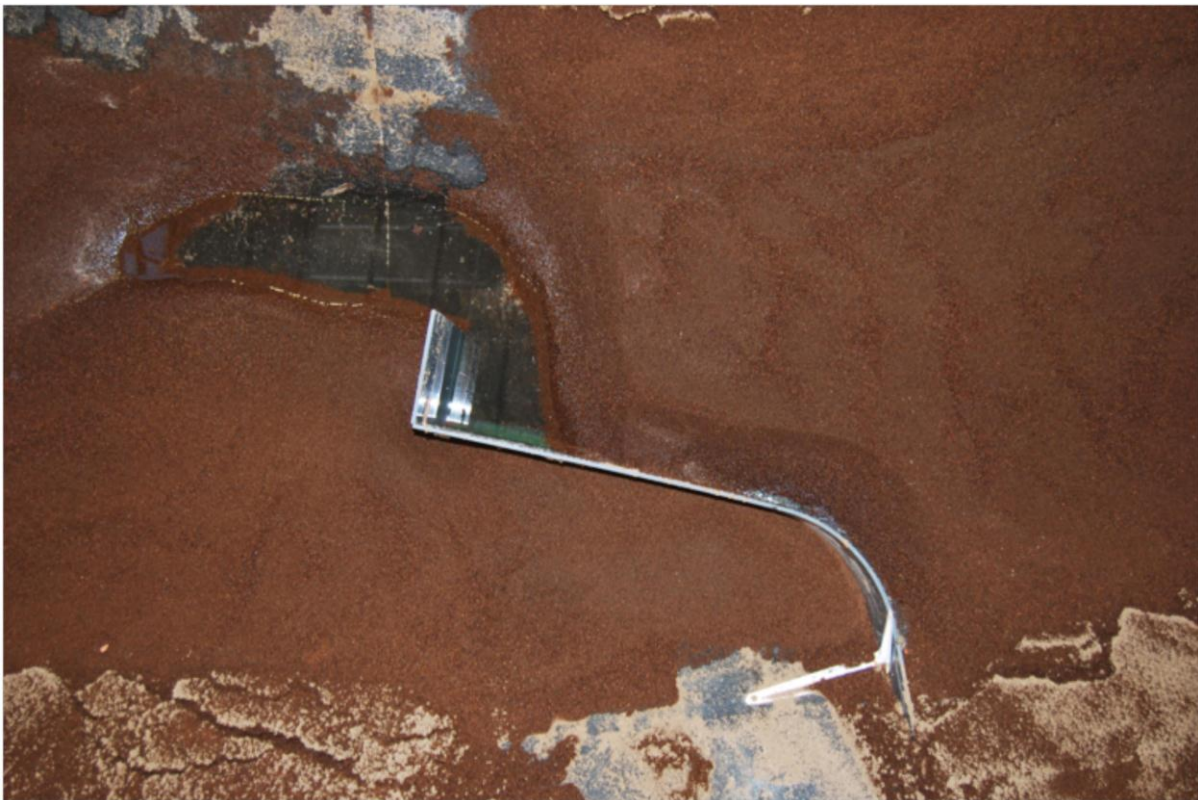


Figure A-16: Photo 2 of 30° structure with L-shaped attachment



Figure A-17: Photo 3 of 30° structure with L-shaped attachment



Figure A-18: Photo 4 of 30° structure with L-shaped attachment

Physical Experiment 6 - 45° Structure with Flow

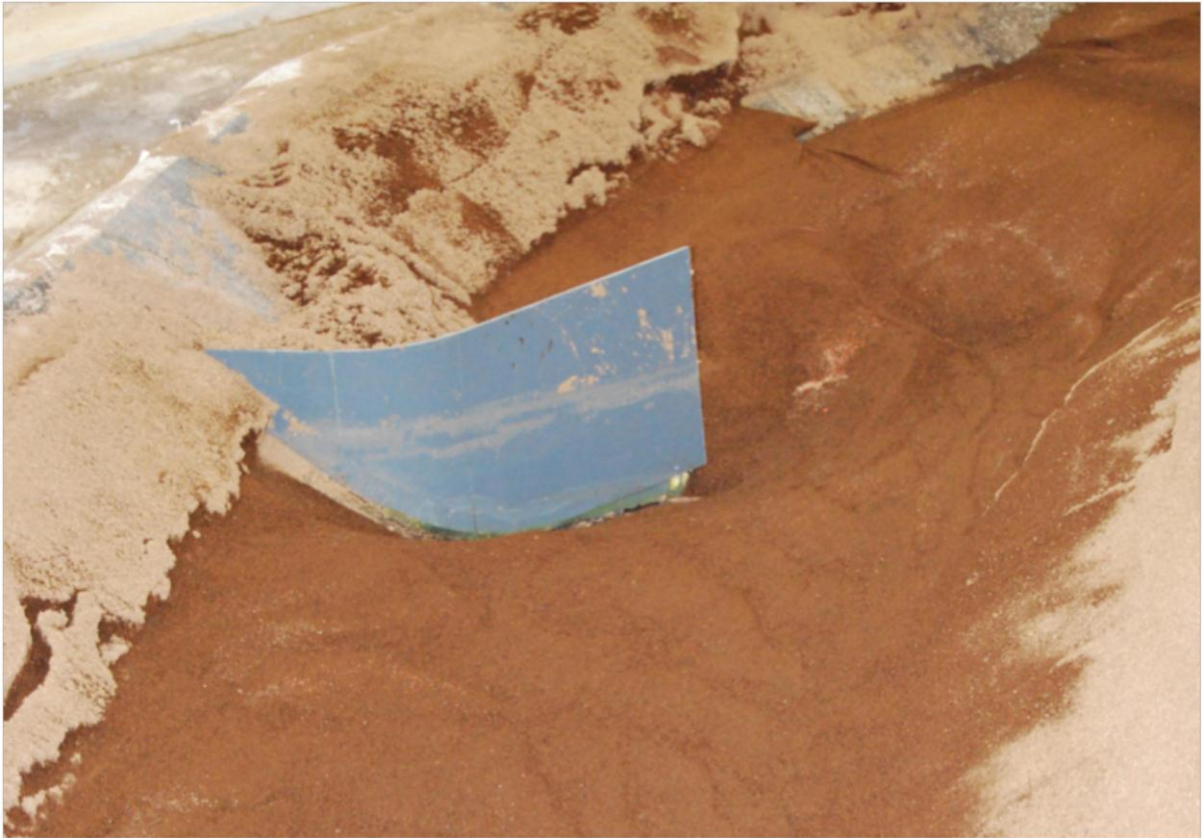


Figure A-19: Photo 1 of 45° structure



Figure A-20: Photo 2 of 45° structure

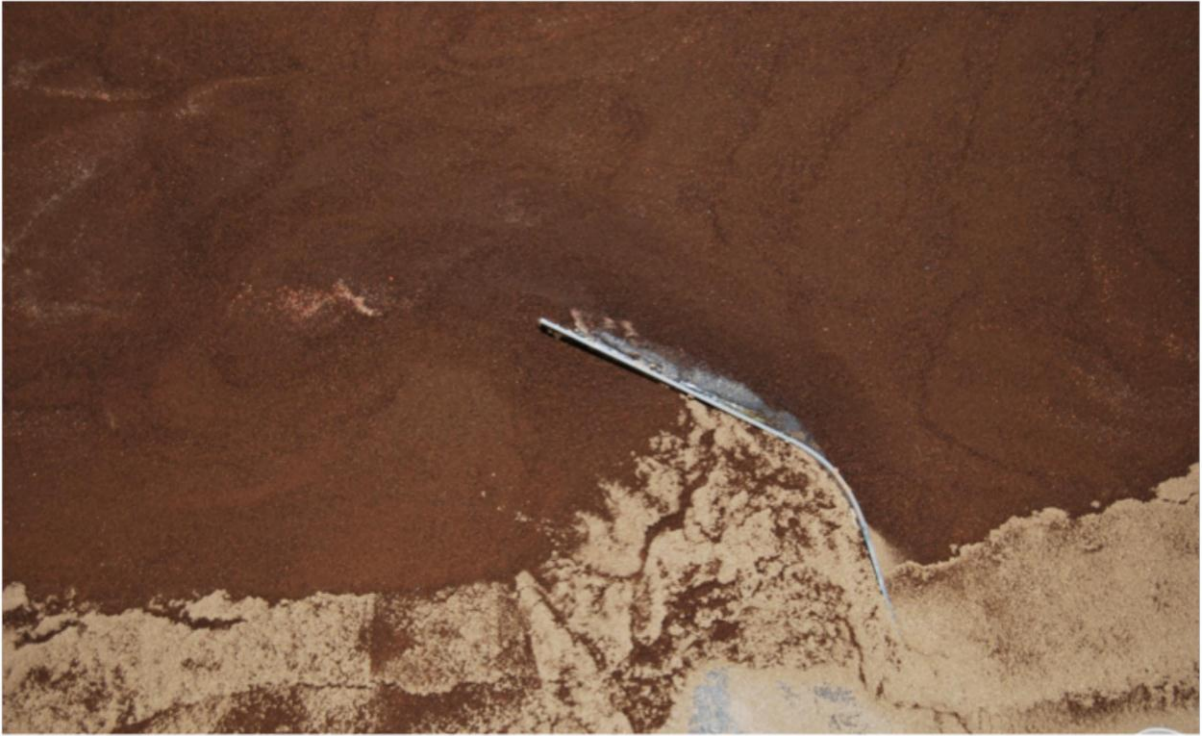


Figure A-21: Photo 3 of 45° structure

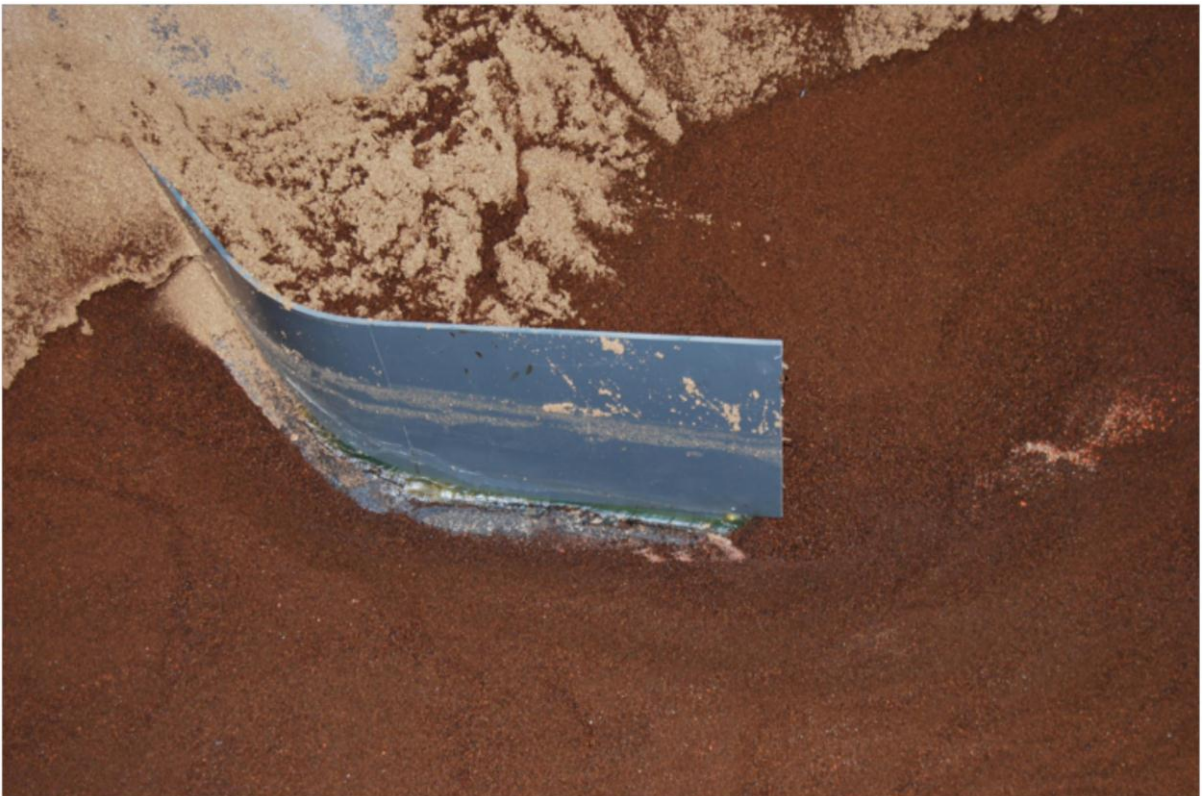


Figure A-22: Photo 4 of 45° structure



Figure A-23: Photo 5 of 45⁰ structure

Physical Experiment 7 - 45° with Flow (L-Shaped Structure)

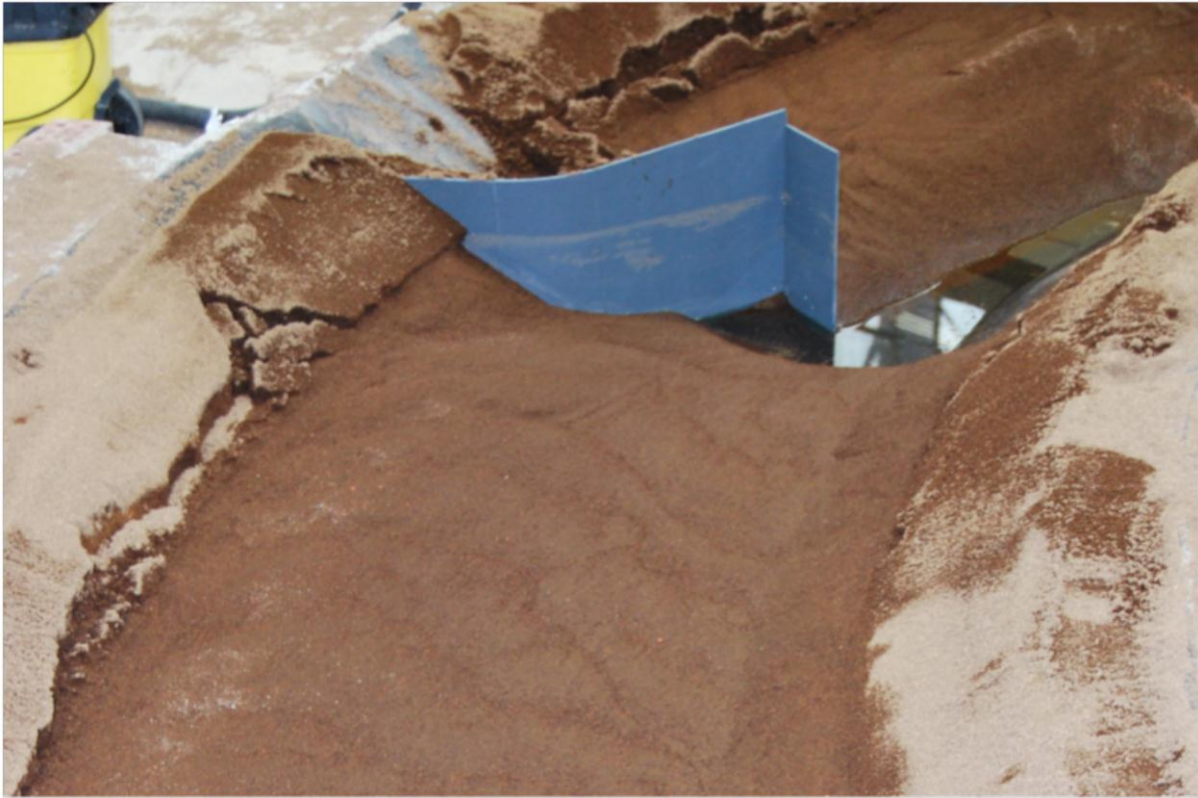


Figure A-24: Photo 1 of 45° structure with L-shaped attachment



Figure A-25: Photo 2 of 45° structure with L-shaped attachment



Figure A-26: Photo 3 of 45° structure with L-shaped attachment



Figure A-27: Photo 4 of 45° structure with L-shaped attachment

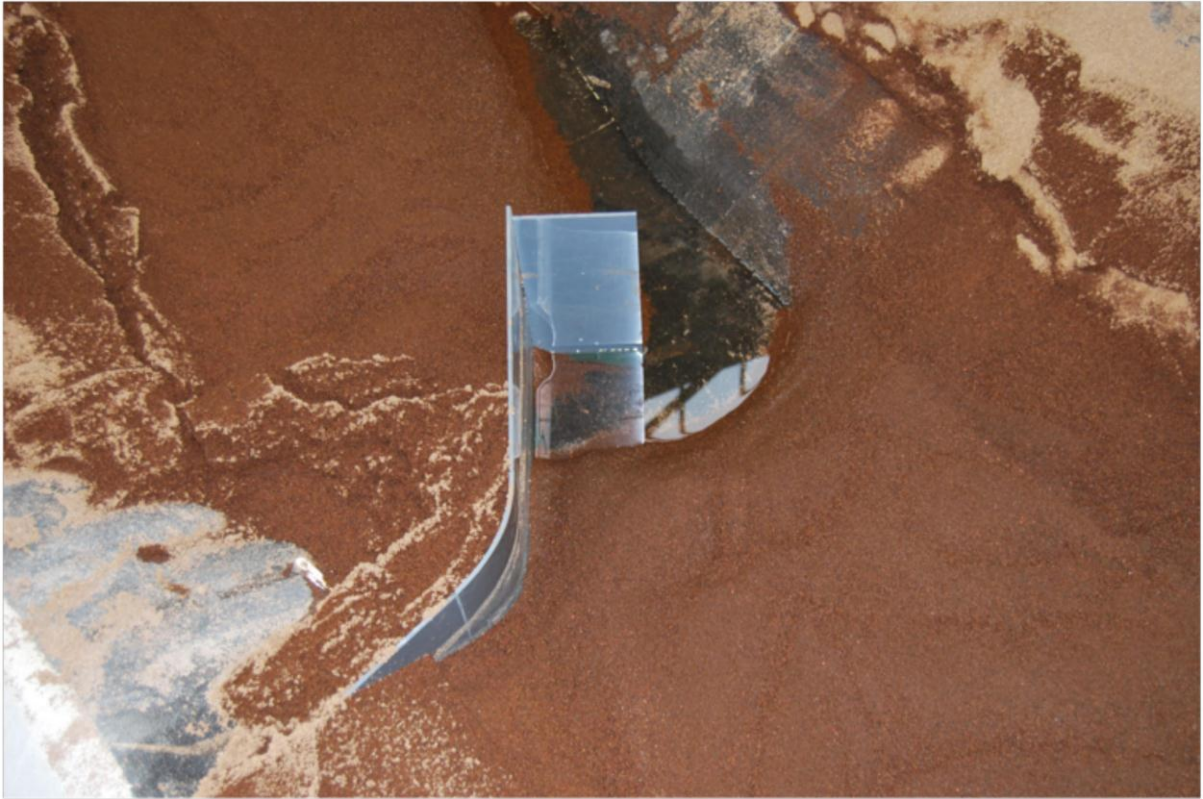


Figure A-28: Photo 5 of 45° structure with L-shaped attachment

Physical Experiment 8 - 60° Structure with Flow



Figure A-29: Photo 1 of 60° structure



Figure A-30: Photo 2 of 60° structure



Figure A-31: Photo 3 of 60° structure



Figure A-32: Photo 4 of 60° structure



Figure A-33: Photo 5 of 60° structure

Physical Experiment 9 - 60° with Flow (L-Shaped Structure)



Figure A-34: Photo 1 of 60° structure with L-shaped attachment



Figure A-35: Photo 2 of 60° structure with L-shaped attachment



Figure A-36: Photo 3 of 60° structure with L-shaped attachment



Figure A-37: Photo 4 of 60° structure with L-shaped attachment



Figure A-38: Photo 5 of 60° structure with L-shaped attachment

Appendix B

Sediment Concentration

Concentration Experiment 10 A

Test 10A 1

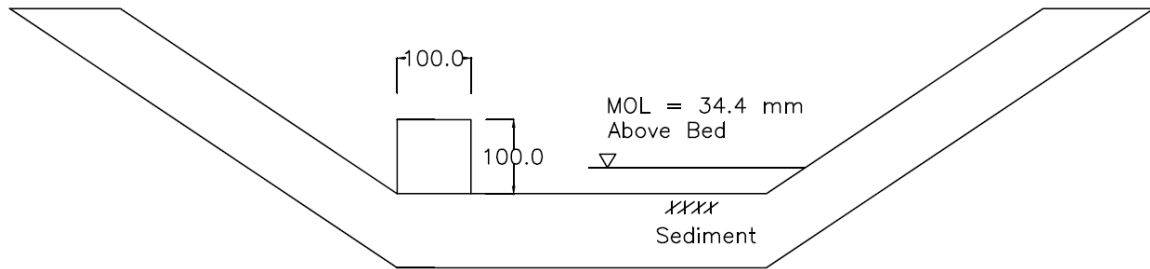


Figure B-1: Dimensions of physical experiment 10A 1

Test 10A 2

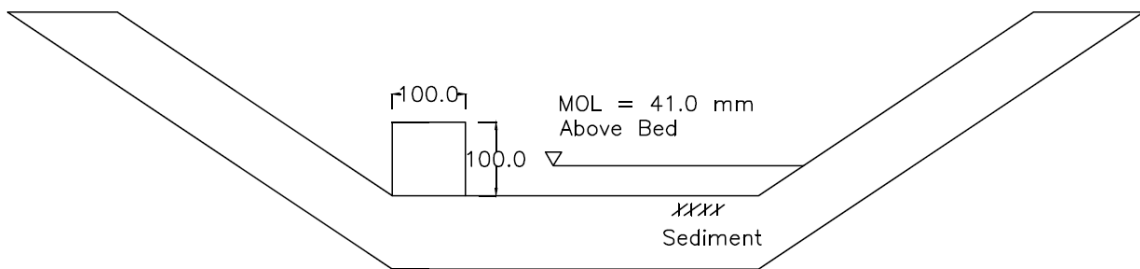


Figure B-2: Dimensions of physical experiment 10A 2

Test 10A 3

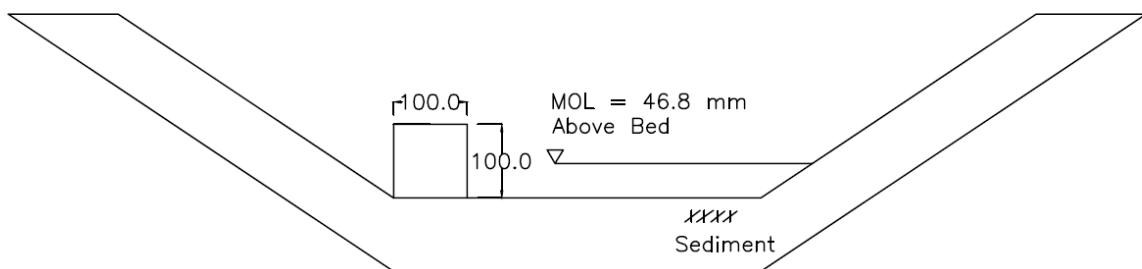


Figure B-3: Dimensions of physical experiment 10A 3

Test 10A 4

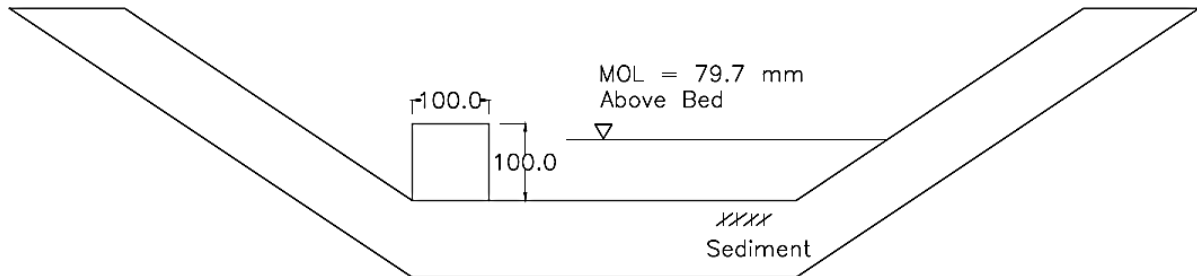


Figure B-4: Dimensions of physical experiment 10A 4

Test 10A 5

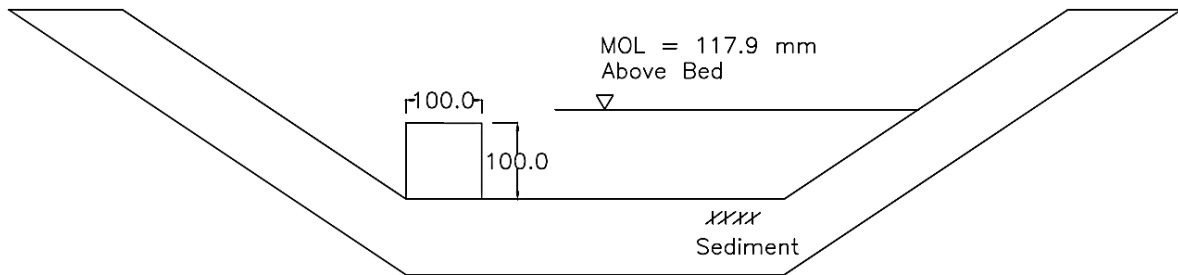


Figure B-5: Dimensions of physical experiment 10A 5

Concentration Experiment 10 B

Test 10B 1

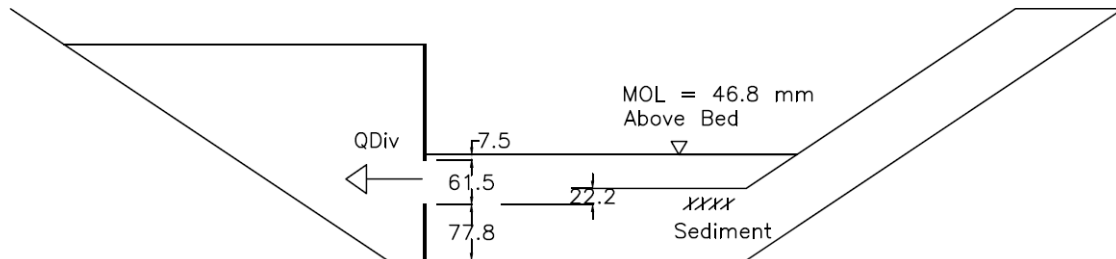


Figure B-6: Dimensions of physical experiment 10B 1



Figure B-7: Photo 1 of experiment 10B 1



Figure B-8: Photo 2 of experiment 10B 1



Figure B-9: Photo 3 of experiment 10B 1

Test 10B 2

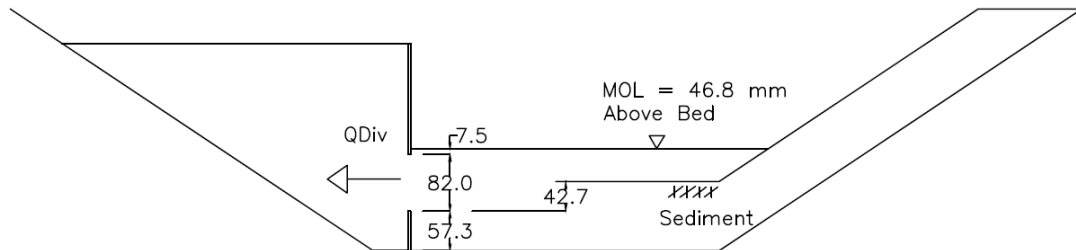


Figure B-10: Dimensions of physical experiment 10B 2



Figure B-11: Photo 1 of experiment 10B 2



Figure B-12: Photo 2 of experiment 10B 2



Figure B-13: Photo 3 of experiment 10B 2

Test 10B 3

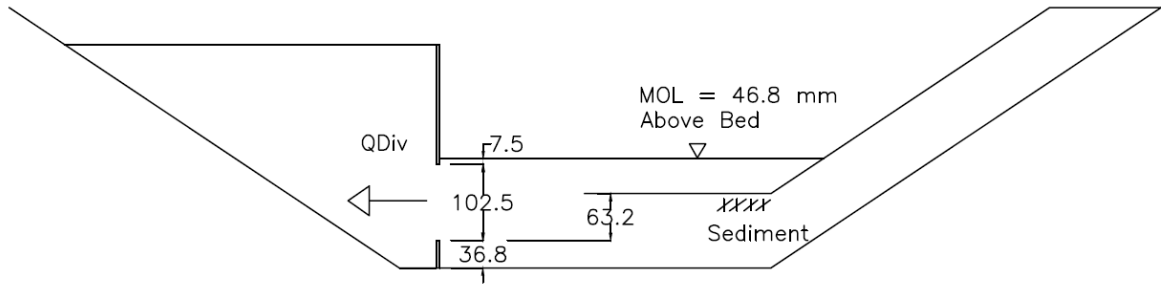


Figure B-14: Dimensions of physical experiment 10B 3



Figure B-15: Photo 1 of experiment 10B 3



Figure B-16: Photo 2 of experiment 10B 3

Concentration Experiment 10 C

Test 10C 1

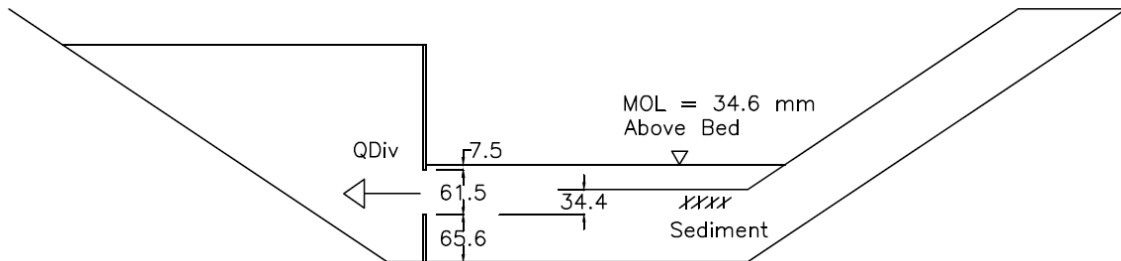


Figure B-17: Dimensions of physical experiment 10C 1



Figure B-18: Photo 1 of experiment 10C 1



Figure B-19: Photo 2 of experiment 10C 1



Figure B-20: Photo 3 of experiment 10C 1

Test 10C 2

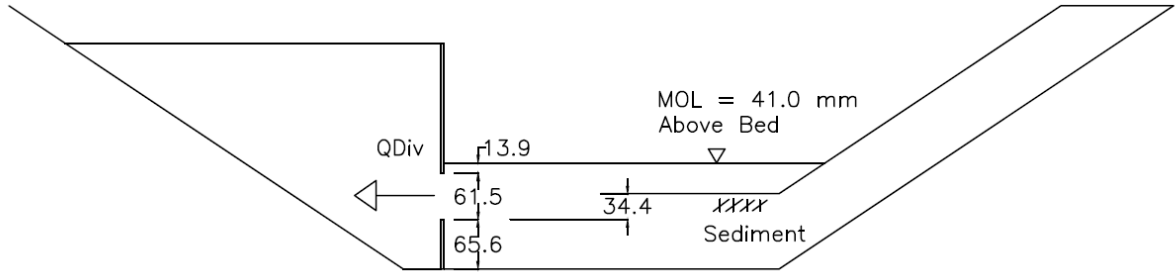


Figure B-21: Dimensions of physical experiment 10C 2



Figure B-22: Photo 1 of experiment 10C 2



Figure B-23: Photo 2 of experiment 10C 2



Figure B-24: Photo 3 of experiment 10C 2

Test 10C 3

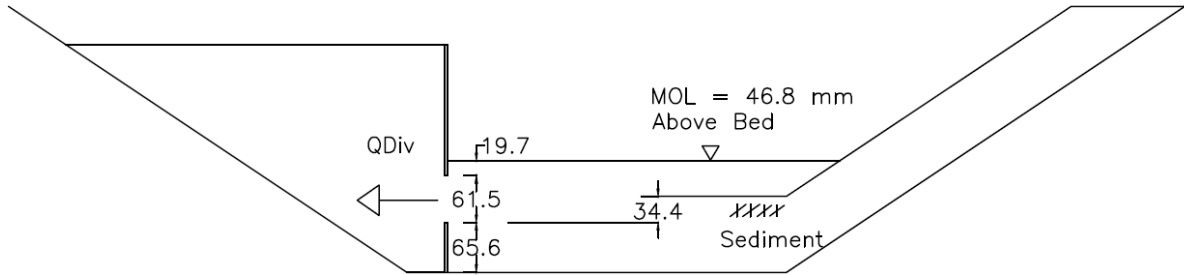


Figure B-25: Dimensions of physical experiment 10C 3



Figure B-26: Photo 1 of experiment 10C 3



Figure B-27: Photo 2 of experiment 10C 3



Figure B-28: Photo 3 of experiment 10C 3

Test 10C 4

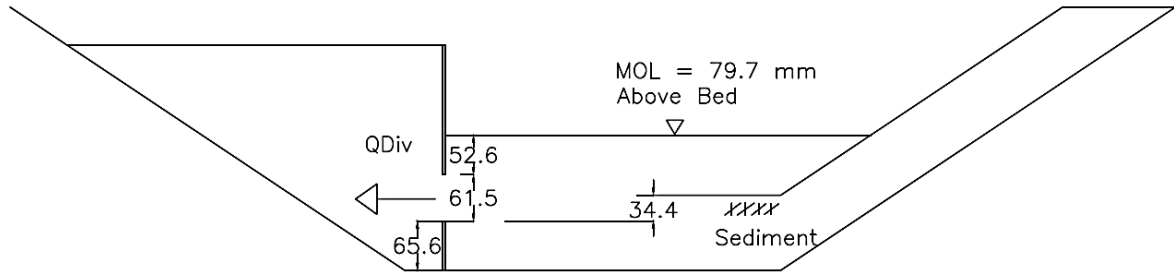


Figure B-29: Dimensions of physical experiment 10C 4



Figure B-30: Photo 1 of experiment 10C 4



Figure B-31: Photo 2 of experiment 10C 4



Figure B-32: Photo 3 of experiment 10C 4

Test 10C 5

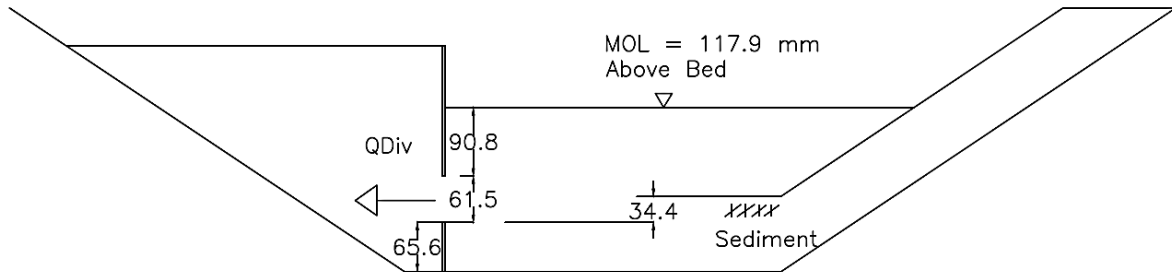


Figure B-33: Dimensions of physical experiment 10C 5



Figure B-34: Photo 1 of experiment 10C 5



Figure B-35: Photo 2 of experiment 10C 5



Figure B-36: Photo 3 of experiment 10C 5

Concentration Experiment 10 D

Test 10D 1

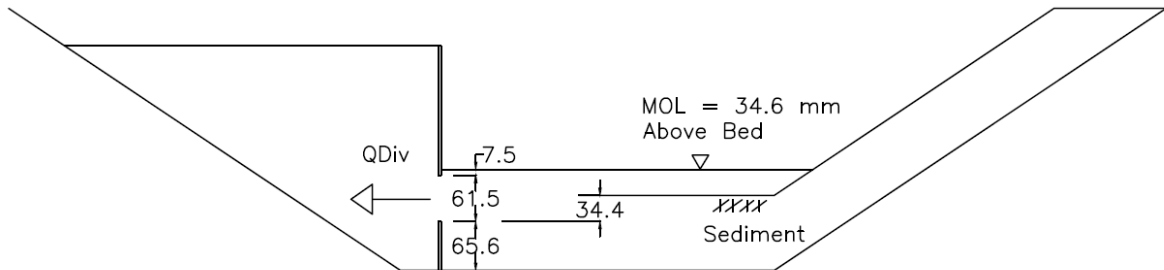


Figure B-37: Dimensions of physical experiment 10D 1



Figure B-38: Photo 1 of experiment 10D 1



Figure B-39: Photo 2 of experiment 10D 1

Test 10D 2

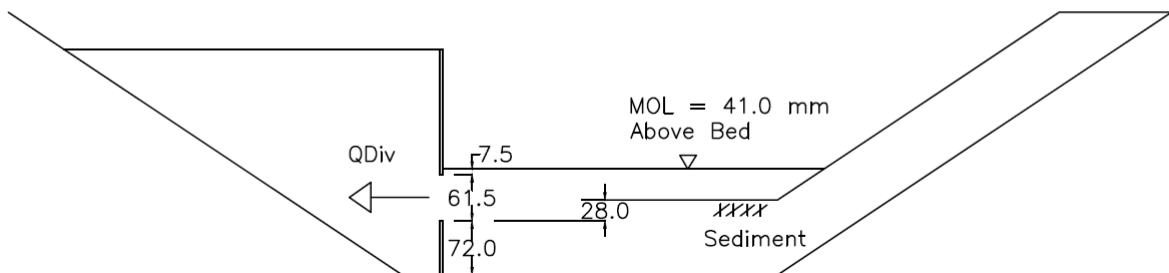


Figure B-40: Dimensions of physical experiment 10D 2



Figure B-41: Photo 1 of experiment 10D 2



Figure B-42: Photo 2 of experiment 10D 2



Figure B-43: Photo 3 of experiment 10D 2

Test 10D 3

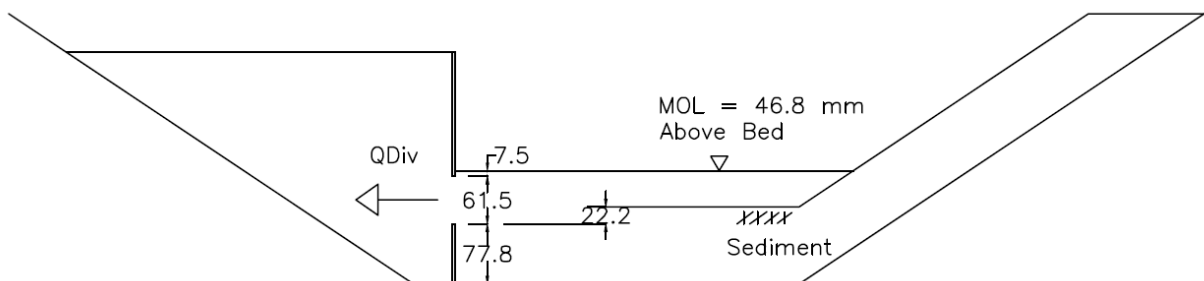


Figure B-44: Dimensions of physical experiment 10D 3



Figure B-45: Photo 1 of experiment 10D 3



Figure B-46: Photo 2 of experiment 10D 3

Appendix C

Numerical Results

Simulation Test 1 – Without Diversion Structure

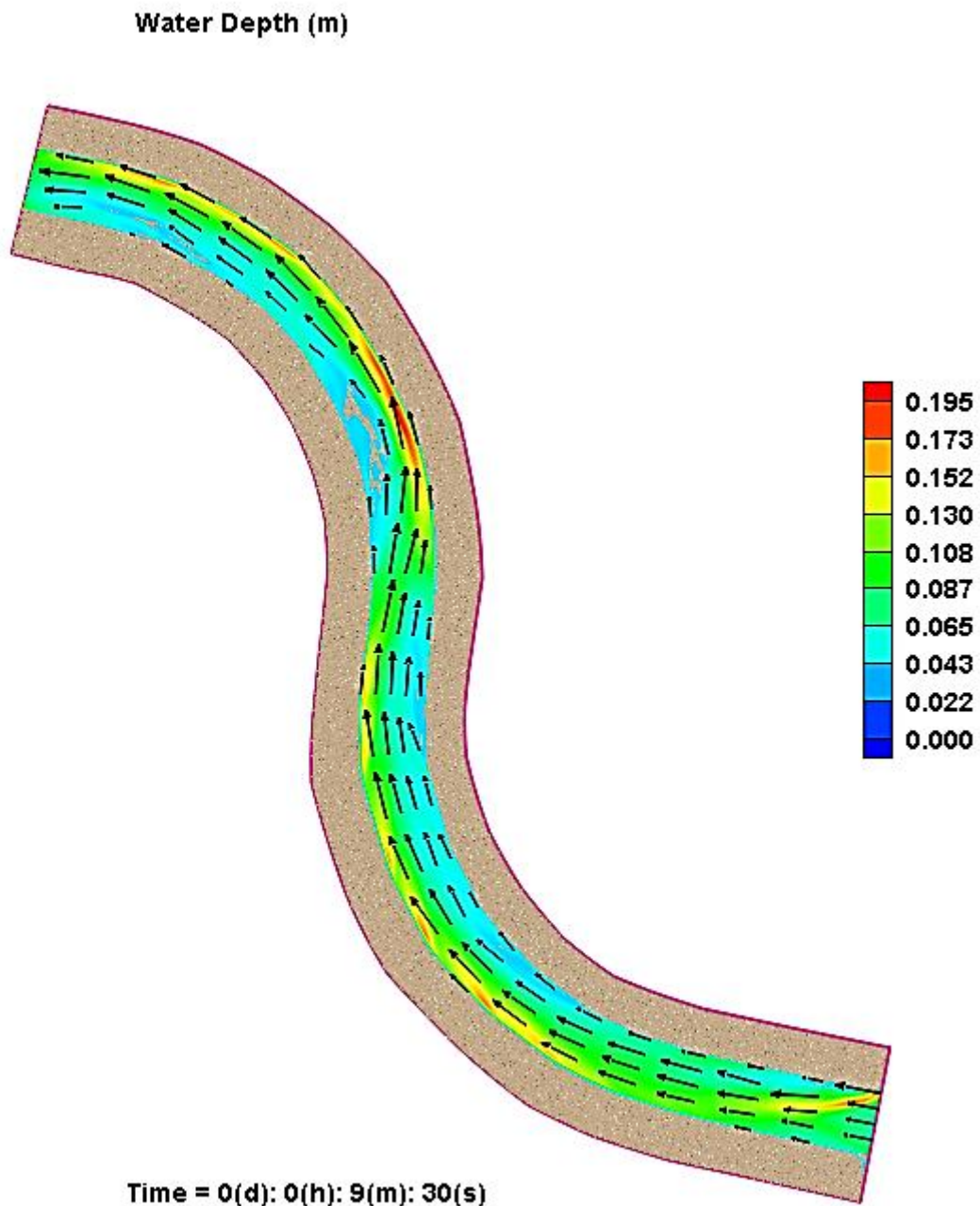


Figure C-2: Water depth (m) with velocity vectors

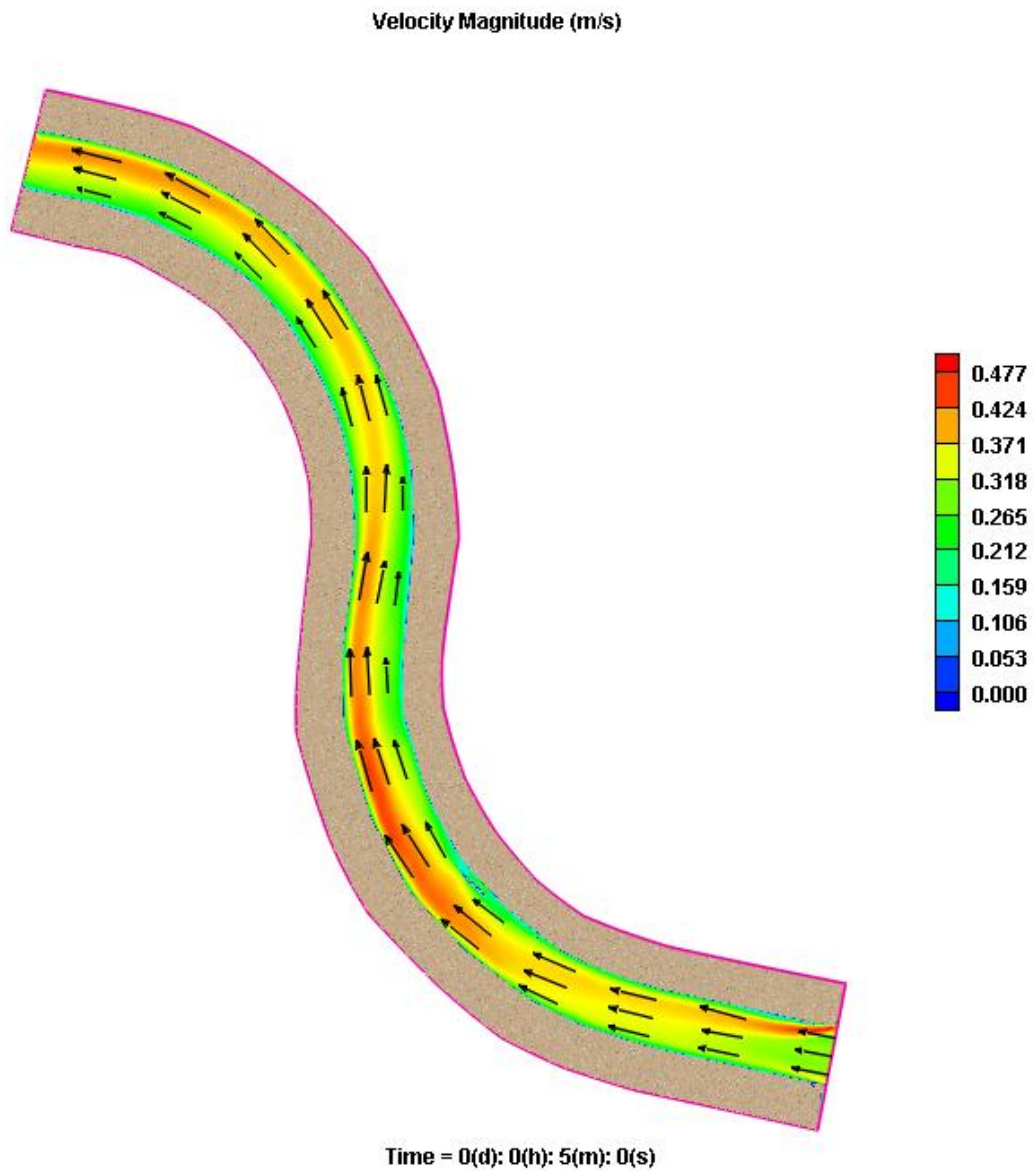


Figure C-3: Velocity magnitude (m/s) with velocity vectors

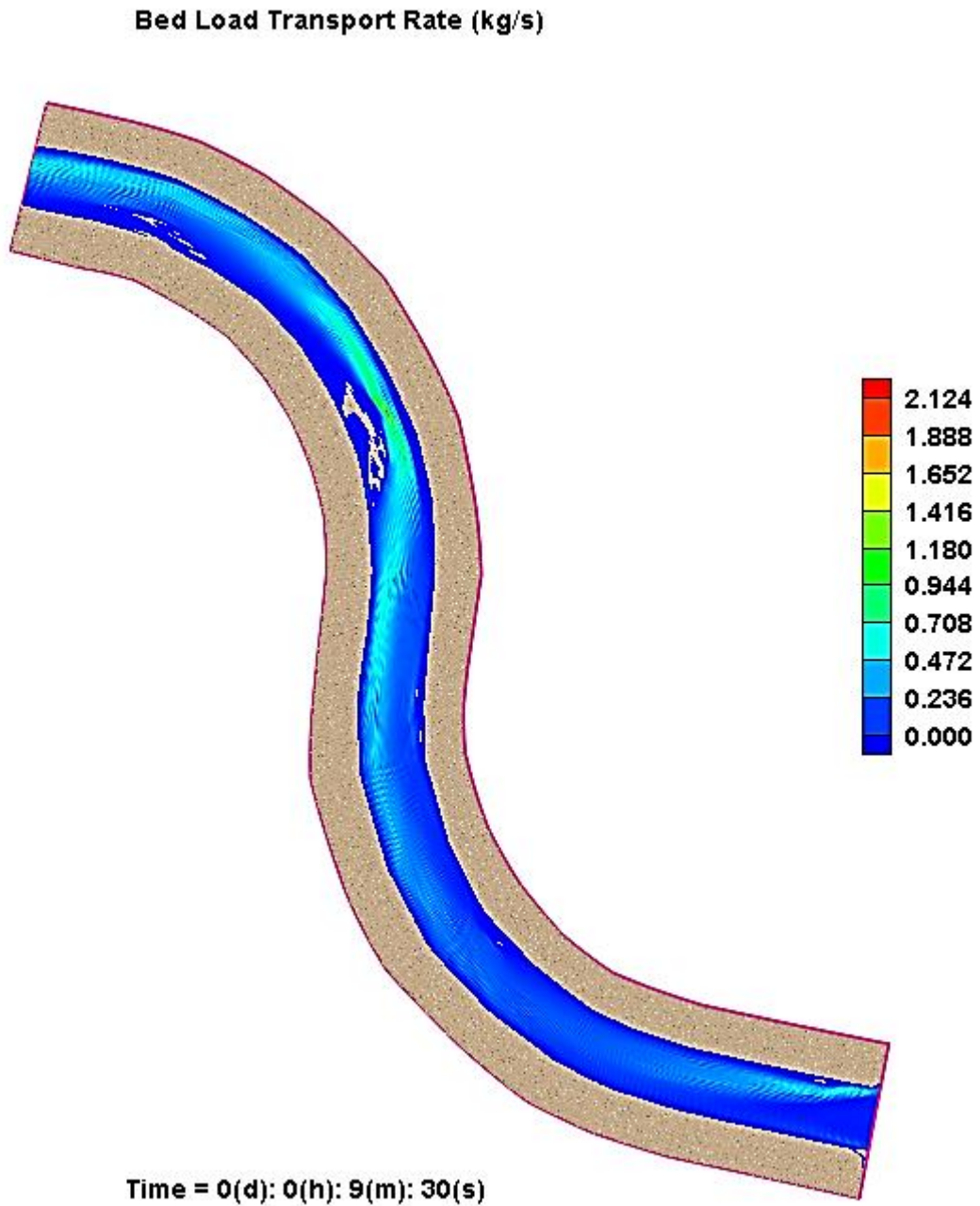


Figure C-4: Bed load transport rate (kg/s) without diversion structure

Bed Change (m)

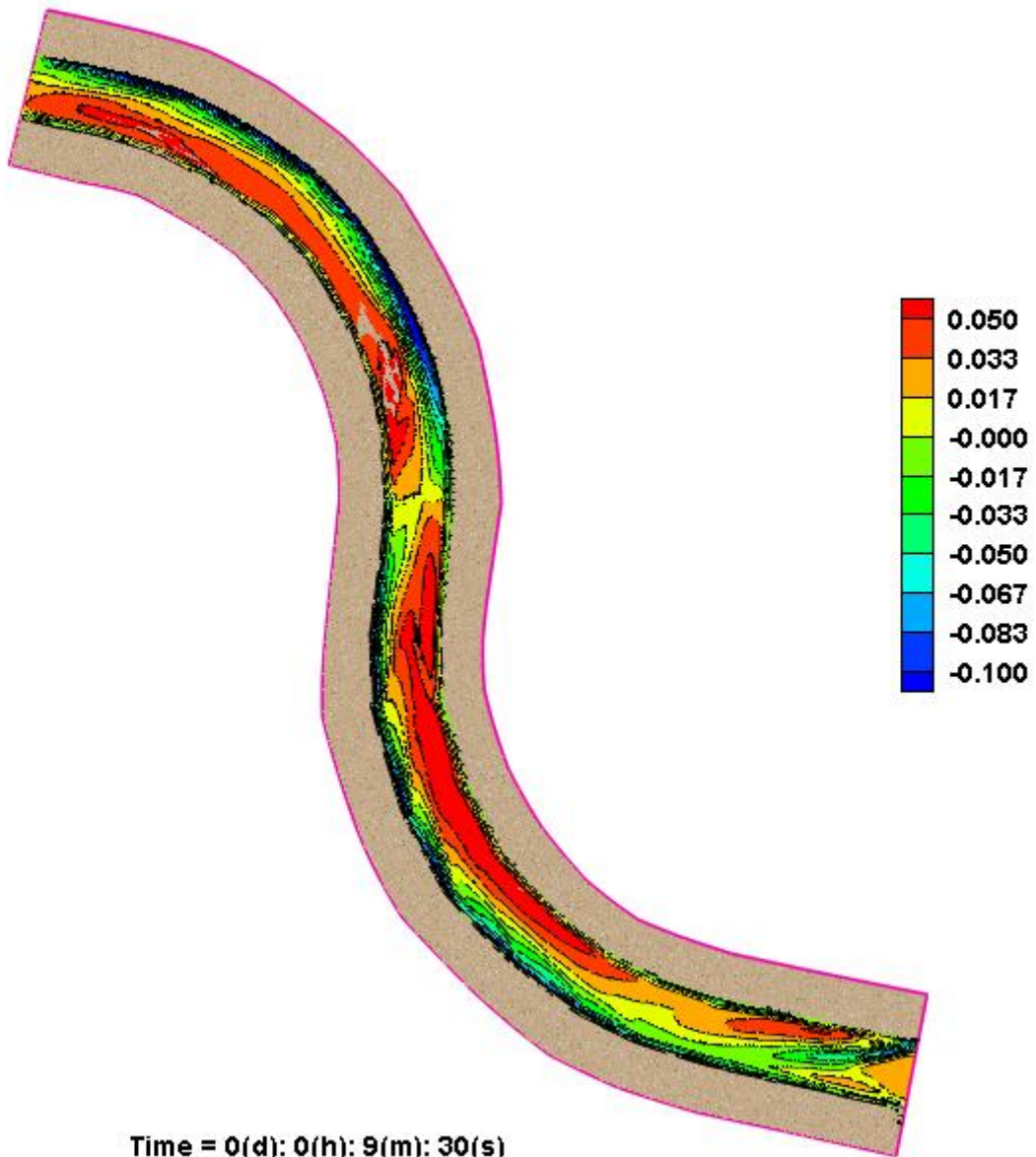


Figure C-5: Bed change (m) without diversion structure

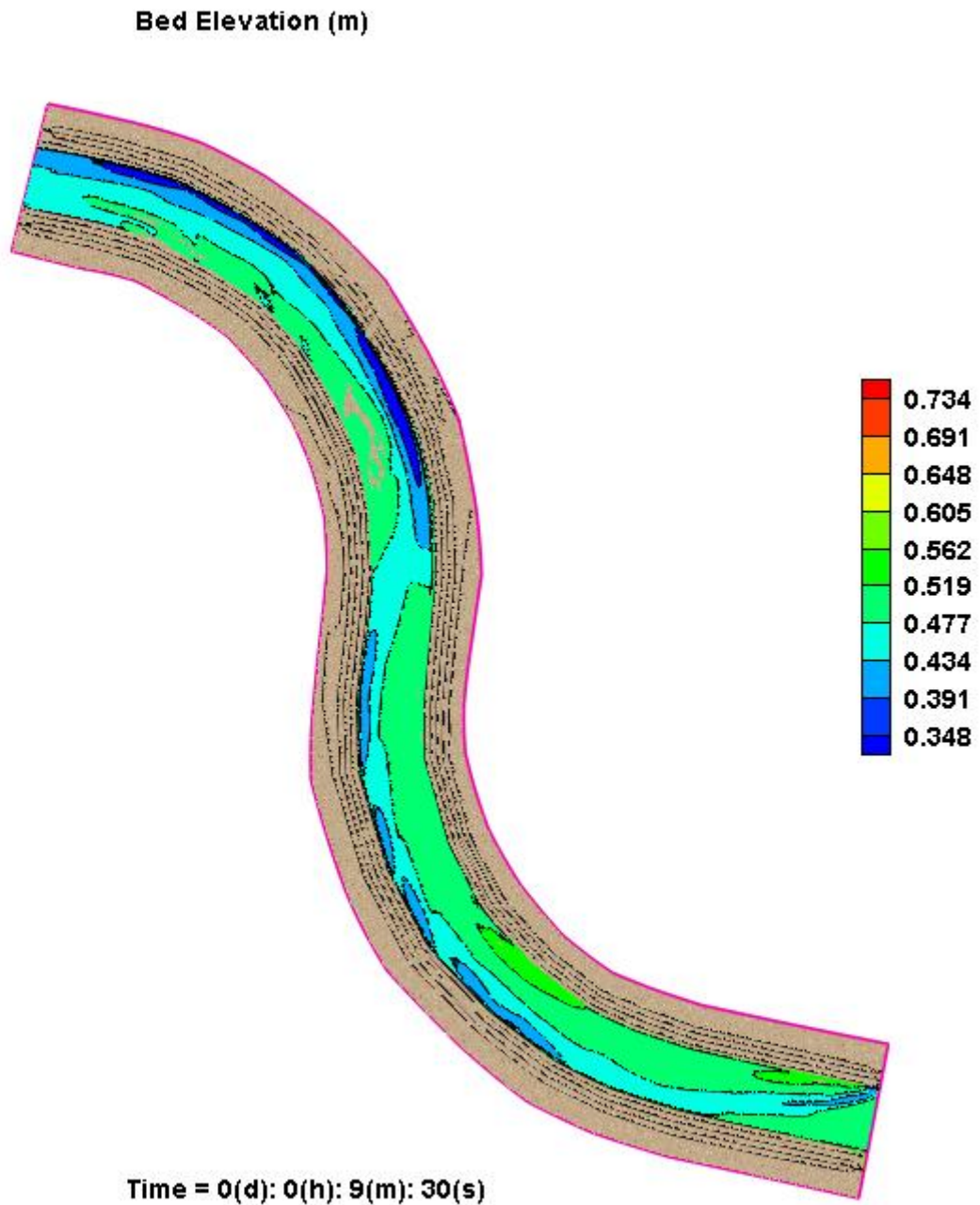


Figure C-6: Scoured bed elevation (without diversion structure)

Simulation Test 2 - 0° Structure with Flow

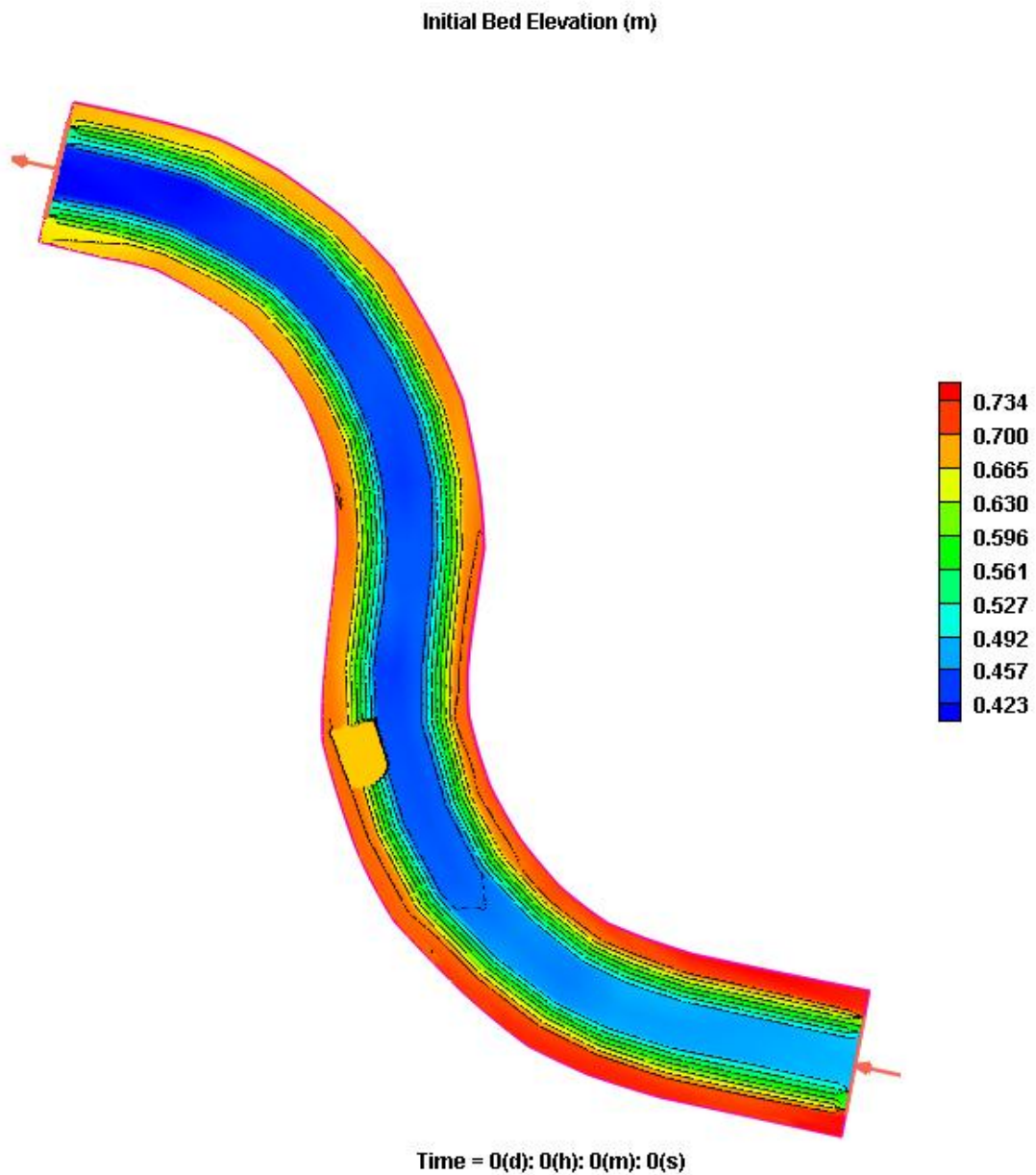


Figure C-7: Bathymetry of 2D model (0° structure with flow)

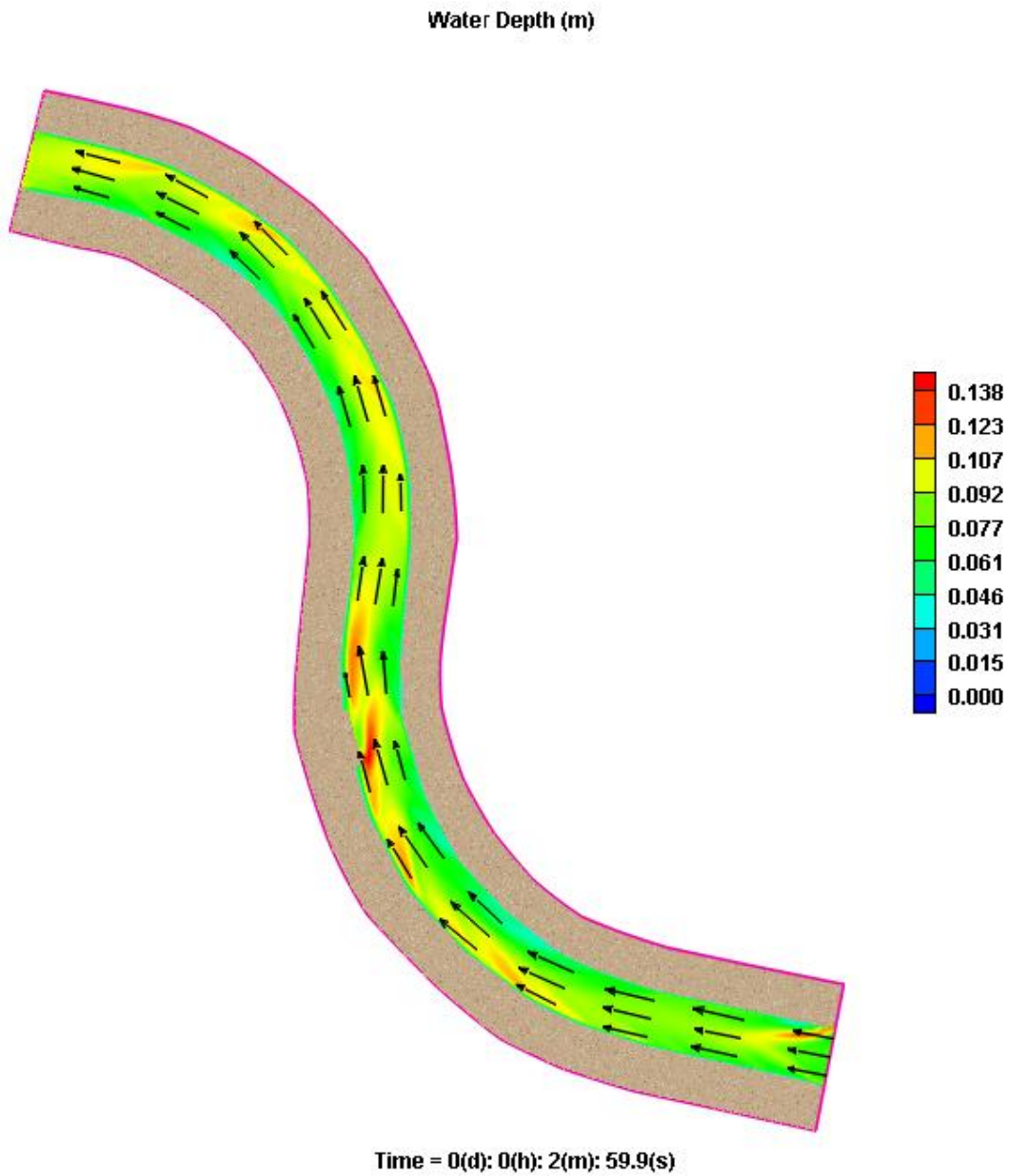


Figure C-8: Water depth (m) with velocity vectors

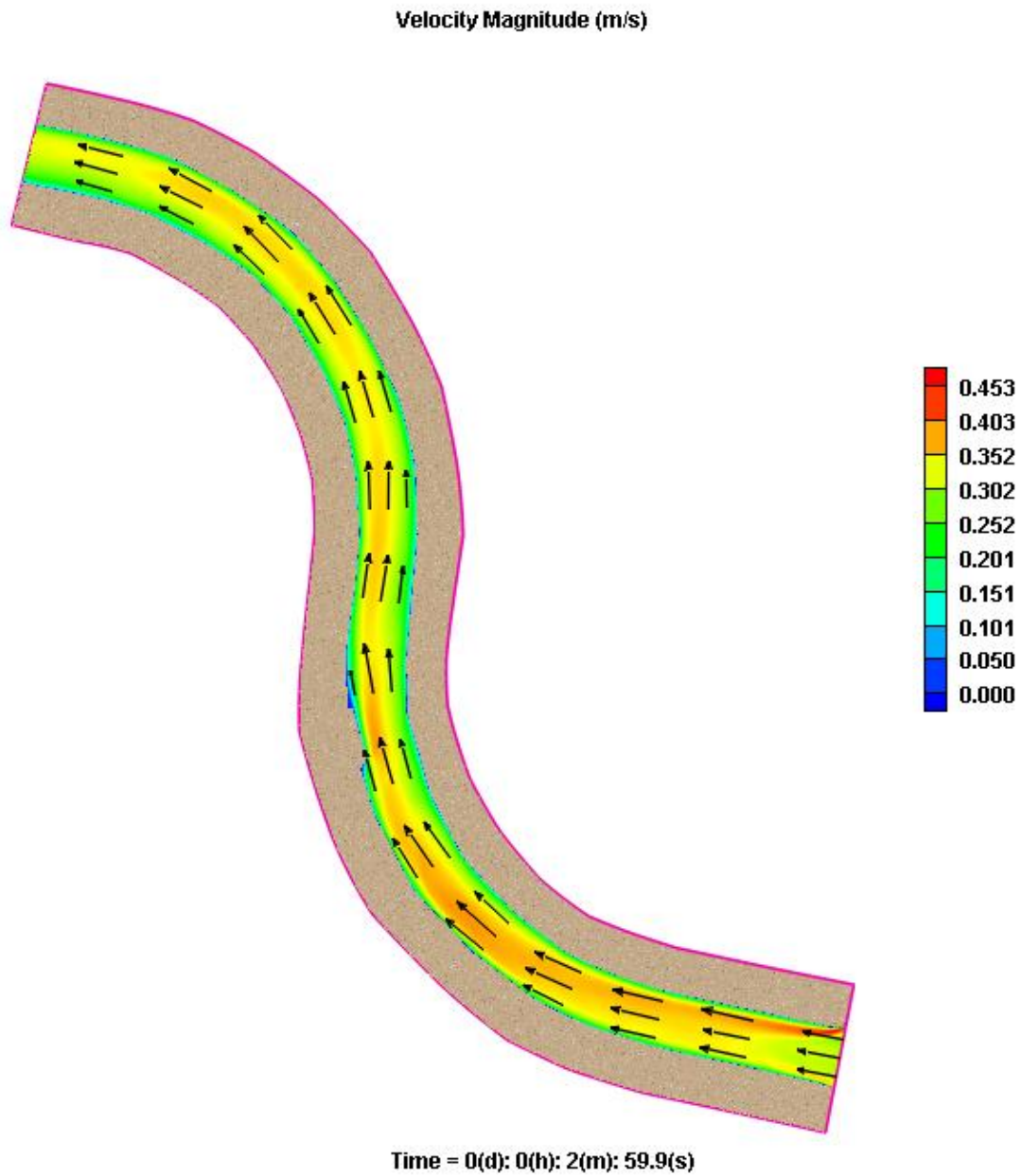


Figure C-9: Velocity magnitude (m/s) with velocity vectors

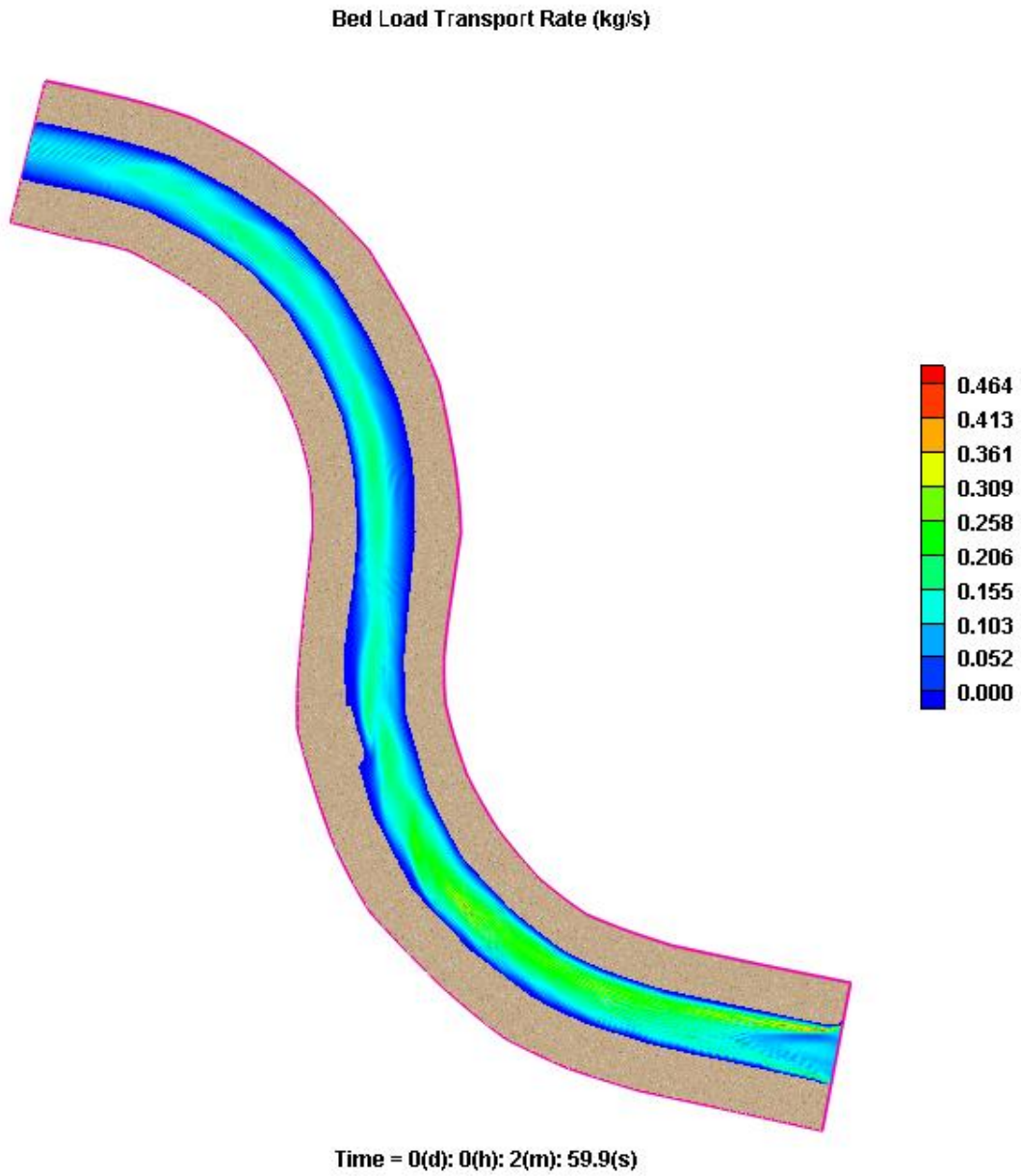


Figure C-10: Bed load transport rate (kg/s) for θ^0 structure with flow

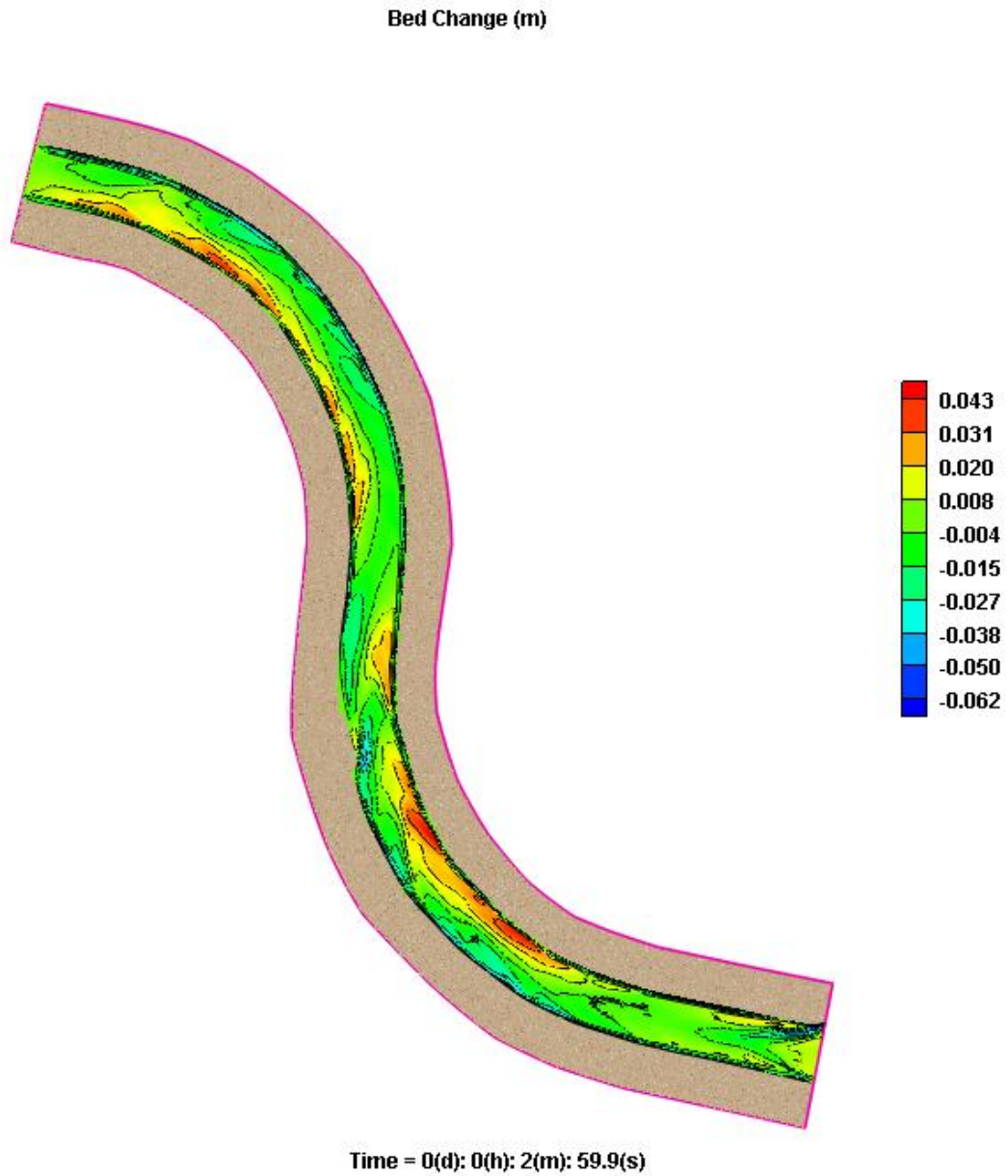


Figure C-11: Bed change (m) for 0° structure with flow

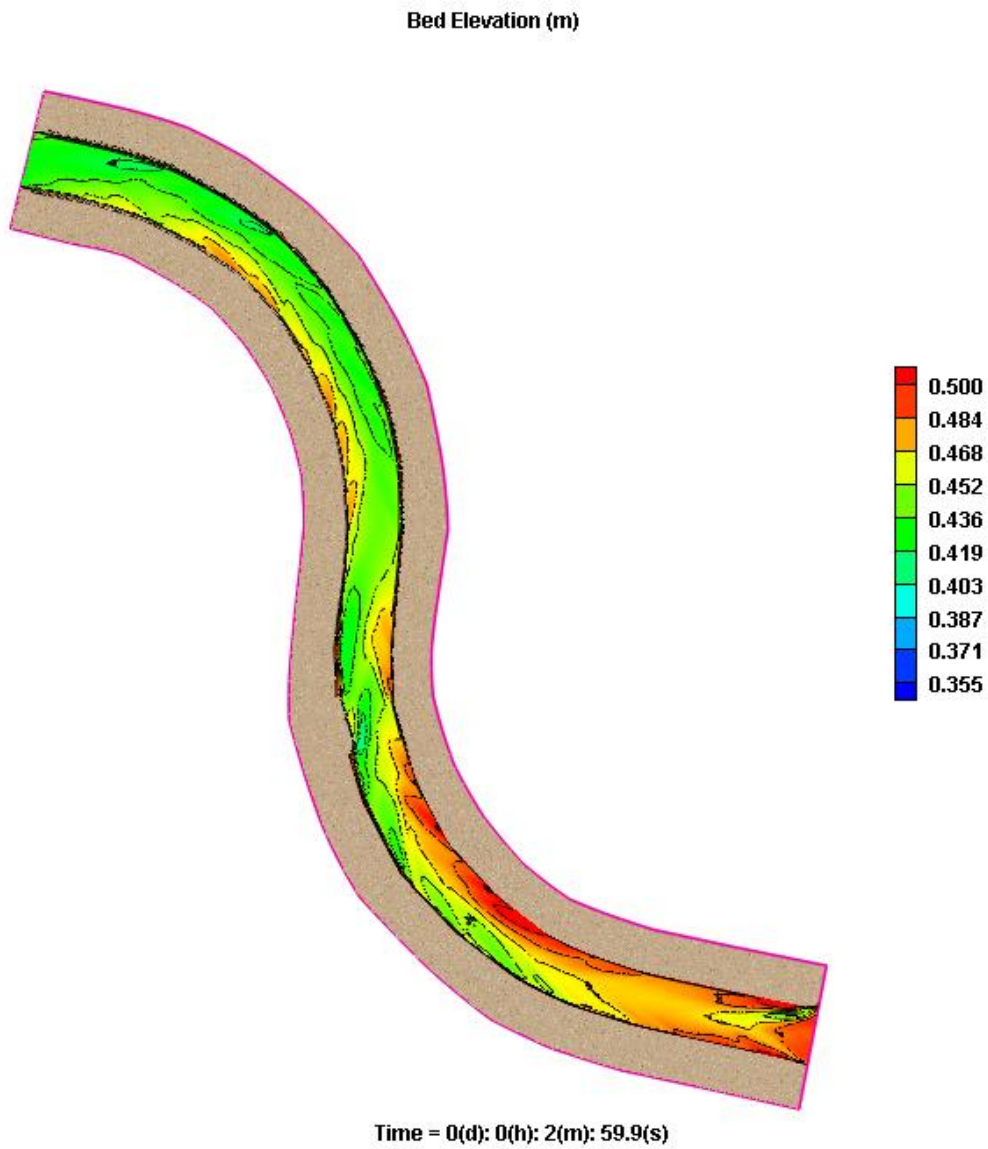


Figure C-12: Scoured bed elevation (0° structure with flow)

Simulation Test 3 - 0° Structure with Flow (L-Shape)

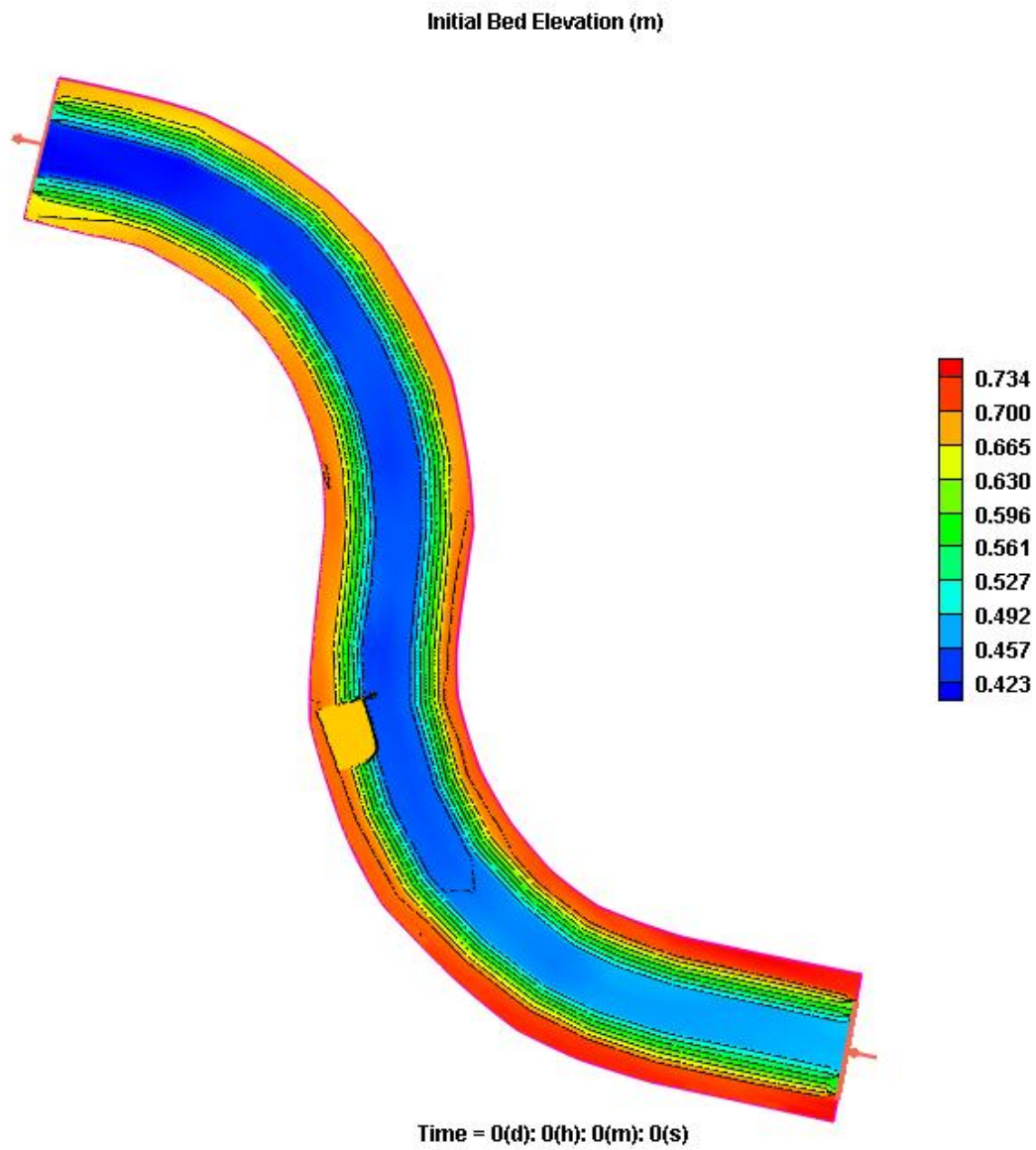


Figure C-13: Bathymetry of 2D model (0° structure with flow (L-shape))

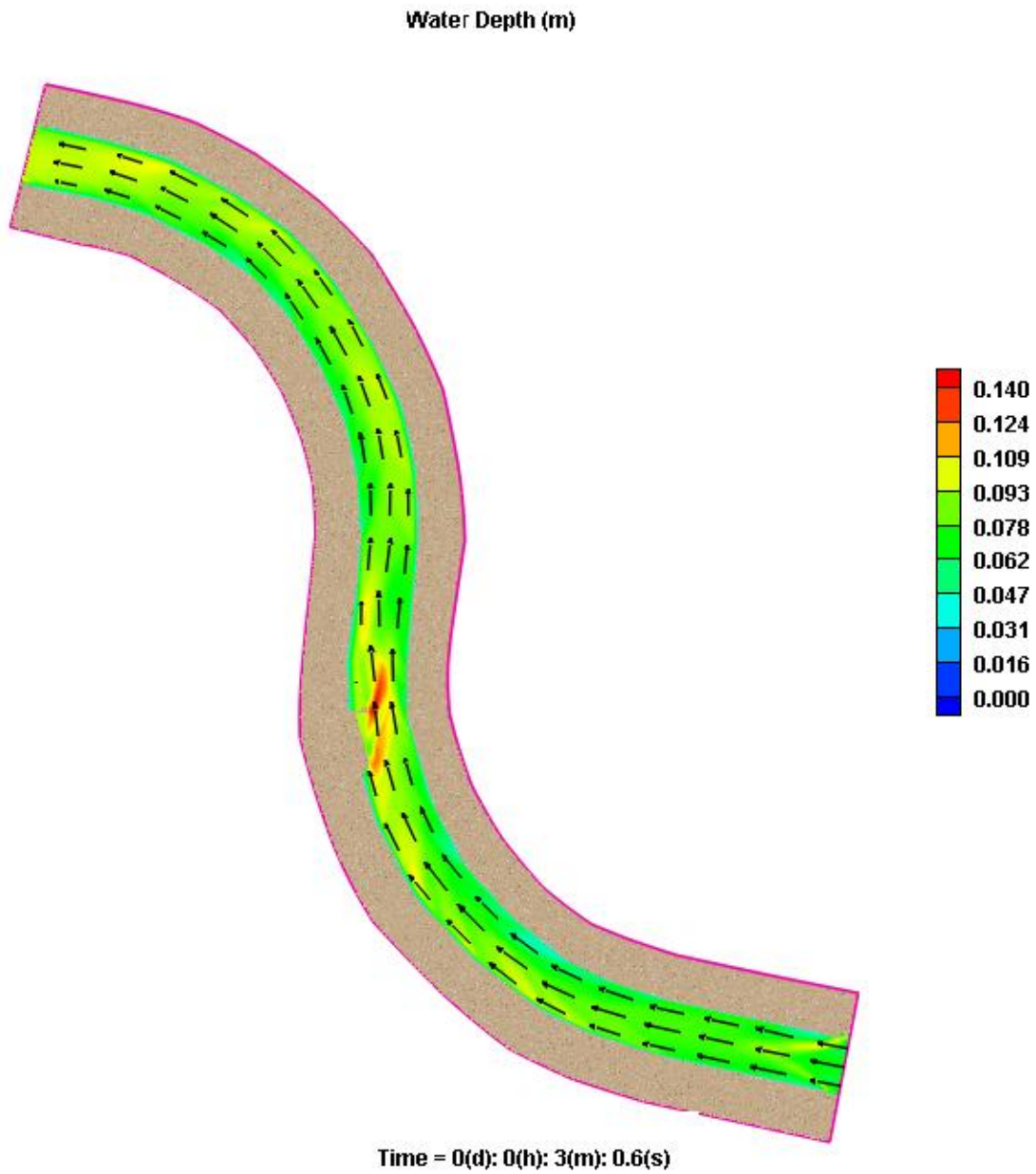


Figure C-14: Water depth (m) with velocity vectors

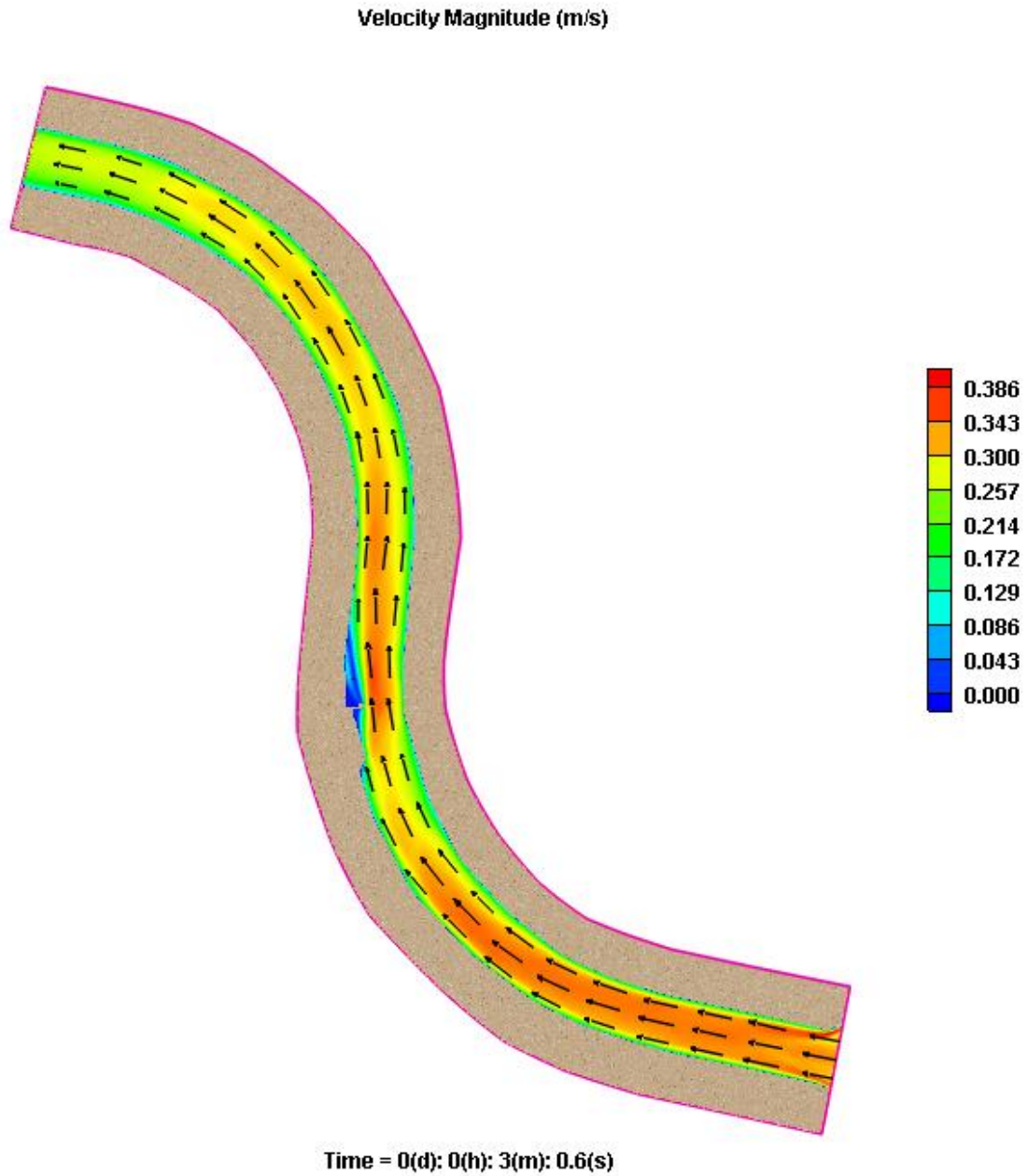


Figure C-15: Velocity magnitude (m/s) with velocity vectors

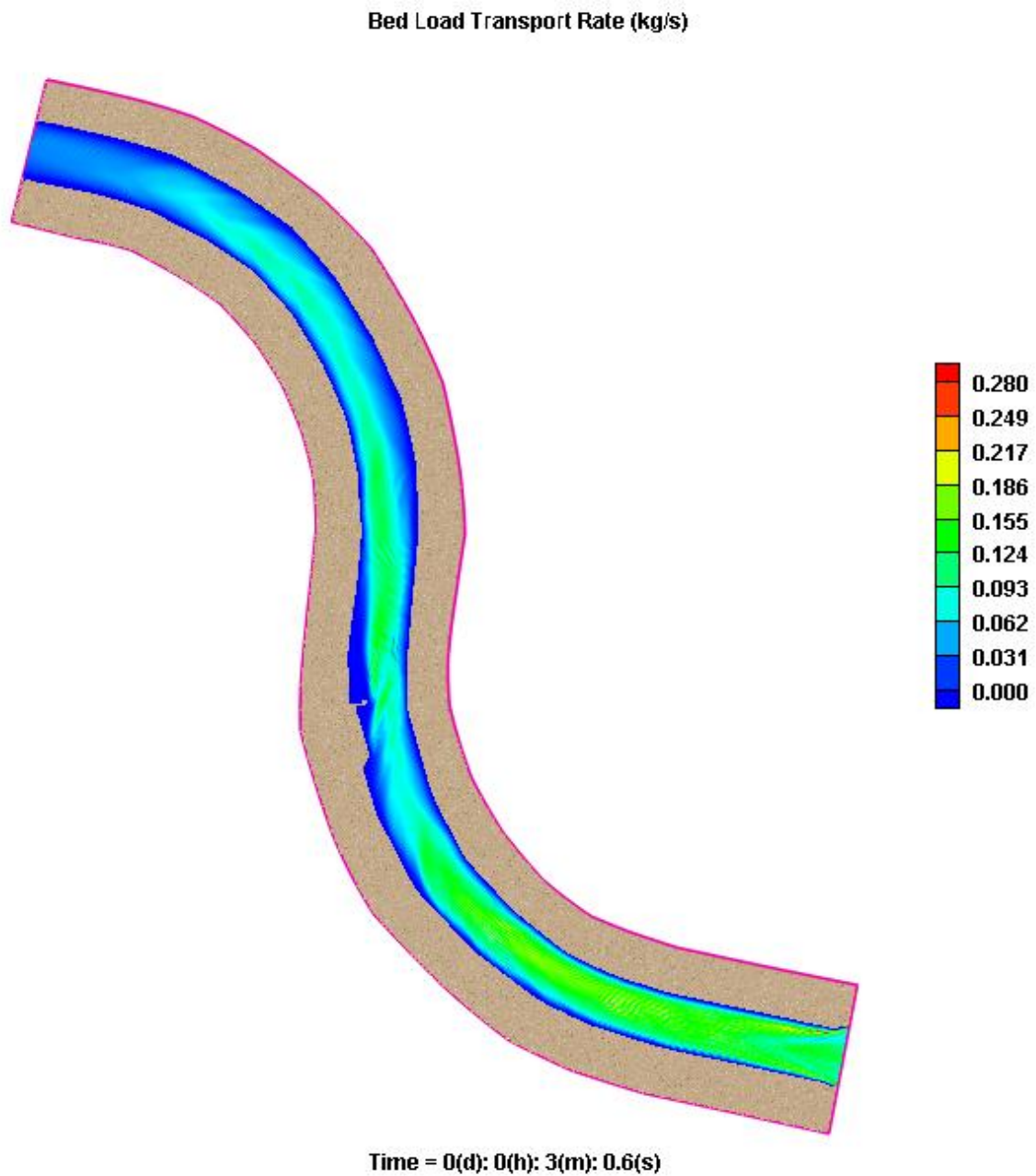


Figure C-16: Bed load transport rate (kg/s) for 0° structure with flow (L-shape)

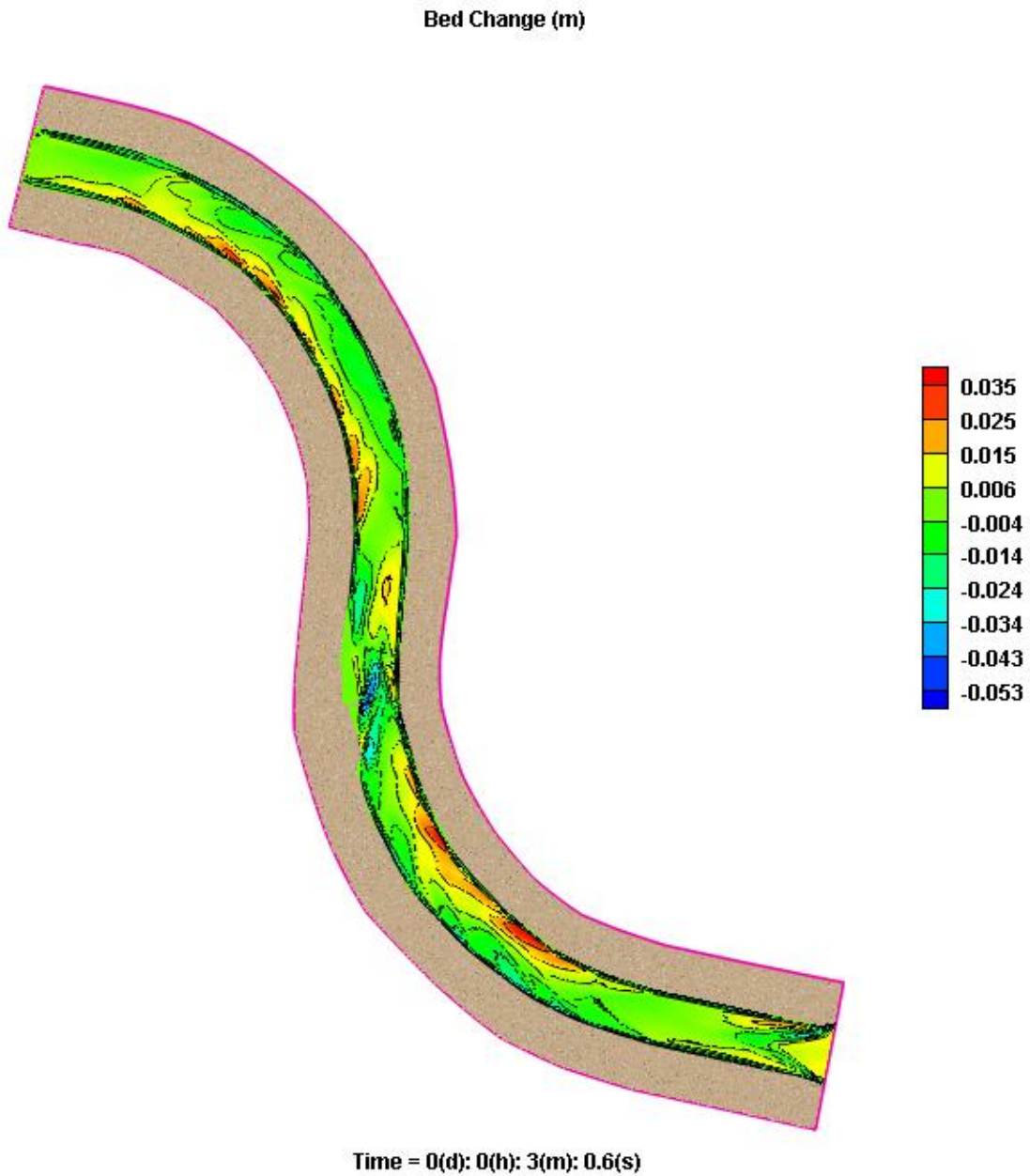


Figure C-17: Bed change (m) for 0° structure with flow (L-shape)

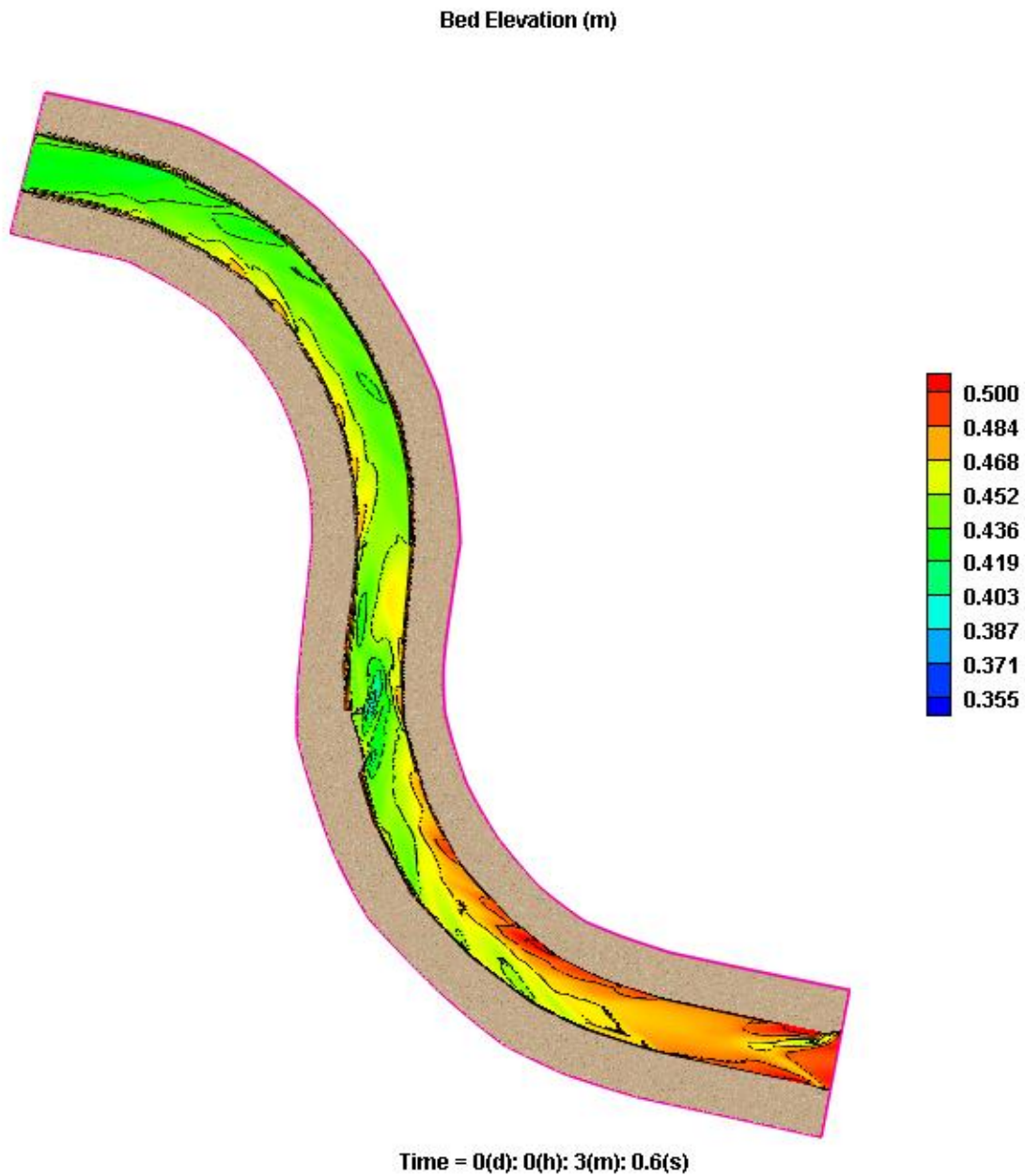


Figure C-18: Scoured bed elevation (0° structure with flow (L-shape))

Simulation Test 4 - 30° Structure with Flow

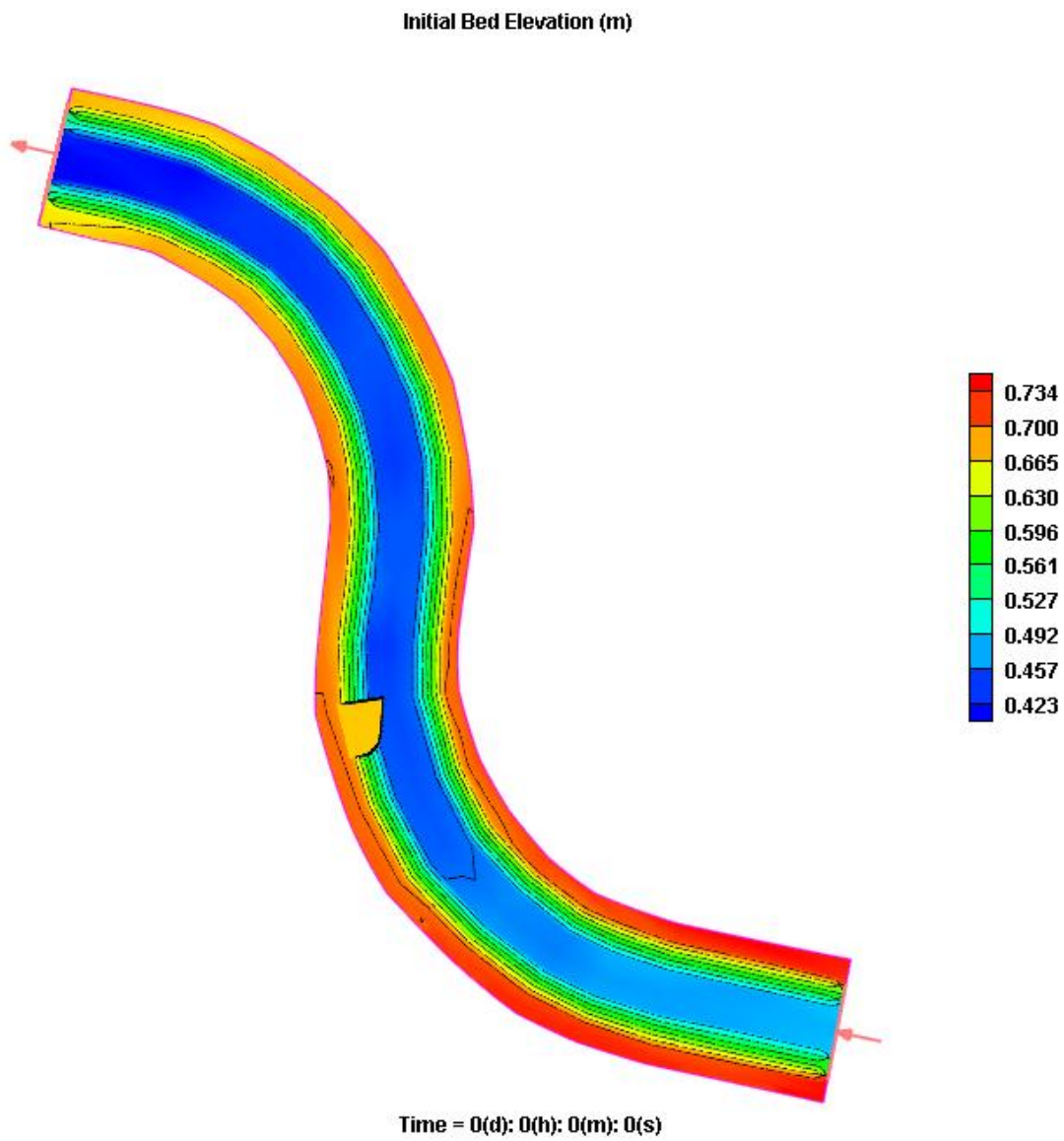


Figure C-19: Bathymetry of 2D model (30° structure with flow)

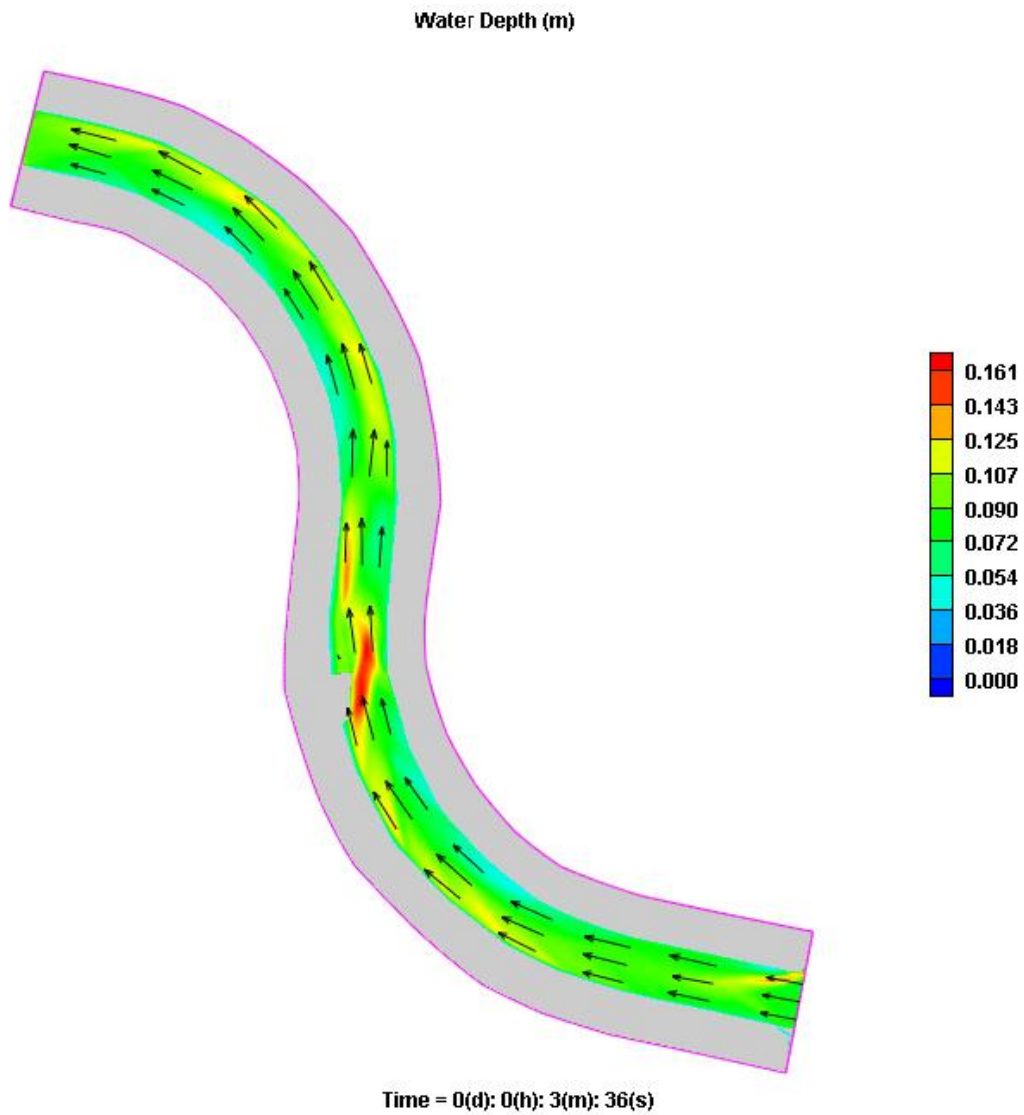


Figure C-20: Water depth (m) with velocity vectors

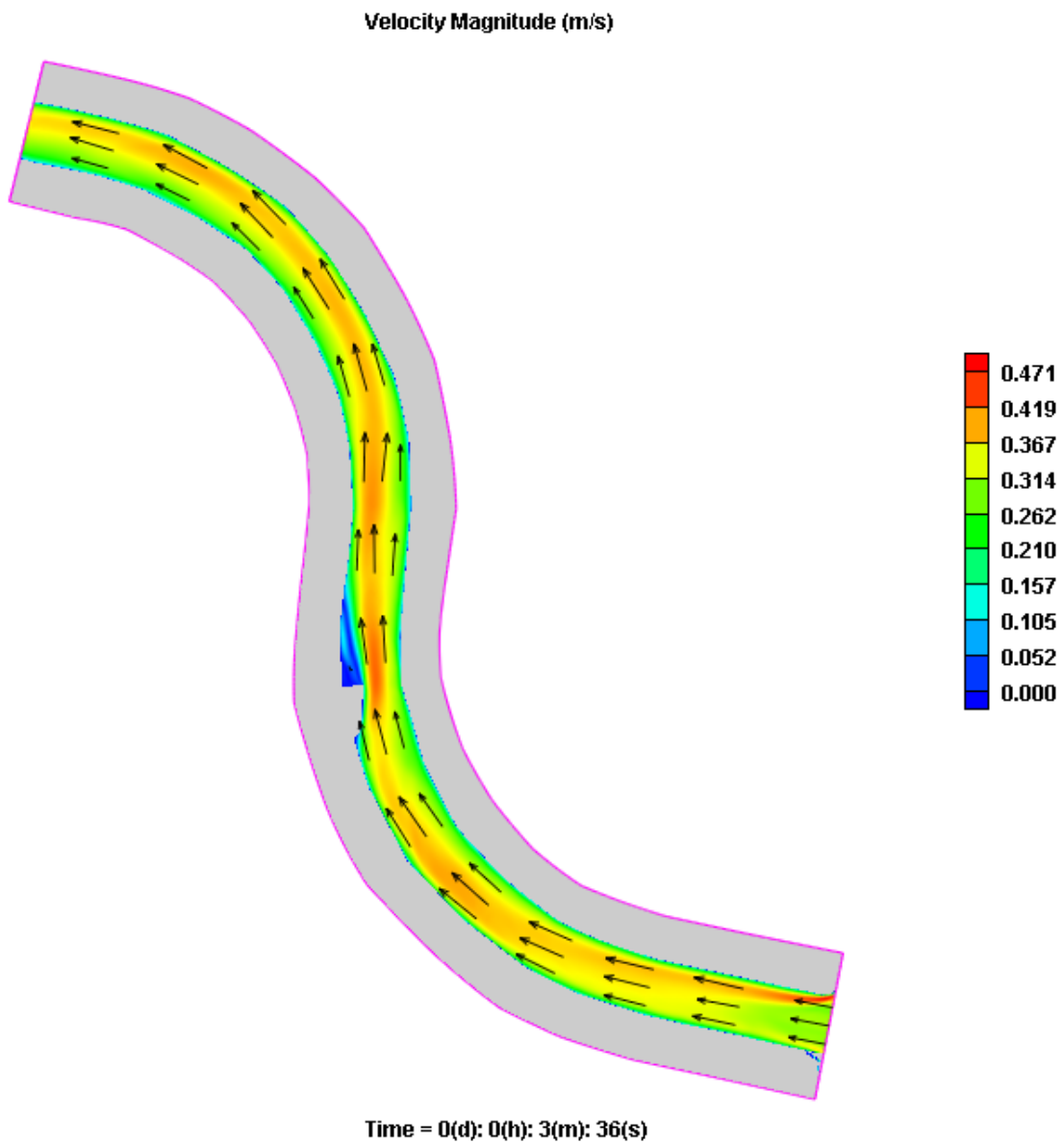


Figure C-21: Velocity magnitude (m/s) with velocity vectors

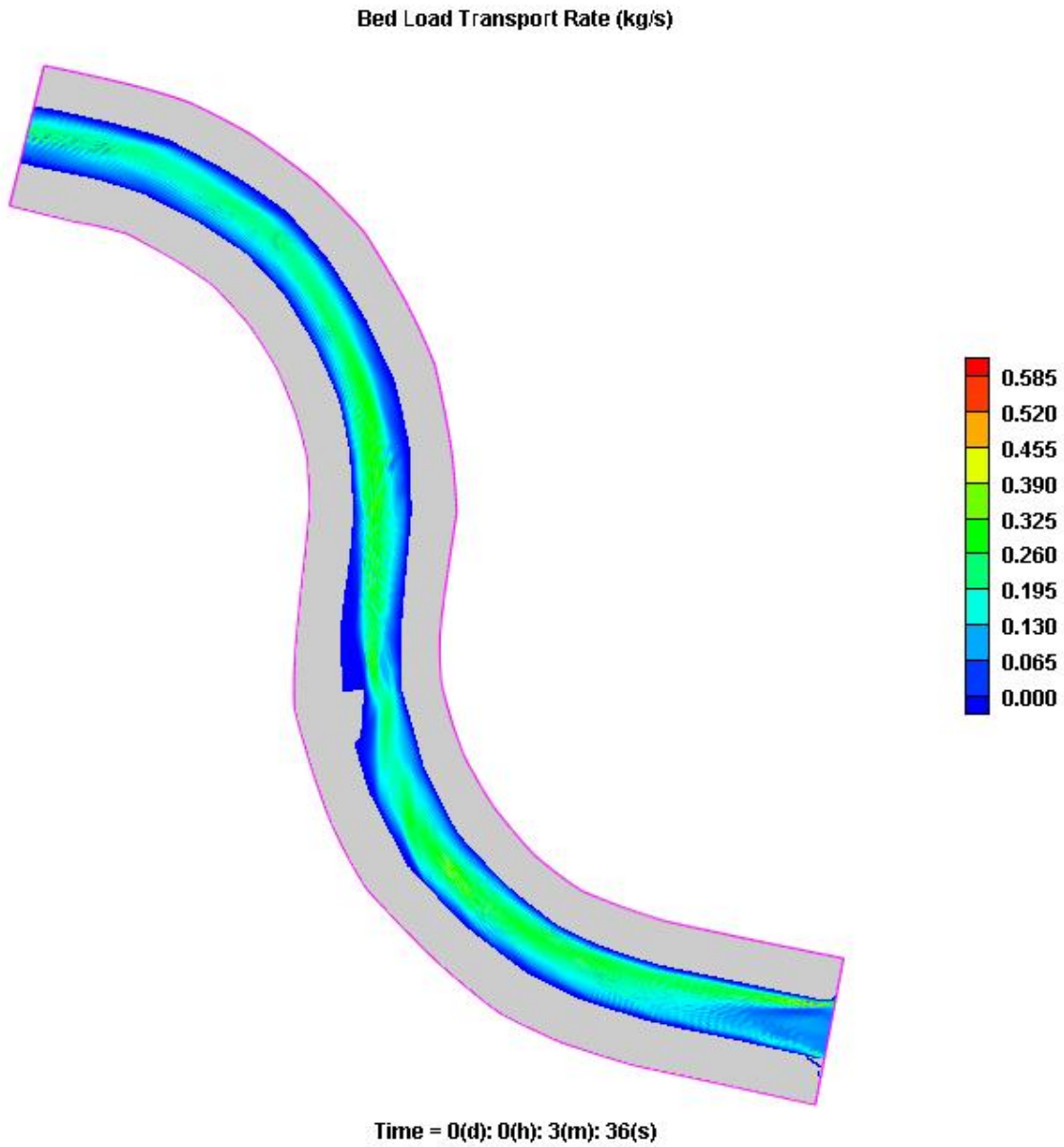


Figure C-22: Bed load transport rate (kg/s) for 30° structure with flow

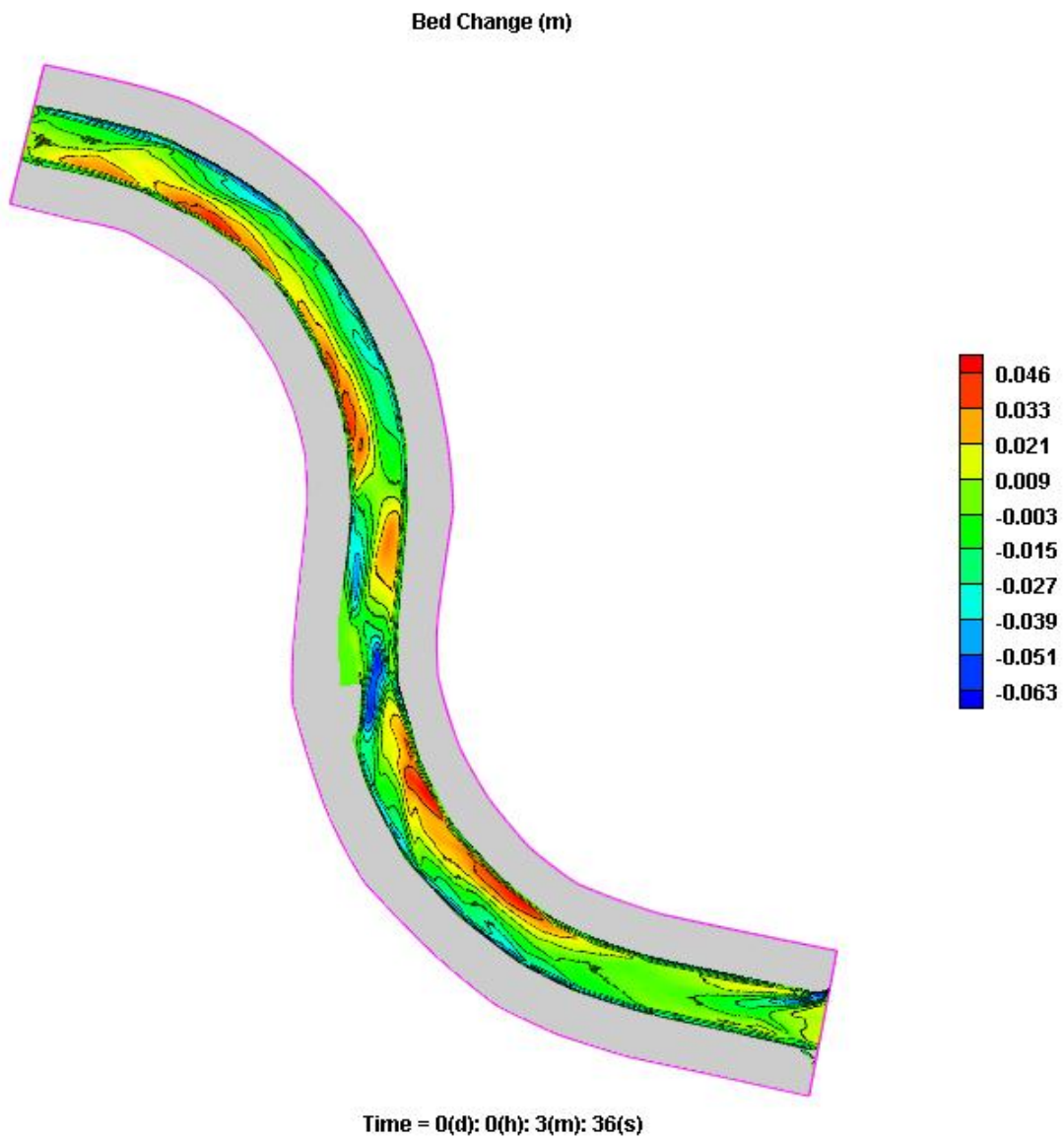


Figure C-23: Bed change (m) for 30° structure with flow

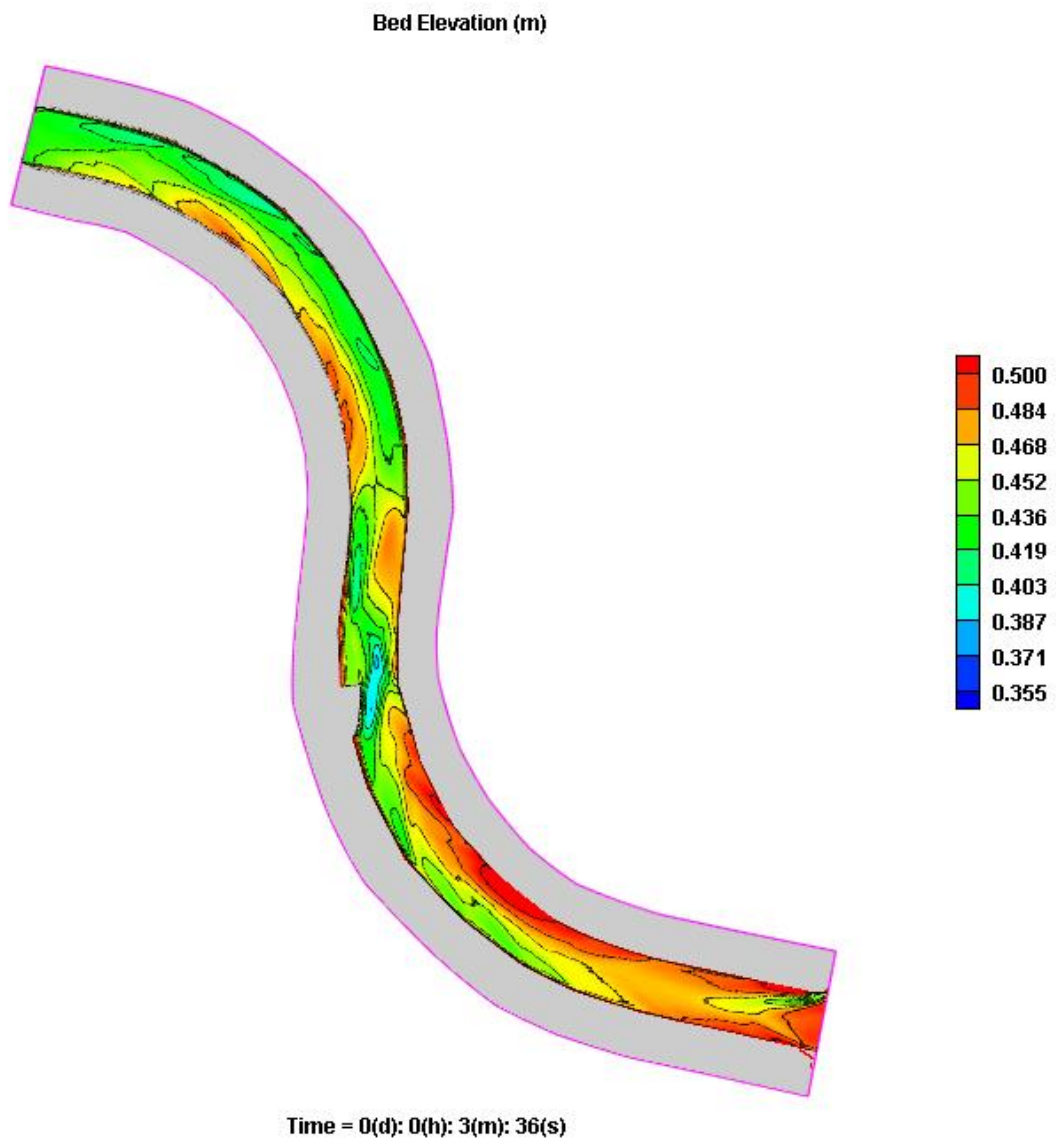


Figure C-24: Scoured bed elevation (30° structure with flow)

Simulation Test 5 - 30° Structure with Flow (L-Shape)

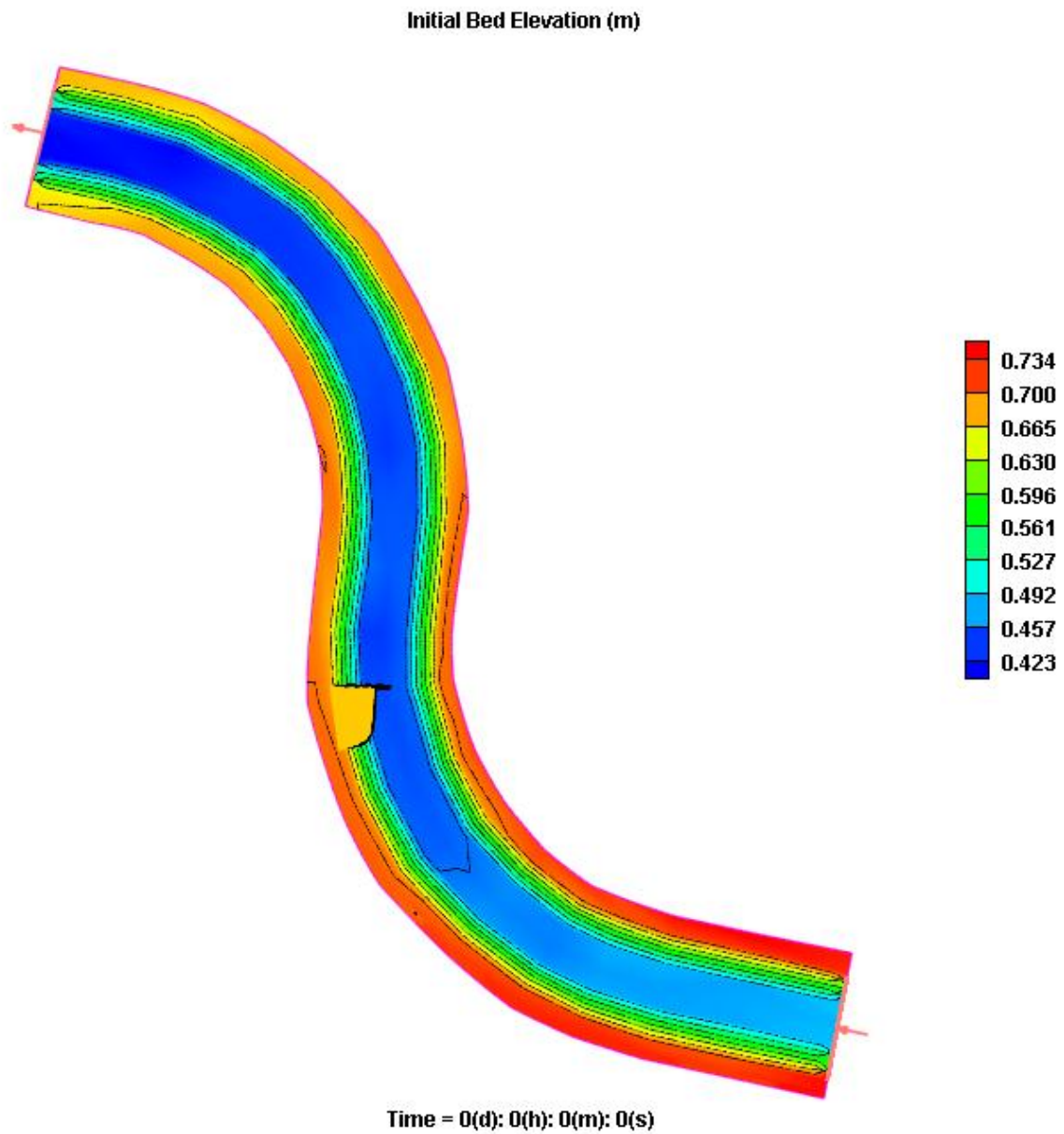


Figure C-25: Bathymetry of 2D model (30° structure with flow (L-shape))

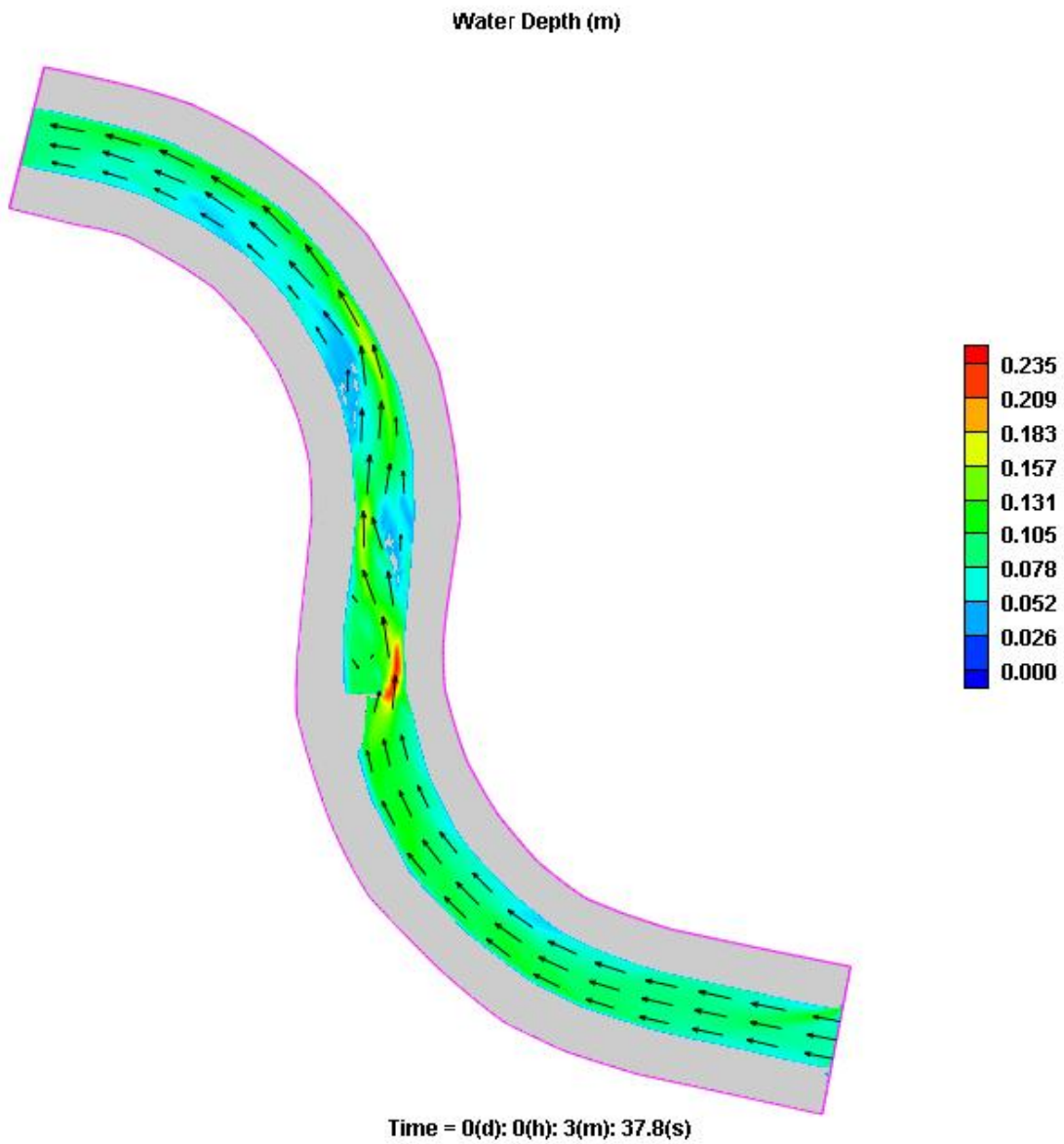


Figure C-26: Water depth (m) with velocity vectors

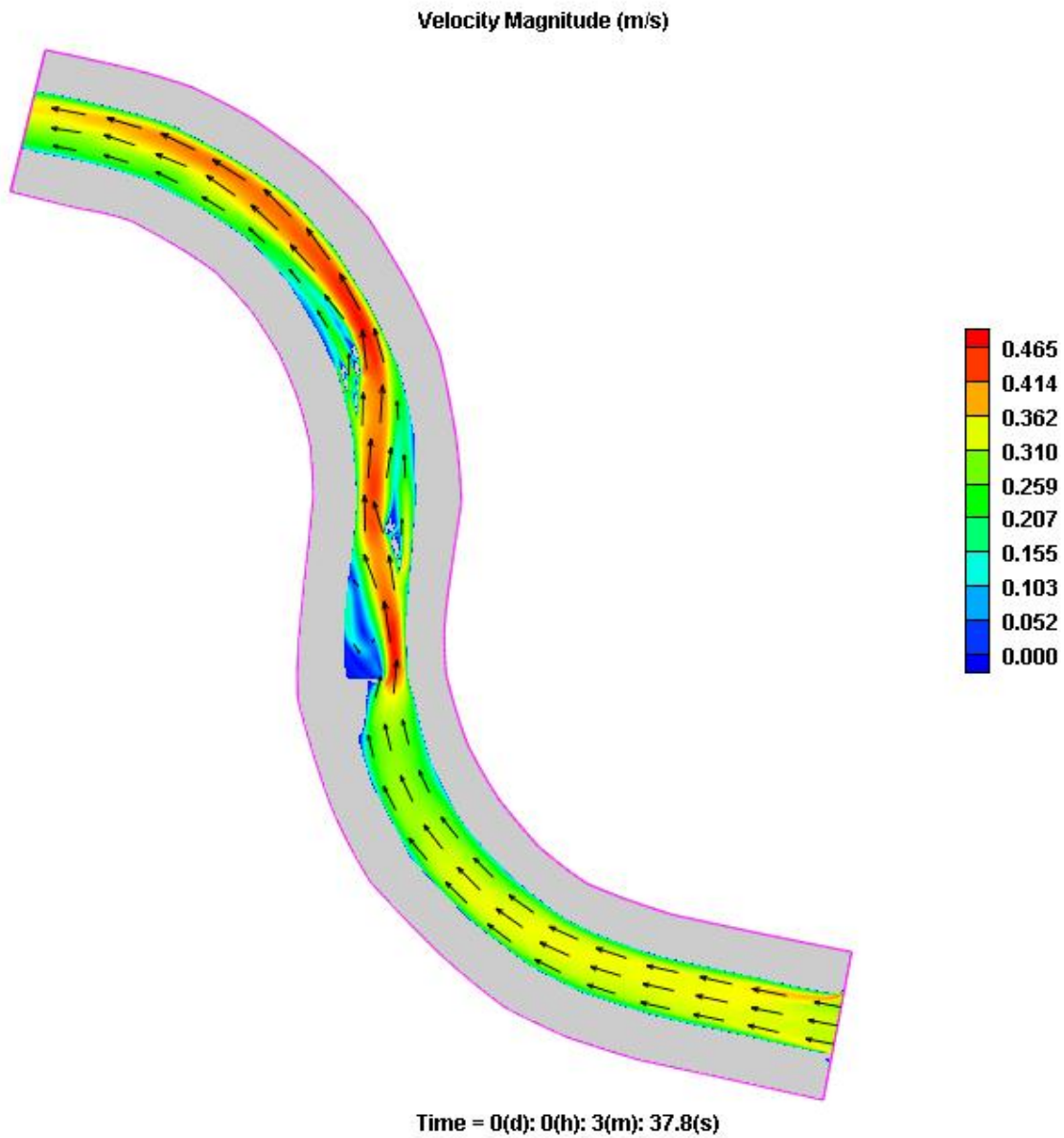


Figure C-27: Velocity magnitude (m/s) with velocity vectors

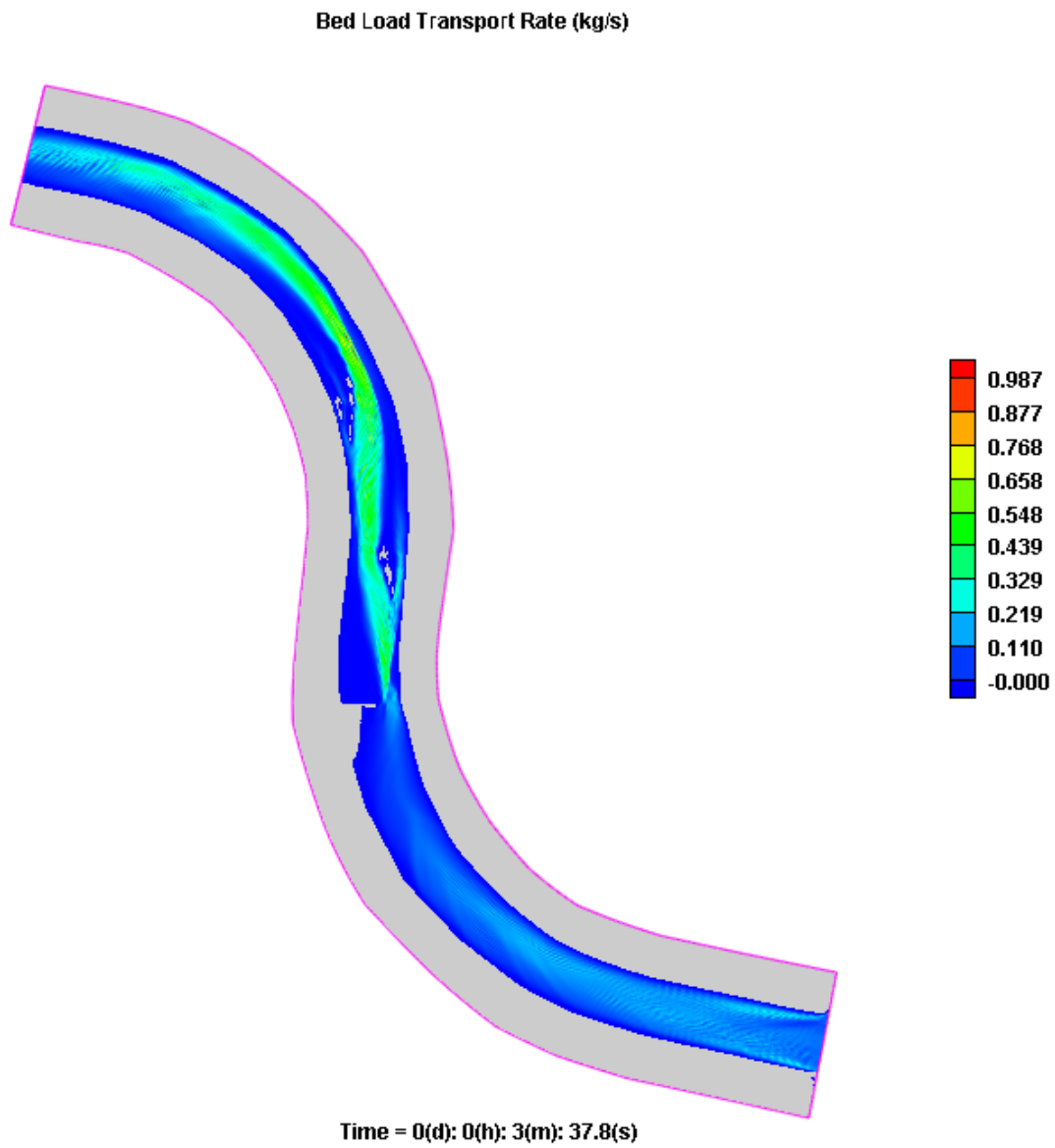


Figure C-28: Bed load transport rate (kg/s) for 30° structure with flow (L-shape)

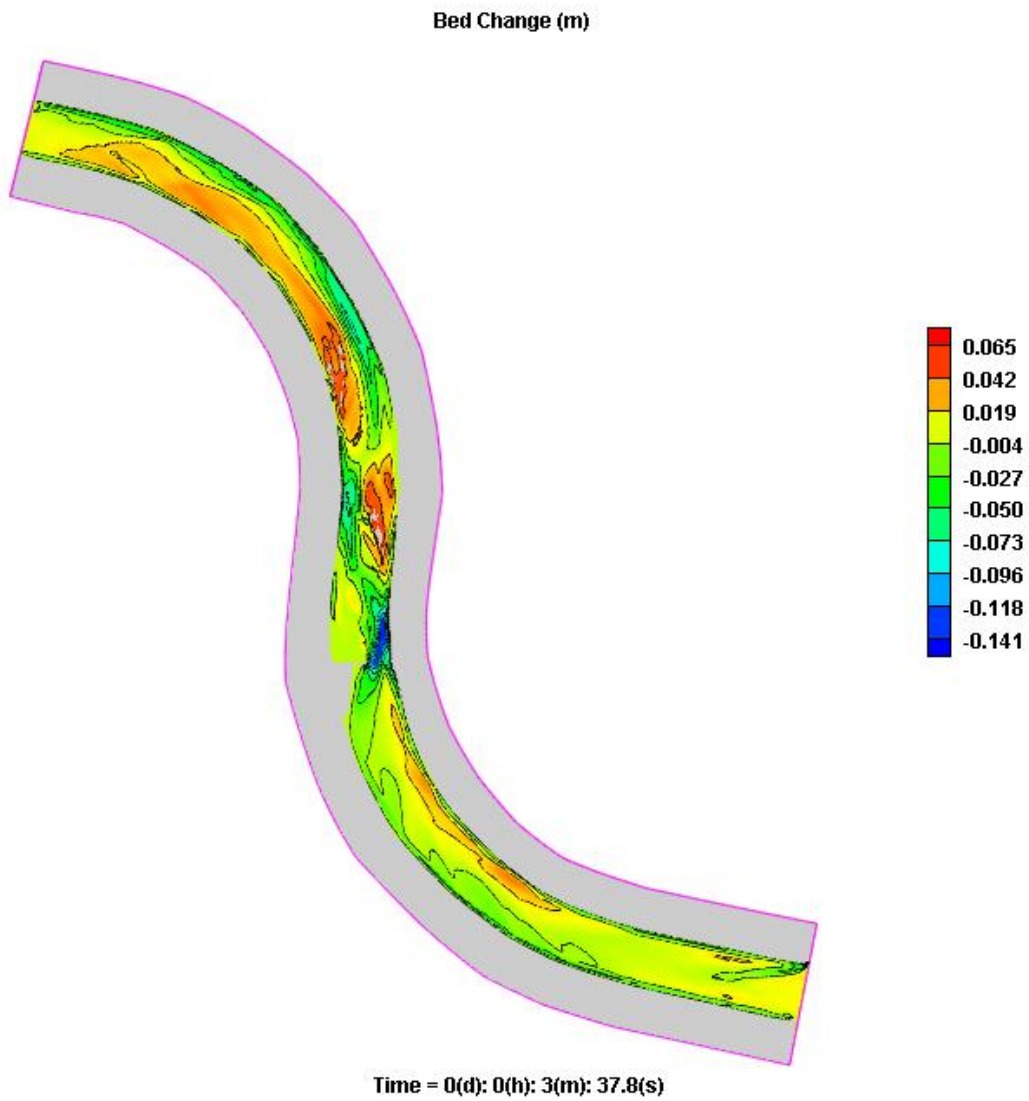


Figure C-29: Bed change (m) for 30° structure with flow (L-shape)

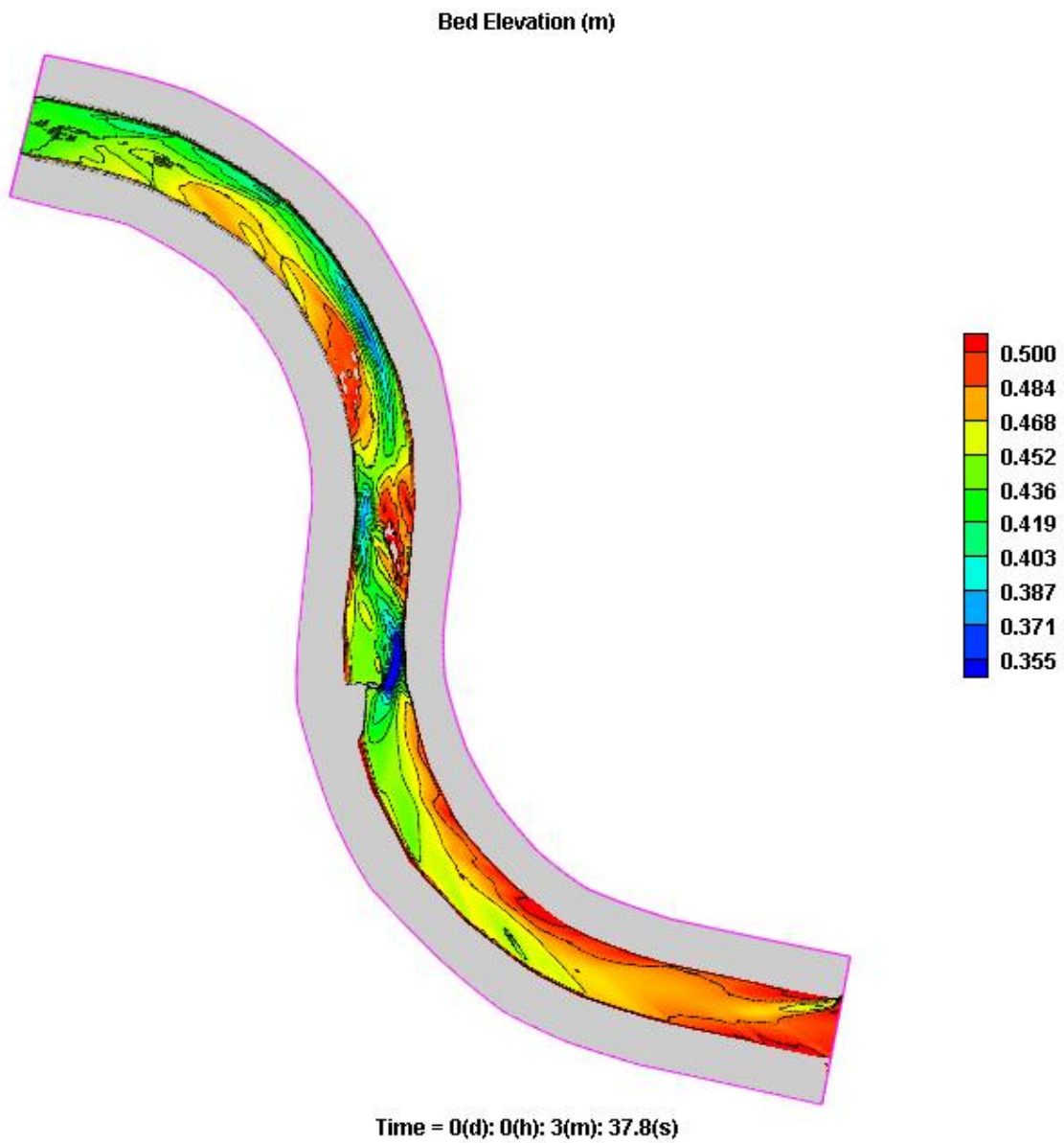


Figure C-30: Scoured bed elevation (30° structure with flow (L-shape))

Simulation Test 6 - 45° Structure with Flow

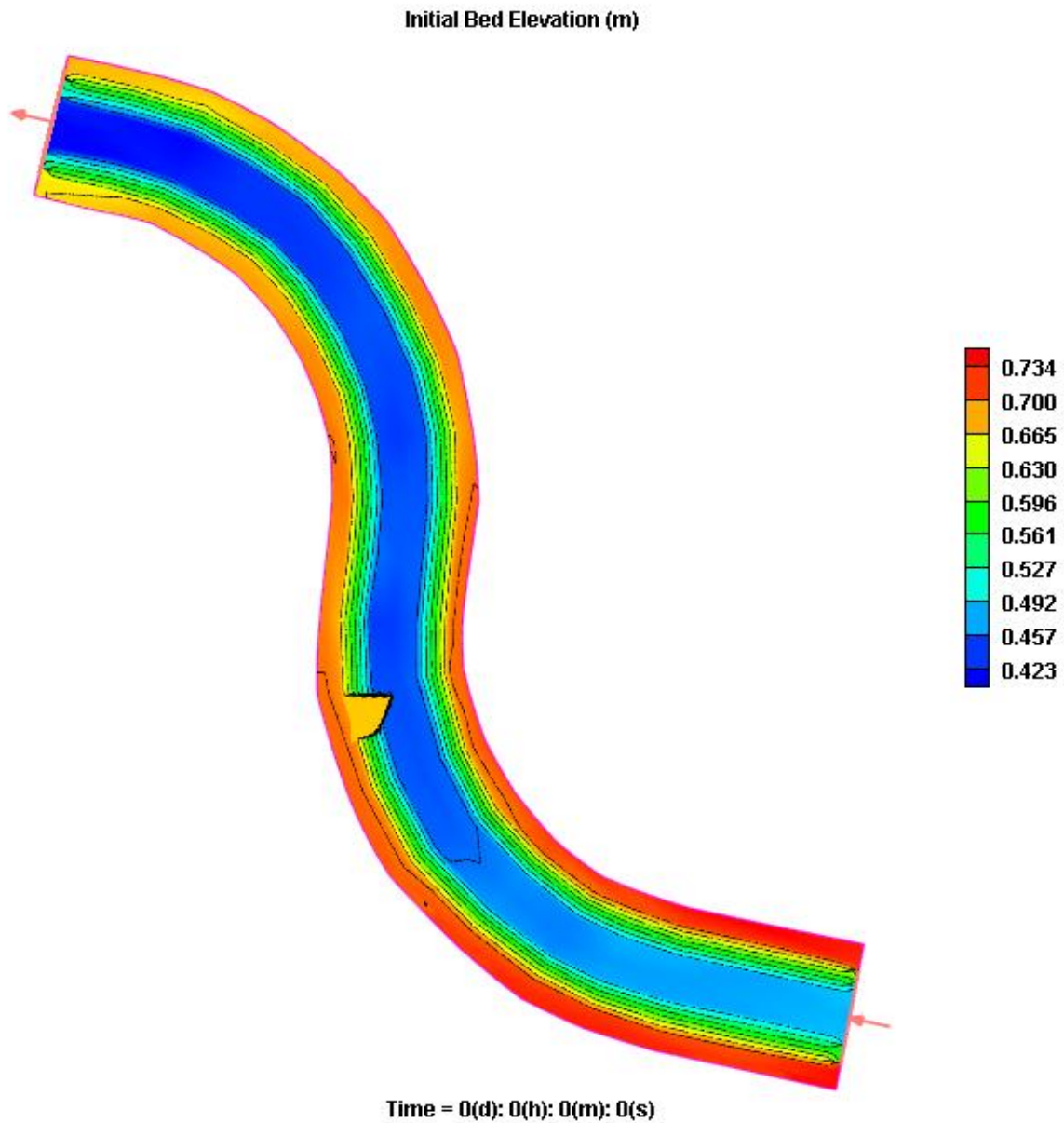


Figure C-31: Bathymetry of 2D model (45° structure with flow)

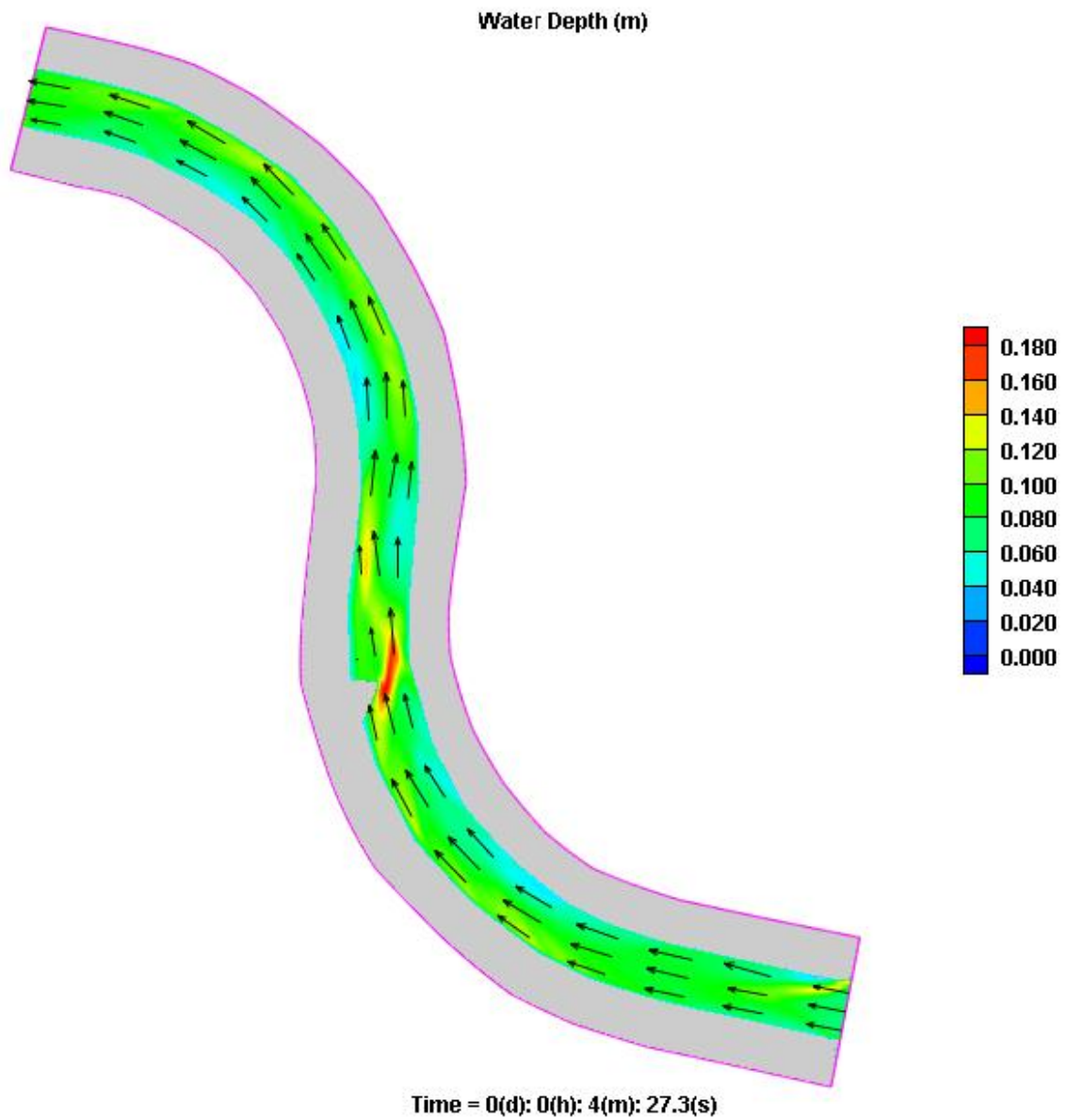


Figure C-32: Water depth (m) with velocity vectors

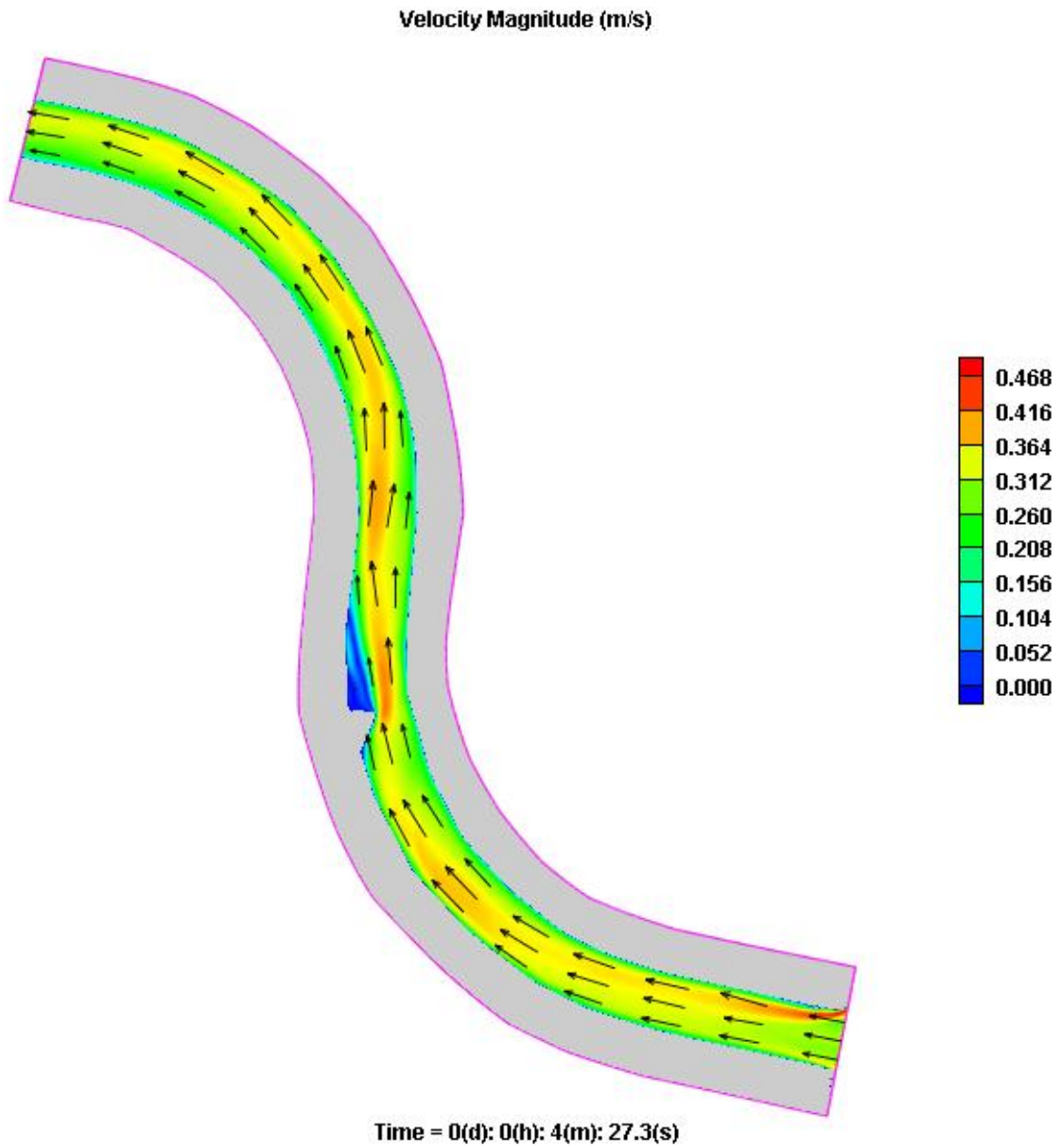


Figure C-33: Velocity magnitude (m/s) with velocity vectors

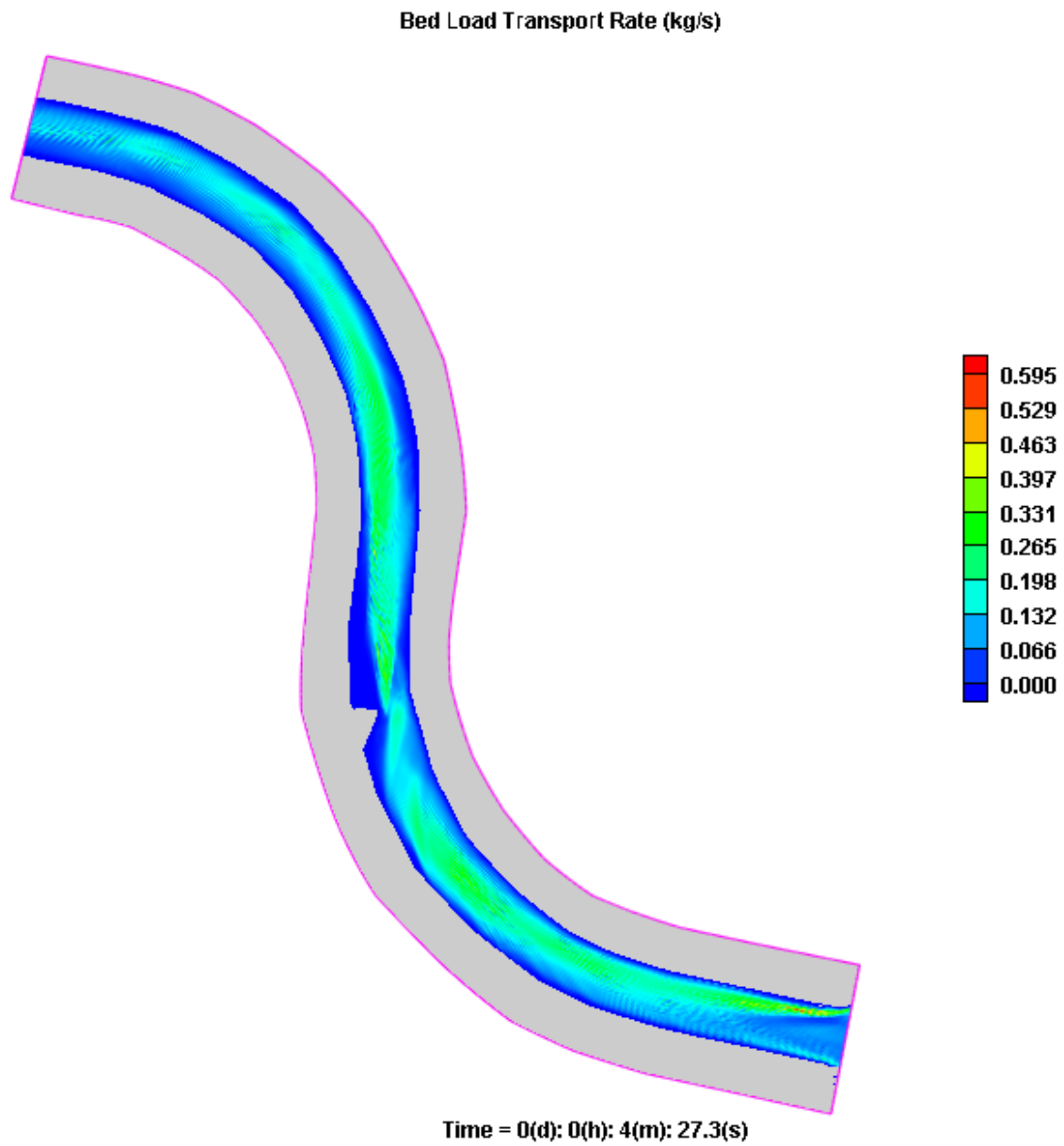


Figure C-34: Bed load transport rate (kg/s) for 45° structure with flow

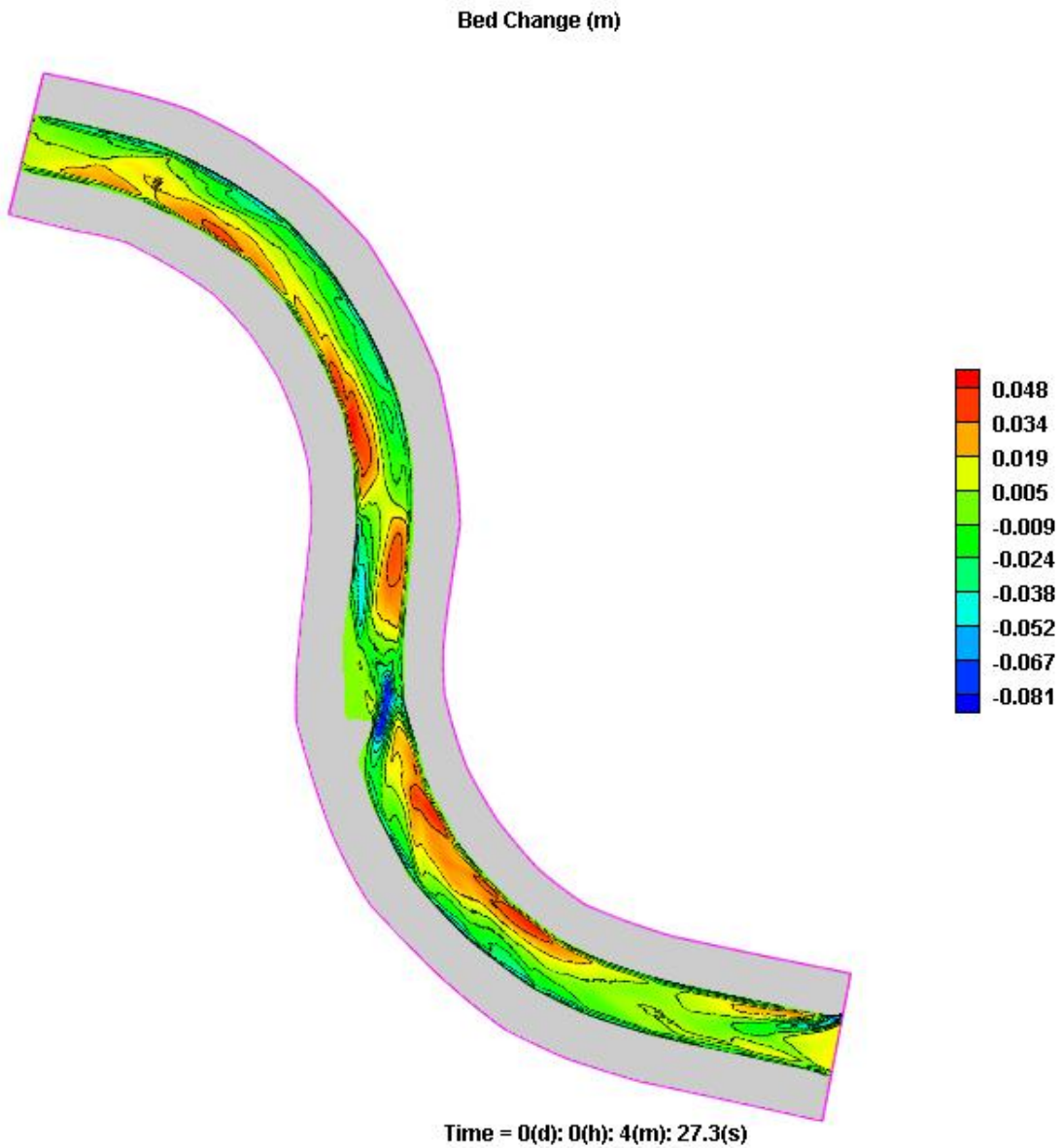


Figure C-35: Bed change (m) for 45° structure with flow

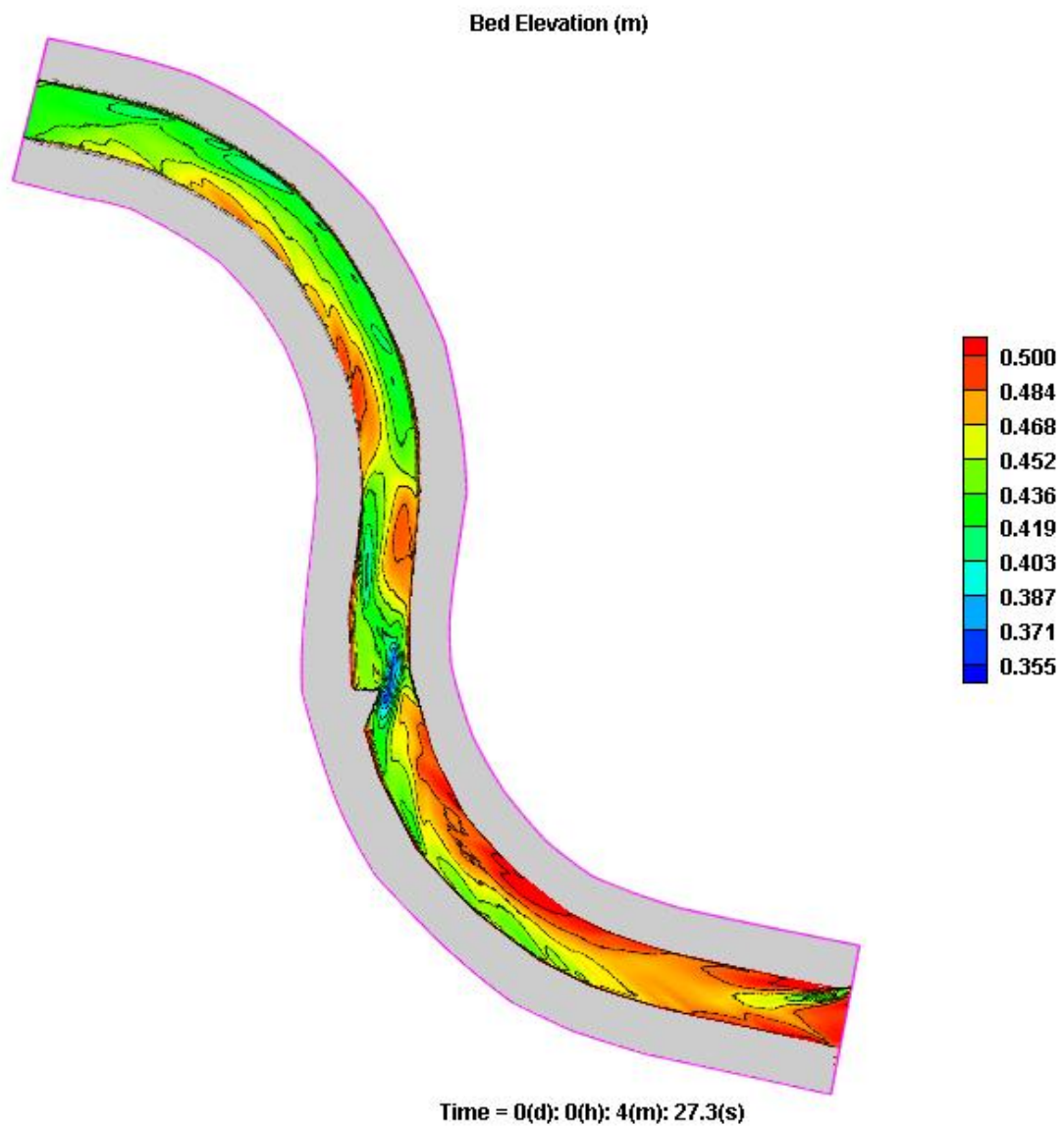


Figure C-36: Scoured bed elevation (45° Structure with flow)

Simulation Test 7 - 45° Structure with Flow (L-Shape)

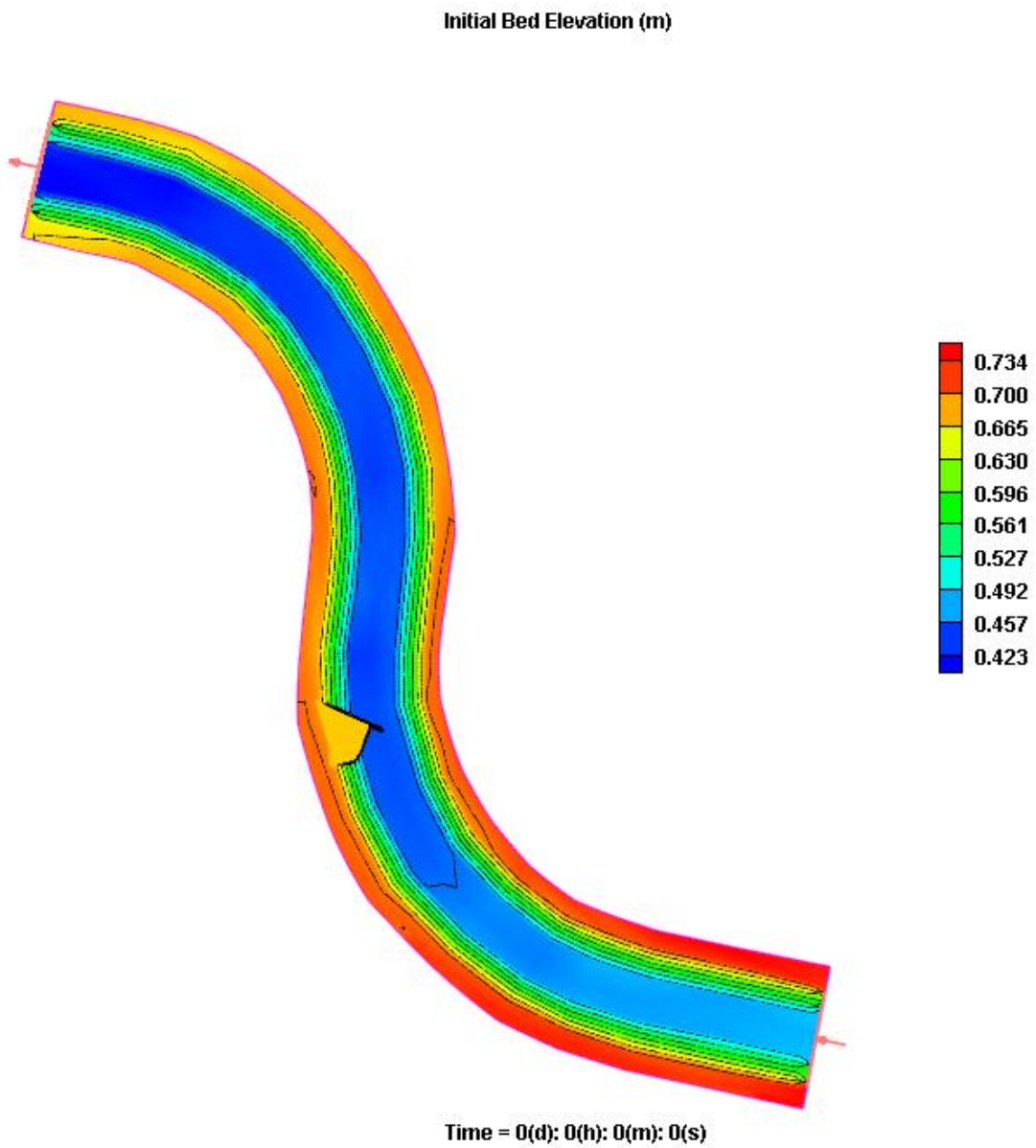


Figure C-37: Bathymetry of 2D model (45° structure with flow (L-shape))

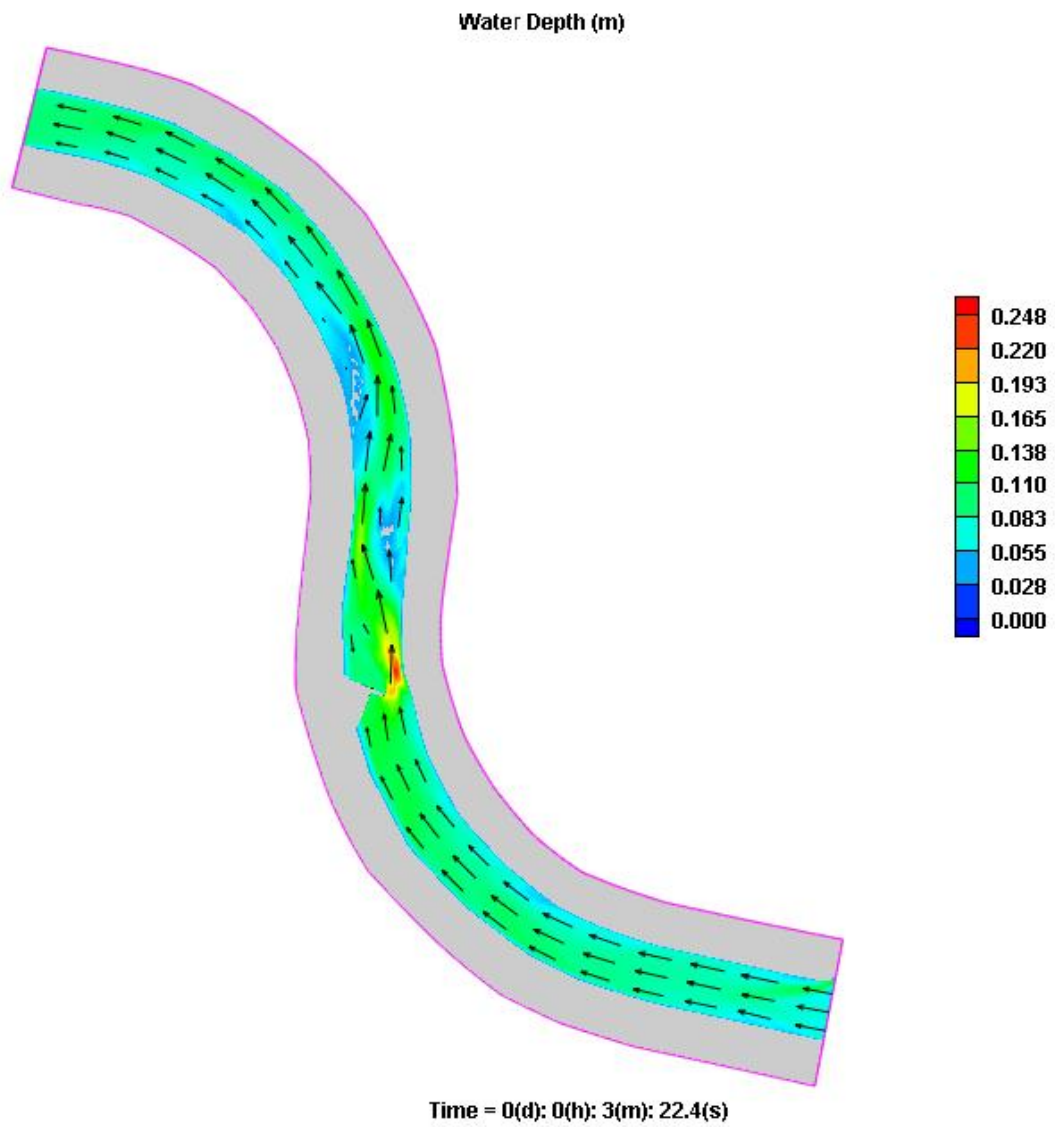


Figure C-38: Water depth (m) with velocity vectors

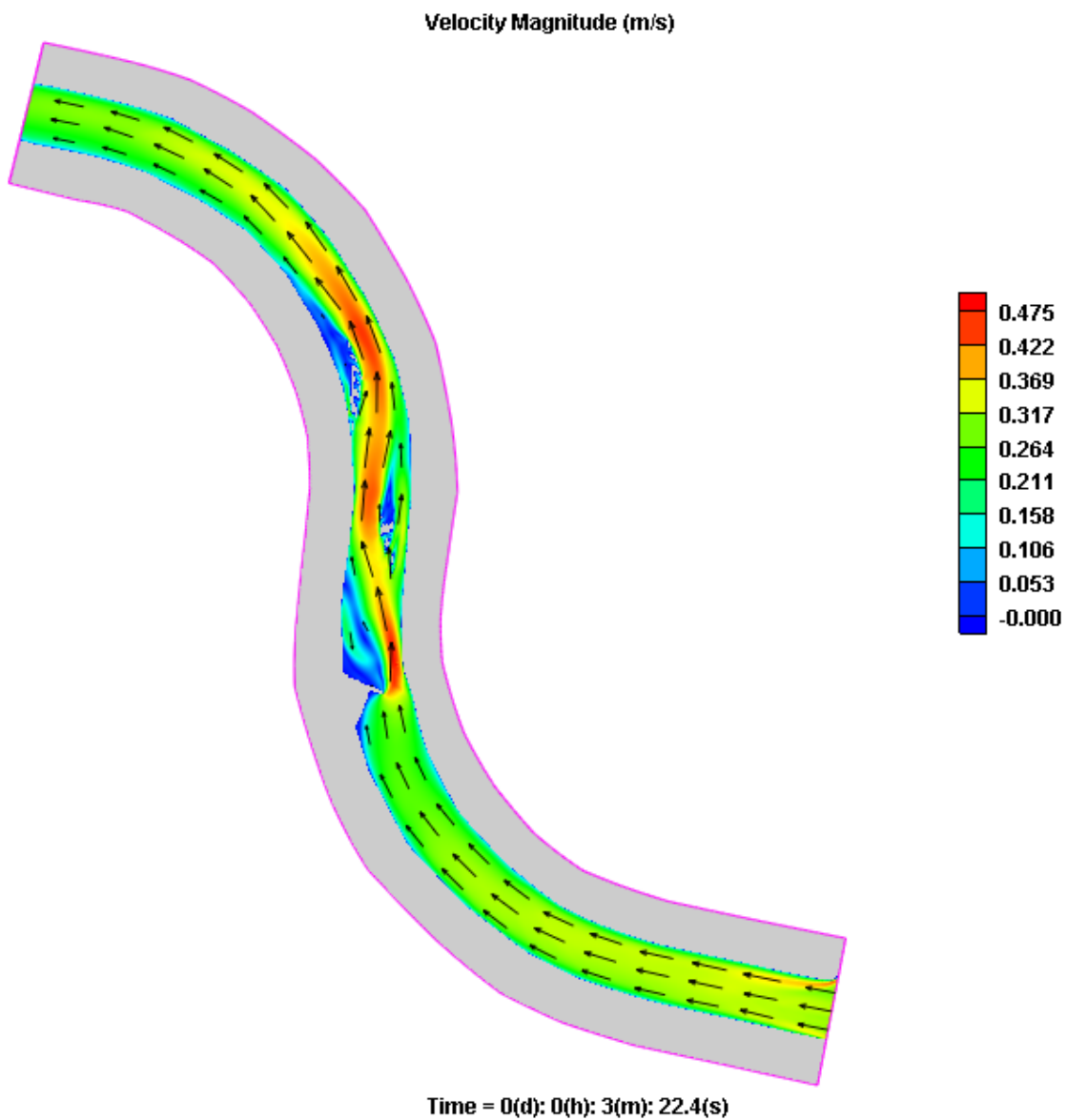


Figure C-39: Velocity magnitude (m/s) with velocity vectors

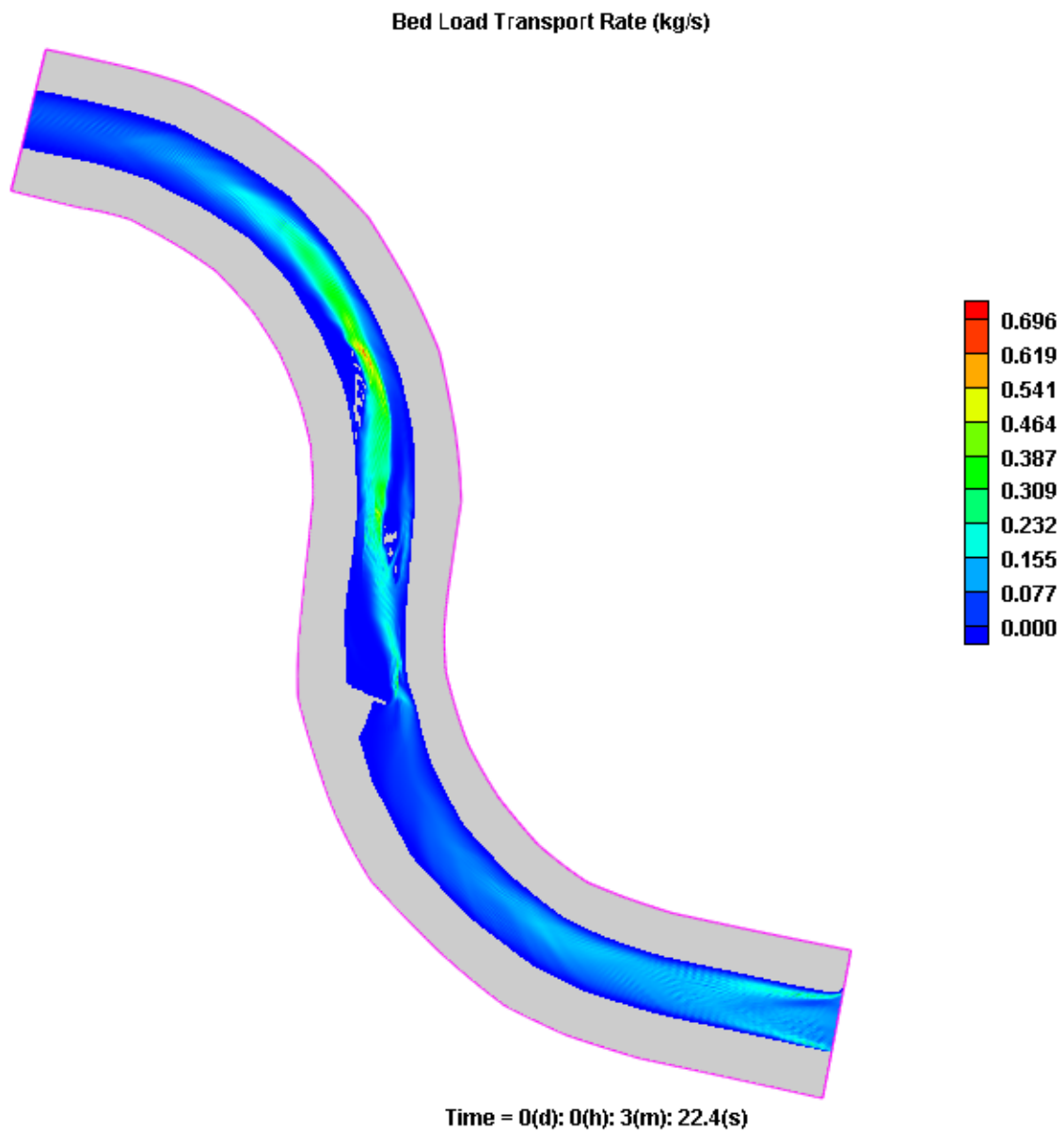


Figure C-40: Bed load transport rate (kg/s) for 45° structure with flow (L-shape)

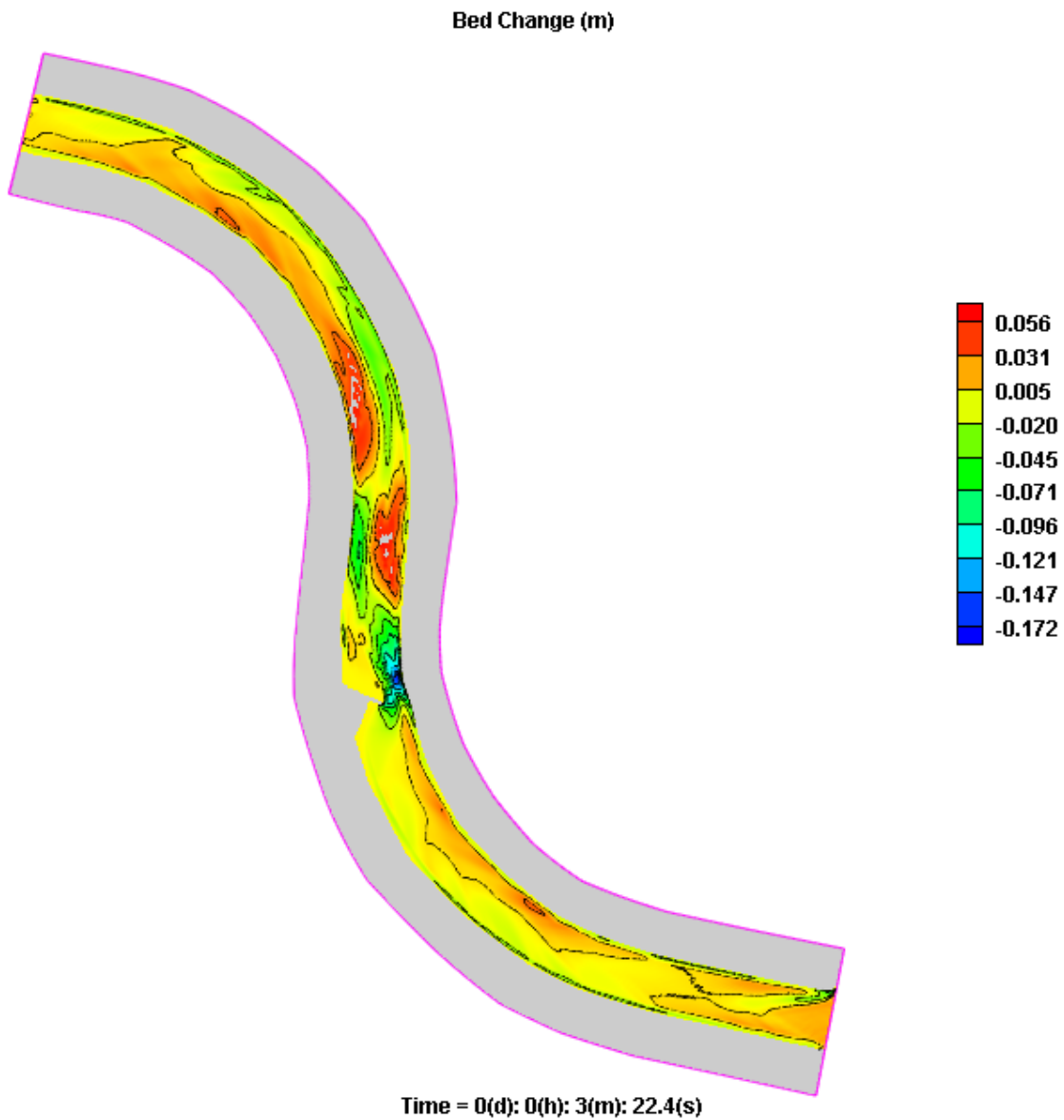


Figure C-41: Bed change (m) for 45° structure with flow (L-shape)

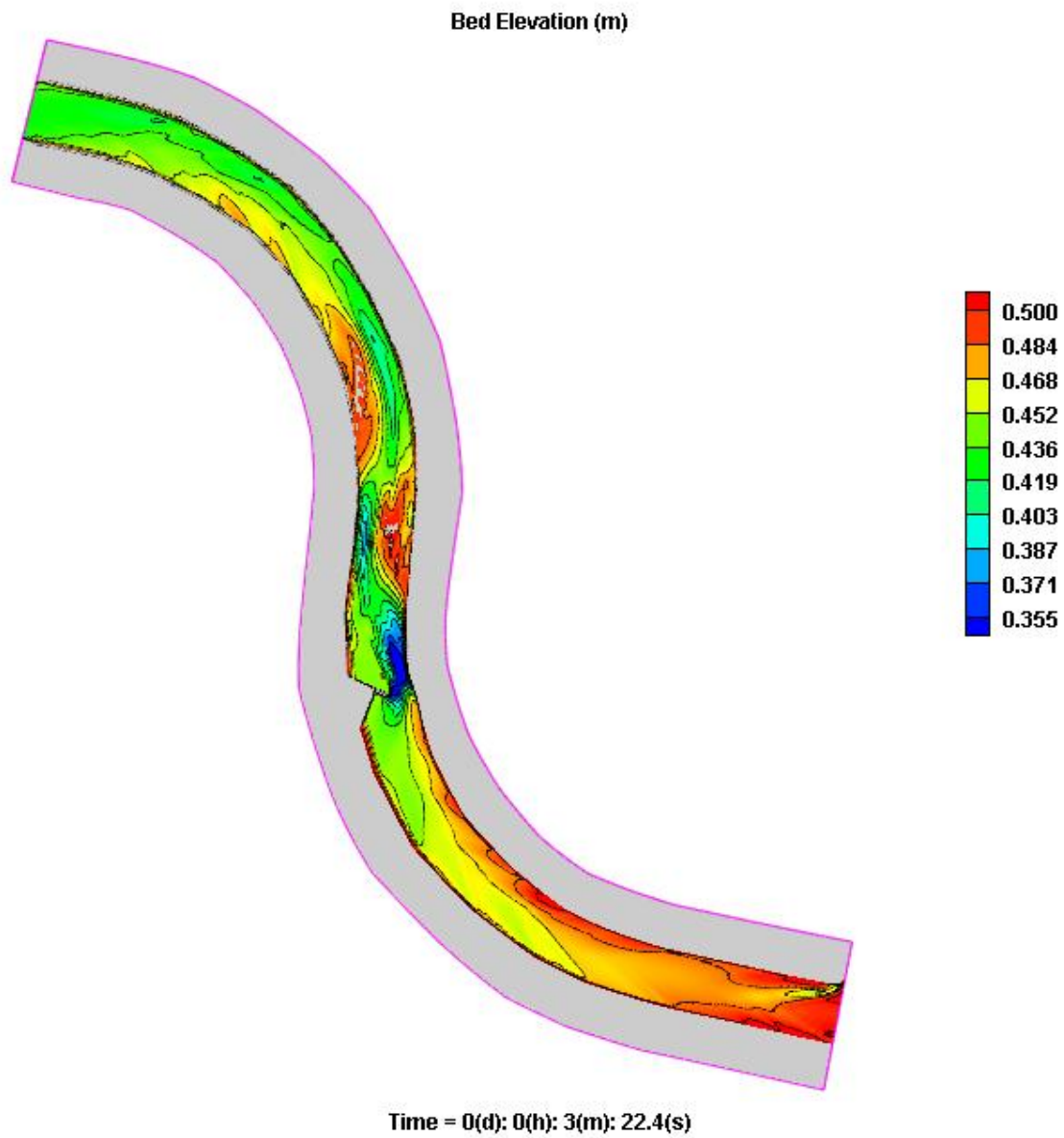


Figure C-42: Scoured bed elevation (45° structure with flow (L-shape))

Simulation Test 8 - 60° Structure with Flow

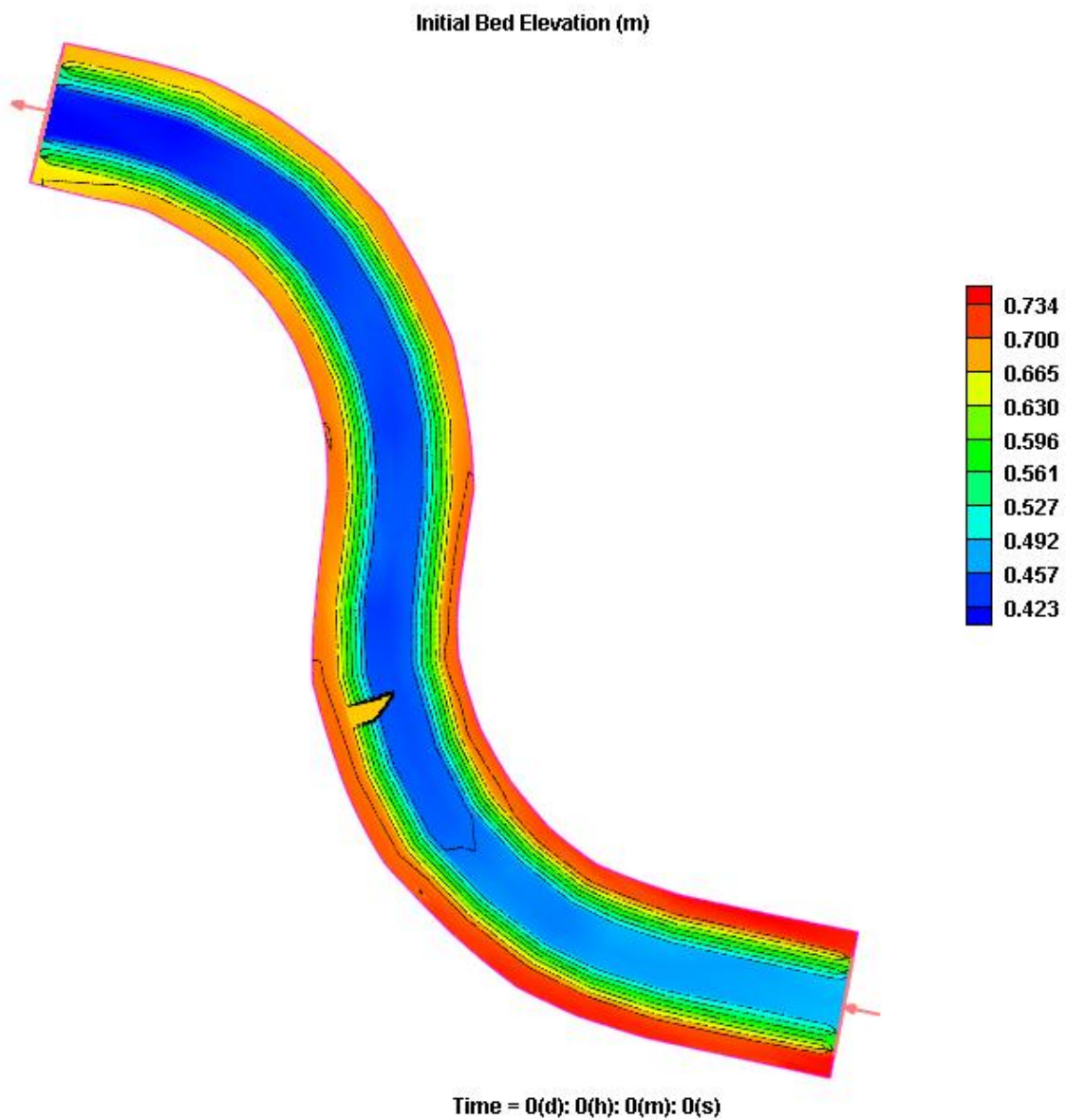


Figure C-43: Bathymetry of 2D model (60° structure with flow)

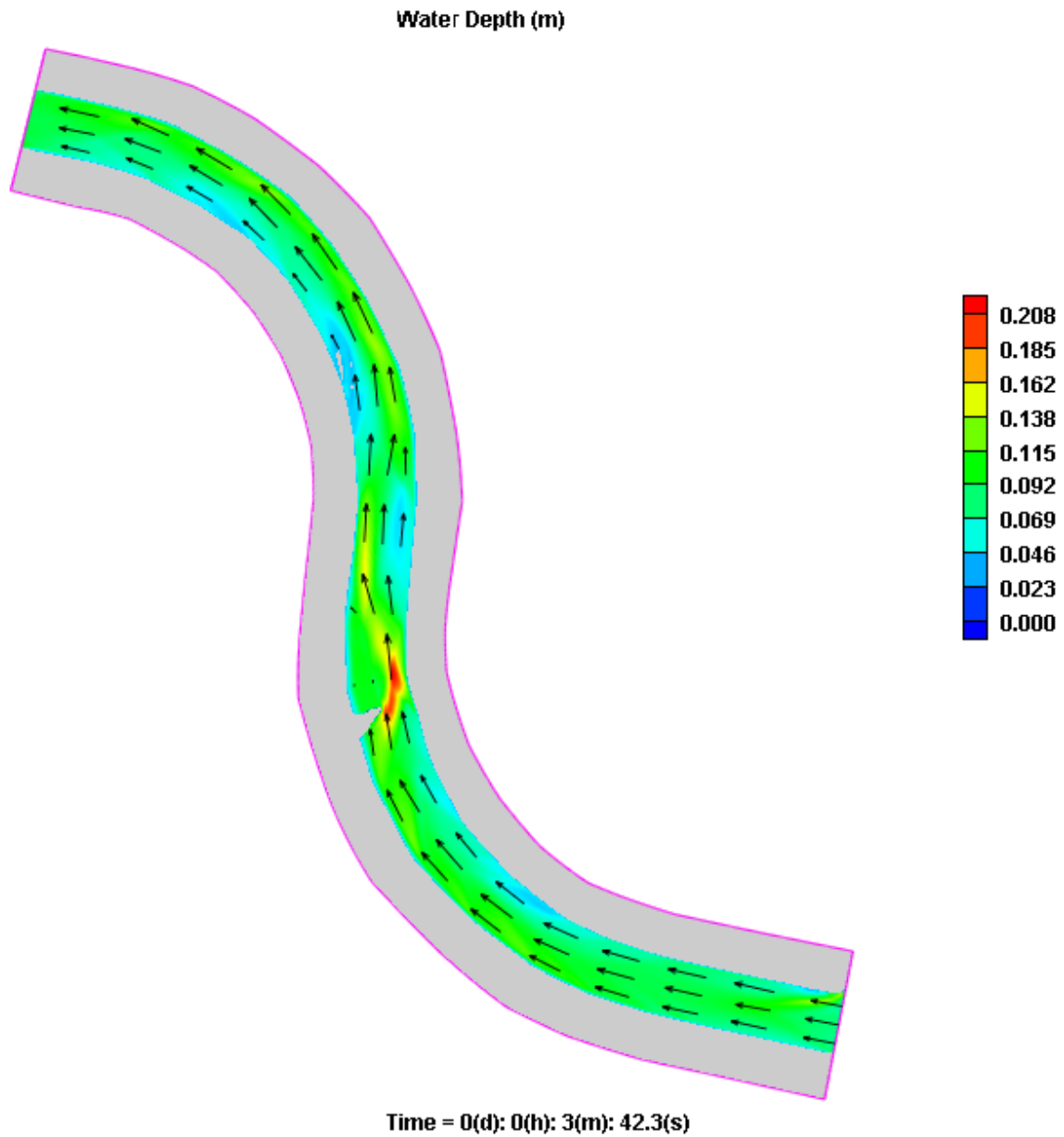


Figure C-44: Water depth (m) with velocity vectors

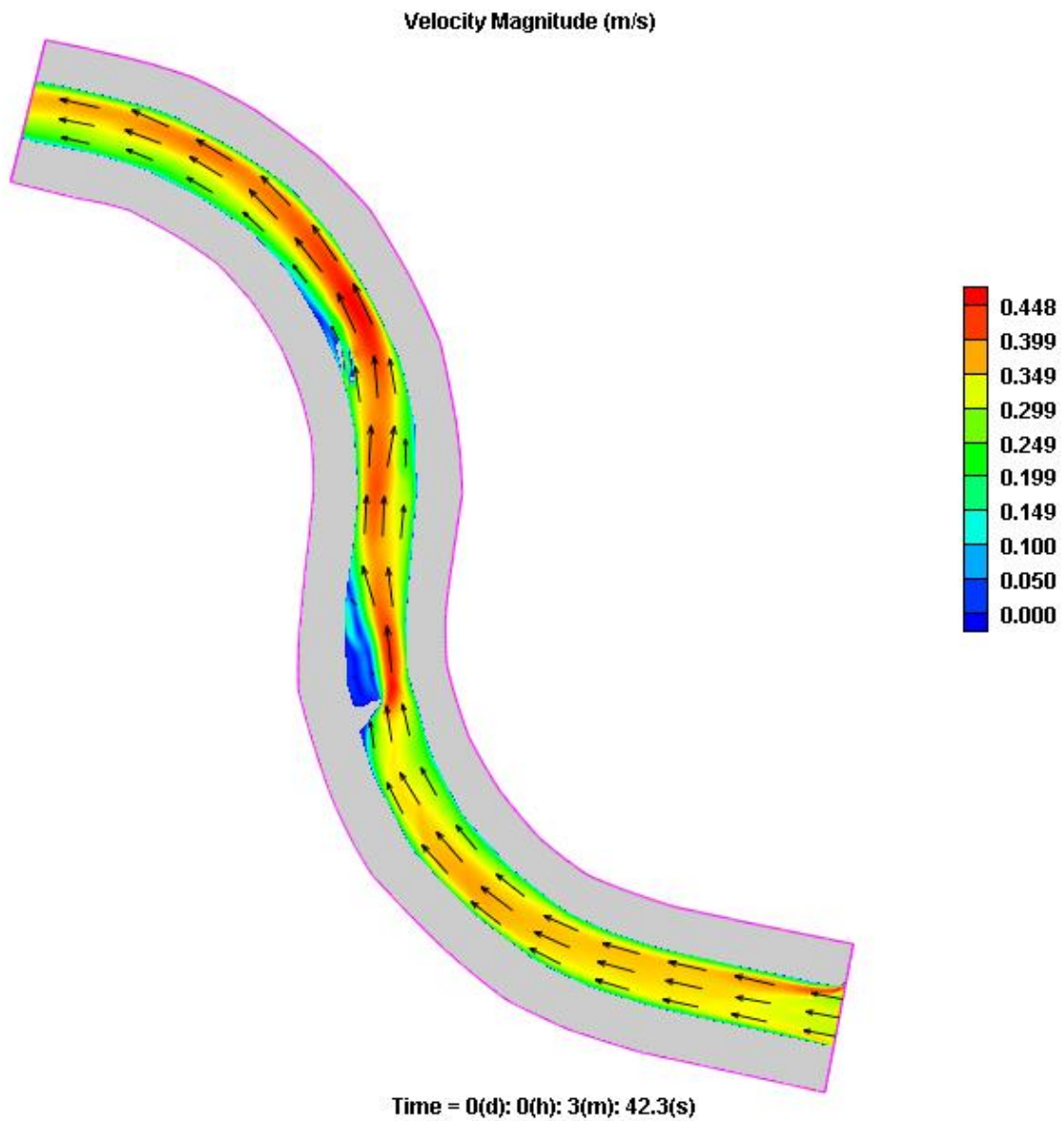


Figure C-45: Velocity magnitude (m/s) with velocity vectors

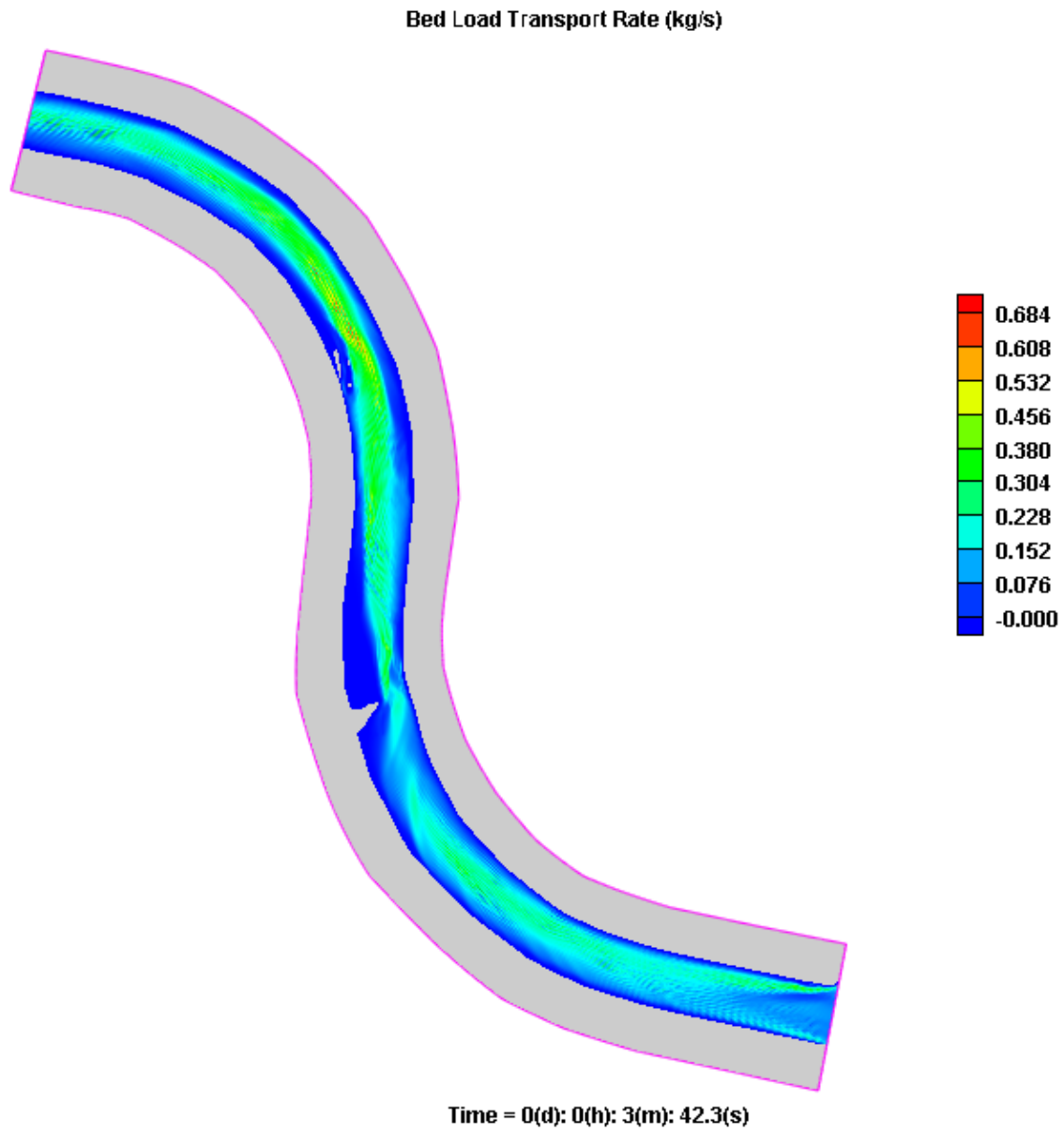


Figure C-46: Bed load transport rate (kg/s) for 60° structure with flow

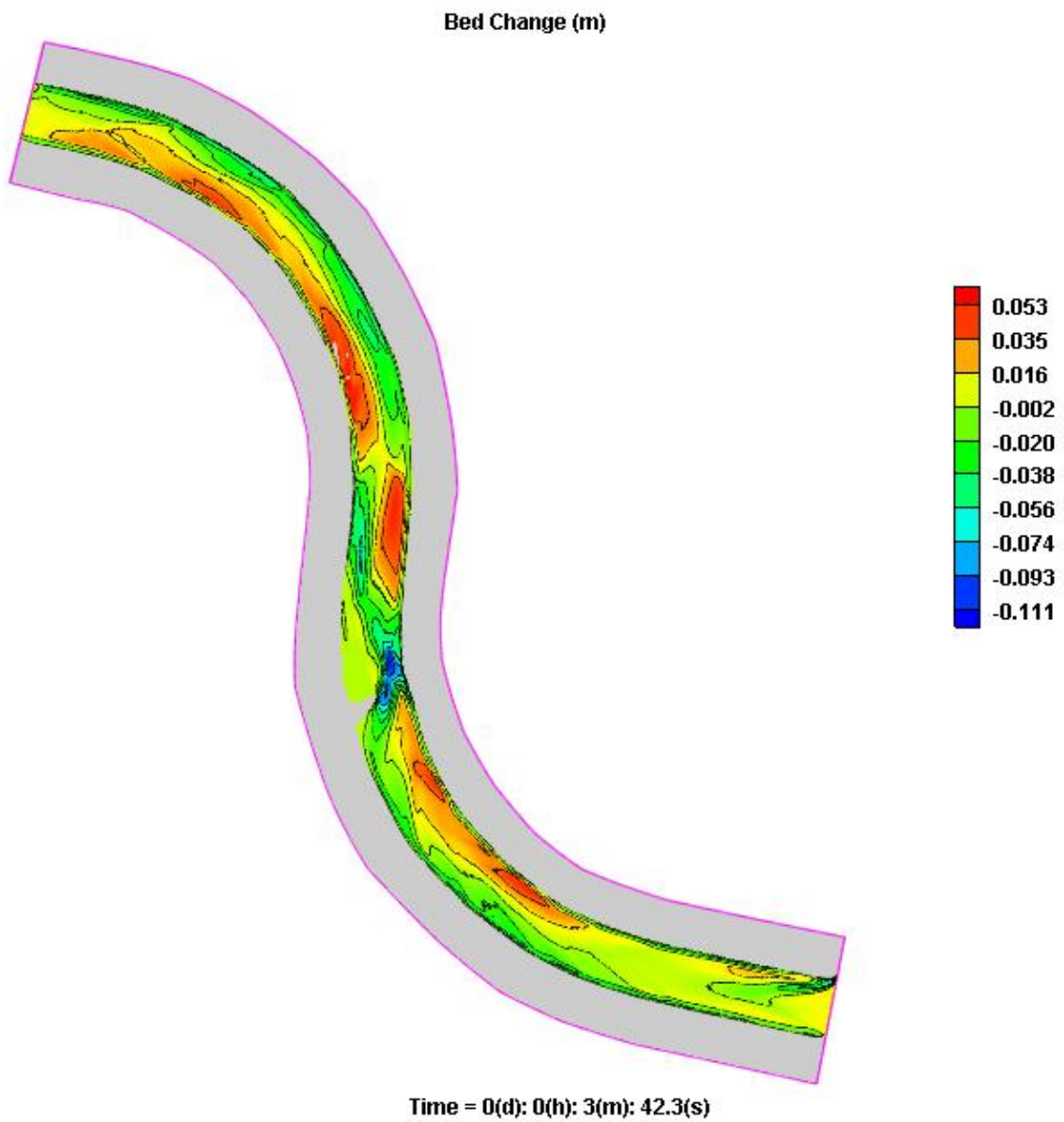


Figure C-47: Bed change (m) for 60° structure with flow

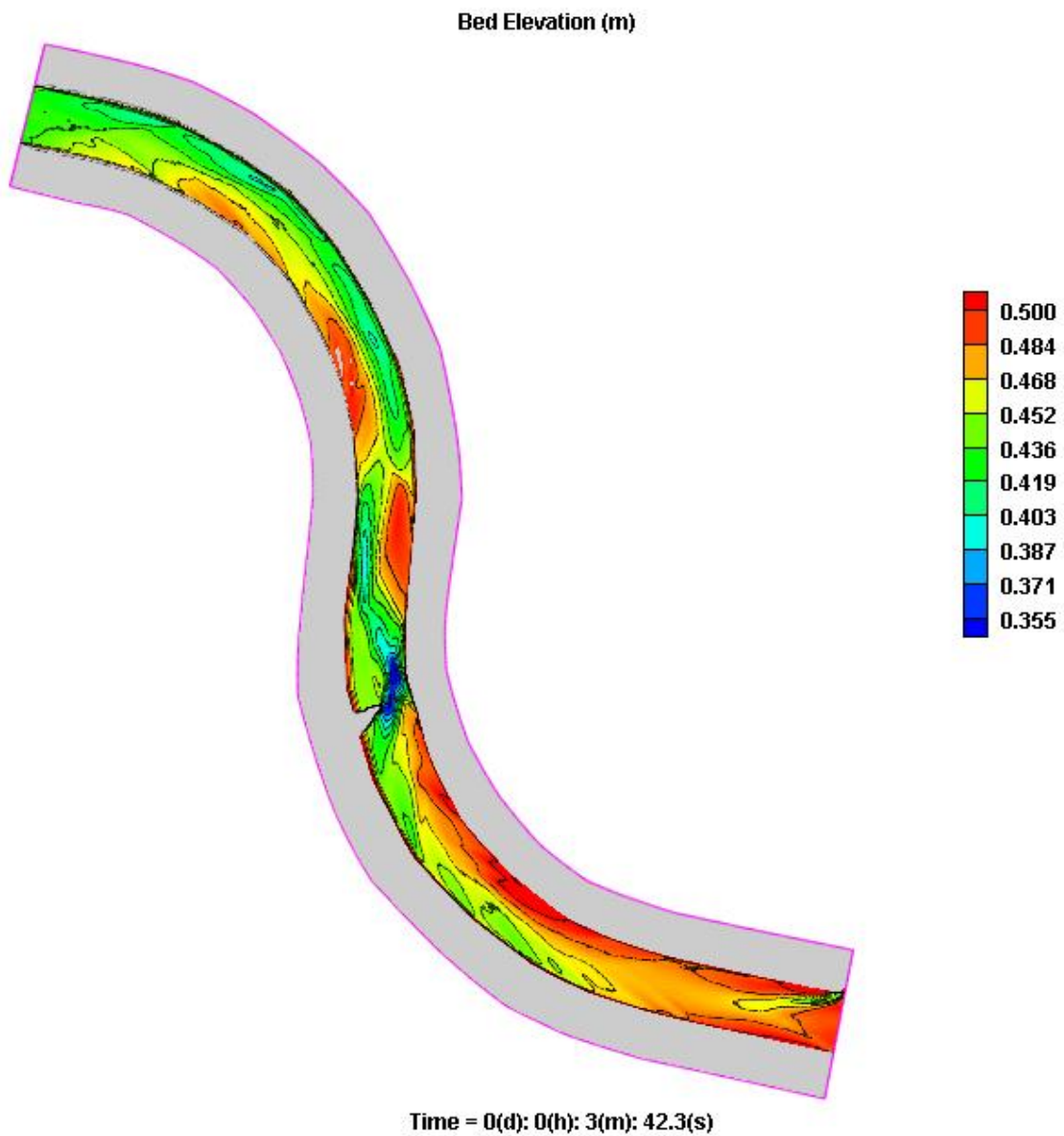


Figure C-48: Scoured bed elevation (60° structure with flow)

Simulation Test 9 - 60° Structure with Flow (L-Shape)

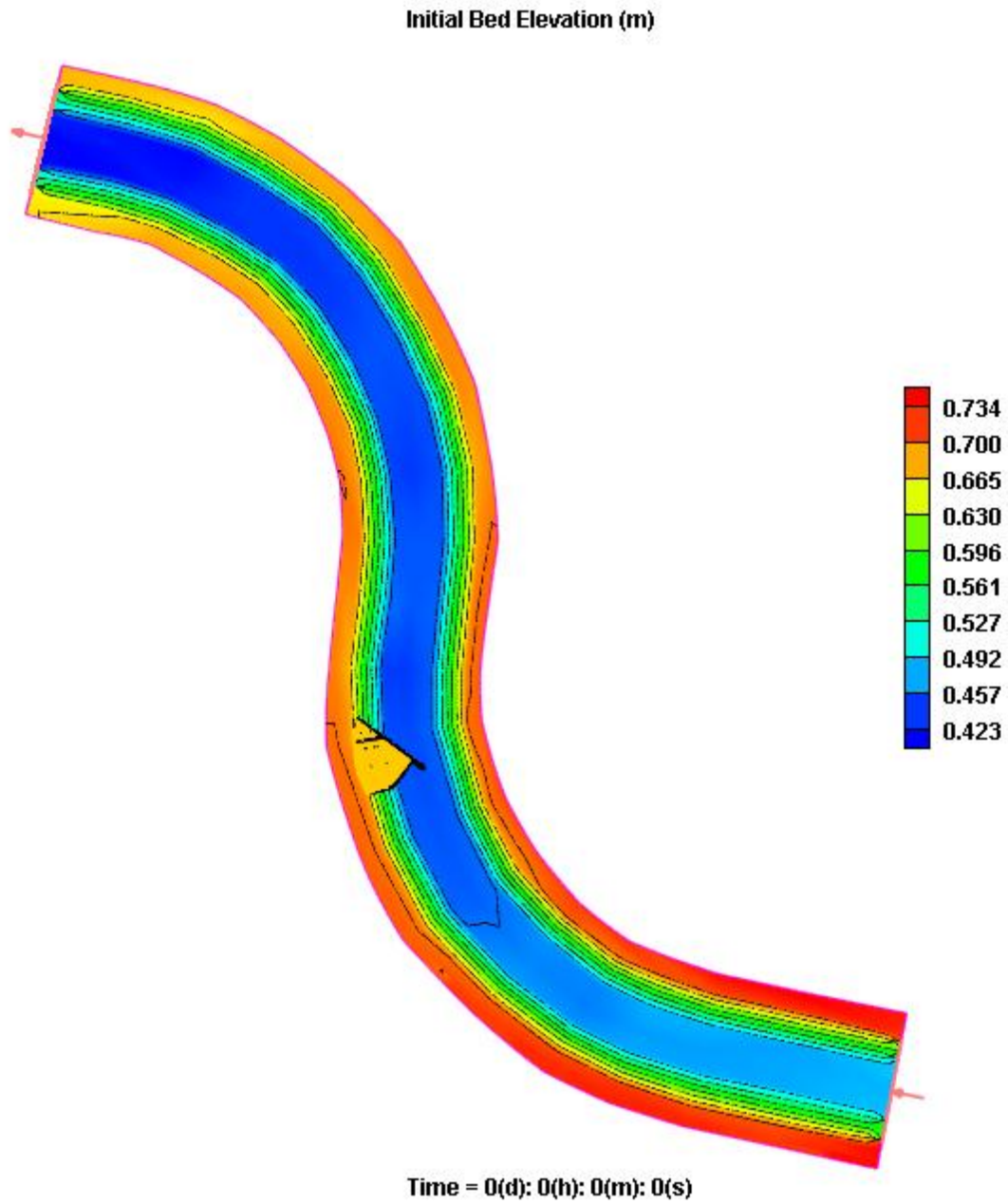


Figure C-49: Bathymetry of 2D model (60° structure with flow (L-shaped))

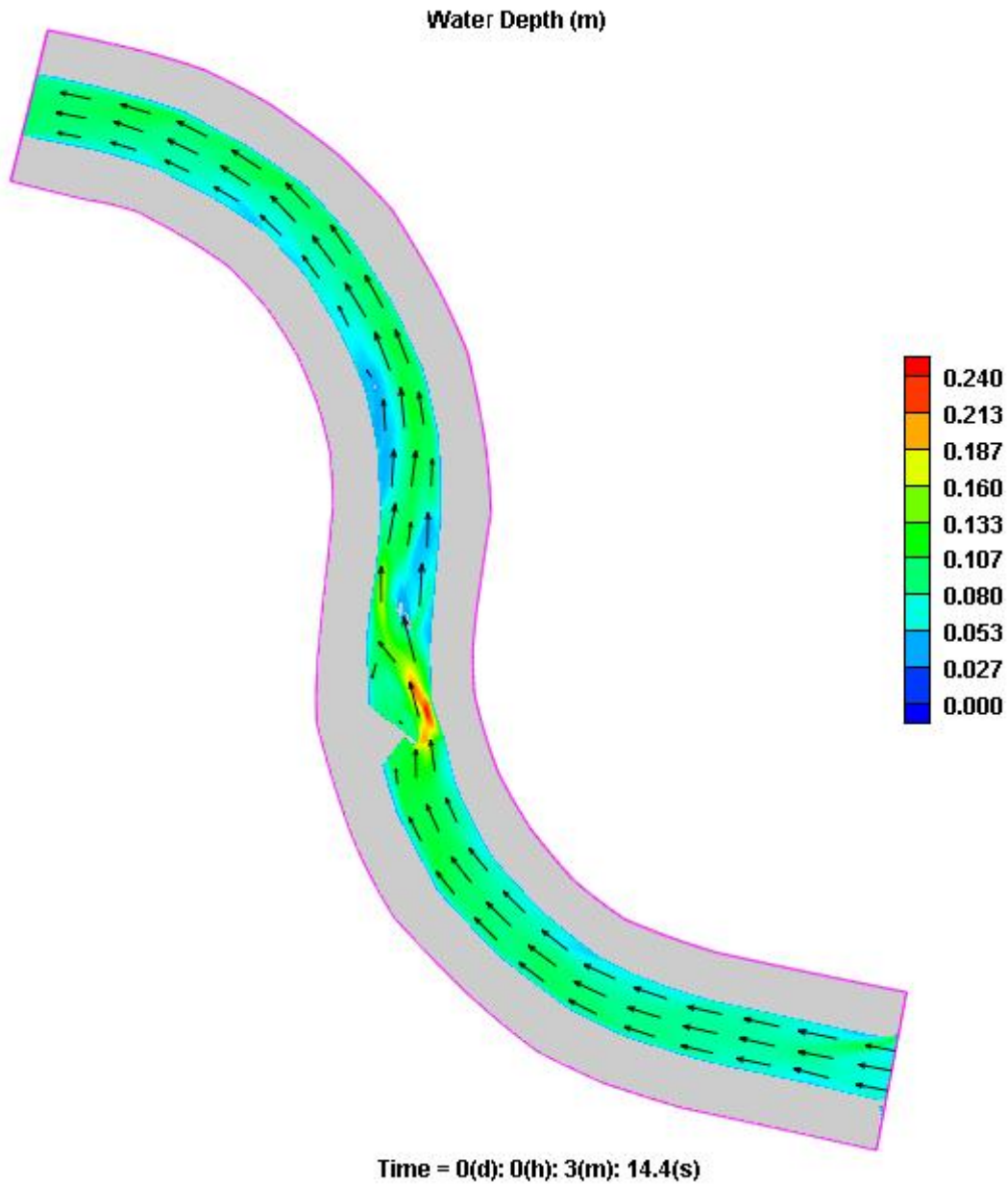


Figure C-50: Water depth (m) with velocity vectors

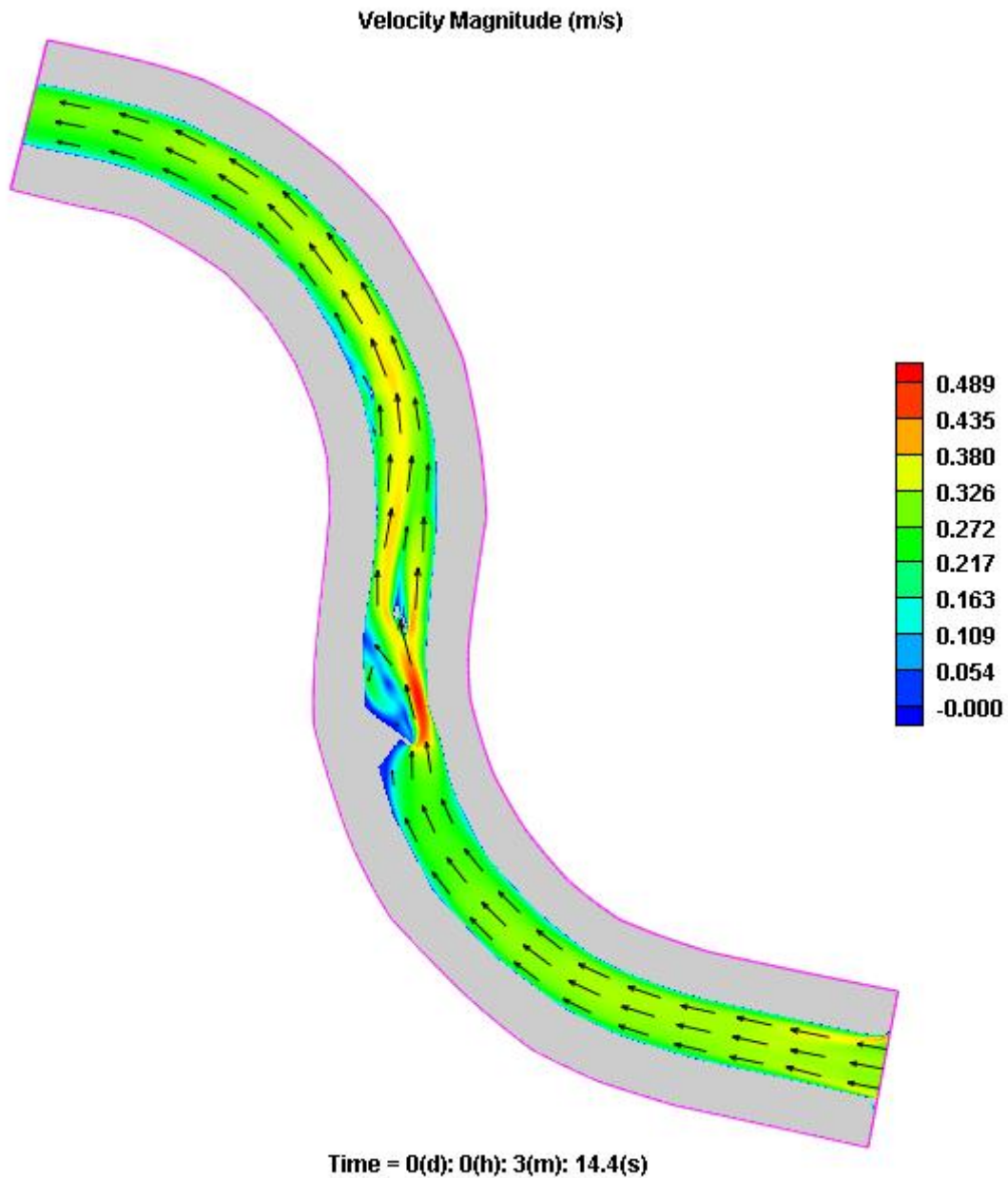


Figure C-51: Velocity magnitude (m/s) with velocity vectors

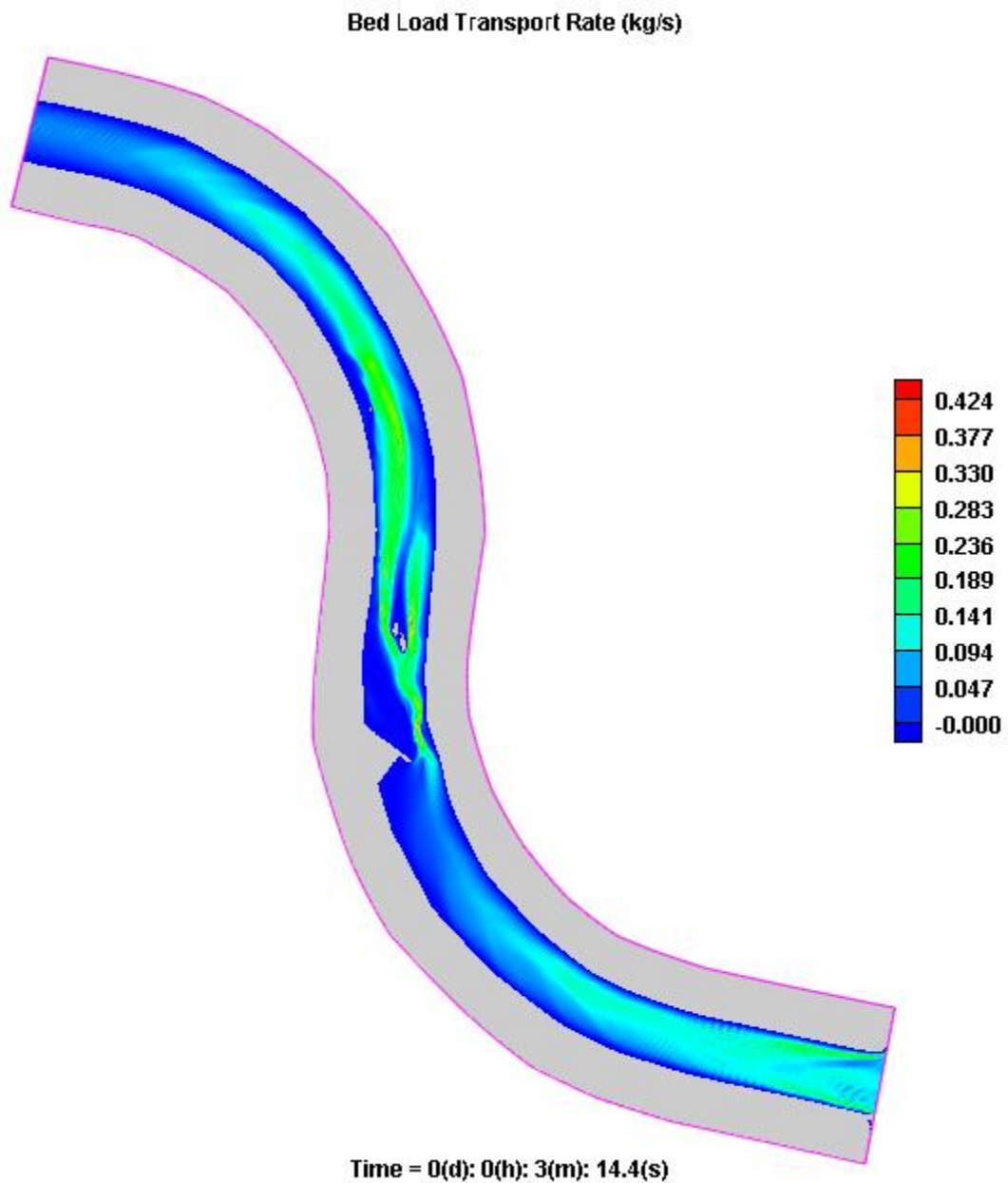


Figure C-52: Bed load transport rate (kg/s) for 60° structure with flow (L-shaped)

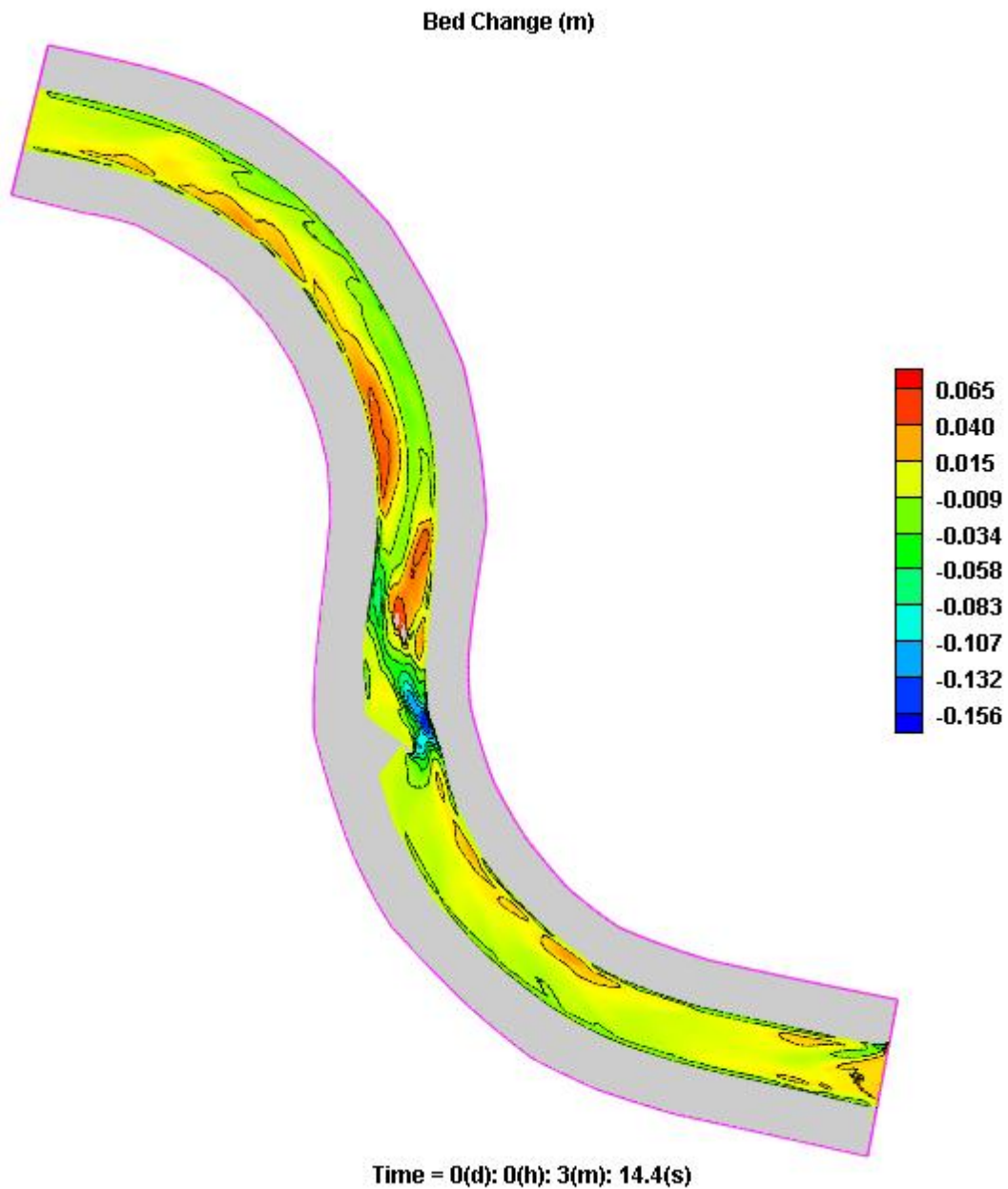


Figure C-53: Bed change (m) for 60° structure with flow (L-shaped)

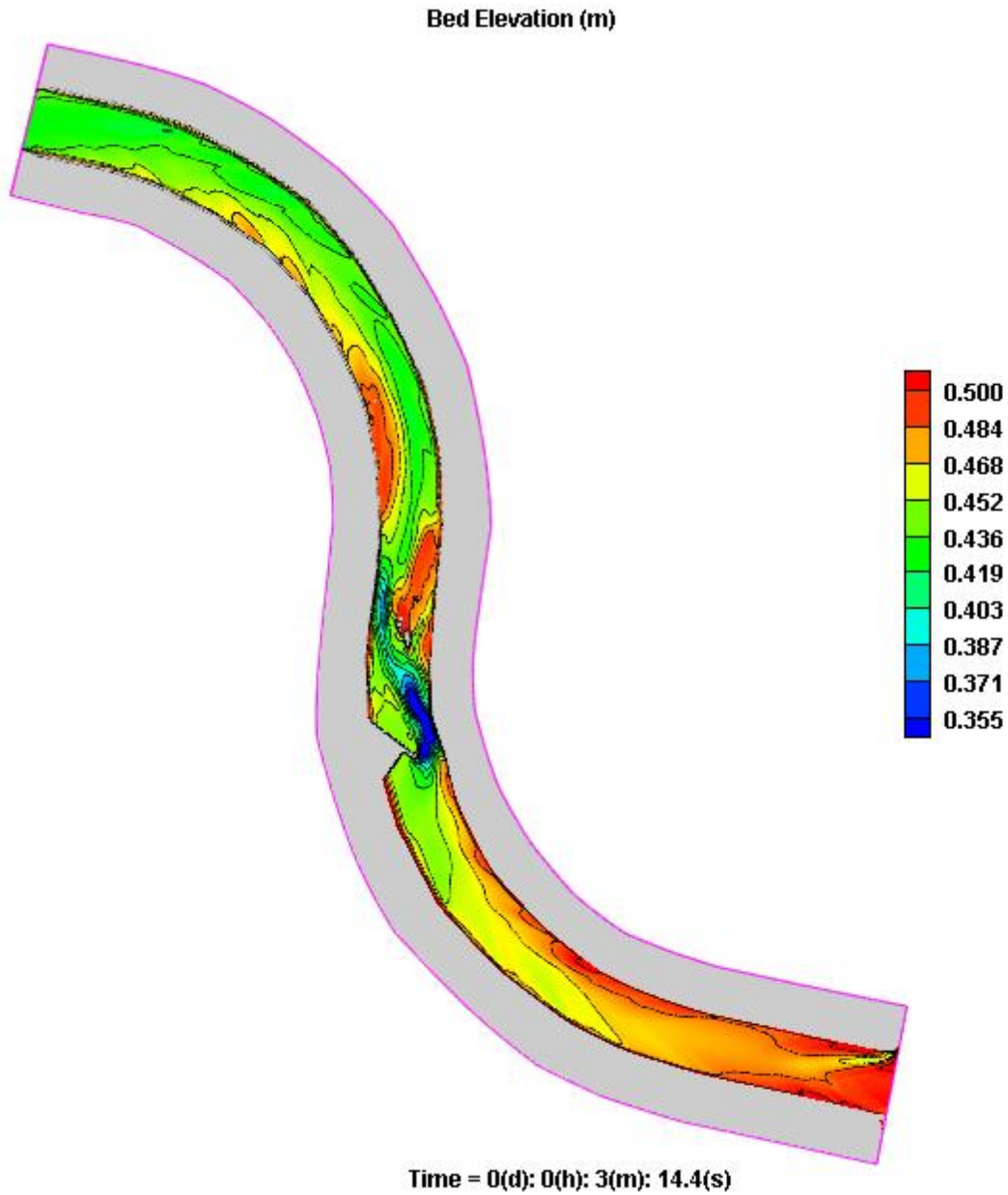


Figure C-54: Scoured bed elevation (60° structure with flow (L-shaped))

Simulation Test 10S 1 - 30° Structure with Flow (One Metre Wide Bottom Width)

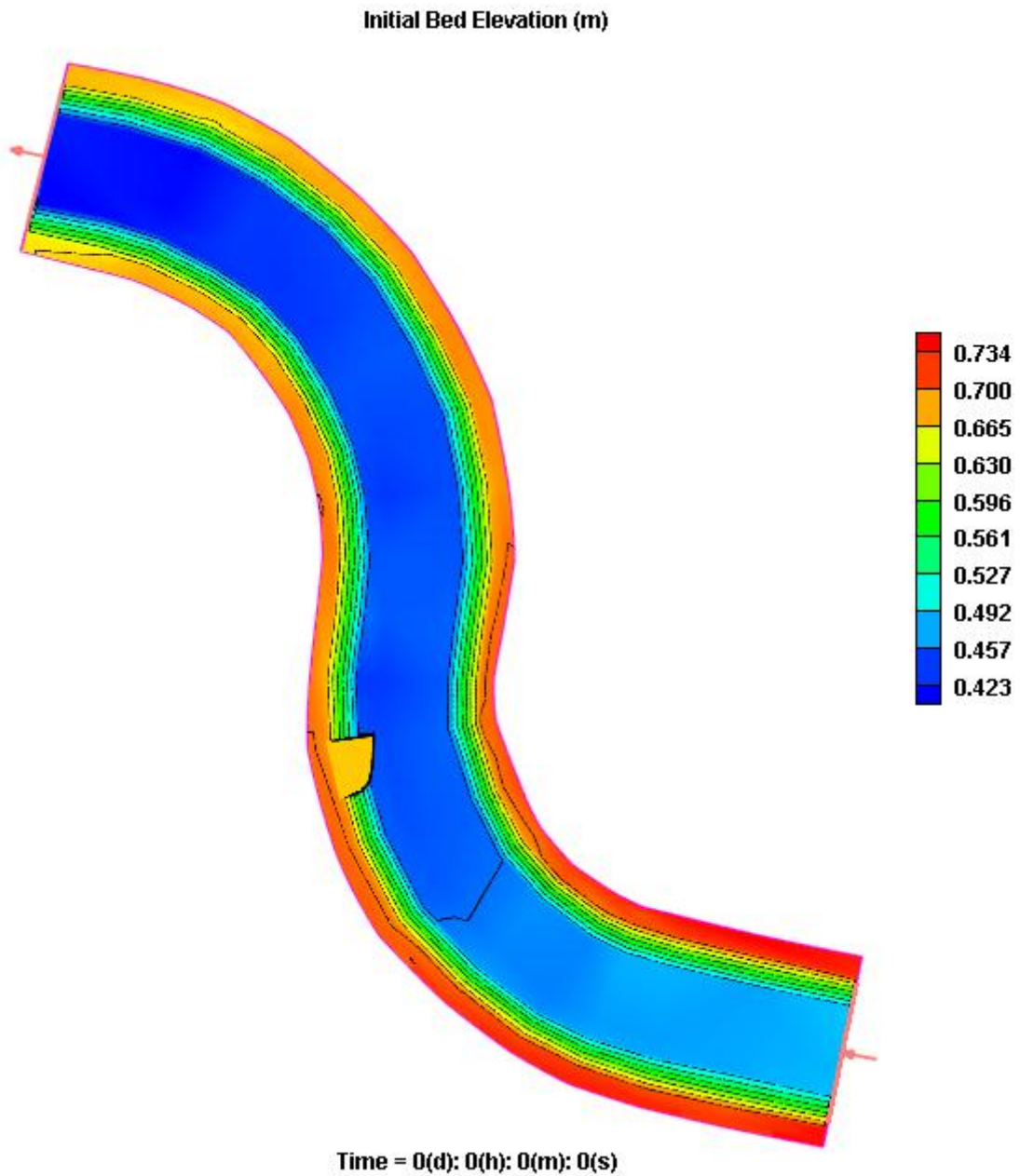


Figure C-55: Bathymetry of 2D model (30° structure with flow (one metre wide bottom width))

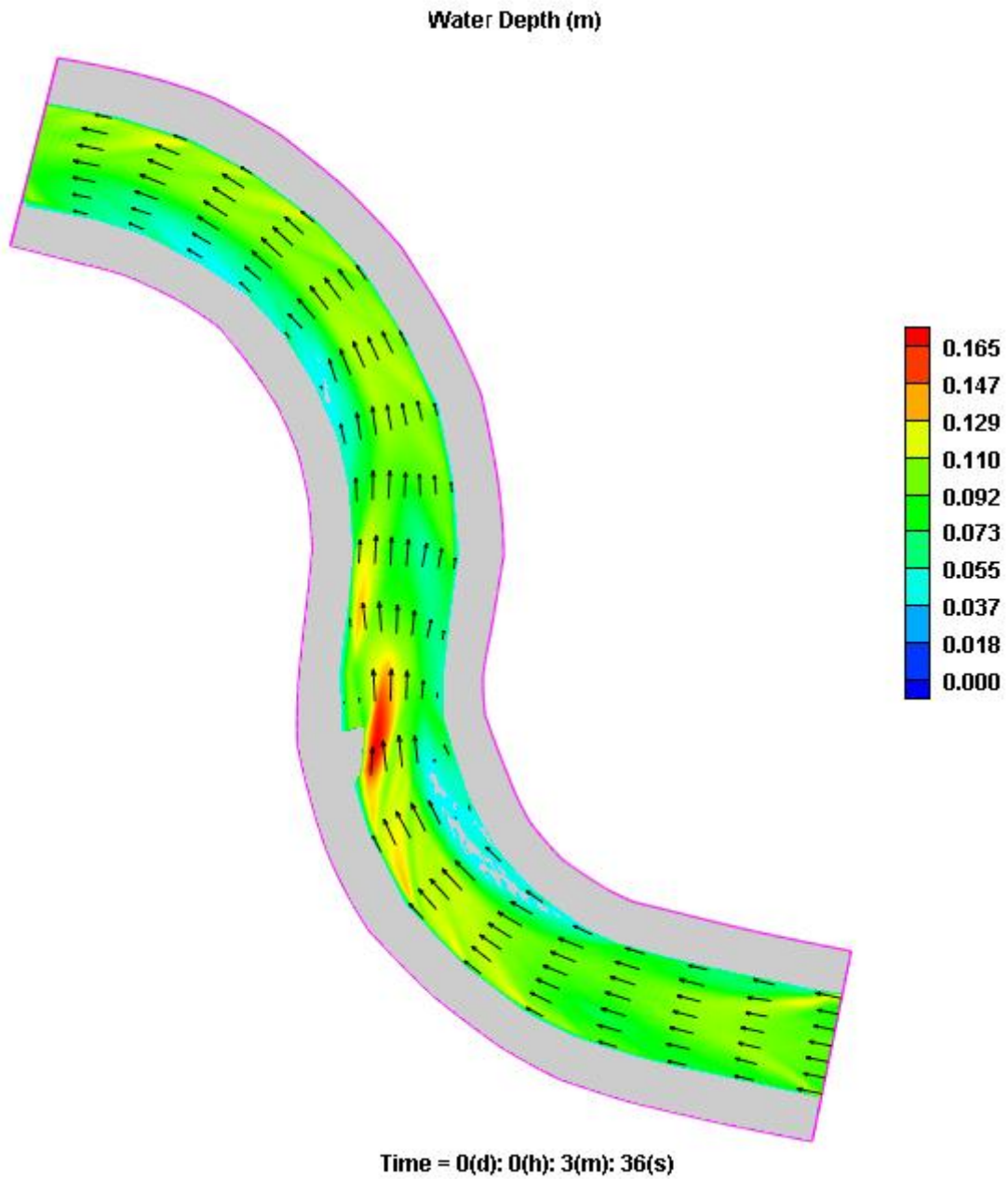


Figure C-56: Water depth (m) with velocity vectors

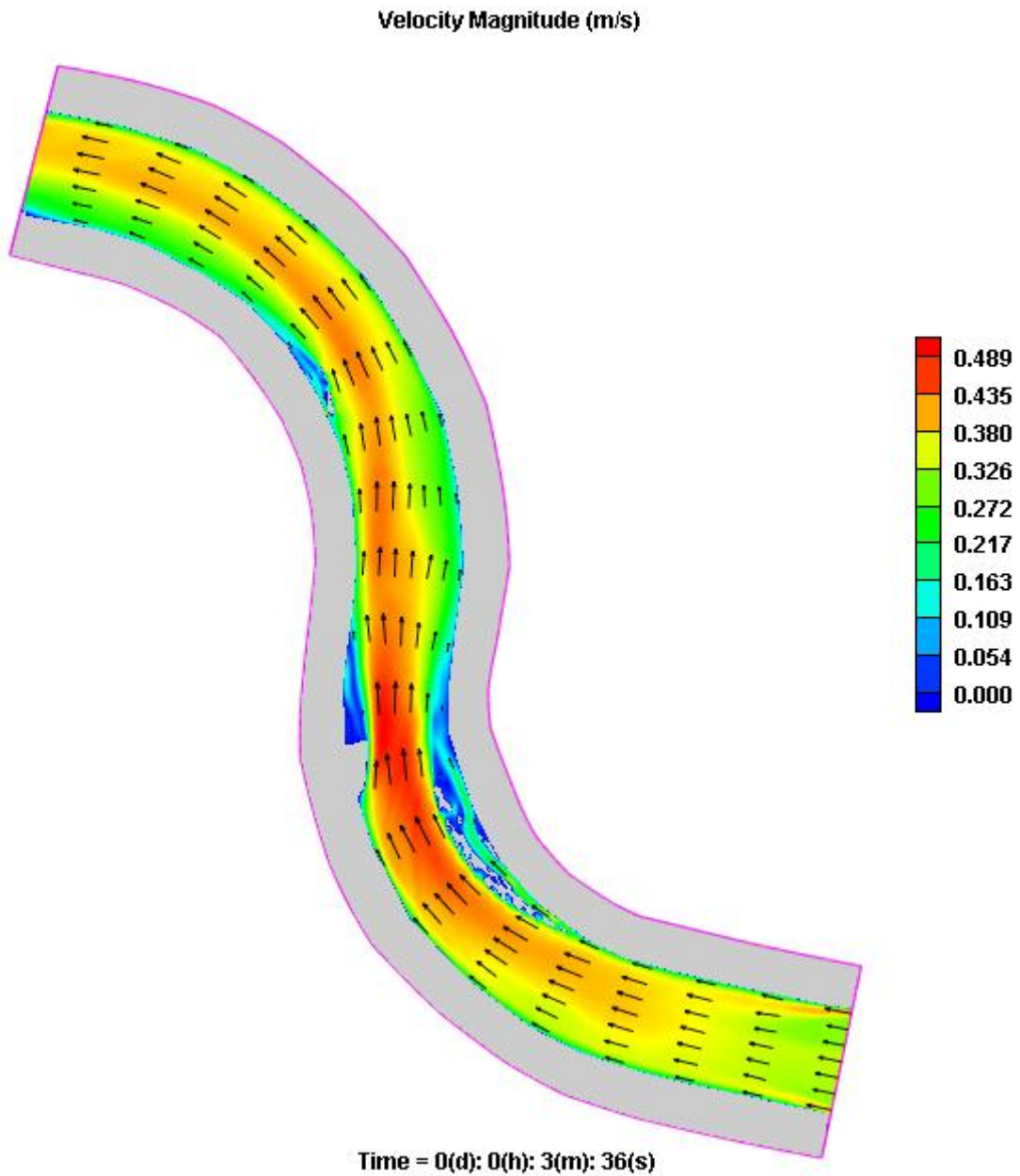


Figure C-57: Velocity magnitude (m/s) with velocity vectors

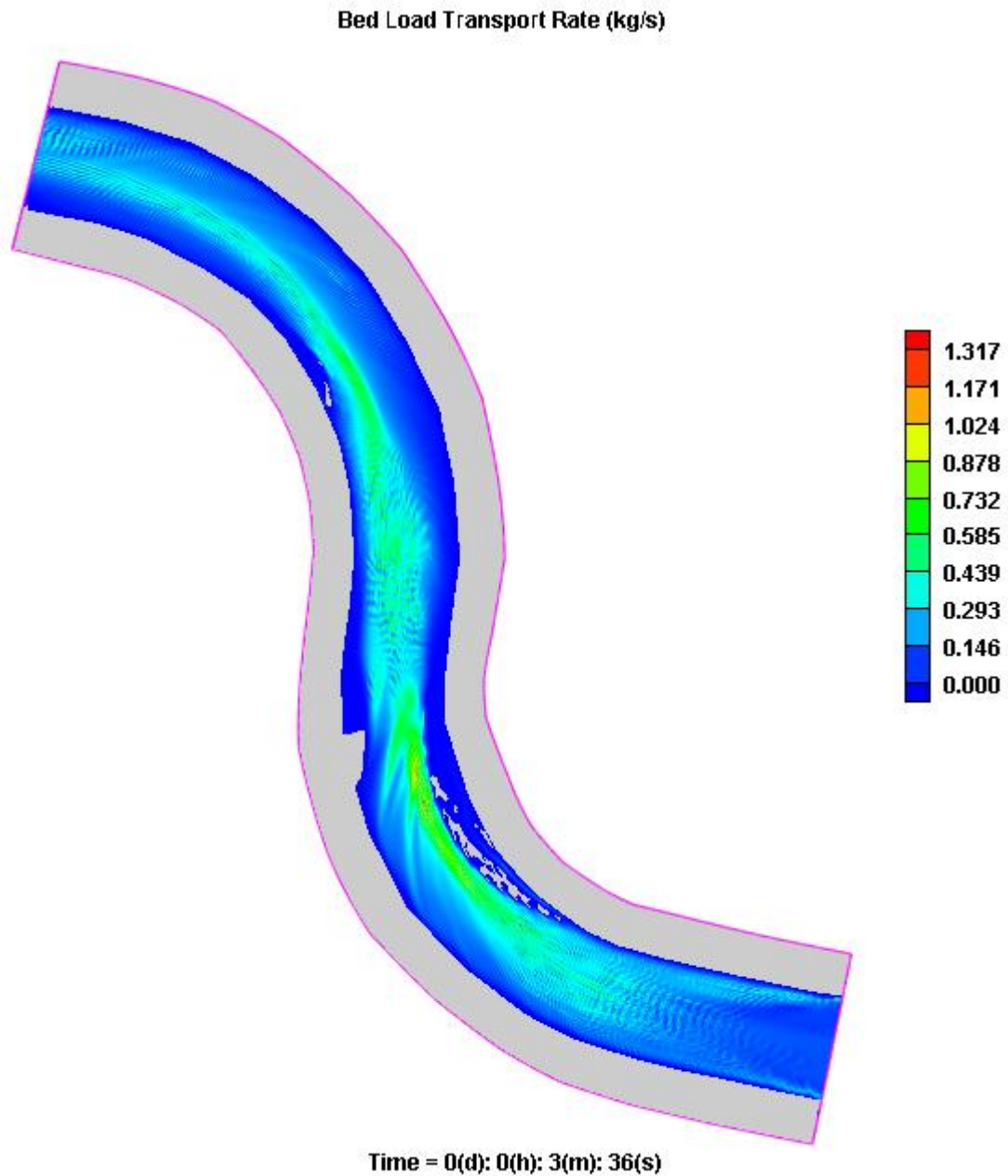


Figure C-58: Bed load transport rate (kg/s) for 30° structure with flow (one metre wide bottom width)

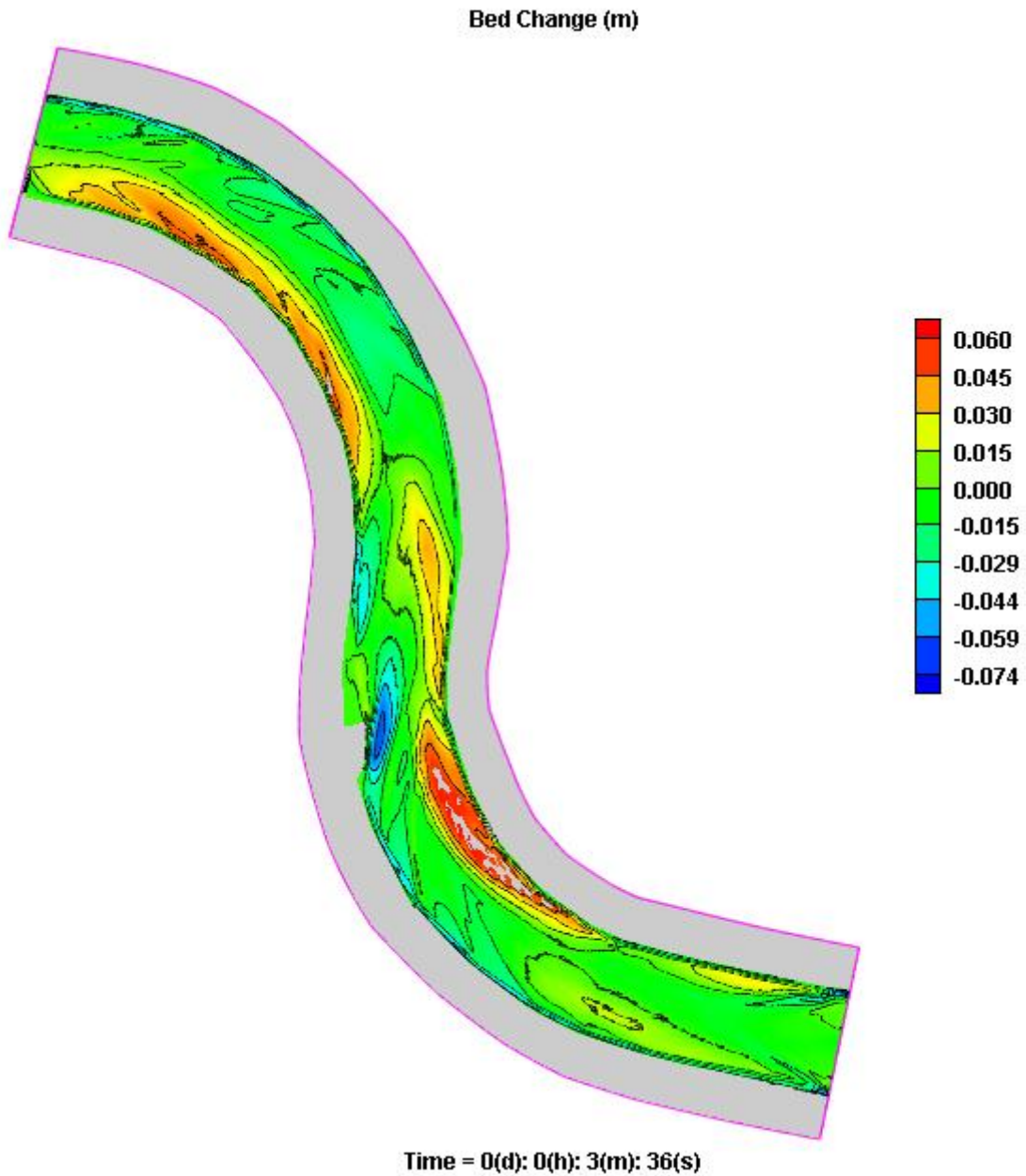


Figure C-59: Bed change (m) for 30° structure with flow (one metre wide bottom width)

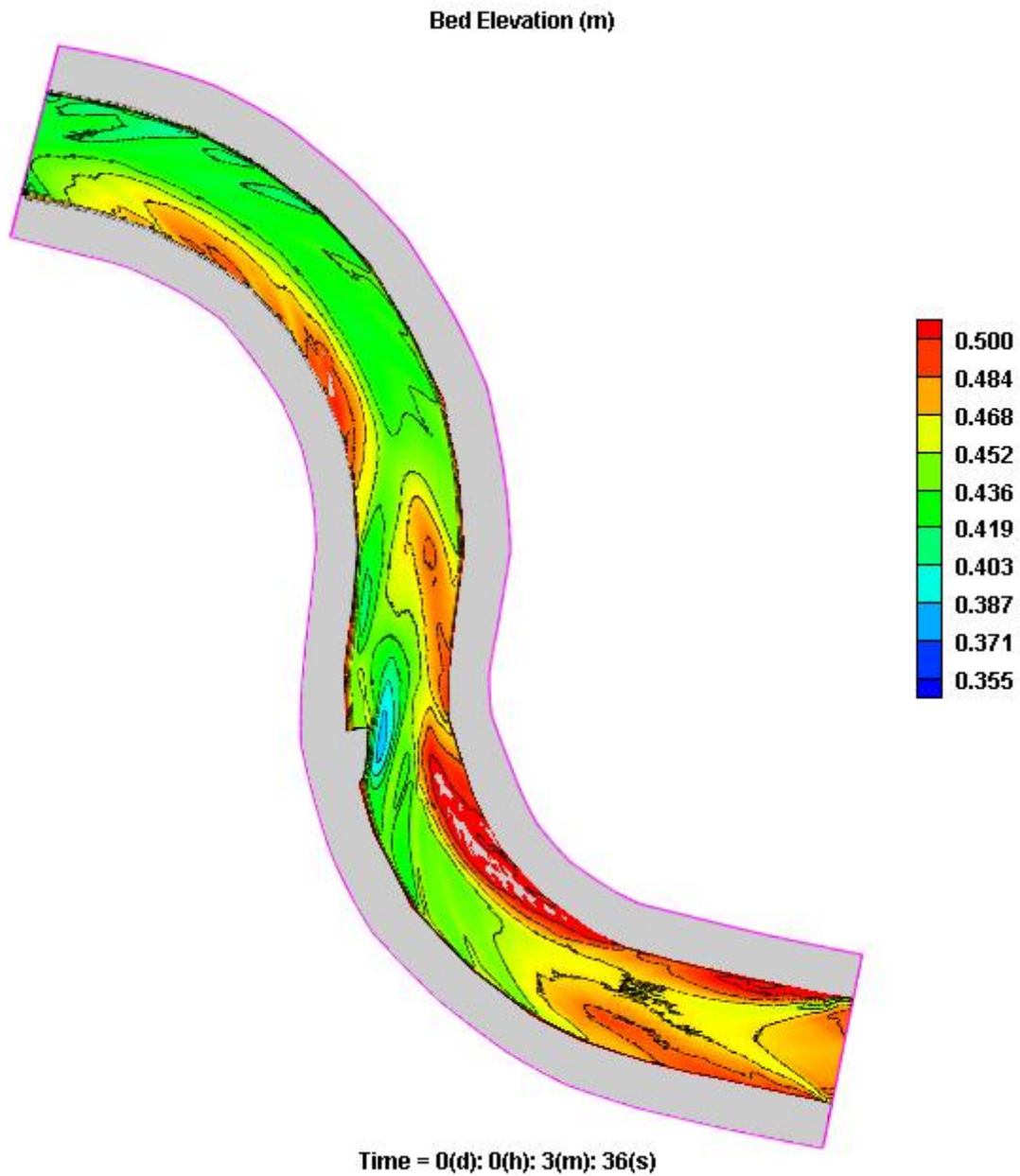


Figure C-60: Scoured bed elevation (30° structure with flow (one metre wide bottom width))

Simulation Test 10S 2 - 60° Structure with Flow (One Metre Wide Bottom Width)

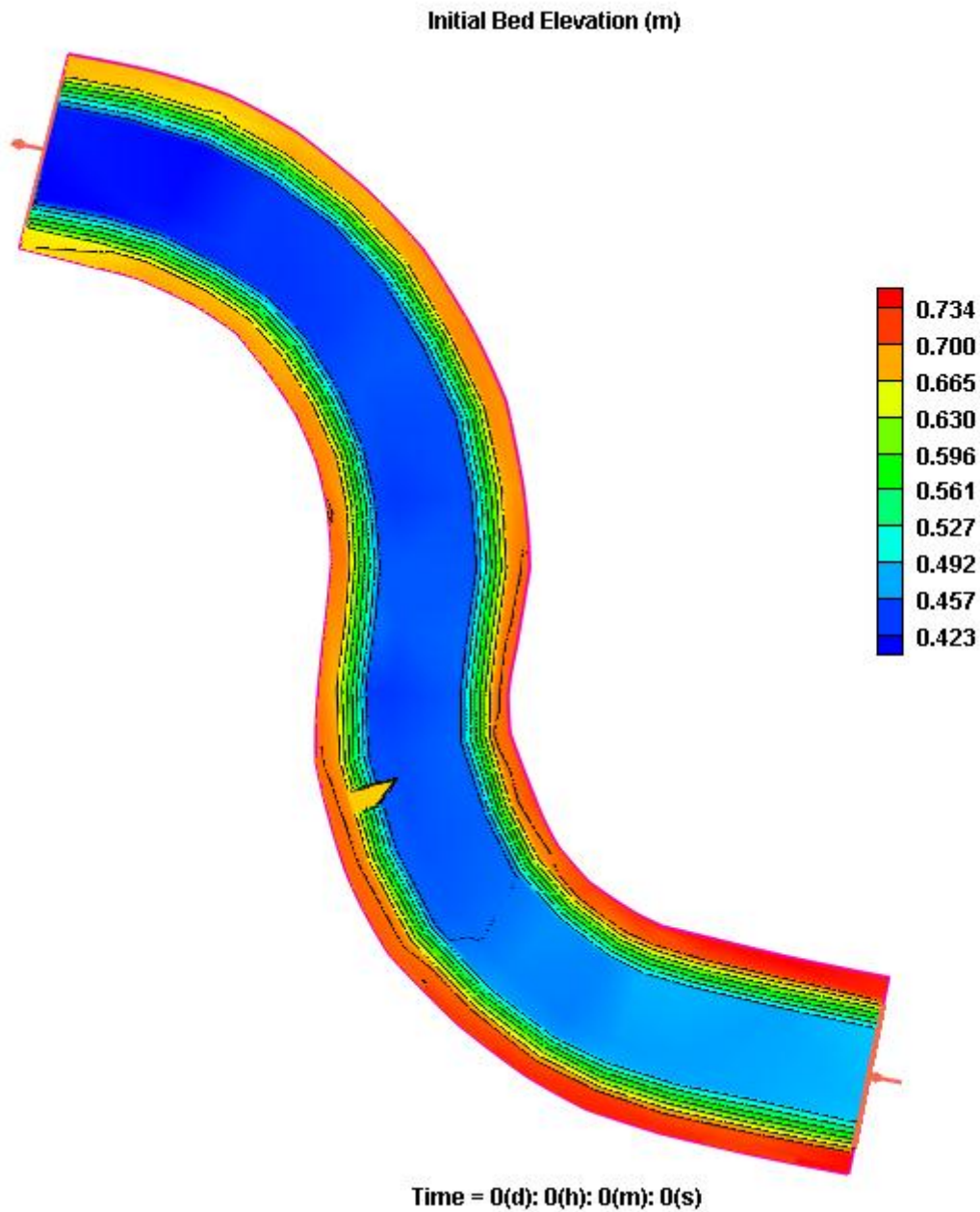


Figure C-61: Bathymetry of 2D model (60° structure with flow (one metre wide bottom width))

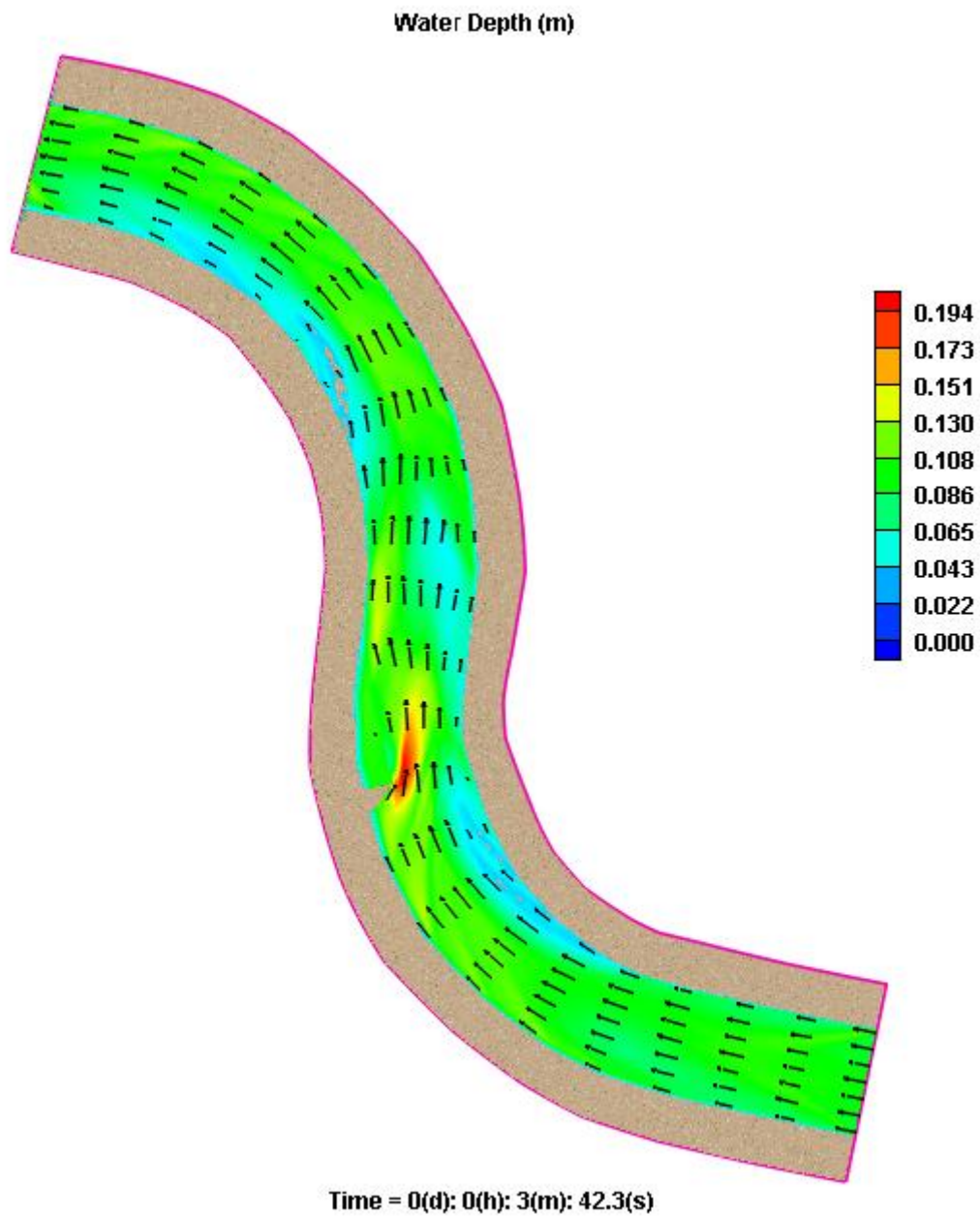


Figure C-62: Water depth (m) with velocity vectors

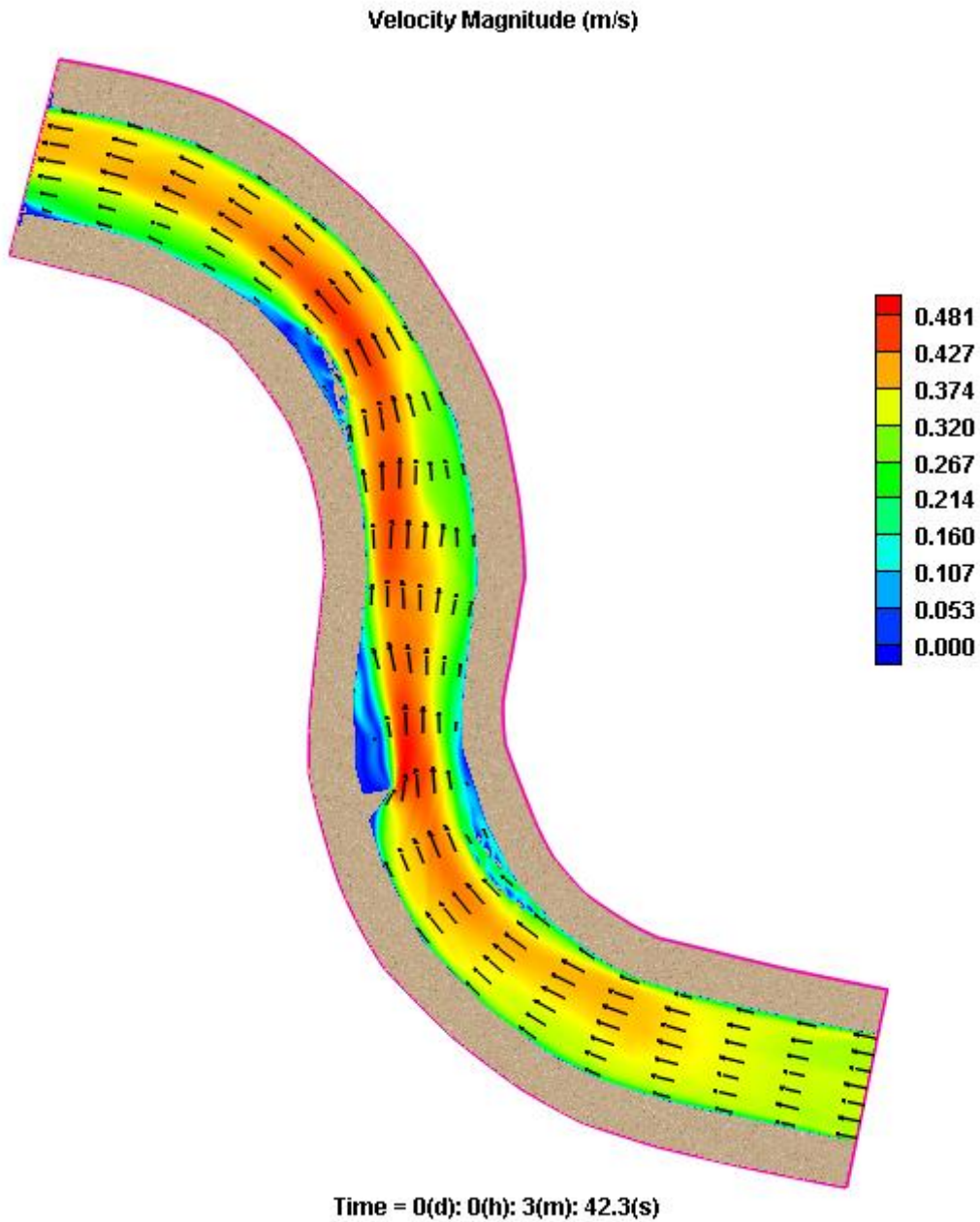


Figure C-63: Velocity magnitude (m/s) with velocity vectors

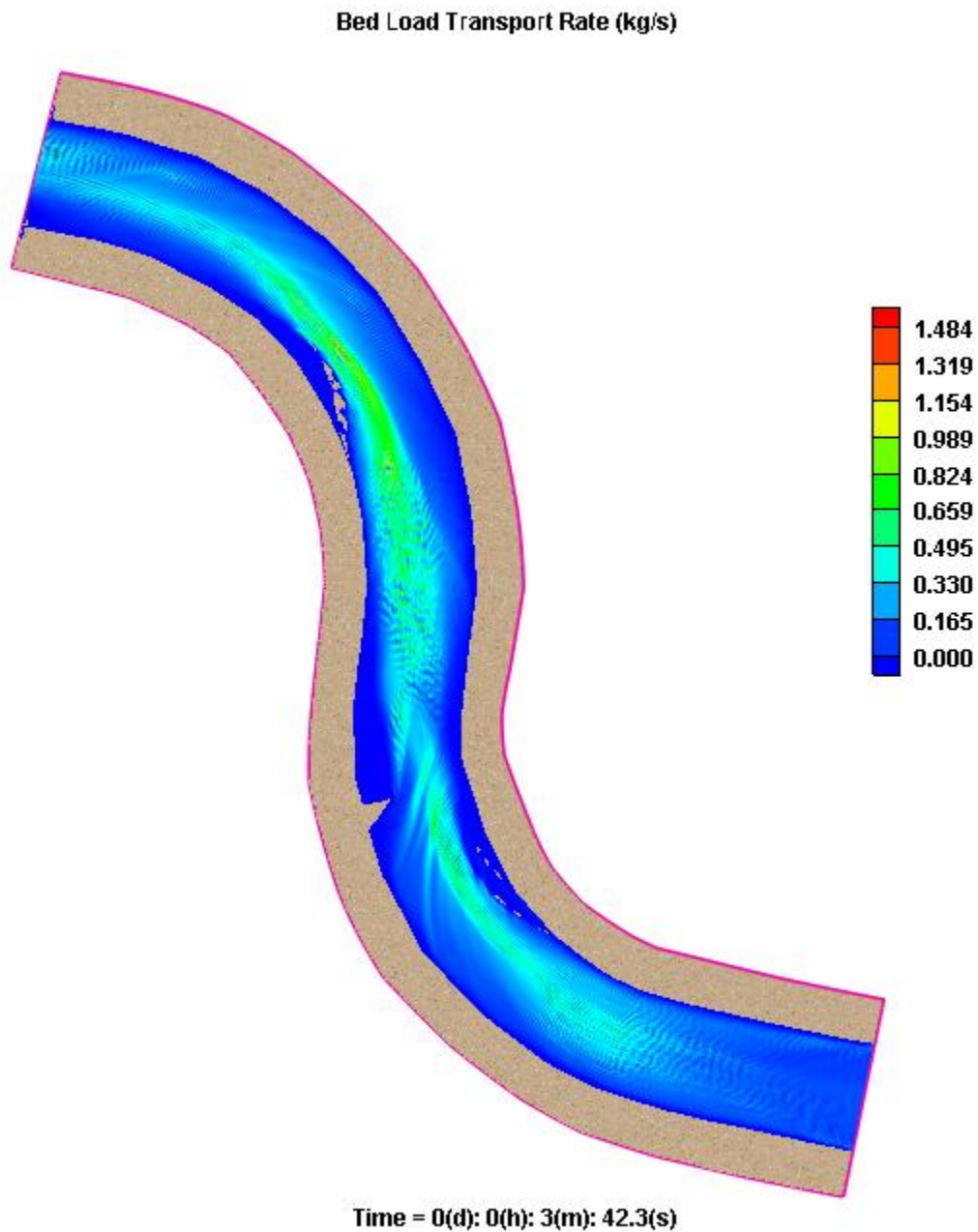


Figure C-64: Bed load transport rate (kg/s) for 60° structure with flow (one metre wide bottom width)

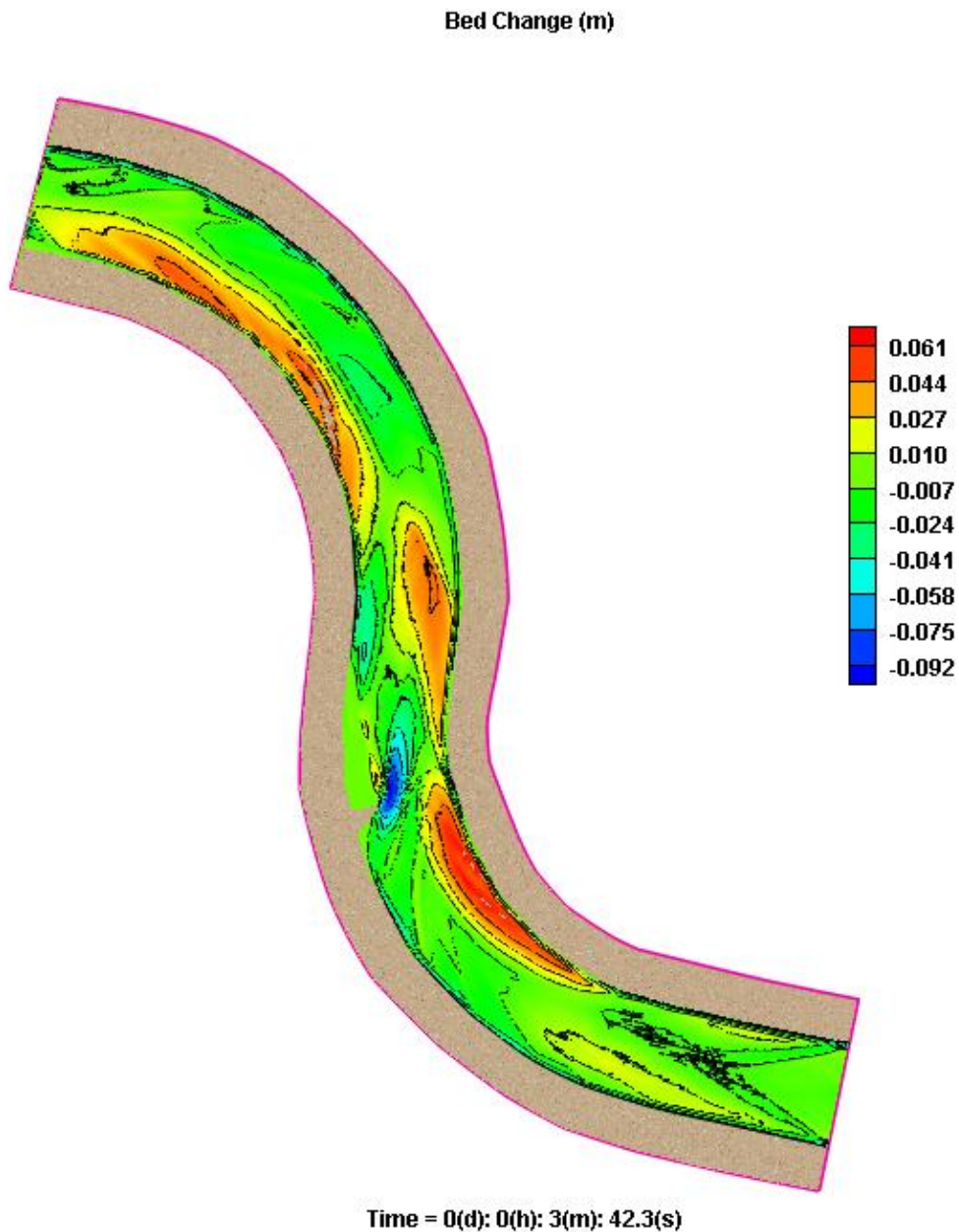


Figure C-65: Bed change (m) for 60° structure with flow (one metre wide bottom width)

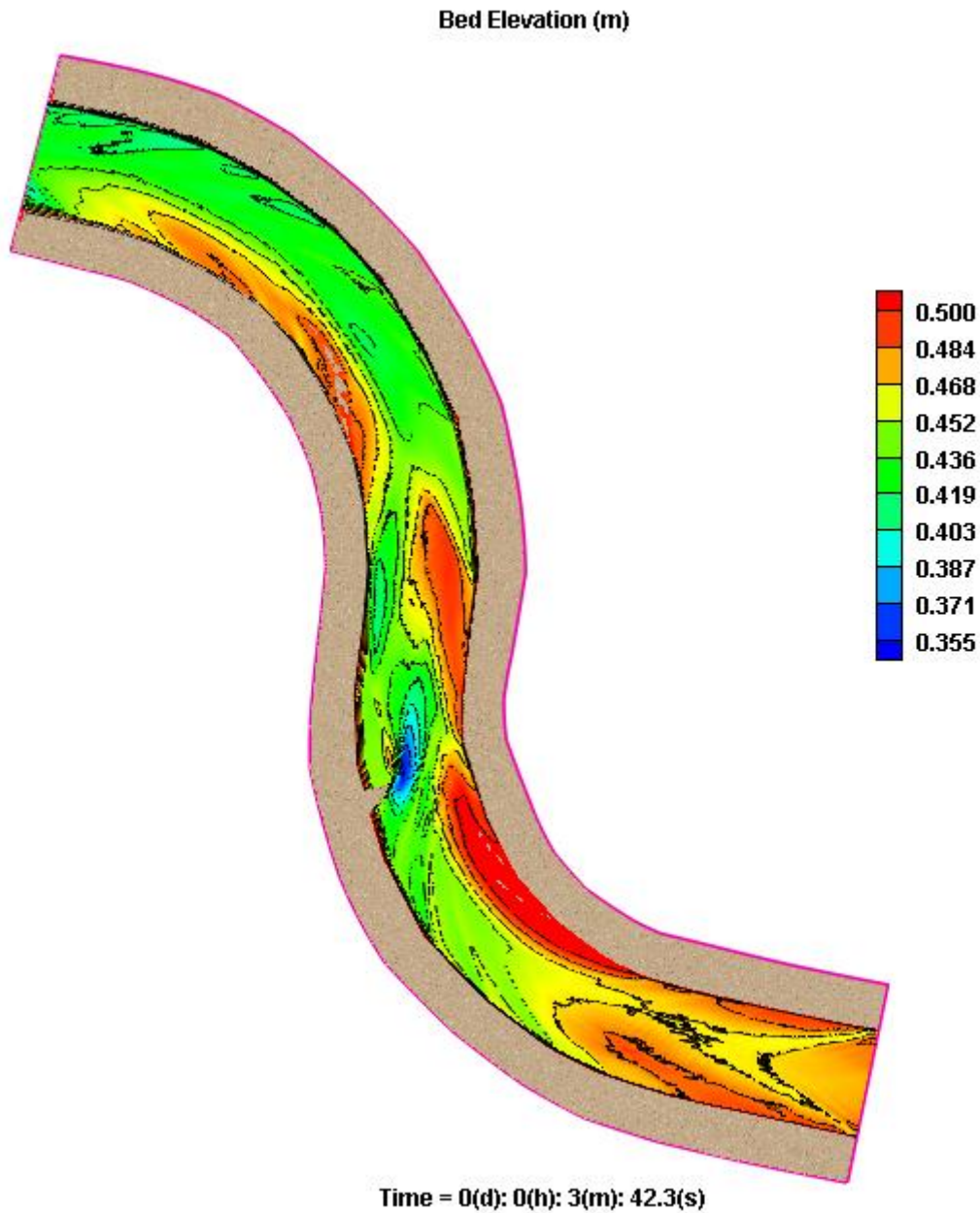


Figure C-66: Scoured bed elevation (60° structure with flow (one metre wide bottom width))